

# TECHNISCHE UNIVERSITÄT MÜNCHEN

Lehrstuhl für Biomolekulare NMR-Spektroskopie,  
Department Chemie

*Structure and molecular recognition of proteins linked to  
pre-mRNA splicing and transcriptional regulation*

Anders R. Friberg

München 2010

# TECHNISCHE UNIVERSITÄT MÜNCHEN

Lehrstuhl für Biomolekulare NMR-Spektroskopie,  
Department Chemie

## *Structure and molecular recognition of proteins linked to pre-mRNA splicing and transcriptional regulation*

Anders R. Friberg

Vollständiger Abdruck der von der Fakultät für Chemie der Technischen Universität München zur Erlangung des akademischen Grades eines Doktors der Naturwissenschaften genehmigten Dissertation.

Vorsitzender: Univ.-Prof. Dr. Chr. F. W. Becker

Prüfer der Dissertation: 1. Univ.-Prof. Dr. M. Sattler  
2. Univ.-Prof. Dr. M. Groll

Die Dissertation wurde am 27.08.2010 bei der Technischen Universität München eingereicht und durch die Fakultät für Chemie am 25.10.2010 angenommen.

"The future doesn't exist yet. Fate is for losers."

*Girlfriend in a Coma* by Douglas Coupland

# Table of contents

---

<b>Abstract</b>	<b>3</b>
<b>Zusammenfassung</b>	<b>4</b>
<b>Chapter 1</b>	<b>5</b>
<b>Regulation of gene expression</b>	
1.1. Central dogma of molecular biology	5
1.2. Regulation of gene expression	6
1.2.1. Regulation at the level of chromatin	8
1.2.2. Transcription: Pol II - a key coordinator	9
1.2.3. Post-transcriptional modifications: Generating mRNA stability	11
1.2.4. <i>Splicing of pre-mRNA: Maturation causing diversity</i>	12
1.2.5. RNA editing: Fine tuning of gene expression	14
1.2.6. mRNA export and localization	15
1.2.7. Gene silencing by RNA interference	18
<b>Chapter 2</b>	<b>21</b>
<b>Methods in structural biology</b>	
2.1. Two siblings: Molecular and structural biology	21
2.1.1. Cloning of a target protein	22
2.2. NMR: Solving structures in solution	24
2.2.1. Basic physical and mathematical description of NMR	25
2.2.2. NMR hardware and experiment setup	27
2.2.3. Fourier transform and NMR	28
2.2.4. The chemical shift and J-coupling	29
2.2.5. The protein fingerprint spectrum, 2D $^1\text{H}$ , $^{15}\text{N}$ HSQC	31
2.2.6. Assignments strategies	32
2.2.7. Ligand binding studies by NMR	34
2.2.8. Relaxation studies in NMR	35
2.2.9. The Nuclear Overhauser Effect	37
2.2.10. Residual dipolar couplings	37
2.2.11. Structure calculations and quality control	38
2.2.12. Literature	39
2.3. X-ray crystallography	40
<b>Chapter 3</b>	<b>43</b>
<b>Structure and ligand binding of Tudor-SN</b>	
3.1. Summary	43
3.2. Published manuscript	45
3.3. Supplementary material	59



<b>Chapter 4</b>	<b>63</b>
<b>NMR structure of an atypical Tudor domain</b>	
4.1. Summary	63
4.2. Published manuscript	65
4.3. Supplementary material	81
<b>Chapter 5</b>	<b>85</b>
<b>Structural characterization of the RES complex</b>	
5.1. Summary	85
5.2. Introduction	86
5.3. Results	89
5.4. Discussion	104
5.5. Conclusions	110
5.6. Materials and Methods	111
<b>Chapter 6</b>	<b>115</b>
<b>Additional collaborations</b>	
6.1. Induction of apoptosis: Evaluation of a potential inhibitor	115
6.2. Proposed interaction between viral LMP1 and human TRADD	116
6.3. Elucidation of a novel structural domain in EBNA-2	118
6.4. Confirming inhibitors of Bcl-xl	119
6.5. STD NMR: Interaction of STAT5b with a putative ligand	120
6.6. Protein chemistry: Ligation of a modified peptide to SMN	121
<b>Acknowledgements</b>	<b>123</b>
<b>References</b>	<b>125</b>
<b>Appendices</b>	<b>135</b>
A.1 Product operator analysis of the HSQC pulse sequence	135
A.2 Sequence and mass spectra of RES expression constructs	137
<b>Abbreviations</b>	<b>141</b>
<b>List of Figures</b>	<b>143</b>
<b>Curriculum Vitae</b>	<b>145</b>

# Abstract

---

Gene expression is a highly regulated process in our eukaryotic cells. To accomplish tight and dynamic control, regulatory functions affect protein production at various stages. The structural and biochemical work presented in this doctoral thesis, focuses on proteins involved in pre-mRNA splicing, one of the key steps in mRNA maturation, as well as on proteins engaged in chromatin remodeling. Notably, post-translational modifications, such as methylation of arginine or lysine residues, have been shown to play critical roles for these processes.

Chapter 1 and 2 serves as an introduction to regulation of gene expression and to structural biology, respectively. The aim is to give an overview of the current knowledge of the fundamental regulatory processes on the way from genes to proteins. The intention is to stress molecular aspects, and to point out how different pathways are intricately interconnected. Structural biology consists of rather different and complementary techniques. Here, mainly basic aspects of nuclear magnetic resonance (NMR), and its use to study the structure, dynamics and interactions of biomolecules, are covered.

Chapter 3 describes the three-dimensional structure of the so-called TSN domain of Tudor-SN, comprising an extended Tudor domain fold. The structure was determined by X-ray crystallography. NMR  $^{15}\text{N}$  relaxation data and residual dipolar coupling measurements show that TSN adopts a compact fold, and that the two subdomains tumble together in solution, consistent with the crystal structure. Using NMR titrations, the TSN domain was found to bind peptides containing symmetrically dimethylated arginines (sDMA). The interaction involves an aromatic cage of the Tudor domain. Dimethylarginine-modified proteins have important functions in various cellular pathways, including the spliceosome. My results suggest how Tudor-SN might interact with the spliceosome, where it has been reported to enhance assembly and splicing efficiency.

Chapter 4 reports the NMR-derived solution structure of the Tudor domain of *Drosophila* Polycomblike (Pcl), which is involved in transcriptional regulation at the level of chromatin remodeling. It was hypothesized that Pcl may act as a targeting factor of a repressive complex by recognition of methylated histone tails through its Tudor domain. Our data, however, show that the Pcl Tudor domain has an atypical aromatic cage, which does not bind to any of the predicted putative Tudor ligands, rendering a role in targeting rather unlikely. A structural comparison to Tudor-SN highlights a hydrophobic surface patch as a potential interaction site, where binding of other domains or proteins in the repressive complex could occur.

In Chapter 5, data on the recently discovered trimeric RES (retention and splicing) complex are presented. RES is involved in splicing and nuclear export of messenger mRNAs. I present a preliminary biophysical characterization, and provide evidence that the interaction of two of the components involves a novel, extended variation of a so-called UHM-ULM (U2AF Homology Motif- UHM Ligand Motif) protein-protein interaction.  $^{15}\text{N}$  relaxation experiments indicate that approximately 25 amino acids in the ULM peptide tightly interact with the UHM domain. Chemical shift analysis suggests that a helix is formed in the ULM peptide upon binding. NMR data has been acquired for a structural elucidation of this protein-peptide complex.

Finally, Chapter 6 briefly covers additional short projects I was involved in during my PhD. Many of them included validation of small-molecule ligands that had been found to interact with their targets in different kinds of primary screens.

# Zusammenfassung

---

Die Expression des genetischen Codes ist ein hoch regulierter Prozess in eukaryontischen Zellen. Die entsprechenden Aspekte der Proteinexpression in der Zelle unterliegen einer strengen und dynamischen Regulation. Die vorliegende Dissertation beschreibt strukturelle und biochemische Untersuchungen von Proteinen, die eine Rolle spielen für das RNA Spleißen, einem Schlüsselschritt der Reifung der Boten RNA, sowie für die Remodellierung des Chromatins spielen.

Kapitel 1 und 2 geben eine Einführung in die verschiedenen Aspekte der Regulation der Genexpression sowie die strukturelle biologische Verfahren. Ziel ist es, einen Überblick über grundlegende regulatorische Prozesse vom Gen zum Protein zu geben. Dabei liegt die Betonung darauf, molekulare Aspekte zu skizzieren und aufzuzeigen, wie die verschiedenen Signalwege eng miteinander verflochten sind. Strukturbiologie umfasst recht unterschiedliche aber komplementäre Methoden. Hier werden vor allem grundlegende Aspekte der Kernspinresonanz („nuclear magnetic resonance“, NMR) Spektroskopie besprochen, sowie ihr Potential für die Untersuchung der Struktur, Dynamik und Wechselwirkungen von biologischen Makromolekülen aufgezeigt.

Kapitel 3 beschreibt die drei-dimensional Struktur der sogenannten TSN Domäne des Tudor-SN Proteins, die ein erweitertes Tudor Domänen Faltungsmotiv darstellt. Die Struktur wurde mittels Röntgenstrukturanalyse bestimmt. NMR  $^{15}\text{N}$  Relaxationsmessungen und dipolare Restkopplungen („residual dipolar couplings“, RDCs) zeigen, dass TSN eine kompakte Struktur einnimmt und dass die beiden Untereinheiten sich in Lösung gemeinsam reorientieren, konsistent mit der Kristallstruktur. Mittels NMR Titrations konnte gezeigt werden, dass die TSN Domäne Peptide mit symmetrisch dimethylierten Argininen (sDMA) bindet. Die Erkennung wird durch einen aromatischen Käfig der Tudor Domäne vermittelt. Dimethylarginin-modifizierte Proteine sind von großer Bedeutung für verschiedene zelluläre Prozesse, einschließlich des Spleißosoms. Meine Ergebnisse liefern Hinweise dafür, wie Tudor-SN mit dem Spleißosom wechselwirken und seine Assemblierung und Effizienz verstärken kann.

Kapitel 4 stellt die NMR Struktur der Tudor Domäne des *Drosophila* „Polycomblike“ (Pcl) Proteins vor, das in die Regulation von Transkription auf der Ebene der Remodellierung des Chromatins impliziert ist. Es wurde vorhergesagt, dass Pcl eine Rolle für die Lokalisierung eines repressiven Komplexes einnimmt, durch Erkennung methylierter Histonendungen mittels seiner Tudor Domäne. Unsere Daten zeigen allerdings, dass die Pcl Tudor Domäne einen atypischen aromatischen Käfig aufweist, der an keinen der vorhergesagten, möglichen Tudor Liganden bindet. Eine Funktion der Tudor Domäne für die Lokalisierung erscheint daher nicht wahrscheinlich. Ein Strukturvergleich mit Tudor-SN zeigt, dass eine hydrophobe Oberfläche existiert, die mögliche Wechselwirkungen mit anderen Domänen oder Proteinen des repressiven Komplexes vermitteln könnte.

In Kapitel 5 werden Untersuchungen zum kürzlich entdeckten ternären RES („retention and splicing“) Komplex vorgestellt. RES spielt eine Rolle im Spleißen und Kernexport von Boten RNAs. Ich stelle meine Ergebnisse hinsichtlich der biophysikalischen Charakterisierung vor und liefere Hinweise dafür, dass die Bindung von zwei Komponenten des RES Komplexes durch eine neue, erweiterte Variante von sogenannten UHM-ULM („U2AF Homology Motif- UHM Ligand Motif“) Protein-Protein Wechselwirkungen vermittelt wird.  $^{15}\text{N}$  Relaxationsexperimente zeigen, dass etwa 25 Aminosäurereste des ULM Peptids an der UHM Bindung beteiligt sind. Eine Analyse von chemischen Verschiebungsänderungen zeigt, dass durch die Bindung eine Helix innerhalb des ULM Peptids induziert wird. Zahlreiche NMR Daten wurden aufgenommen, die eine Strukturbestimmung des Protein-Peptidkomplexes ermöglichen.

Im abschließenden Kapitel 6 werden einige kurze Projekte beschrieben, an denen ich im Laufe meiner Promotion beteiligt war. Viele dieser Projekte betreffen die Validierung der Bindung von kleinen organischen Molekülen an verschiedene Zielproteine, die aufgrund verschiedener primärer Assays beschrieben war.

# Chapter 1

---

## Regulation of gene expression

At no single instance of cellular life, gene expression is left out of regulation. Regulation of our genes is inherently dynamic which allows it to respond to new stimuli and stress of different kinds. Loss of regulation, in contrast, is directly linked to various diseases and, perhaps most notably, to development of cancer. Regulation of gene expression controls the amount of gene products, proteins or functional RNAs in the cell, and is an intense field of research. In recent years, not only has the saying: "one gene, one protein" become obsolete, but also entirely new layers of regulation have been discovered, such as RNA interference (RNAi) and within chromatin remodeling.

This biological introduction will focus on the control of gene expression in the eukaryotic cell rather than the prokaryotic. Some processes are, of course, similar in both types of cells, but the differences are many. One aim is to point out the massive regulation going on in the cells at any given moment, also when obvious external demands are not present. Another intention is to illustrate how a molecular understanding of these regulatory processes is required, and has paved the road for many discoveries. Finally, the intriguing interconnectivity between specific concepts will be highlighted.

### 1.1. Central dogma of molecular biology

How traits are inherited and articulated had been a well-disputed subject for a long time, until the flow of genetic information in the cell was laid out during the middle of the last century. Taking this knowledge into account, Francis Crick then formulated the famous *Central dogma of Molecular Biology*.<sup>1</sup> In the nucleus the messenger-RNA (mRNA) is transcribed from DNA, and using the mRNA as a blueprint, a protein is synthesized in the cytoplasm (Figure 1.1.1). Over the years, the original hypothesis has been modified and extended, and now also comes in many flavors depending on which organism is studied. Starting from the early discoveries, numerous levels of regulation of gene expression were discovered. In the next sections the main topics and themes will be introduced, adding complexity to the original oversimplified hypothesis on a straightforward cellular protein production. Various regulatory processes will be addressed, starting with chromatin remodeling, going through transcriptional control and RNA maturation, until just prior translation at the ribosome.

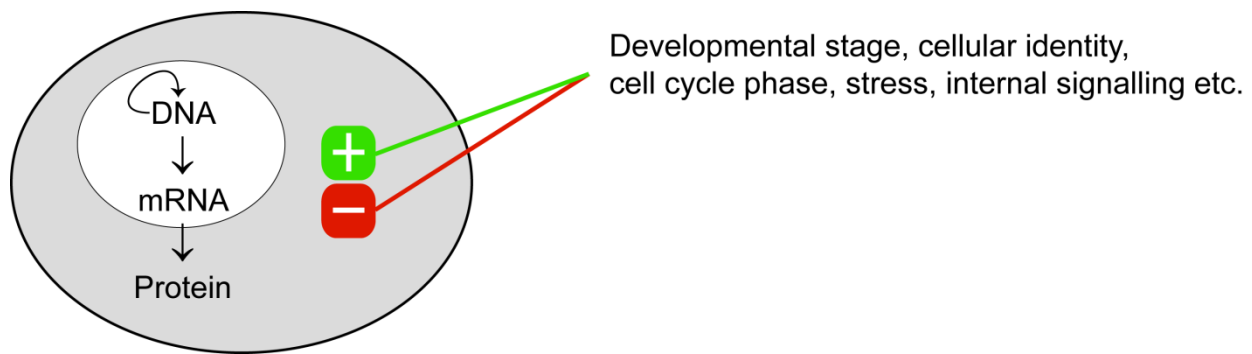


**Figure 1.1.1 Central dogma of molecular biology.** DNA contains our genetic information and is replicated during each round of the cell cycle. Proteins, carrying out most of the functions in the cell, are produced using mRNA as a blueprint of the gene. The genetic material (DNA) stays in the cell nucleus, while the mRNA is transported out into the cytoplasm, where the protein is synthesized. All of these processes are intricately influenced, activated or repressed, by various internal and external factors.

## 1.2. Regulation of gene expression

Simpler organisms, such as bacteria, have to be able to respond to changes in the surroundings and adapt to their new environment.<sup>2</sup> This is in part done by regulation on the level of gene expression. However, the importance of a tight and dynamic regulation of genes becomes even more evident in the development of multicellular organisms. Here, all cells have the same set of genes in their chromosomes, but serve very diverse purposes: Bone cells provide structure, nerve cells pass on electro-chemical signals, gut cells produce acid, immune cells fight infections. In higher eukaryotes, the maintenance of cellular identity is based on control over long-term gene expression. The whole field of stem cell research relies on the understanding of such processes and on working out how to manipulate them.<sup>3</sup>

Light, nutrition and toxic compounds are obvious external stimuli, that cells have to be able to respond. Stress on cells and organisms is a topic that has been studied thoroughly, here one can include for example heat shock, starvation, DNA damage by UV light, as well as infection of viruses or other organisms. Another main theme is gene expression regulated by the cell cycle, or other rhythmic processes (circadian clocks). Especially in multicellular organisms, signaling between individual cells by hormones, peptides and metabolites, or through direct contact, plays a key role in gene regulation.

In the eukaryotic cell, the importance of compartmentalization must be stressed. The untangling of transcription and translation, taking place in the nucleus and in the cytoplasm respectively, facilitates regulation and opens up for steps of quality control. The overview figure on the next page introduces topics later discussed, and place them according to their apparent sequential order (Figure 1.2.1).

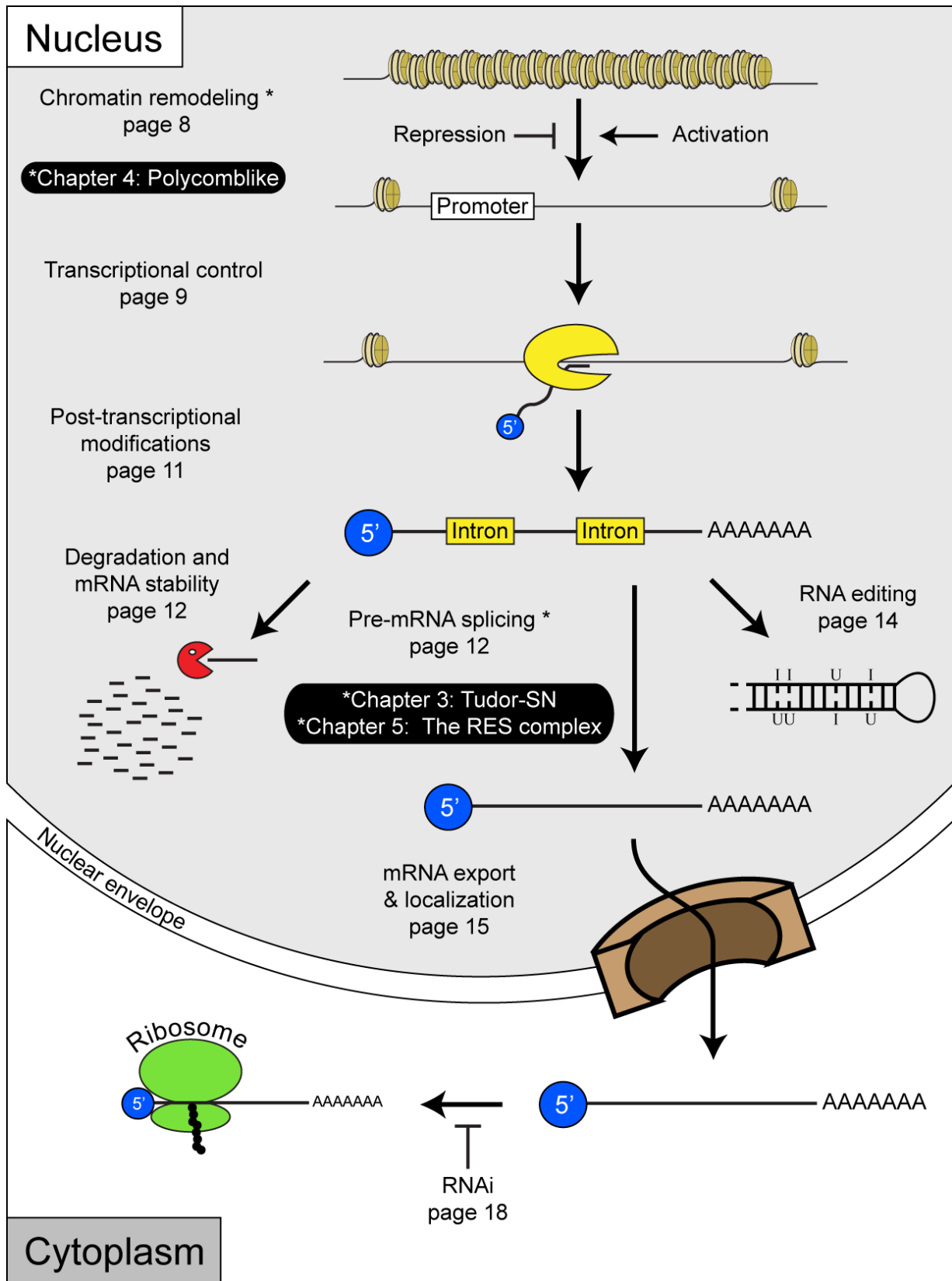


**Figure 1.2.1 Overview of regulation in gene expression: From transcription to translation.** Each step of gene expression, starting at transcription, through mRNA maturation, until export and translation, is tightly regulated. The topics of the three main projects of this thesis are highlighted (black boxes) and put into their context. Page numbers refer to the biological introduction found in Chapter 1.

### 1.2.1. Regulation at the level of chromatin

Chromatin, comprising DNA wound up on histone proteins and together forming nucleosomes, should not be considered only a depository structure for the genetic material, since it is actively involved in regulation of gene expression. Furthermore, chromatin structure is not static but is continuously remodeled.<sup>4</sup> Changes in its structure, make genes or loci accessible, or not, to transcription (Figure 1.2.2 A). A compact state of chromatin also hinders the required interaction of gene promoter and enhancer regions, which in eukaryotic chromosomes can be far apart.<sup>5</sup>

The processes mentioned below, all play their roles in epigenetic regulation. Broadly speaking, epigenetic regulation includes such processes that affect cell identity over longer time periods, also cell generations, and that are caused by mechanisms other than changes in the DNA sequence.<sup>6</sup> Epigenetics has become important to diverse fields such as developmental<sup>7</sup>, tumor<sup>8</sup> and stem cell biology<sup>9</sup>

Methylation of the DNA itself has a basic gene silencing function in for example imprinting and X-chromosome inactivation.<sup>6</sup> Both processes are related to the fact that the cell has pairs of equivalent chromosomes from the parents. In some cases, parts or an entire chromosome have to be silenced so that proteins only are expressed from one of the original two chromosomes. DNA methylation is carried out by certain enzymatic complexes, the DNA methyltransferases (DNMTs)<sup>10</sup>, and mainly affect gene expression by acting as a platform for methyl-binding proteins (Figure 1.2.2 B).<sup>11</sup> Methyl-CpG-binding protein 2 (MeCP2) is one example of such protein and mutations in its gene give rise to the Rett syndrome, a disorder related to autism.<sup>12</sup> However, DNA methylation *per-se* alters the nature of the DNA molecule and thereby decrease transcription. Interestingly, X-chromosome inactivation is targeted by a non-coding RNA (ncRNA).<sup>13,14</sup>

Additionally, chromatin structure and gene expression are modulated by post-translational modifications in the flexible tails of histones (Figure 1.2.2 C).<sup>15</sup> These modifications include amongst others: acetylation, methylation, ubiquitination and phosphorylation. The position of each functional group, and the combination of them, is thought to form a *histone code*. This *histone code* can then be read by many different adaptor and effector proteins, carrying out diverse functions. For instance, acetylation of histone tails typically lead to a more open chromatin structure, while methylation of lysine 27 in histone protein 3 (H3K27me) is indicative of transcriptionally repressed genes (see Chapter 4).<sup>16,17</sup> Also DNA damage is connected to certain histone modifications and is thought to recruit repair factors.<sup>18</sup>

Nucleosome repositioning is an energy-dependent process capable of moving the histone octamer, to which the DNA is attached.<sup>19</sup> When nucleosomes slide or are removed, specific genes are opened up to transcription (Figure 1.2.2 D). RCS<sup>20</sup> and SWI/SNF<sup>21</sup> are two well-characterized nucleosome remodeling complexes. Furthermore, topoisomerases have been shown to affect chromatin dynamics and facilitate remodeling processes.<sup>22</sup>



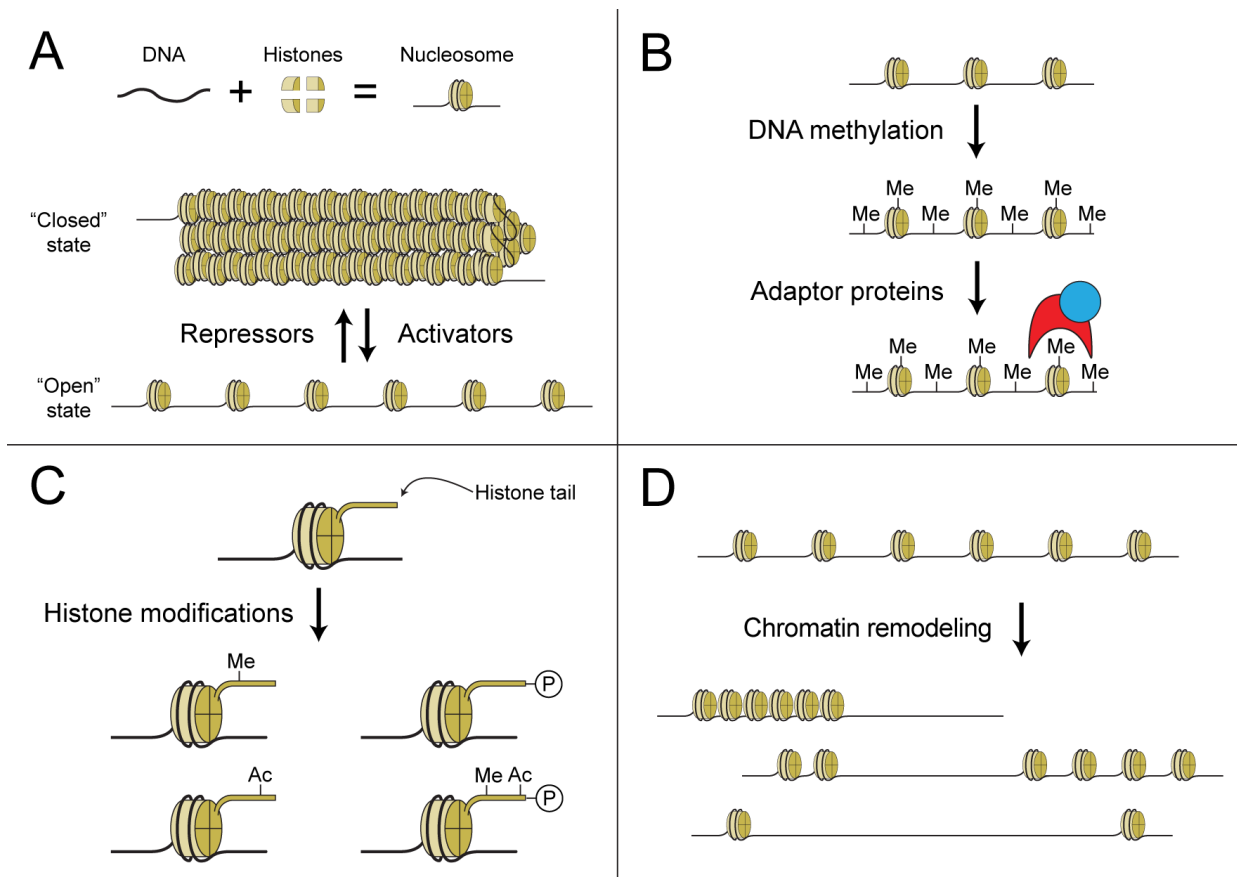


**Figure 1.2.2 Chromatin is a dynamic structure.** (A) In a repressed state the nucleosomes are tightly packed against each other, but when activated the chromatin state is relaxed. (B) DNA methylation by DNMTs creates a possible interaction surface for adaptor proteins, such as MeCP2. (C) Post-translational modifications of the flexible histone tails regulates the transcription activity. Also, a combination of different epigenetic marks can be interpreted jointly. (D) Chromatin remodeling complexes can move and/or remove nucleosomes to guarantee polymerases access to promoters.

### 1.2.2. Transcription: Pol II - a key coordinator

The primary level of regulation of gene expression is taking place at transcription, including the steps of initiation, elongation and termination.<sup>23</sup> The actual production of the correct amount of the specific RNA at the right moment is fundamental to proper gene expression. Transcription of RNA, as such, is relatively well understood, nonetheless the regulation of this process still remains to be elucidated further.<sup>24</sup> There are many different types of RNAs transcribed in eukaryotes, however, here the regulation of messenger-RNA (mRNA) synthesis is briefly introduced (Figure 1.2.3).

In eukaryotes, transcription of mRNA is accomplished by RNA polymerase II (Pol II), a multi-subunit enzyme.<sup>25</sup> In brief, transcription initiation takes place at an accessible promoter including a TATA-box, where a set of general transcription factors binds together with Pol II.<sup>26</sup> After formation of a pre-initiation complex, the DNA duplex is melted and transcription can start. The C-terminal domain (CTD) of the largest subunit of Pol II is an essential site for regulation. At this stage, the CTD is phosphorylated which allows the polymerase to enter the elongation phase.<sup>27</sup> Different Pol II subunits and stages of the transcription process have been characterized by structural



biology.<sup>28</sup> At a specific sequence the mRNA is polyadenylated (poly(A)) and this causes transcription termination. The polymerase detaches from the DNA, and the mRNA is cleaved just after the poly(A)-tail. Although, the exact termination mechanism differs depending on the type of RNA, and is still not completely understood, it has been shown to be required for optimal protein expression.<sup>29-31</sup>

The CTD of Pol II is essential for efficient transcription and coordinates many processing steps described in later sections. These include 5' capping, synthesis of the poly(A)-tail, splicing and RNA editing.<sup>32,33</sup> It seems evident that it is correct to consider these processes as highly interconnected and not sequential or separate. Thus, their regulation is expected to depend on the transcription process as well.

In addition to the TATA-box, many genes have important regulatory DNA sequences slightly upstream of the start site. These sequences bind transcription factors (TFs), which in eukaryotes most often are activators of transcription. The TFs generally contain a DNA binding module, a response domain, which responds to a particular signal, as well as an activation module, which interacts with the transcription machinery. Two examples of families of TFs are C/EBPs and CREBs. Both families are binding to certain DNA sequences and are themselves regulated by plethora of signal pathways.<sup>34,35</sup> See also Section 5.5 for another example.

In addition, eukaryotic genes have enhancer regions much further away from the transcription initiation site. The TFs and the enhancer regions are linked to Pol II by a large multi-protein and essential co-activating complex known as the Mediator.<sup>36</sup> However, structures and functions of the individual domains are not as well characterized as for Pol II.<sup>37</sup> All the regulatory molecules described have to come together at the same time to allow transcription to take place, like a lock where several keys are needed simultaneously to unlock it.

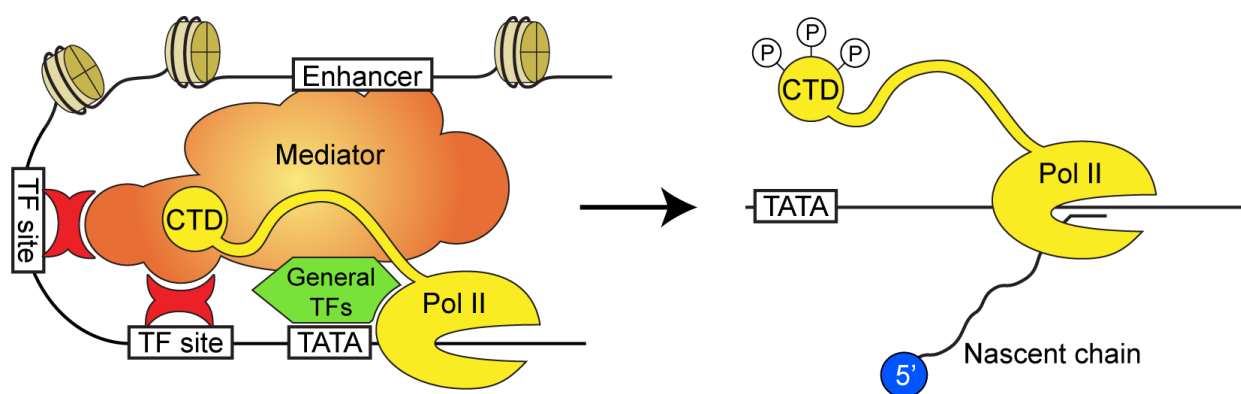


**Figure 1.2.3 Transcription initiation.** Regulation of transcription is a crucial step in protein production. In addition to general transcription factors, the transcription initiation of Pol II needs Mediator, which is thought to combine the co-activating effect of specific transcription factors and distant enhancer regions. The CTD is phosphorylated prior to elongation, and is responsible for linking many of the downstream RNA-processing steps to transcription. The 5' cap is acquired early on to stabilize the nascent chain.

### 1.2.3. Post-transcriptional modifications: Generating mRNA stability

Transcribed mRNAs need to be stable, but not too stable, to allow fluctuations in the amount of protein produced. The dynamic equilibrium between those two states are closely linked to post-transcriptional modifications. However, as commented on previously, processing of the transcribed and immature precursor mRNA (pre-mRNA) is coordinated with transcription itself. Hence, the term '*post-transcriptional*' is misleading, since processing takes place during transcription, and not strictly in a sequential fashion. Interestingly, mRNA decay has been suggested to be profoundly involved in the regulation of gene expression.<sup>38</sup>

5' capping is the first step in pre-mRNA processing. Just after transcription elongation has started, three enzymatic activities come together to modify the 5' end of the nascent transcript: a triphosphatase, a guanyltransferase and a methyltransferase. The modifiers reside at the CTD, awaiting CTD phosphorylation, a signal which activates elongation, as well as these capping enzymes.<sup>33</sup>

The 3' poly(A) tail is generated at a specific sequence, present at the very end of the gene. This sequence recruits another enzymatic complex to the pre-mRNA. It comprises a polyadenylase, which synthesizes the poly(A)-tail, and subsequently an endonuclease, that cleaves the transcript. The poly(A)-tail is initially approximately 250 nucleotides long.

Both the 5' cap and the poly(A)-tail are key modifications which are required to produce a stable mRNA, and have been shown to promote efficient nuclear export. Before degradation, generally, either decapping at the 5' end or shortening of the poly(A)-tail has to occur. Thus, such enzymatic activities are tightly regulated.<sup>39,40</sup> The main actor in the subsequent degradation of mRNA is the exosome, which has a 3' → 5' RNase activity and is found in both the nucleus and the cytoplasm.<sup>41</sup> The exosome core contains RNase and structural subunits, but specificity and regulation are coupled to other associated proteins.<sup>41,42</sup> In addition to its basic function, the exosome is also partially responsible for degradation of RNA fragments coming from aberrant transcripts, miRNA pathways, splicing or even viral infections. Such molecules could cause problems if translated, or through interference with other processes.

Quality control of transcribed mRNAs is essential, and one particular pathway, the so-called nonsense mediated decay (NMD), is connected with both the exosome and the topic of the next section, splicing. Correct splicing of introns will result in deposition of an exon-junction complex (EJC) at the reaction site. This signal is identified by the NMD pathway, and if a premature and erroneous stop-codon exist upstream, the exosome will degrade the mRNA.<sup>43</sup>

In conclusion, starting at transcription, the mRNA obtains various modifications, which affects its stability and downstream processing steps (Figure 1.2.4).

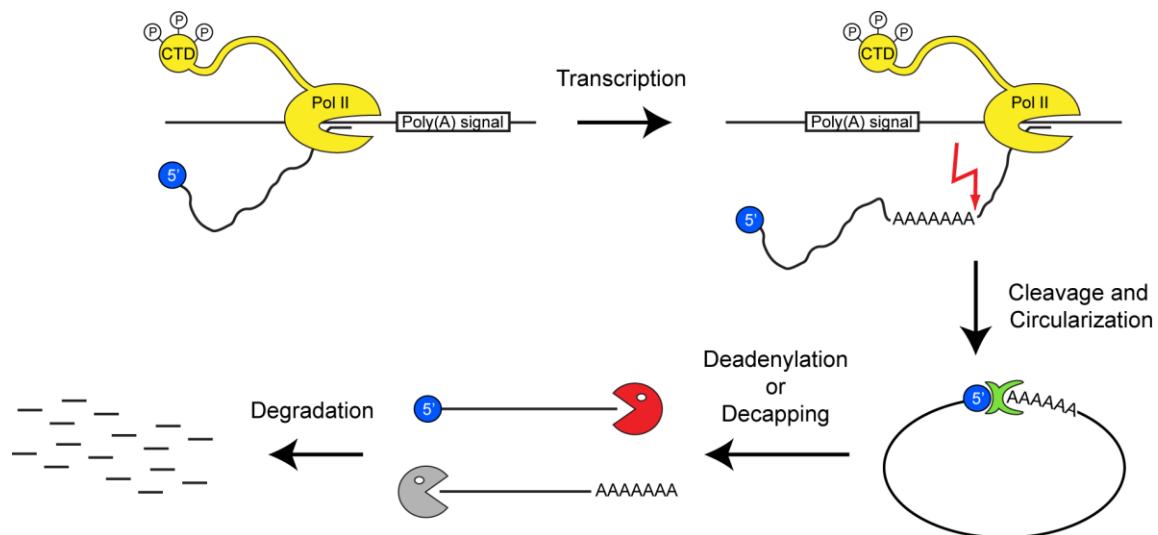


**Figure 1.2.4 mRNA stability depends on the 5' cap and on a intact Poly(A)-tail.** Upon a sequence signal in the gene a Poly(A)-tail is synthesized into the mRNA. Endonucleolytic cleavage releases the mRNA, which is thought to circularize via adaptor proteins (green). As soon as decapping or deadenylation occurs the mRNA is receptive to nucleases, such as the 3'→5' degrading exosome (red).

#### 1.2.4. Splicing of pre-mRNA: Maturation causing diversity

In lower eukaryotes, e.g. baker's yeast, the separation of genes into protein-coding *exons* and non-protein-coding *introns* is rare, however, in higher eukaryotes it is virtually standard. The process of removal of introns and of joining exons is known as splicing, and is carried out by a dynamic and highly regulated machinery, the spliceosome.<sup>44</sup> The spliceosome is of megadalton size, only including the ~50 core proteins and RNAs, and assembles for every round of splicing in an ordered and sequential fashion. Mass spectrometry data estimates a coupled of hundred proteins to be additionally associated with the spliceosome.<sup>44,45</sup> It can be expected that many of those proteins are involved in splicing regulation.

The three subunits of the RES complex are examples of such spliceosome-associated proteins.<sup>46</sup> See Chapter 5 for details on our work with this recently discovered complex. Additionally, Chapter 3 presents structural and ligand binding data on Tudor-SN, a splicing enhancer.<sup>47</sup> Tudor-SN contains a domain with the ability to interact with methylated arginines. Such modifications have been found in the spliceosome.

The five small nuclear ribonucleoprotein particles (snRNPs) are central spliceosomal multimeric complexes, and are named according to the small nuclear RNA (snRNA) contained in them (U1, U2, U4, U5 and U6).<sup>48</sup> In brief, spliceosome assembly and reaction cycle starts with the definition of 5' and 3' splice site by U1 snRNP and U2 associated factors, respectively (Figure 1.2.5). Second, the U2 snRNP binds at the so-called branch point. A catalytic complex is then formed by addition of the last three snRNPs. Together, they are known as the tri-snRNP. The catalytic splicing reaction cycle includes major structural rearrangements leading to two transesterification reactions, and results in the excision of a intron lariat.<sup>49</sup> What is an intron, or an exon, is defined by the mRNA sequence itself, together with the involved spliceosomal

complexes. The strength of the splice site varies with the nucleotide composition, but might also be affected by the rate of transcription elongation<sup>50</sup>.

A majority of the human genes exhibits alternative splicing, through which different combinations of exons are joined. This allows the production of diverse protein isoforms, from a minimal set of genes.<sup>51</sup> For instance, the Titin gene consists of 363 exons, which theoretically could give rise to over a million different protein isoforms.<sup>52</sup> Alternative splicing has important implications in processes ranging from development<sup>53</sup> to apoptosis<sup>54</sup>, and affects tissue specific gene expression<sup>55</sup>. Not surprisingly, alternative splicing is therefore closely connected to disease<sup>56</sup>.

It is believed that alternative splicing depends on additional factors, that are capable of competing with the constitutive splice factors and thereby affect splice site definition. For example, FOX2 inhibits the inclusion of exons by blocking branch point identification.<sup>57</sup> RBM5 influences splicing at a later stage by promoting binding of the tri-snRNP to two non-sequential exons.<sup>51</sup> Interestingly, some proteins involved in constitutive splicing are known to induce alternative splicing upon post-translational modifications, such as phosphorylation.<sup>58</sup> Furthermore, alternative splicing can also be introduced by the identification of additional weak splice sites.

As described previously, splicing is connected to mRNA degradation via the NMD pathway<sup>59</sup>, however, splicing is also coupled to transcription.<sup>33</sup> During transcription splicing factors are recruited to the nascent chain and can perform the first reactions before cleavage and poly(A)-tail synthesis.<sup>60</sup> In addition, splicing is linked to mRNA export from the nucleus to the cytoplasm where translation into protein occurs. In this regard - How far is it possible to study splicing regulation as an isolated event, outside the context of transcription and pre-mRNA processing?

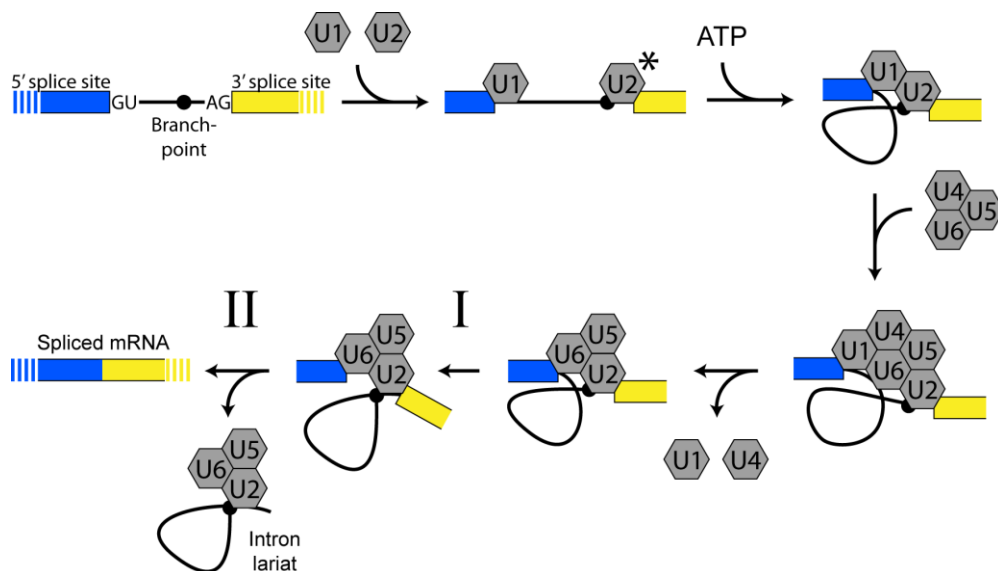


**Figure 1.2.5 Basics of pre-mRNA splicing.** The spliceosome assembles anew for every round of splicing. The snRNPs join in a specific order but each step is dynamically regulated. The asterisk highlights the possibility of alternative splicing regulation taking place at the 3' splice site. ATP is required to overcome conformational barriers. In the first catalytic step (I), the 2'-OH of the branch point adenosine attacks the 5' splice site. Subsequently, the two exons are joined (II) and the intron lariat is spliced out. The individual snRNPs are then recycled to be re-used for another round of splicing.

### 1.2.5. RNA editing: Fine tuning of gene expression

Editing of RNA includes deletion, insertion and, perhaps most well-known, modification of single nucleotides in the RNA. These reactions are carried out by different families of editing enzymes, located in the nucleus as well as in the cytoplasm. Editing influences not only the protein amino acid sequence, but also splice site selection, as well as structure and function of non-coding RNAs. Until recently, RNA editing was a rather exotic research field, but has lately gained momentum. It has become especially influential in neuron function and RNA interference (RNAi).<sup>61-63</sup>

Since RNA editing is a relatively rare event, it can be considered as fine tuning of gene expression. RNA editing leads to subtle, although essential, changes on the nucleotide. Here, adenosine-to-inosine (A-to-I) editing will be presented as an example of RNA editing. Also A-to-I editing has been suggested to be coupled to transcription.<sup>32</sup> See Chapter 3 for details on our work with Tudor-SN, a protein suggested to be involved in the metabolism of A-to-I edited RNA.<sup>64,65</sup>

A-to-I editing is carried out by enzymes named ADARs (adenosine deaminases that act on RNAs). The substrate is a dsRNA molecule (>20bp), in which the exocyclic purine amine group of an adenosine nucleotide is deaminated to a carbonyl. Importantly, inosines are decoded as guanosines by the ribosome. A direct link between editing and modulation of protein function by differential amino acid incorporation, has been shown for two neuronal receptors, GABA and voltage-activated potassium channels.<sup>66,67</sup> Additionally, alternative splicing of the glutamate receptor is regulated by RNA editing.<sup>68</sup>

Several reports have been published on the interference between A-to-I editing and RNAi pathways.<sup>69</sup> The main theme is how the dsRNA molecule can be directed into either RNA editing, or into RNAi.<sup>70</sup> Competition over the dsRNA has been shown to affect biogenesis of miRNAs and their silencing profile.<sup>71,72</sup>

Interestingly, hyper-editing of transcripts from Alu repeats have been discovered.<sup>73</sup> Alu repeats account for at least 10% of the human genome, and are expected to play a role in gene silencing and genomic diversity.<sup>74,75</sup> RNA editing has also been suggested to be linked to development of a certain prostate cancer.<sup>76</sup>

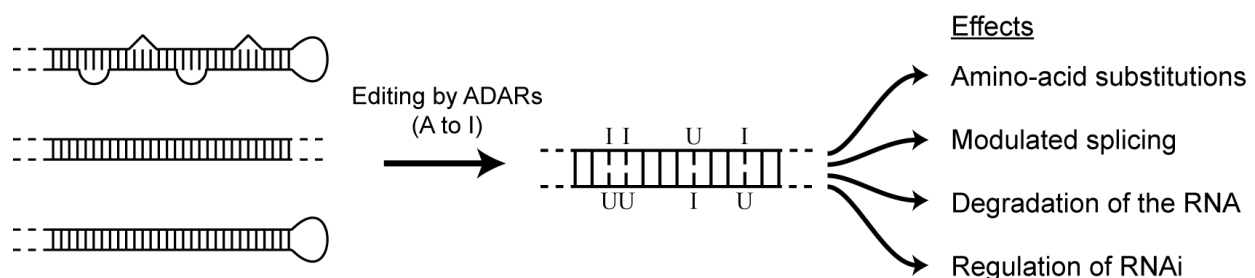


**Figure 1.2.6 RNA editing by ADARs.** Double stranded RNAs can be modified by editing enzymes, such as the ADARs (adenosine deaminases that act on RNAs), which deaminate adenosines to inosines. The editing have effects on many downstream pathways, for instance, on translation and splicing. The appearance of inosines alters the primary sequence and modulate the possible interactions of the RNA. Additionally, editing has been shown to regulate RNAi, and the degradation of RNAs.

### 1.2.6. mRNA export and localization

Because transcription and subsequent translation takes place in the nucleus and in the cytoplasm, respectively, the mature mRNA has to be transported across the nuclear envelope (Figure 1.2.7). Smaller molecules, i.e. metabolites, peptides etc, can diffuse through non-specific channels in the membrane, however, larger molecules depend on active transport through the nuclear pores. These pores are created by vast assemblies of approximately thirty core proteins (nucleoporins) and are called nuclear pore complexes (NPCs; ~125 nm Ø; ~125 MDa).<sup>77</sup> Here, we focus on the export of mature mRNA into the cytoplasm destined for translation, and leave out import/export of proteins. Notably, the by now very diverse group of functional RNAs (tRNA, rRNA, snRNA, miRNA etc.) utilizes quite different export pathways.<sup>78</sup>

In brief, to facilitate the bidirectional transport of very diverse macromolecules, the NPC utilizes various adaptor proteins. These are mobile export receptors (exportins) that identify a specific cargo and cycle between the nucleus and the cytoplasm. For the larger mRNA molecule the most important exportins are TAP and p15, which together form a stable heterodimer. The TAP-p15 complex interacts with the 5' UTR of the mRNA where it replaces the TREX complex, which was placed on the mRNA during elongation in a cap-dependent manner. In comparison to export of many other macromolecules, including other RNAs, mRNA export is generally not driven by the Ran-GTP/GDP gradient. One hypothesis, is that export relies on ATP-dependent rearrangements occurring at the 5' cap in the cytoplasm. Although, for some mRNA Crm1 is involved in nucleocytoplasmic export and is thus driven by GTP-hydrolysis.<sup>78</sup> Once the mRNA is transported through the pore, it is prepared for translation. The 5' cap is bound by eIF4E, a translation initiation factor, and at the 3' end, several proteins associate with the poly(A)-tail. It is not unusual, that the mRNA directly associates with the ribosome after passage through the NPC.

In addition to physically transporting the mRNA over the nuclear envelope, the NPC is closely coupled to quality control and to gene regulation. The mRNA is exported together with many proteins attached to it. This composite particle is called messenger ribonucleoprotein particle (mRNP). The SR (Ser/Arg-rich) proteins bind early to the mRNA and have a key role in many steps of the mRNA lifecycle.<sup>79</sup> This includes nucleocytoplasmic export where it functions as a adaptor protein to the TAP-p15 complex after hypophosphorylation. After export, the SR proteins dissociate from the mRNA and are recycled back into the nucleus.

The exon-junction complex (EJC) is another member of the mRNP which affects export efficiency. Export is known to be coupled to splicing, and is one major quality control pathway. The presence or lack of EJCs, creates a checkpoint for selection between spliced or unspliced mRNA, respectively. Other proteins at the NPC are involved in similar tasks, for example the Mlp1-Mlp2 system.<sup>80</sup> Pre-mRNA leakage into the cytoplasm is a quite common result due to decreased splicing capabilities, just because the nucleus is full of newly synthesized unspliced transcripts. See Chapter 5 for a structural characterization of the RES complex, which is important to efficient splicing, and in retention of unspliced pre-mRNA in the nucleus.

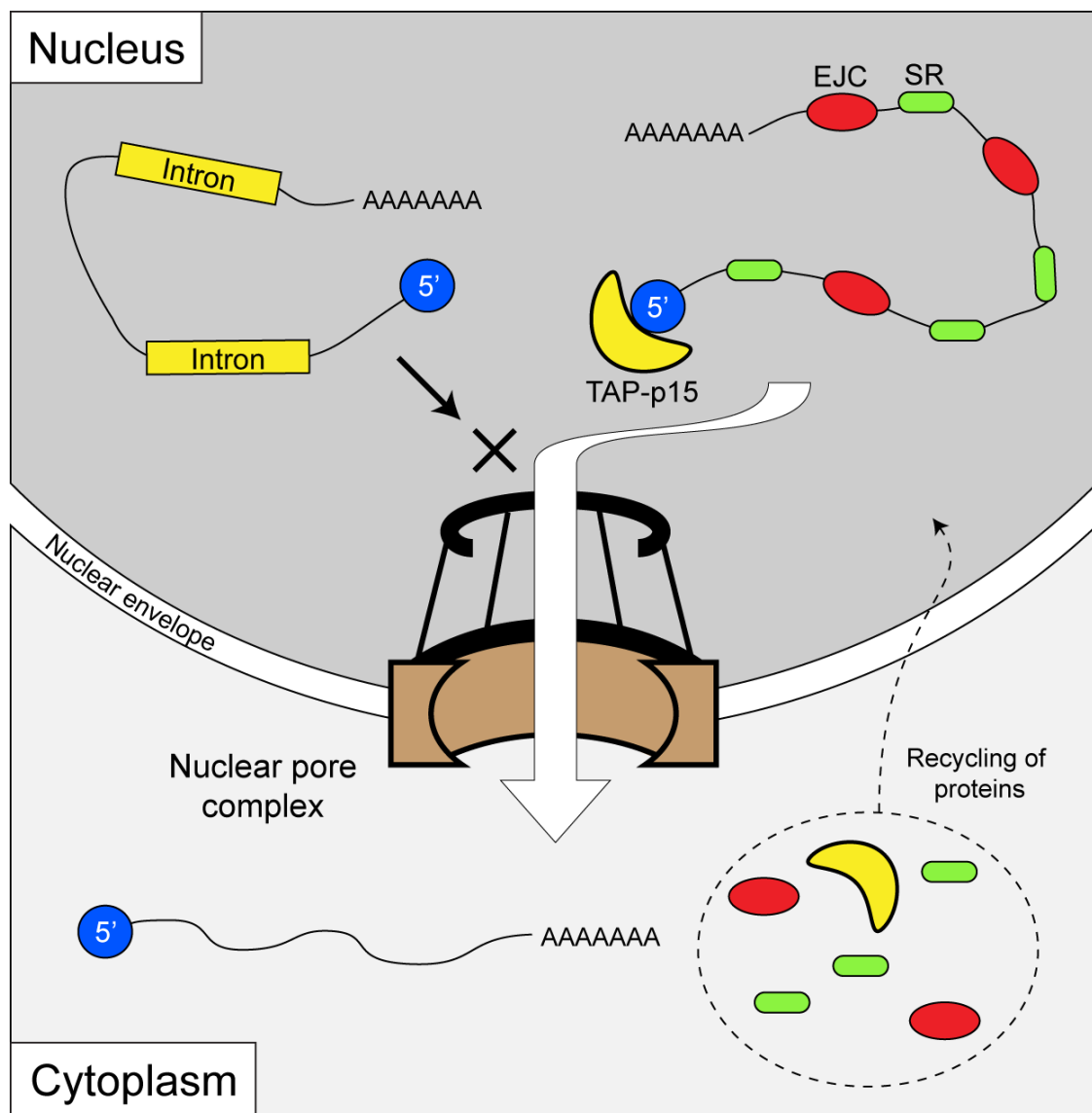


**Figure 1.2.7 The nuclear pore complex (NPC) controls mRNA export from the nucleus.** As a gatekeeper the NPC decides which biomolecules to import from the nucleus, and which to export to the cytoplasm. Non-processed pre-mRNAs contain introns and are not ready to be exported. However, the exon-junction complex (EJC; red) is deposited onto the mRNA after splicing and acts as an export signal. The EJC creates, together with SR proteins (green) and 5' cap-associated TAP-p15 (yellow), affinity for the NPC and enhance export efficiency. These proteins are recycled to be used for new rounds of export. The exported mRNA is now ready to be translated by ribosomes available in the cytoplasm.

Human immunodeficiency virus (HIV) is a retrovirus, and therefore requires unspliced RNA for the assembly of new virus particles. To circumvent the suppressed export of unspliced RNAs in the host cell, the virus encodes a protein that specifically binds to unspliced viral RNA. This protein, named Rev, includes an export signal and hijacks the endogenous protein export system, which allows the unspliced RNA to escape through the NPC without being detected as aberrant.<sup>81</sup>

Interestingly, there is some evidence that transcription, in yeast, sometimes is directly taking place at the NPC.<sup>82</sup> This model of gene-looping is the source of interesting ideas about transcription termination and gene surveillance, and explains observations on transcriptional memory.<sup>33,83</sup>

In addition to the reallocation of mature mRNA from the nucleus to the cytoplasm, subcellular localization of mRNA within the cytoplasm can further affect protein expression. Instead of being translated straight away, mRNA can be targeted to special cytoplasmic RNA granules, which are actually visible by light microscopy.<sup>84</sup> Those granules have been shown to be used for storage, transport and decay of mRNA, and are associated with particular cellular events. Some classical examples of cytoplasmic targeted mRNAs are found in cells with rather asymmetric shapes, for instance oocytes and budding yeast cells, where mRNA accumulation generates cell polarity. In case of the *Drosophila* oocyte, *oscar*, *bicoid* and *nanos* regulates the establishment of spatial patterning of the embryo.<sup>85</sup> A special case of translationally repressed mRNPs is found in neurons. Here, mRNAs are transported far distances through the axons, before being released and translated in the synaptic region.<sup>84</sup> Recent studies, however, suggest that the subcellular localization of mRNA is far more widespread than previously thought, and not only linked to specific cell types or proteins.<sup>86</sup>

Stress granules and Processing bodies (P-bodies) are two examples of more general RNA granules. The assembly of either granule can be induced by stress on the cell. Furthermore, both of the granules share overlapping groups of proteins, however, while the stress granules contain members of the translation initiation machinery, the P-bodies contain proteins involved in RNA decay. Interestingly, the assembly is reversible and the granules can, upon changes in the environment be disentangled. This property is expected to make RNA granules key post-transcriptional and epigenetic modulators of gene expression.<sup>87</sup>



### 1.2.7. Gene silencing by RNA interference

RNA molecules have been discovered to play a more central role in gene regulation than ever anticipated a couple of decades ago. One major breakthrough, was the observation that short transcripts are actively used in sequence specific degradation of other RNA molecules, which results in silencing of that particular protein.<sup>88</sup> This silencing process is known as the RNA interference (RNAi) pathway, and involves molecules known as microRNAs (miRNAs) and small interfering RNAs (siRNAs). miRNAs are mostly endogenously encoded and consist of a single strand folded into a non-perfect double stranded RNA hairpin. In contrast, the siRNA usually comprises two separate strands with perfect complementarity which normally, but not always, originate from an exogenous source, for example a virus genome or transposons.<sup>89</sup>

These two types of RNA molecules, both ~20-30 nucleotides long in their final form, are nevertheless closely related, especially in that they share many associated processing and effector proteins (Figure 1.2.8). Briefly, non-processed duplex precursors are cut by a ribonuclease enzyme called Dicer, creating a two nucleotide overhangs at the 3' ends. miRNAs are initially also processed by Drosha. In the cytoplasm, one of the strands from the processed duplex is loaded onto the so-called Argonaute protein. Which strand is selected, depends on the thermodynamic stability of the duplex.<sup>90</sup> The RNA-loaded Argonaute protein is then assembled with other effector proteins into a RNA-induced silencing complex (RISC). The mature RISC is now ready to perform its effector functions.<sup>91</sup>

The short RNA molecule from RISC acts as a sequence specific targeting factor, that binds to the corresponding mRNA. In general, RISC cleaves the identified mRNA if there is complete base-pairing (mainly siRNAs), whereas if the base-pairing is not perfect (normally miRNAs), gene expression is decreased by inhibition of translation. The latter case involves mRNA binding and localization to so-called P-bodies<sup>92</sup>, in which translation is impeded. RISC can also repress translation initiation.<sup>89</sup> The function of RISC differs between organisms, and depends on the proteins and RNA involved. For instance, humans have eight Argonaute paralogs which allows for specialization. RNAi affects many biological processes, ranging from development to tumor growth.<sup>93,94</sup>

The RNAi research field changes rapidly and many important discoveries probably lie ahead. The functional boundaries between miRNAs and siRNAs are constantly being blurred. To summarize however, siRNA mostly silences the expression of its own gene product, whereas miRNA normally targets another gene or group of genes. In part, this can be explained by the absence of mature miRNA-containing RISC in the nucleus.

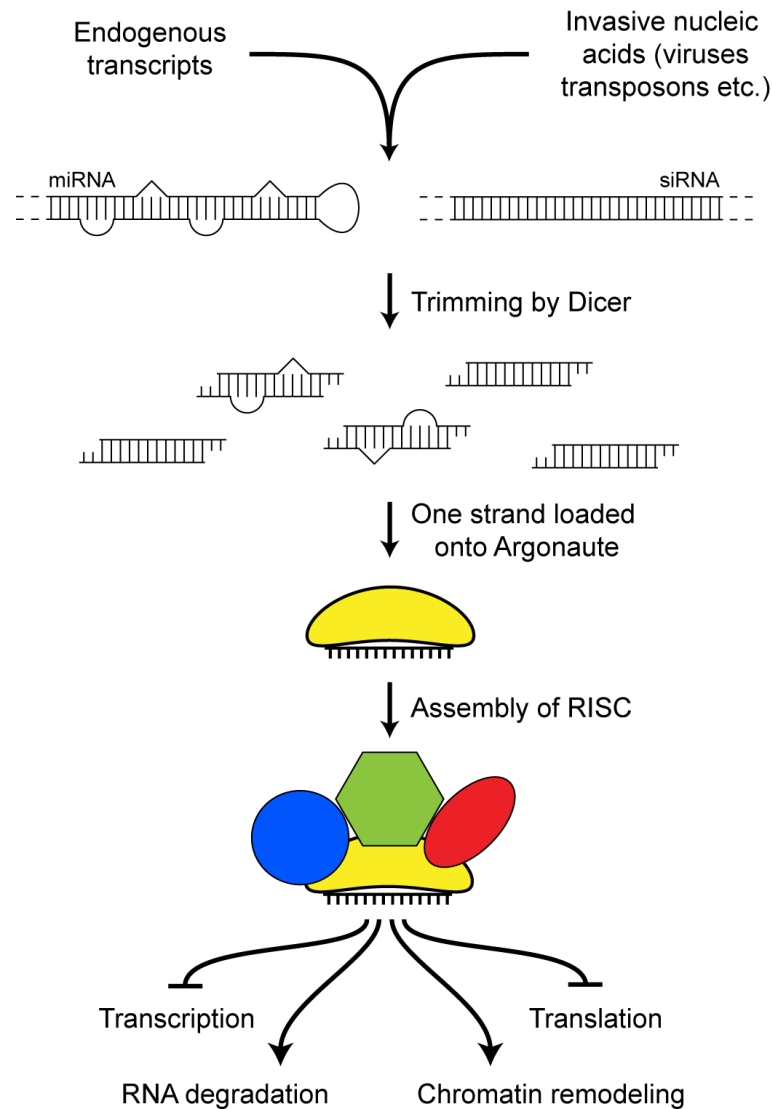


**Figure 1.2.8 RNA interference (RNAi) in eukaryotic cells.** Short double stranded RNA molecules (siRNAs or miRNAs) are after initial trimming loaded on to Argonaute proteins. The Argonaute is primed with additional proteins and act site-specifically in a variety of different regulatory pathways. (Adapted from Carthew et al.<sup>89</sup>)

It is rather appropriate to conclude this introduction of gene regulation with the focus on RNA, around which it is all centered. In addition to mRNA degradation, several other regulatory roles of functional RNA molecules have been described. This somewhat extends the simplified picture presented and points out the full complexity of cellular life that we are about to unravel. For instance, non-coding RNA has been shown to participate directly in epigenetic transcriptional repression.<sup>95-97</sup> Interestingly, small RNAs have also been demonstrated to inhibit RNA polymerase II during elongation.<sup>98</sup> Finally, the cellular defense against transposon spread, is suggested to be closely linked to genome evolution.<sup>99</sup> One discovery that suggest there is more to learn from the research on RNA-mediated gene regulation, is that bidirectional promoters give rise to many uncharacterized non-coding RNAs.<sup>100</sup> All in all, gene regulation increases the plasticity of the organism, so that it is able to respond and adapt to various stimuli, and ensures the maintenance of cellular identity.



# Chapter 2

---

## Methods in structural biology

### 2.1. Two siblings: Molecular and structural biology

Structural biology is interested in explaining biological processes by characterizing the three-dimensional structure of the involved biomolecules, typically on an atomic level, and in connecting that knowledge to functional data. Its big brother, molecular biology, became a flourishing research field towards the middle of the last century when specific biological functions was starting to be attributed to certain biomolecules. Molecular biology can be described as the coming together of biology and chemistry, and is more of an approach or perception than a specific technique.<sup>101</sup>

Without the development of modern molecular biology the field of structural biology would be an obscure small research interest of a few. One has to remember, that early on all proteins were purified from their natural source, which limited biological experiments and especially structural studies. This limitation was overcome by the possibility to produce any protein, or protein fragment, in high amounts using recombinant techniques and bacterial expression strains. Recombinant DNA cloning is one main reason structural biology had the chance to become one of the major players in life science, as it is today.

Several reasons can be given to why a molecular understanding of biology is important:

- It is the basic organization of biology. Biological pathways relies on single molecules to perform their function. How all the various processes functions together, is rather studied in the field of systems biology.
- Seeing is understanding. Only when the fine details of a process are laid out, it is possible to grasp its full mechanism and how it actually works.
- New hypotheses. Understanding a process at its fundamental level opens up for novel scientific questions, that otherwise would have been overlooked.
- Drug discovery. In modern pharmaceutical research it is essential to have a molecular perspective. This enables efficient development of synthetic compounds modulating a specific biological pathway.

Maybe the most well-known example of structural biology, which not only changed biology, is the elucidation of the DNA helix in the 1950s.<sup>102</sup> For the first time it was now possible to see the molecule which carried the inherited traits of our parents.

### 2.1.1. Cloning of a target protein

Once a target molecule has been selected, samples need to be prepared for the experiments planned. In structural biology, the sample in the majority of cases is a pure and highly concentrated solution of protein. Generally, recombinant protein is produced in *Escherichia coli* (*E. coli*), into which foreign DNA has been transfected using a bacterial plasmid as a vector (Figure 2.1.1). Such plasmids normally contain the T7 promoter and can nowadays be prepared by using standardized protocols.<sup>103</sup> The first step of classic ligation-based cloning is the design of primers for the polymerase chain reaction (PCR). The primers facilitate the amplification of a specific gene fragment. The next step is to cleave the PCR product at the ends with restriction enzymes. These enzymes are highly specific and usually leave an overhang at each DNA end, also known as "sticky ends". The vector is then digested using the same enzymes, so that the PCR fragment can be inserted into it by the help of a DNA ligase. The sticky ends helps directing the fragment and enhances the efficiency of the insertion. Finally, the plasmid containing the gene of interest, and additional functional sequences for selection and expression, can be transferred into the host bacterial cell.

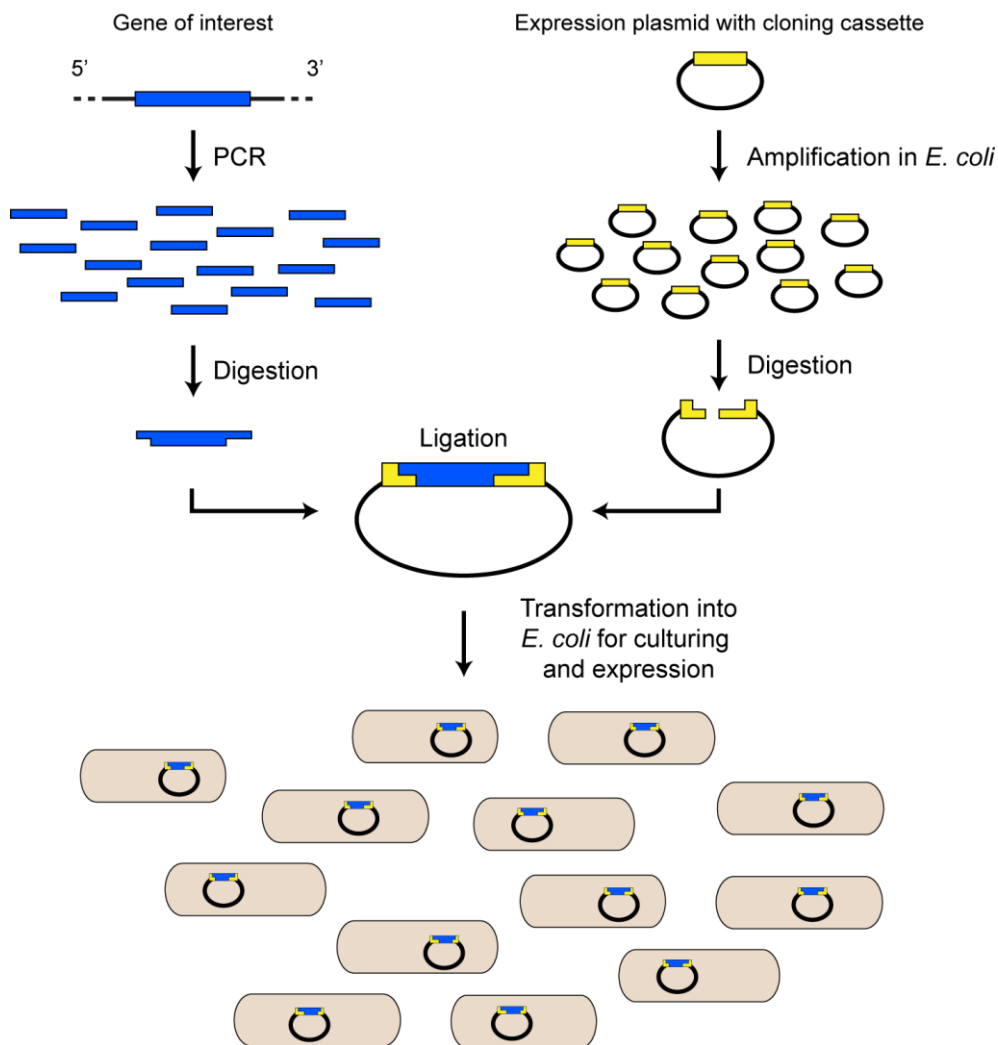


**Figure 2.1.1** Basic workflow of molecular cloning for protein expression.

Many important considerations have to be taken into account at this early stage of sample preparations.<sup>104</sup> The construct design will often determine how successful the project will be, and/or which quality the data will have.<sup>105</sup> First, it is usually important to clone a fragment of the full-length protein that is likely to give rise to a stable and mono-disperse protein solution. This can be facilitated by bioinformatics tools available online.<sup>106</sup> These can tell you about conservation, compared to other homologous proteins, as well as where you can expect secondary structures or unfolded regions. Second, if the target is exhibiting low purification yields, the incorporation of solubility or expression tags should be considered. Usually a His-tag or a GST-tag is available in the plasmid, to simplify protein purification. Importantly, the tags are typically cleavable upon the addition of a sequence specific protease, such as the Tobacco etch virus (TEV) protease. Third, if human genes are to be expressed in *E. coli*, problems with codon usage can arise due to differences in tRNA levels.<sup>107</sup> This can be avoided by changing specific rare codons through site-specific mutations, or by transfecting the plasmid into special *E. coli* expression strains, carrying an extra plasmid for production of rare tRNAs.

Additionally, it is now possible to buy codon-optimized constructs from companies specialized in gene synthesis. Finally, it is important to realize the importance of trial and error in cloning. It is usually suggested to make several constructs of the same protein, and check the expression quality of them all. Subtle differences in at N- or C-terminus can affect the sample quality drastically, as can residue specific mutations, or shortening of internal loops.<sup>108</sup> Varying the incorporated solubility-tag, so-called parallel cloning, is also to be considered. Constructs of difficult targets must be extensively optimized and is often pursued in a high-throughput setting.<sup>109,110</sup>

In addition to ligation-dependent cloning, alternatives exist that might simplify laboratory work drastically. *Homologous recombination* (e.g. Gateway® from Invitrogen), *Ligase Independent Cloning* (LIC)<sup>111</sup> and *Sequence and Ligase Independent Cloning* (SLIC)<sup>112</sup>, are all established options with their respective pros and cons.

For protocols and vector maps: <http://www.helmholtz-muenchen.de/en/pepf/>

For practical details regarding expression and purification of cloned proteins, see the *Materials and methods* section of the published papers, or in Chapter 5.

## 2.2. NMR: Solving structures in solution

Nuclear magnetic resonance (NMR) is a basic physical phenomenon of certain atomic nuclei. Such spin- $\frac{1}{2}$  nuclei orient in an applied magnetic field, either in an parallel or in anti-parallel way, and will therefore populate two different energy states. The system can be perturbed using radiofrequencies, meaning that the difference between the energy states can be measured, hence the name NMR spectroscopy. The difference in energy corresponds to a resonance frequency. The NMR spectroscopist tries to measure as many of these frequencies as possible, and then assigns from which atom they arise. A closer analysis of the acquired NMR data can later give specific information on the structure and dynamics of the molecule studied.

In the coming sections, the physical background of NMR and its applications in structural biology will be introduced. However, this is a formidable task and the reader is encouraged to follow references and to check the suggested literature (page 39) for additional information. It should be pointed out that this text is largely dealing with solution NMR, i.e. the sample molecule is dissolved in a liquid. Solid state NMR, using crystalline or amorphous samples, has increased in popularity due to technological and methodological improvements.<sup>113</sup> It should also be kept in mind, that the medically important field of magnetic resonance imaging (MRI) is based on the same physical phenomenon as NMR.

The history of NMR really starts in the middle of the 1940s when American physicists first recorded an NMR signal with the purpose of measuring the magnetic dipole moments of different elements.<sup>114</sup> What Purcell, Bloch and colleagues overlooked was that those values are affected by the electrochemical environment of the nuclei. In fact, the discrepancies gave rise to the understanding of the chemical shift, which led to a lot of interest among chemists. In chemical molecules the hydrogen nuclei, which frequencies normally are recorded, will sense those differences and give rise to specific and separate signals. One important breakthrough then came in the early 50s when the nuclear Overhauser effect (NOE) was described.<sup>115</sup> The NOE would later be used for structure elucidation of molecules. The progress of NMR is closely linked to advancement of technology, in particular the construction of very strong and stable magnets, increasing resolution and signal intensity. A crucial development was also the use of Fourier transform NMR (FT NMR)<sup>116</sup> (page 28), and its use in combination with multi-dimensional techniques<sup>117</sup> (page 31). This paved the road for detection of heteronuclei (e.g.  $^{15}\text{N}$  and  $^{13}\text{C}$ ) which are inherently insensitive. Today, with state of the art equipment, NMR is an integral part of biological and pharmaceutical research, with continuous improvements regarding limitations of molecular size<sup>118,119</sup> and of sample amounts<sup>120,121</sup>.

Throughout the years several Nobel prizes have been awarded for discoveries connected to the development of NMR and to its applications. To mention two; Richard Ernst (1991) for the development of two-dimensional FT NMR. Kurt Wüthrich (2002) for the determination of the first protein structure by NMR.

### 2.2.1. Basic physical and mathematical description of NMR

One intrinsic property of atomic nuclei is that they frequently, depending on the composition of protons and neutrons, possess a magnetic angular momentum,

$$\mu_z = \gamma \times \hbar \times m ,$$

where  $\gamma$  is a nucleus dependent value called the gyromagnetic ratio,  $\hbar$  the Planck constant divided by  $2\pi$ , and  $m$  the magnetic quantum number. This feature causes the nuclei to behave like a small magnet and is sometimes referred to as nuclear spin, since a rotating charged body is known to create a magnetic field. However, there is no evidence that the proton is actually spinning.  $^1\text{H}$ ,  $^{13}\text{C}$  and  $^{15}\text{N}$  are the most common NMR active nuclei studied, but also other isotopes, for example,  $^{19}\text{F}$  or and  $^{31}\text{P}$  can be utilized. When for an example a hydrogen nuclei, which only includes one proton, is put in an external magnetic there is only two possible values of the  $\mu_z$ , because  $m$  is quantized and only can be  $+\frac{1}{2}$  or  $-\frac{1}{2}$ .

If  $B_0$  is the applied magnetic field then the energy of each state and the difference between them is,

$$E = -\mu_z \times B_0 = -\gamma\hbar m \times B_0 \Rightarrow \Delta E = \gamma\hbar \times B_0 .$$

As we can see that the energy difference is increasing with higher magnetic fields (Figure 2.2.1). In a sample, including billions of spins, the population of these energy states will follow the Boltzmann distribution,

$$N_{-\frac{1}{2}}/N_{+\frac{1}{2}} = e^{-\Delta E/kT}$$

, where  $N$  is the number of protons in each respective state,  $k$  the Boltzmann constant and  $T$  the temperature. Together the spins will create a net bulk magnetization along  $B_0$ , which allow manipulation of the system during an NMR experiment. Unfortunately, the bulk magnetization is small and cause the inherently low sensitivity of NMR.

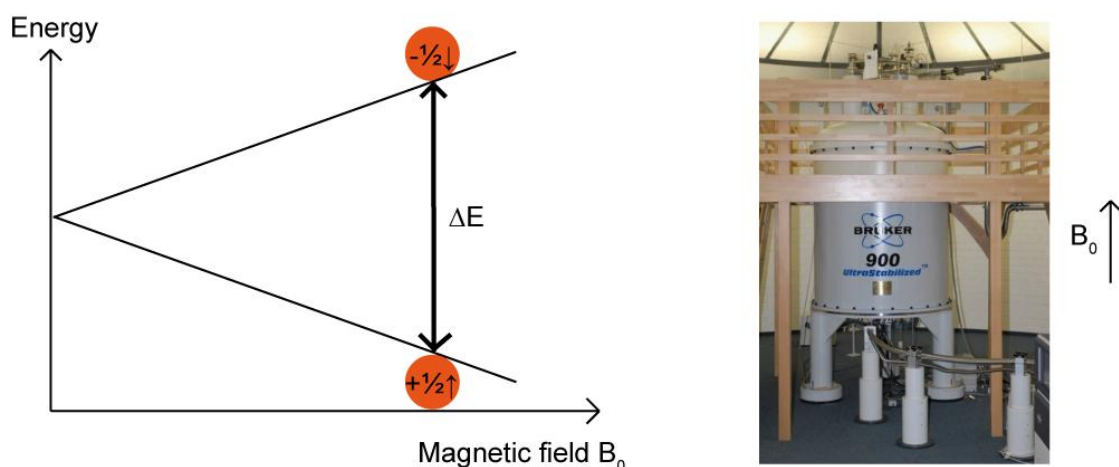


**Figure 2.2.1** In a magnetic field the proton can only populate two energy states, between which the difference increases with the strength of the  $B_0$  field. The population distribution follows the Boltzmann equation and will create a favorable bulk magnetization in the sample along  $B_0$ . This bulk magnetization is manipulated during NMR experiments.



Now the question comes how we manipulate the spin system, and what the readout actually is. The resonance condition of the system is fulfilled using electromagnetic radiation of the correct frequency:  $\Delta E = h \times \nu$ , where  $\nu$  is the frequency in Hertz. In the case of NMR this is typically in the range 100-1000 MHz, corresponding to the normal FM radio frequency band.

Put into a Cartesian coordinate system, the bulk magnetization can be represented by a vector, **M**. Initially, **M** is pointing along the z-axis and  $B_0$  (Figure 2.2.2 A). If a radio pulse,  $B_1$ , is applied along y-axis the magnetization will turn towards the x-axis. The angle  $\alpha$  will increase depending on how long the radio pulse is (Figure 2.2.2 B). The direction of the vector rotation is determined by the right-hand rule known from basic physics of electromagnetism. The vector and the system is now out of equilibrium but will try to return to the low energy state. As a gyroscope (a rotating mass), in a gravity field, the magnetization vector will not go straight back to the original position, but will precess around the magnetic field (Figure 2.2.2 C). This precession frequency, also known as the Larmor frequency,  $\omega$ , is the actual readout of each NMR experiment, since it induces an electric current in the receiver coils. The NMR signal is, however, affected by relaxation, and the **M** returns to the ground state (Figure 2.2.2 D).

Importantly, this basic vector model can only explain simple NMR experiments on isolated spins. Furthermore, most pulse programs normally only include pulses where  $\alpha = 90^\circ$  or  $180^\circ$  degree, which make the analysis and setup less complicated.

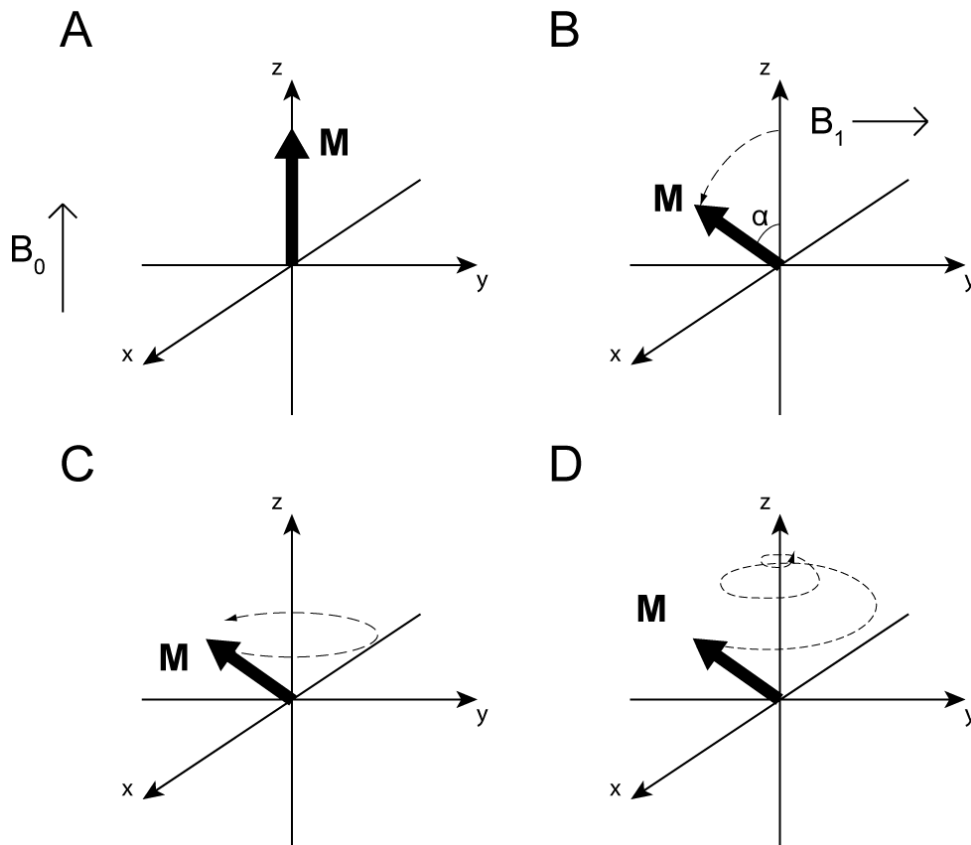


**Figure 2.2.2** Basic explanation of the NMR phenomenon using the vector model. See text for details.

## 2.2.2. NMR hardware and experiment setup

Figure 2.2.3 outlines the hardware setup and how a spectrum is acquired. Most modern NMR experiments utilize rather complex sequences of radio pulses and delays, which together manipulate the spins in a desired way. The commands are sent to a radio frequency (RF) synthesizer which executes the pulseprogram. The electric pulses are converted to radio pulses in the probe coils and transferred to the sample. Directly after execution of the pulse program, the same probe coils are used to detect whatever NMR signal is returned back. An amplifier is needed due to the very low signal intensity. The oscillating output signal, called free induction decay (FID), is then digitized so that it can be recorded and processed by a normal desktop computer. The oscillating output signal, called free induction decay (FID), is then digitized so that it can be recorded and processed by a normal desktop computer.

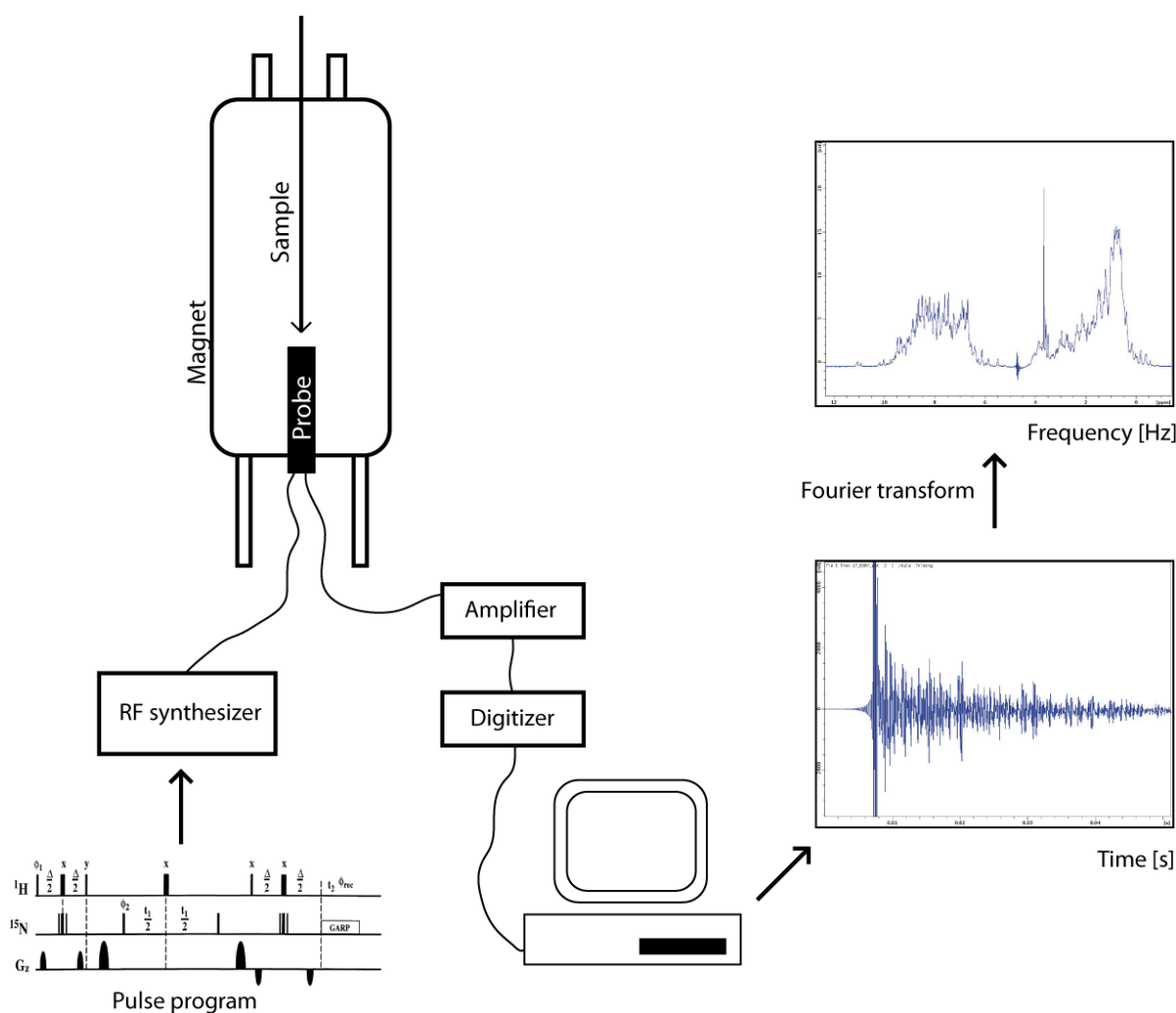


**Figure 2.2.3** Outline of NMR hardware setup and acquisition. See text for further details.

There are many important practical considerations to be aware of when acquiring NMR spectra, because of the low signal-to-noise ratio. Depending on the type of experiment, the sample has to be concentrated enough, and stable over the acquisition time. Additionally, the NMR instrumentation has to be carefully set up. First, the hardware should be checked and adjusted. Matching and tuning of the resonance circuit in the probe head, will optimize the transfer of the radio pulse from the coil to the sample,

and is affected by salt concentration etc. A proper shimming process will create a homogenous magnetic field over the whole sample. Remember, that the  $B_0$  directly affects the resonance frequency, and if it is not constant this will result in broad lines in the final spectrum. Shimming is accomplished by adjusting the current in a set of additional electromagnets in the probe. Secondly, the pulses (length, power and sometimes the phase) included in the pulseprogram have to be calibrated, so that manipulation of the spins are optimal. Finally, the user should control that the water suppression is good enough. If not, the protein signals of typical NMR samples,  $\sim 100 \mu\text{M}$ , would be obscured by a huge water signal,  $\sim 110 \text{ M}$  (proton concentration). Instead of always buffer exchanging the protein into a  $\text{D}_2\text{O}$ -based buffer, which would also eliminate any exchangeable protons, several techniques have been developed. In addition to pre-saturation, where the water signal is specifically saturated before each experiment, the most common procedures include water-flip-back, or the WATERGATE sequence.<sup>122</sup> With optimized water-suppression hardly any signal from the water are visible in the NMR spectrum. Inappropriate shimming usually leads to diminished water suppression.

### 2.2.3. Fourier transform and NMR

Old NMR instruments used to sweep the frequency (continuous wave, CW NMR), and when a resonance condition was fulfilled this would result in a spike in the spectrum. With this technique there would be a direct correlation between the frequency recorded and the signal, but it was indeed very time-consuming. In the 1970s it was realized that one could excite all frequencies at the same time, record the response and then deconvolute the output signal, which now retained all signals in an overlapped fashion.<sup>117</sup> The problem was of course how to reconstruct the frequency spectrum from a time-domain signal (Figure 2.2.3). The answer came from an old known mathematical trick, the Fourier transform (FT), and because FT was used for the deconvolution process this was called FT NMR. FT appreciate the possibility to express any periodic, and continuous function, as a sum of sine and cosine functions. The oscillating FID fulfills these criteria and can be evaluated, allowing extraction of the unknown frequencies contained in the signal.

Formally, the frequency spectrum,  $f(\nu)$ , is found by integrating the time domain function,  $f(t)$ ,

$$f(\nu) = \int_0^{+\infty} f(t) \times e^{-2\pi i \nu t} dt .$$

FT NMR opened up for the development of modern NMR, because the output of rapid consecutive scans could be added together. Importantly, while the NMR signal of  $N$  scans directly adds up, the noise only adds up with  $\sqrt{N}$ . Hence, four times as many scans are needed, to double the signal-to-noise ratio. The FT technique increased the relative sensitivity and made it possible to record more insensitive nuclei, such as  $^{13}\text{C}$  and  $^{15}\text{N}$ , by coherence transfer. Additionally, FT NMR was essential to the

implementation of complex pulseprograms, comprising multiple pulses on different nuclei. For instance, multi-dimensional experiments and studies of relaxation would otherwise have been difficult to realize.

Practically, experiments on Bruker NMR instruments are setup using their Topspin® software, however, the final processing of the FID is often done in NMRPipe<sup>123</sup>. Here, the user has the opportunity to include several additional processing steps prior and after the FT step. Amongst those, choosing the appropriate window function, that make sure the FID reaches zero at last time point, and applying zero-filling, which enhances the digital resolution of the spectrum, as well as adding a phase correction in the dimensions at hand, are the most important. In addition, linear prediction of further data points can be implemented, which might increase the resolution of the spectrum, but sometimes introduces artifacts.

#### 2.2.4. The chemical shift and J-coupling

As previously touched on, depending on the electrochemical environment of the NMR active nucleus, it will acquire slightly different resonance frequencies. This feature is known as the chemical shift. The resonance frequency of NMR signals are rarely given in Hertz, but rather by their chemical shift (in parts per million, ppm). The latter unit is also independent of the field strength,

$$\delta(ppm) = 10^6 \times \frac{\nu - \nu_{ref}}{\nu_{ref}}$$

, where  $\nu$  is the frequency of the signal and  $\nu_{ref}$  is the frequency of the reference compound decided upon.

Another basic aspect of NMR, is that nuclei connected by electron pairs, i.e. chemical bonds, are known to communicate with each other. For example, if one hydrogen nuclei has been excited, the behavior of this magnetization can be influenced by a neighboring *coupled* <sup>13</sup>C nuclei. This coupling, named scalar or J-coupling, can be measured (usually in Hz), and is stronger with increasing values. J-couplings reaching over up to three chemical bonds are often utilized in NMR experiments. The J-coupling make it possible to transfer magnetization between coupled nuclei. This means, not only the NMR frequency of the initial nucleus can be measure, but also additional resonances in the vicinity.

The product operator nomenclature has been very successfully introduced in NMR. It is used to analyze the NMR properties mentioned above, especially in the context of more complex pulseprograms.<sup>124</sup> Product operators are based on quantum mechanics of the populated energy states and can handle multiple coupled nuclei. The product operators do not include the treatment of relaxation, or strongly coupled nuclei. In brief, the initial bulk magnetization is described by a basic operator,  $I_z$ , and depending on the pulseprogram this initial state is transformed during the experiment. The final state, i.e. the outcome of the experiment, can be calculated by the sequential application of easy

rules, and by simple computations. To start with, the effect of 90° and 180° pulses is introduced:

$$\begin{array}{ccc}
 I_z \xrightarrow{90^\circ I_x} -I_y & I_z \xrightarrow{90^\circ I_y} I_x & I_z \xrightarrow{90^\circ I_z} I_z \\
 I_z \xrightarrow{180^\circ I_x} -I_z & I_z \xrightarrow{180^\circ I_y} -I_z & I_z \xrightarrow{180^\circ I_z} I_z
 \end{array}$$

Please notice that a pulse along the axis of the initial operator leaves it untouched, and that a 180° pulse along the x- or y-axis inverts the  $I_z$  operator. The chemical shift is treated in more complicated since it evolves with the offset  $\Omega$  during the time  $t$  of free precession:

$$\begin{array}{l}
 I_x \xrightarrow{\Omega t} I_x \cos \Omega t + I_y \sin \Omega t \\
 I_y \xrightarrow{\Omega t} I_y \cos \Omega t - I_x \sin \Omega t \\
 I_z \xrightarrow{\Omega t} I_z
 \end{array}$$

Free precession always takes place around the applied magnetic field, which by definition is along  $I_z$ . The offset ( $\Omega$ ) is the difference between a signal and a reference value, i.e.  $\nu - \nu_{\text{ref}}$ .

So far, only single isolated spins have been treated, but to explain the J-coupling a coupled heteronuclear nuclei, S, is introduced. The S spin is typically  $^{15}\text{N}$  or  $^{13}\text{C}$  in real experiments. Due to the large difference in resonance frequency, pulses on either the I or the S spins, will leave the state of other spin unchanged. The product operator rules for the evolution of this J-coupling,  $J_{IS}$ , are again more complicated than the evolution of chemical shift. This is because the state of the I spin, is mixed with the state of the S spin. The results is a product of two operators, which is underlining the importance and convenience of product operators. Figure 2.2.4A illustrates how  $I_x$  and  $I_y$  evolves under  $J_{IS}$ , over time  $t$ . Neither the  $I_z$ , or the  $S_z$  operator evolves under J-coupling. Two-spin IS product operators evolve in a similar way as one-spin operators under free precession (Figure 2.2.4 B), only the x- or y-component change. In the next section, these product operator rules will be used to analyze the HSQC pulse sequence.

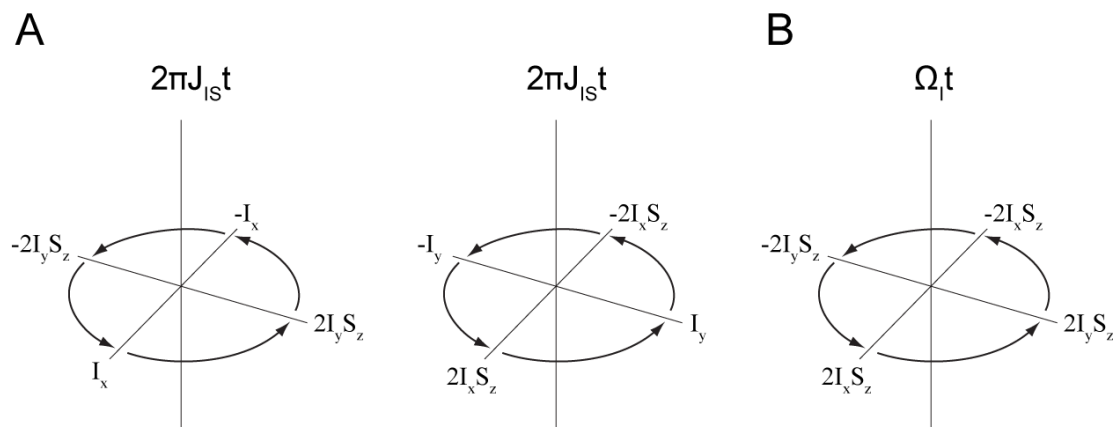


**Figure 2.2.4** (A) Illustrates how  $I_x$  and  $I_y$  evolves under J-coupling over time  $t$ , when coupled with another spin S. (B) Depicts how the two-spin operators in (A) evolve under free precession.

## 2.2.5. The protein fingerprint spectrum, 2D $^1\text{H}$ , $^{15}\text{N}$ HSQC

Signal overlap in the NMR spectrum will occur with increasing molecular size, and will soon be so severe that separation is impossible. The solution to this problem is to apply selection criteria. In the two-dimensional  $^1\text{H}$ ,  $^{15}\text{N}$  heteronuclear single-quantum correlation (HSQC) spectrum only the frequencies of amide nitrogens, and their paired hydrogen, will be recorded (Figure 2.2.5). Another selection criteria could be to record proton resonances correlated to  $^{13}\text{C}$  atoms. For a 10 kDa protein this results in a reduction from ~700 hydrogen signals in a normal 1D spectrum, to ~100 signals in a 2D  $^1\text{H}$ ,  $^{15}\text{N}$  HSQC. Recording the nitrogen frequency also enables the separation of the 100 signals in two dimensions instead of one. This is accomplished by the stepwise increase of the  $t_1$  delay, and the subsequent FT processing of both time domains. The HSQC is sometimes considered to give a "fingerprint spectrum" of a protein, since each signal correspond to one residue and together produce a unique spectrum.

To be able to acquire heteronuclear spectra, the protein needs to be isotopically enriched with the required NMR active nuclei. In general, this is accomplished by growing protein producing bacteria on minimal media, supplied with  $^{15}\text{N}$   $\text{NH}_4\text{Cl}$  and/or  $^{13}\text{C}$ -glucose as the sole nitrogen and carbon source, respectively.

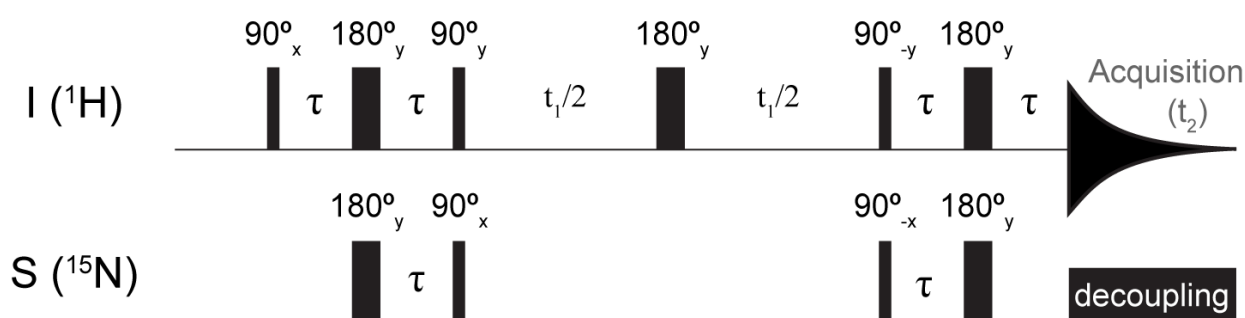


**Figure 2.2.5** The basic version of the HSQC pulse sequence. See Appendix A.1 for details.

In summary, the outcome of the HSQC pulseprogram just prior to acquisition,

$$I_y \cos \Omega_S t_1$$

, indicate that  $I_y$ , which was created by the initial  $90^\circ$  pulse, has acquired the chemical shift (or frequency) of the S spin ( $\Omega_S$ ) during  $t_1$ . During acquisition ( $t_2$ )  $I_y$  will then evolve the chemical shift of the I spin. For the full product operator analysis of the HSQC pulse sequence see Appendix A.1.

If additional signal dispersion is needed, the dimensionality of a NMR spectrum can be increased to three or more, of course at the cost of lower sensitivity which leads to long acquisition times (Figure 2.2.6).

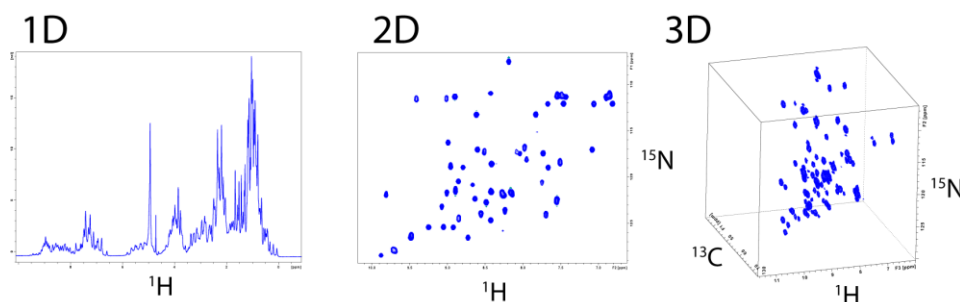


**Figure 2.2.6** The application of selection criteria and the acquisition of correlated NMR resonances, will enhance the dispersion of the NMR signals by introducing additional dimensions.

## 2.2.6. Assignments strategies

The  $^1\text{H}$ ,  $^{15}\text{N}$  HSQC spectrum is often used for ligand binding studies. However, the possibility to map the binding site onto a model of the protein, requires knowledge about the resonance assignment. This means that each NMR signal has to be correlated to the atom from which it arises. For this purpose several multidimensional heteronuclear NMR experiments based on J-couplings has been developed (Figure 2.2.7). To assign the protein backbone amides, i.e. the HSQC spectrum, triple resonance experiments, which correlate the amide to the  $\text{C}\alpha$  and  $\text{C}\beta$  chemical shift, are acquired. The experiments are named according to the atoms involved in magnetization transfer. For instance, a HNCACB gives the frequency of  $\text{C}\alpha$  and  $\text{C}\beta$  of the current residue, while HN(CO)CACB gives the frequency of  $\text{C}\alpha$  and  $\text{C}\beta$  of the previous residue.<sup>125</sup> Using the data of each spin system, they can be now be connected, put together like pieces of a jigsaw puzzle. Stretches of combined spin systems are then assigned to the primary sequence of the protein (Figure 2.2.8). This is feasible, because the  $\text{C}\alpha/\text{C}\beta$  chemical shift is dependent on the type of residue. The backbone assignment is often guided by computer programs.<sup>126,127</sup>

The side-chain atoms of a protein are assign using a slightly different strategy. Normally, starting from the  $\text{C}\alpha/\text{C}\beta$  chemical shifts and the backbone assignment, the correlation to additional carbon atoms, e.g.  $\text{C}\gamma$  and  $\text{C}\delta$ , are found by TOCSY-based (total correlation spectroscopy) experiments. In the next step, all carbons are correlated to their attached hydrogens.<sup>125</sup>

Assigned chemical shifts can be used as such for characterizing a protein. The chemical shift index (CSI) method exploit the fact that  $\text{C}\alpha/\text{C}\beta$  chemical shifts is influenced by the secondary structure.<sup>128</sup> A simple comparison to average values from disordered peptides, can give the propensity of alpha-helices, beta-strands and loops along the protein sequence. The TALOS program includes a database of high-resolution crystal structures with assigned chemical shifts, and is used to predict  $\phi$  and  $\psi$  torsion angles.<sup>129</sup> In general, torsion angles will also give information on secondary structures. A more recent and intriguing development, is the direct calculation of structures using only chemical shift data, or in combination with additional but sparse NMR data. CS-Rosetta is the most known procedure, but other labs have developed similar algorithms.<sup>130-132</sup>

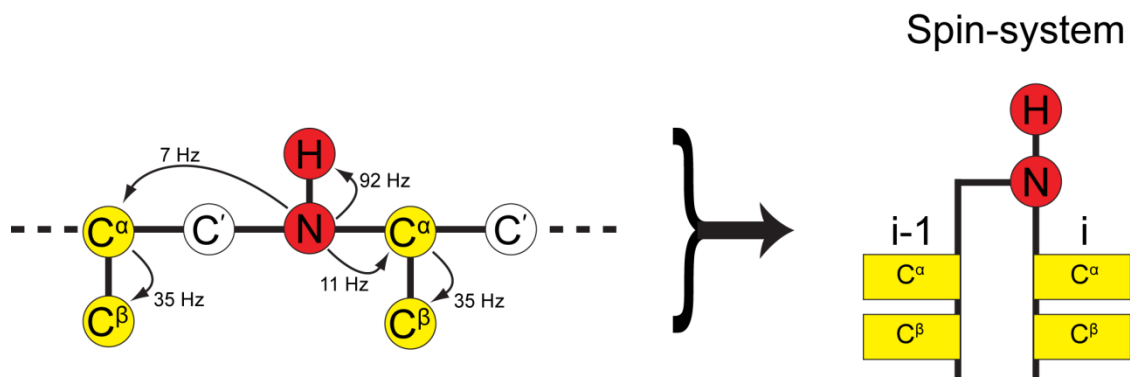


**Figure 2.2.7** J-couplings utilized in backbone assignment experiments (left). Together the experiments give the chemical shift of the  $C^\alpha/C^\beta$  atoms of the current as well as of the previous residue (right). The spin system can be compared to a piece of a jigsaw puzzle with its characteristic edges.

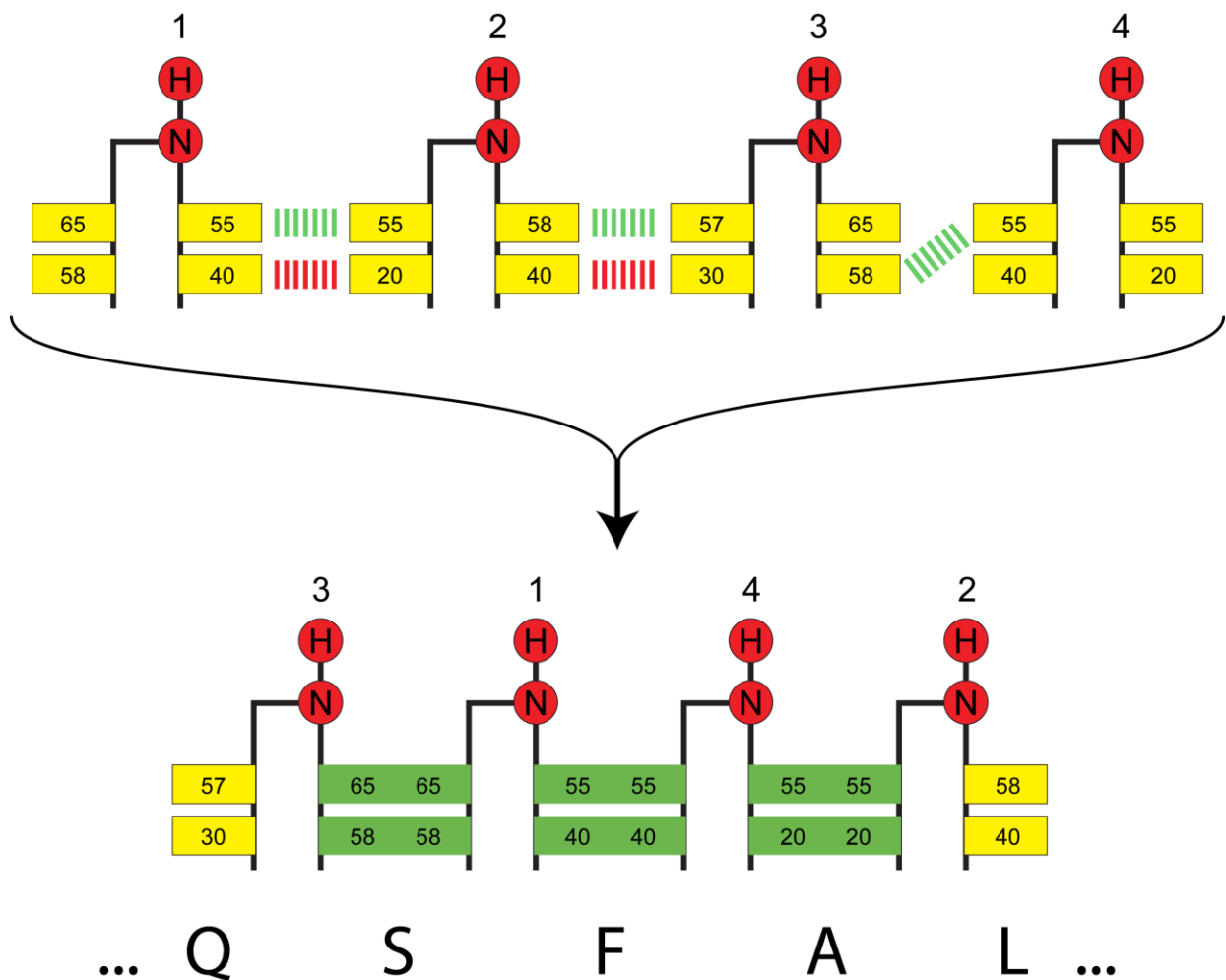


**Figure 2.2.8** Cartoon illustrating the backbone assignment strategy. All  $C^\alpha$  and  $C^\beta$  chemical shifts have been measured for four different spin systems, but the initial order is incorrect (top). The values [ppm] do not correspond very well with each other. After rearrangement the chemical shifts match perfectly (bottom). The complete fragment is now used to search the protein sequence for a match. In this example the serine and the alanine have very characteristic chemical shifts, which facilitates final assignment. The result is that resonances 1-4 corresponds to the residues of S-F-A-L. This information can now be used for ligand binding studies. It is also the first step in structure determination.



## 2.2.7. Ligand binding studies by NMR

NMR is not restricted only to the study of structural or dynamic properties, but can also be used to examine the interactions of biomolecules. The 2D  $^1\text{H}$ ,  $^{15}\text{N}$  HSQC spectrum, is maybe the simplest and the most widely used experiment to monitor ligand binding. A ligand that interacts with a protein will affect the chemical environment of the amides in the binding site. As a consequence the resonance frequency of those particular proton and nitrogen nuclei will change. This can be observed as a shift of the signal position, and is called a chemical shift perturbation (CSP) (Figure 2.2.9).

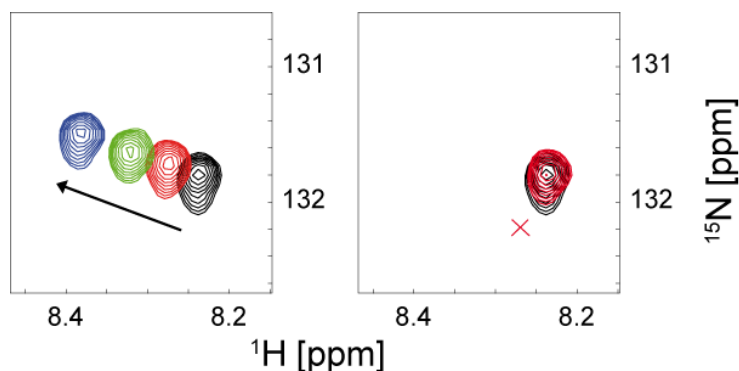


**Figure 2.2.9** Ligand binding monitored by consecutive acquisition of  $^1\text{H}$ ,  $^{15}\text{N}$  HSQC spectra. To the left an example of CSPs induced by a ligand interacting in the fast-exchange regime, and to the right a spectrum after addition of a ligand with no, or very weak affinity for the protein. The black reference spectrum is recorded on a sample without any ligand.

Using this technique, libraries of compounds can be screened for binding, or hits from other experimental methods can be validated.<sup>133</sup> Moreover, if the two molecules are in fast exchange, the affinity between them can be estimated, (see Chapter 3). Fast, intermediate or slow exchange ( $k_{ex}$ ) refer to the NMR timescale as,

Fast exchange:  $k_{ex} \gg \Delta\nu$

Intermediate exchange:  $k_{ex} \approx \Delta\nu$

Slow exchange:  $k_{ex} \ll \Delta\nu$

, where  $\Delta\nu$  is the resonance frequency difference (in Hz), between the free and bound (saturated) state. The behaviour influences the appearance of the spectra during titration of a ligand and is illustrated in Figure 2.2.10. To push the equilibrium into another exchange regime, one can change the temperature or field strength.

Due to the high sensitivity of CSPs, and their correlation to structural information, NMR has been successfully established as a powerful technique in drug discovery and development. "SAR by NMR" is based on the possibility to map the interaction of small and weakly interacting fragments, which are then joined together by linkers to form high-affinity drug-like lead compounds.<sup>134</sup> Many NMR experiments that detect the ligand have also been developed. In contrast to the protein detecting experiments, the ligand-detected experiments do not suffer from the slow tumbling of a large receptor, which results in broad NMR signals. STD-NMR<sup>135</sup> (saturation transfer difference NMR) and INPHARMA<sup>136</sup> are good examples of such experiments useful in drug design.

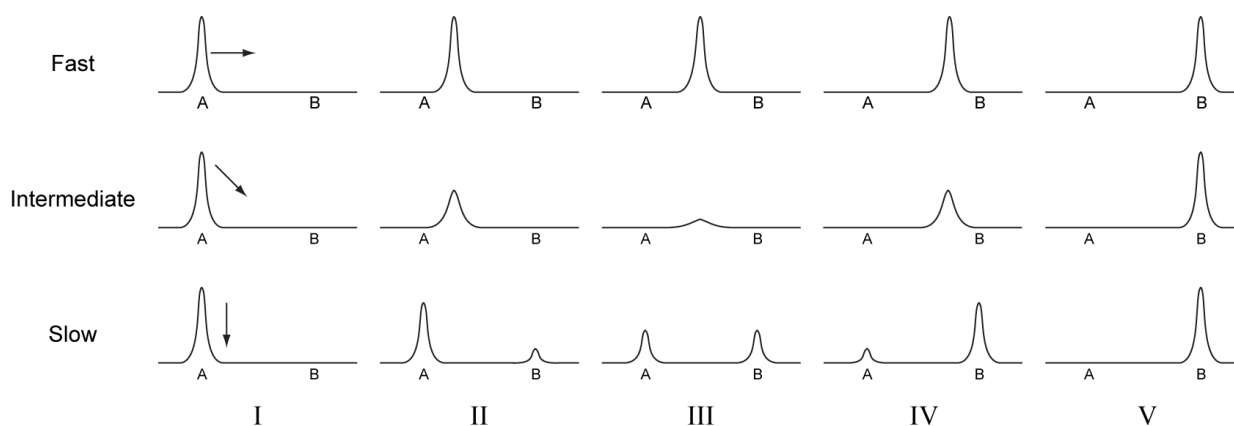


**Figure 2.2.10** The exchange rate of the ligand influence the appearance of a signal during titration. A ligand is titrated to the free form of the protein (A) until the fully saturated or bound state (B) is reached. I-V denote the amount of ligand added. For a fast exchanging ligand the peak position is an average chemical shift, weighted by the relative amounts of free and bound protein. In the intermediate case the peak is broadened until coalescence, but recover upon saturation. Finally, for slow exchanging ligands, the population of free and bound state, can be observed simultaneously. The area under the peaks correspond to their relative amounts.

## 2.2.8. Relaxation studies in NMR

The function of a protein is determined by its structure and, importantly, by the motions present in the molecule. The dynamic properties of a protein, or any other biomolecule, can be studied by following the relaxation of NMR signals. Two constants are usually used to characterize NMR relaxation in biomolecules,  $T_1$  and  $T_2$ , and these are typically studied separately.  $T_1$  describes the *longitudinal relaxation*, which is the return from the symmetrically populated excited state to the low-energy equilibrium state.  $T_2$  on the other hand, known as *transverse relaxation*, is related to the loss of coherence between the individual precessing spins in the sample. The bulk magnetization, which is manipulated and detected during the NMR experiment, is indeed produced by the individual spins, and disappears once those vectors are not precessing in a synchronized and organized way. Both longitudinal and transverse relaxation follow an exponential decay function, where  $T_1$  and  $T_2$  are the single time constants.

The physical understanding and mathematical description of relaxation is very demanding. In short, relaxation comes from the interaction of the individual spin with its environment. The molecule is tumbling and diffusing, additionally there might be internal motion. This creates several relaxation pathways, through which energy and entropy is lost, and causes the return of the polarization, from an excited state, back to equilibrium. A major relaxation contribution comes from the dipole-dipole interactions of a spin. Relaxation increases with molecular size, and can create severe problems regarding acquisition, thereby creating an upper limit for structural studies by NMR (~30kDa). The "positive" thing with relaxation is that consecutive scans can be executed with relatively short intervals. Additionally,  $T_1$  and  $T_2$  can give information on the relative flexibility of an amino acid residue.

Generally,  $T_1$  of macromolecules increases with the molecular weight, as well as with high rigidity of a residue.  $T_2$ , on the contrary, is normally decreasing in such cases. The flexibility of the protein backbone can be estimated by measuring those two constants using HSQC based NMR experiments.<sup>137</sup> In such pulseprograms a relaxation delay has been incorporated, and the intensity of each signal is then followed over a range of delay values. Extending the relaxation delay results in a decrease of the signal intensity. The data is then fitted to an exponential decay function and the time constants are calculated (Figure 2.2.11). The error is normally based on a Monte Carlo simulation, which adds the noise of the experiment onto the signal intensity of the data.

In Chapter 4,  $T_1$  and  $T_2$  measurements could be correlated to the precision of structure calculations. The  $\{^1\text{H}\}$ - $^{15}\text{N}$  heteronuclear NOE is a complementary experiment, which quickly provides data on which protein stretches are flexible. This is practical for optimization of protein constructs.<sup>138</sup>

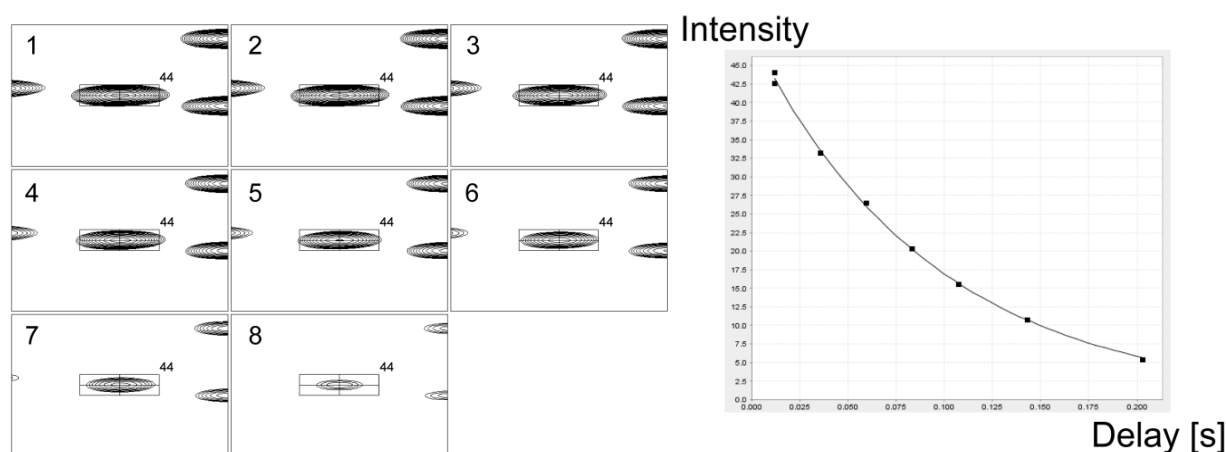


**Figure 2.2.11**  $T_2$  measurements using the rate analysis module of NMRViewJ v8. The intensity of each peak is plotted and fitted to an exponential decay function. The calculated (per-residue)  $T_2$  value gives information on which residues are rigid (structured domain) and which are flexible (termini and loops), as well as information on motions on a slower timescale undergone by the system under study.

Certain labeling techniques can be used to study the relaxation, and therefore the dynamics, of methyl groups in large macromolecular complexes.<sup>119</sup> This helps in delineating the molecular function of such cellular machines.<sup>139</sup> Non-linear sampling is another recent development that might facilitate such studies.<sup>140</sup> Here, not all time-points of the Nyquist-grid are recorded but rather only a randomly distributed subset. This opens up for increased sensitivity with maintained resolution, but need alternatives to the classical FT processing approach.

Structure determination by NMR is heavily dependent on measuring distances between nuclei. This is possible due to an important feature of relaxation called the nuclear Overhauser effect (NOE), which will be described in the following section.

## 2.2.9. The Nuclear Overhauser Effect

The nuclear Overhauser effect (NOE) make it possible to measure inter-atomic distances by NMR, usually between hydrogen atoms. The NOE is arising from the cross relaxation of two dipole-coupled spins.<sup>115</sup> The dipolar coupling enables the transfer of spin polarization (magnetization along the z-axis), from one nuclei to another, while remembering its previous resonance frequency. This transfer opens up for the design NMR experiments, where a hydrogen resonance frequency is correlated to all other hydrogen signals in the vicinity ( $< 5 \text{ \AA}$ ). In contrast to J-coupled systems, where the coherence transfer is via the molecular bonds, the NOE polarization transfer is through space. The distance dependence is strong, and the transfer efficiency decreases with  $r^{-6}$ , where  $r$  is the atomic distance.

Many NOE spectroscopy (NOESY) pulse sequence have been developed to measure the NOE between certain nuclei. Apart from applying different selection criteria (see Section 2.2.5) they all share the incorporation of a crucial *mixing period*. During this period ( $\sim 100$  ms) the spins have to be along the magnetic field. In addition to the homonuclear  $^1\text{H}$ - $^1\text{H}$  NOESY, the key experiments for structural biology include  $^{13}\text{C}$  and  $^{15}\text{N}$  *editing*.<sup>125</sup> This means that only protons connected to carbons or nitrogens are recorded, i.e.  $^{13}\text{C}$ - $^1\text{H} \cdots ^1\text{H}$  or  $^{15}\text{N}$ - $^1\text{H} \cdots ^1\text{H}$  correlations. In combination with editing, insertion of *filtering* steps are important to the characterization of macromolecular complexes. Such pulse sequences are used for instance for protein-peptide complexes where the protein is  $^{13}\text{C}/^{15}\text{N}$  labeled and the peptide not. The resulting spectrum would give the correlations of the following kind,  $^{13}\text{C}$ - $^1\text{H} \cdots ^1\text{H}$ - $^{12}\text{C}/^{14}\text{N}$ .

Automated techniques have been implemented to assign the usually very complex NOESY spectra. The most popular algorithms to derive distance restraints are CYANA and ARIA.<sup>141,142</sup> Both are based on iterative rounds of assignment and re-assignment, and include ambiguous restraints, network anchoring and simplified torsion angle molecular dynamics to obtain initial structural models.

## 2.2.10. Residual dipolar couplings

The dipolar interaction between two nuclei (two dipoles) is dependent on the orientation and distance,

$$\nu_D = \nu_{\parallel} \frac{(3\cos^2\theta - 1)}{2} \quad \left( \nu_{\parallel} = -\frac{\gamma_I\gamma_S h}{4\pi^2 r^3} \right)$$

, where  $\nu_D$  is the frequency contribution to the chemical shift from the dipolar coupling, whereas  $\nu_{\parallel}$  is the maximum dipolar coupling, which occurs when the vector is along the external magnetic field ( $\theta = 0^\circ$  or  $180^\circ$ ).  $\theta$  is the angle between the inter-nuclei vector and the applied magnetic field,  $\gamma$  is gyromagnetic ratio of the involved nuclei,  $h$  the Plank constant, and  $r$  the inter-nuclei distance. The dipolar interaction is averaged out in solution because of the  $\theta$  dependence. This simplifies the NMR spectra

significantly, since the coupling is very strong, e.g. between two protons it is in the kilohertz range.

The dipolar coupling has to be scaled down if the geometric information, hidden in the dipolar coupling is to be used. A *residual dipolar coupling* (RDC) is revealed if the molecules are slightly aligned in the sample and, thus, to the magnetic field.<sup>143</sup> Several media have been established to allow RDC measurements. The most common are bacteriophages<sup>144</sup>, liquid crystalline media<sup>145,146</sup>, and stretched or compressed gels<sup>147</sup>. The RDC is commonly measured as the difference of the J-coupling in two non-decoupled spectra, one of the non-aligned sample, and the other of an aligned sample. Then, the RDCs are analyzed by the computer programs and connected to the molecular frame.<sup>148-150</sup> The best data come from measurements of different RDCs, in combination with multiple types of alignment media.

RDC data can be used for structure refinement by incorporating them as restraints into the calculations. RDCs are particularly important for large complexes, due to their inherent global character.<sup>151</sup> Here, they give important information on the relative domain orientations. If not used in the structure calculation, RDCs can be used in for structure validation. A quality factor (Q-factor) can be calculated as,

$$Q = \frac{\sqrt{\sum (RDC_{exp} - RDC_{calc})^2}}{\sqrt{\sum (RDC_{exp})^2}}$$

and gives the agreement between experimental ( $RDC_{exp}$ ) and back-calculated ( $RDC_{calc}$ ) RDC values. Q values ranging between 0.2-0.3 can be considered reasonable.<sup>152</sup>

In relation to X-ray crystallography, RDCs can be used to compare a crystal structure to its solution conformation, without completing a structural determination by NMR. Also dynamics can be studied by RDC measurements. Examples include studies of inter-domain motions<sup>153</sup> (and Chapter 3), as well as the investigation of the solution dynamics of whole proteins.<sup>154,155</sup> This is possible since the RDC, due to averaging, contains conformational data up the microsecond timescale.

### 2.2.11. Structure calculations and quality control

Compared to X-ray crystallography, where a structural model is built into the electron density, NMR relies on the simulated folding of a macromolecule. The folding is caused by the application of structural restraints (e.g. NOEs, RDCs and torsion angles). Importantly, the restrained simulation is rather a simulated annealing procedure, since the goal is only to minimize the target function, and does not try give a physically realistic trajectory of the molecular dynamics. In brief, after an initial high-temperature phase the energy of the system is slowly lowered. The cooling allow the efficient minimization of the penalties that arise from violated restraints. When, which and how

strongly a specific type of restraint is applied, are important features to modify for a successful result.

The two most used programs for structural determination by NMR are CNS<sup>156</sup> and XPLOR-NIH<sup>157</sup>. Both packages can also be used for a final refinement in explicit solvents, which is important to improve the surface electrostatics. Furthermore, additional restraints to the ones mentioned above can be incorporated in the calculations. These include paramagnetic relaxation enhancement (PRE) data<sup>151,158</sup>, hydrogen bonds (characterized by H/D-exchange) and predicted torsion angles<sup>129</sup>.

After completed calculations the structure quality has to be assessed. The parameters to examine can be divided into two categories, one is how well the final structure fulfills the given restraints, and the other is how the structure compares to other previously determined structures (often high-resolution crystal structures). Two terms useful to quality analysis, are *precision* and *accuracy*, as is the understanding that something that is precise do not have to be accurate.<sup>159</sup> The actual analysis is facilitated by readily available programs and online services. One recommendation is iCING<sup>160</sup>, which includes PROCHECK<sup>161</sup> and WHATCHECK<sup>162</sup>, as well as detailed per-residue reports on violations, and a calculation on completeness. The recommendation is to perform iterative rounds of quality checks and setting up of new structure calculations. This will increase the chances of discovering and relieving problems early in the process. Suggestions have been made to introduce R-factors as in X-ray crystallography.<sup>163</sup>

## 2.2.12. Literature

As a complement to the article references given, I suggest the following books for further reading. They span from introductory texts on basic NMR concepts, to detailed descriptions on more exotic topics.

Introductory:

*NMR: The Toolkit*, P.J. Hore; Concise introduction to NMR in general  
*Structural Biology - Practical NMR Applications*, Q. Teng; NMR focused on structural biology  
*Understanding NMR Spectroscopy*, J. Keeler; A great introduction to the mathematics of NMR

More advanced:

*Fundamentals of Protein NMR Spectroscopy*, G.S. Rule; Protein NMR, quite mathematical.  
*Spin Dynamics*, M.H. Levitt; Comprehensive book explaining the physics behind NMR.  
*Protein NMR Spectroscopy: Principles and Practice*, J. Cavanagh et al.; The standard reference for a protein NMR spectroscopist. Covers most of the relevant topics.

Practical advice on setup and acquisition:

*200 and more NMR Experiments*, S. Berger et al.; Good when setting up new experiments.

### 2.3. X-ray crystallography

X-ray crystallography is the method of choice to solve large structures or complexes of biomolecules (>25 kDa).<sup>164-166</sup> The technique is dependent on the strong X-ray diffraction of a well-ordered crystal. The photons of the X-ray beam are scattered by the electrons of the molecules in the crystal lattice. However, due to the crystal periodicity, there is a constructive interference at certain distances and angles. All these signals, known as reflections, can be recorded by rotating the crystal in the beam. Through back-calculation the underlying electron density can be reconstructed. Here, one hurdle is solving the *phase problem*. The phases are lost during the acquisition but can be recovered by computational or experimental procedures.<sup>167</sup> The back-calculation is performed by Fourier-transform algorithms similar to those used in NMR. Once the electron density is available, the crystallographer tries to build a model of the macromolecule that fits the data the best. Refinement of the model is an iterative process of building and re-building (Figure 2.3.1).

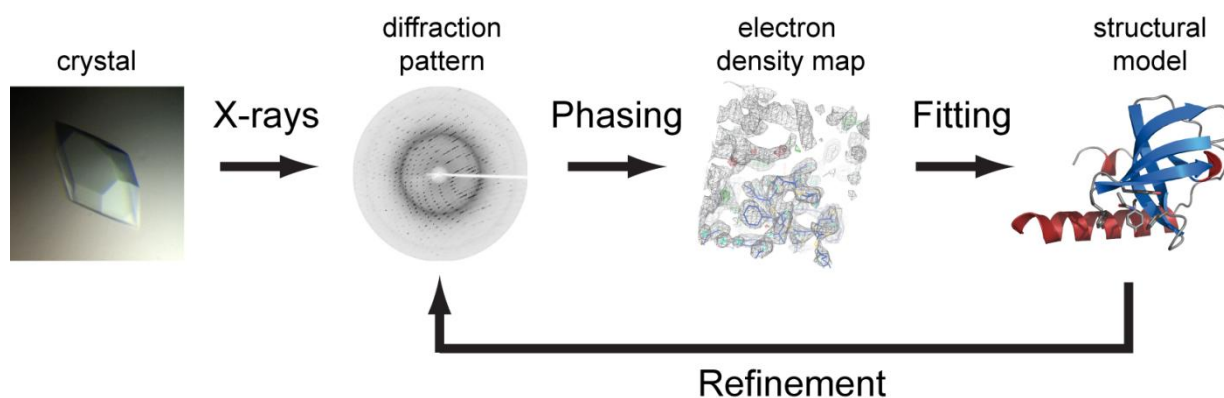


**Figure 2.3.1** Basic workflow of X-ray crystallography. Today, the major bottleneck is the production of high-quality crystals. The refinement cycle ends when no further improvements are possible.

Because of the short wavelength of X-ray radiation, it is possible to resolve the atom coordinates with high accuracy. The precision, on the other hand, depends on the crystal and the equipment used. Conditions for growing protein crystals, or similar, are screened by automated procedures at sub-microliter scale. The difficulty of growing usable crystals makes this the major bottleneck in the field.<sup>168</sup> For instance, the EBNA-2 protein (page 118) yields huge and good-looking crystals, however, those do not diffract at all. Due to the seemingly complete lack of correlation, between a proteins properties and its crystallization condition, one can only outline some basic principles for what will increase the chances to obtain diffracting crystals; First, use an optimized protein construct, without long flexible termini. A complementary practice is the use of proteolysis.<sup>169</sup> Second, make sure the sample is as pure as possible (> 95%) and is in a defined and non-aggregated state. Third, consider making site-specific mutations of exposed residues to lower the surface entropy.<sup>168</sup> Finally, the addition of a ligand might improve the conformational stability of the protein, and could change the outcome of the crystal screen.

As been touch on previously, the strength of X-ray crystallography is the apparent absence of a size-limitation. It is also a direct method of modeling the structure, and most often yield highly accurate atom coordinates. Additionally, no expensive isotope labeling is needed and once crystals are available it is normally a very fast procedure. One important feature is the possibility of structural quality assessment. The R-factor defined as,

$$R = \frac{\sum |F_{obs}| - |F_{calc}|}{\sum |F_{obs}|}$$

, where  $F_{obs}$  and  $F_{calc}$  are the observed and calculated structure factors, respectively, gives an easy measure on how well the model corresponds to the data. In contrast to NMR, an R-factor can also be calculated for a subset of reflections not used in the refinement. Such an  $R_{free}$  factor is a cross-validation test, used not to over-interpret the crystallographic data.<sup>170</sup> This type of validation is possible due to the nature of the crystallographic data. Single reflections are not alone responsible for the electron density in a certain position. However, such removal of specific restraints in the NMR structure calculation can be harmful to the output.

As described, the weakness of X-ray crystallography lies in the difficulty to obtain crystals, as well as in the time invested in solving the phase problem. One inherent difference to NMR is that the information on dynamic motions is limited, as the crystal is consisting of an ordered solid phase array of molecules. Additionally, the crystals are usually cooled down to approximately 100K during data acquisition to minimize radiation damage. Another reason why to use NMR, when possible, is the straightforward implementation of ligand binding studies.

In conclusion, the two major techniques of structural biology, X-ray crystallography and solution NMR spectroscopy, have their own strengths and weaknesses. Depending on the specific research question at hand, one technique can be selected, or, a combination of the two can be used. There are several examples of when the synergy of combining the two methods, lead to increased understanding of biology at a very molecular level. For instance, Sprangers et al. have studied the function of the proteasome, and Christodoulou et al. have described motions in the E. coli ribosome.<sup>139,171</sup> An additional example, on a somewhat different scale, is given in the next chapter. Here, we present the crystal structure of a double-domain construct of Tudor-SN, and give NMR evidence that those two domains tumble together in solution.





## Chapter 3

---

### Structure and ligand binding of Tudor-SN

#### 3.1. Summary

Splicing is one out of many levels at which cellular gene expression is regulated. The exclusion of introns is an essential step in the maturation of mRNA, before its export into the cytoplasm, and translation into protein by the ribosome (see also Chapter 5). Tudor-SN, first described to act as a transcriptional co-activator important to the Epstein-Barr virus, was recently shown to possess the ability to enhance early steps of splicing. To better understand the molecular mechanism we determined the structure of an extended Tudor domain in *Drosophila* Tudor-SN using X-ray crystallography, and analyzed the ligand binding preferences of this domain by NMR.

The extended Tudor domain of Tudor-SN (TSN) exhibits an interesting structure, in which a Tudor domain is intertwined with a staphylococcal nuclease domain. During the evolution of the protein, the Tudor domain has been inserted with additional linker residues into a loop of the nuclease domain. Solution NMR data show that the two domains tumble together. A comparison to known nuclease domains and their active-sites, strongly implies that the TSN domain has no remaining nuclease activity. However, its binding site for methylated amino acids, located in the Tudor domain, is intact. We decided to probe the ligand binding of the TSN domain by NMR. By adding ligands in increasing amounts and recording consecutive 2D  $^1\text{H}$ ,  $^{15}\text{N}$  HSQC spectra, we were able to deduce that Tudor-SN has affinity for methylated arginines, as well as peptides comprising such residues. In particular, the strongest interaction was observed between Tudor-SN and symmetrically dimethylated arginines (sDMA).

sDMA can be found in proteins important to splicing, for instance in the C-terminal tails of various Sm-proteins. Sm-proteins are an integral part of most small nuclear ribonucleoproteins (snRNPs), which build up the core of the spliceosome. Our data shows that Tudor-SN is capable of interacting with sDMA-modified proteins, and suggest how the protein can affect the spliceosome assembly. Further studies will be needed to establish the interaction partners of Tudor-SN *in vivo*.



## Structure and Ligand Binding of the Extended Tudor Domain of *D. melanogaster* Tudor-SN

Anders Friberg<sup>1,2</sup>, Lorenzo Corsini<sup>3</sup>, André Mourão<sup>1,2,3</sup>  
and Michael Sattler<sup>1,2\*</sup>

<sup>1</sup>Institute of Structural Biology,  
Helmholtz Zentrum München,  
Ingolstädter Landstr. 1, 85764  
Neuherberg, Germany

<sup>2</sup>Munich Center for Integrated  
Protein Science and Chair of  
Biomolecular NMR,  
Department Chemie, Technische  
Universität München,  
Lichtenbergstr. 4, 85747  
Garching, Germany

<sup>3</sup>European Molecular Biology  
Laboratory (EMBL),  
Meyerhofstr. 1, 69117  
Heidelberg, Germany

Received 29 October 2008;  
received in revised form  
4 February 2009;  
accepted 10 February 2009  
Available online  
14 February 2009

The Tudor-SN protein (p100, SND1) has been implicated in a variety of cellular processes, such as transcription, processing of edited double-stranded RNA, and splicing regulation. Molecular details of these functions are not yet understood. Tudor domains have previously been shown to bind methylated ligands, such as methylated lysines and arginines. It has been suggested that the role of Tudor-SN in splicing may involve binding to such methylated ligands or to the methylated 5' cap of spliceosomal snRNAs.

Here, we report the crystal structure of the extended Tudor domain of Tudor-SN from *Drosophila melanogaster* to a resolution of 2.1 Å. NMR secondary chemical shifts, relaxation data, and residual dipolar couplings indicate that the solution and crystal structures are similar. Binding of various ligands was investigated by NMR. Binding sites and affinities were characterized by chemical shift perturbations. We show that the aromatic cage of the Tudor domain specifically binds a peptide containing symmetrically dimethylated arginines (sDMA) with micromolar affinity, while the same peptide comprising nonmethylated arginines does not show significant chemical shift perturbations. Tudor-SN preferentially recognizes sDMA over asymmetrically dimethylated arginine (aDMA). In contrast, two 5' cap analogues with different methylation patterns, as well as mono-, di-, and trimethyllysines, show no binding.

Our data demonstrate that the Tudor domain of Tudor-SN specifically recognizes sDMA-containing ligands. The aromatic cage of Tudor-SN is very similar to the one in the Tudor domain of the survival of motor neuron protein, which also recognizes sDMA peptides, indicating a conserved binding motif for this methylation mark. Recognition of sDMA in the C-terminal tails of spliceosomal Sm proteins suggests how Tudor-SN may interact with small nuclear ribonucleoprotein particles during the regulation of splicing.

© 2009 Elsevier Ltd. All rights reserved.

Edited by R. Huber

Keywords: Tudor-SN; p100; NMR; crystallography; sDMA

\*Corresponding author. E-mail address:  
sattler@helmholtz-muenchen.de.

Abbreviations used: sDMA, symmetrically dimethylated arginine; aDMA, asymmetrically dimethylated arginine; snRNP, small nuclear ribonucleoprotein; SMN, survival of motor neuron; CSP, chemical shift perturbation; RDC, residual dipolar coupling; HSQC, heteronuclear single quantum correlation; EBNA-2, Epstein–Barr virus nuclear antigen 2; dsRNA, double-stranded RNA; PDB, Protein Data Bank; NOE, nuclear Overhauser enhancement; EMBL, European Molecular Biology Laboratory.

### Introduction

Tudor-SN (p100, SND1) is a multifunctional protein found in many eukaryotic organisms by genome sequencing†. It was initially discovered as a factor important for Epstein–Barr virus nuclear antigen 2 (EBNA-2)-activated gene expression by acting as a bridge to the general transcription factor TFIIE.<sup>1</sup> Tudor-SN was later shown to be a coactivator of several other transcription factors, such as STAT5<sup>2</sup> and STAT6.<sup>3</sup> In both cases, the protein mediates interactions to the basal transcription machinery.

† [www.ensembl.org](http://www.ensembl.org)

Furthermore, Pim-1 kinase activates c-Myb via Tudor-SN as a response to a number of cytokines.<sup>4</sup> Recently, Tudor-SN was also discovered to interact with components of the U5 small nuclear ribonucleoproteins (snRNPs), to facilitate spliceosome assembly, and to enhance the kinetics of the first stage of splicing.<sup>5</sup> The multiple functions of Tudor-SN might play a role in the context of the coordination of transcription and splicing,<sup>6,7</sup> as have been seen for other steps of mRNA maturation in the nucleus.<sup>8</sup>

In addition to its role in transcription and splicing, Tudor-SN has been implicated in the modulation of RNA interference pathways. Long double-stranded RNAs (dsRNAs) can be specifically or nonspecifically edited by adenosine deaminases acting on RNA.<sup>9</sup> This modification, a conversion of adenosines to inosines (A-to-I editing), can lead to cleavage of the dsRNA.<sup>10</sup> Moreover, A-to-I editing of dsRNAs can lead to amino acid substitutions (I is translated as G by the ribosome)<sup>11</sup> and changes in gene

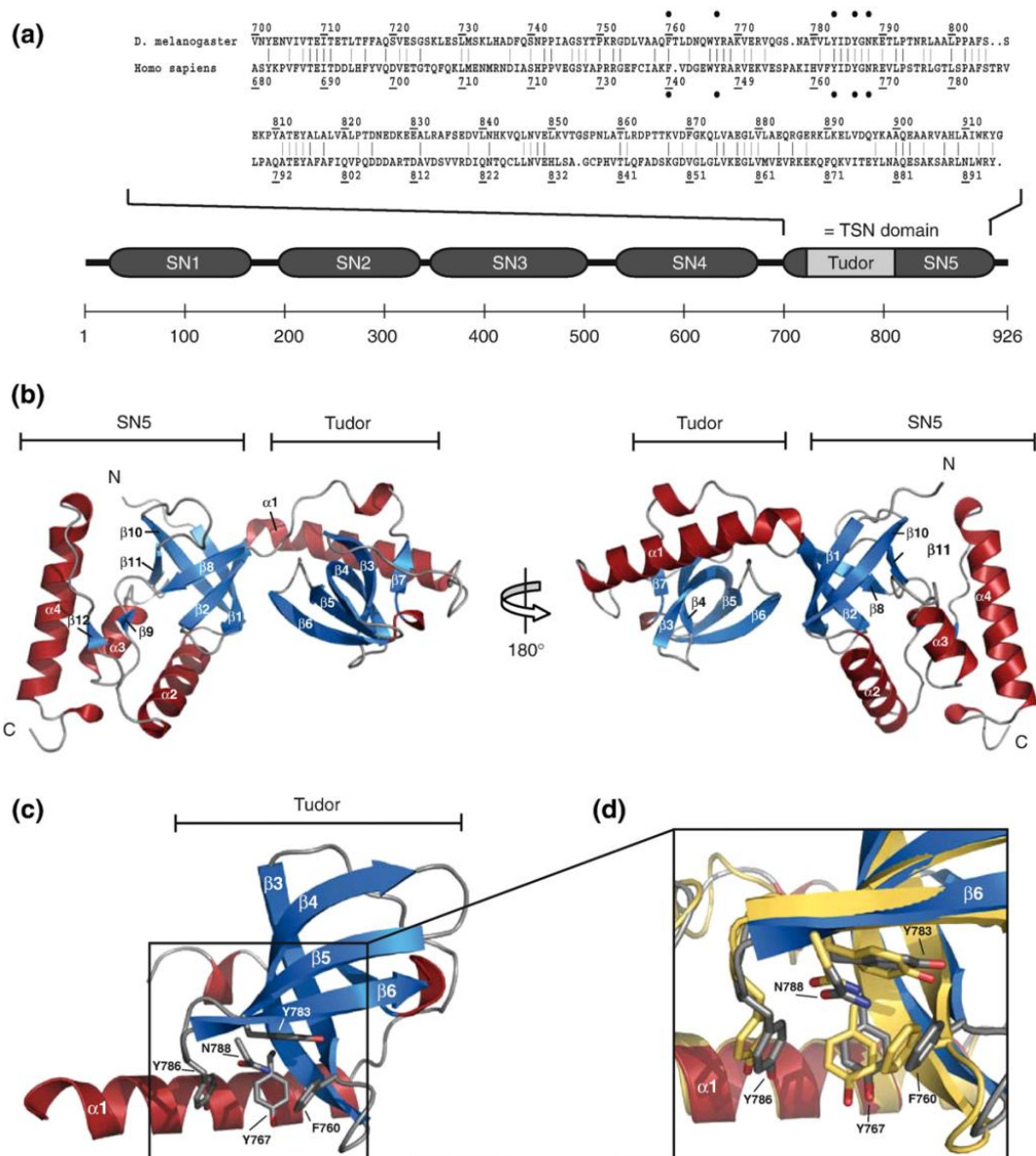


**Fig. 1.** Sequence and crystal structure of the TSN domain of *D. melanogaster* Tudor-SN. (a) Sequence alignment of the TSN domain from *D. melanogaster* and the human homologue (42% identity). Aromatic cage residues are marked with filled circles. Below, the domain structure of full-length Tudor-SN. (b) Crystal structure of the TSN domain (chain A), viewed from two opposite sides. The N- and C-termini are labeled;  $\alpha$ -helices,  $\beta$ -strands, and loops are colored red, blue, and gray, respectively. (c) Close-up view of the Tudor domain in Tudor-SN with the aromatic cage residues highlighted as gray sticks. Coloring of secondary-structure elements as in (b). (d) Comparison of the aromatic cages in *D. melanogaster* and human (yellow) Tudor-SN.



regulation.<sup>12,13</sup> Edited dsRNAs bind to Tudor-SN, but it is unclear if the protein alone can accomplish the subsequent cleavage reaction.<sup>14,15</sup> A-to-I editing of micro-RNAs has been shown to occur *in vivo* and affects the biogenesis<sup>16</sup> and the silencing profile<sup>17</sup> of these molecules. Notably, Tudor-SN has been identified as a subunit of the RNA-induced silencing complex,<sup>18</sup> although its function there remains unknown. Recently, Tudor-SN was shown to influence expression of angiotensin II type 1 receptor by interactions mapped to the 3'-untranslated region of the mRNA.<sup>19</sup>

Full-length Tudor-SN consists of five staphylococcal nuclease domains (SN1–5) and one Tudor domain (Fig. 1a). The first four SN domains have been shown to mediate an interaction between STAT6 and the large subunit of RNA Polymerase II,<sup>3</sup> as well as between STAT6 and the CREB binding protein, thereby recruiting histone acetyl transferase activity to the promoter site.<sup>20</sup> Recent data revealed that the same SN domains also bind dsRNAs.<sup>15</sup> Bioinformatical analysis suggests that—at the primary sequence level—the Tudor domain is inserted into the C-terminal SN domain (SN5).<sup>21,22</sup> The existence of such an extended Tudor domain (TSN) was confirmed by structural studies of human Tudor-SN.<sup>23</sup> The study provided biochemical evidence for an interaction between the TSN domain and several snRNPs. It has also been reported that the TSN domain of human Tudor-SN alone facilitates spliceosome assembly *in vitro*.<sup>5</sup> However, although mutations in the Tudor domain interfere with the binding of snRNPs,<sup>23</sup> this interaction is not understood on a molecular level.

Tudor domains have previously been shown to interact with methylated ligands, such as symmetrically dimethylated arginines (sDMAs) in the C-terminal tails of Sm proteins<sup>24–26</sup> and methylated lysines in histone tails.<sup>27,28</sup> The recognition involves the so-called aromatic cage, which consists of a number of aromatic residues that, together with polar side chains, interact with the methylated ligand. For example, the survival of motor neuron (SMN) Tudor domain interacts with sDMAs in Sm proteins *in vivo* and plays an important role in snRNP biogenesis.<sup>24,29</sup> Yet, other Tudor domains bind methylated lysines found in histone tails. For example, 53BP1 is recruited to DNA double-strand breaks by its tandem Tudor domain.<sup>27,30</sup> Thus, it may be expected that the TSN domain recognizes arginine- and/or lysine-methylated ligands. In addition, the 5' cap of snRNAs, which exists in different methylated states,<sup>31</sup> has been suggested as a possible ligand of Tudor-SN.

Here, we present the crystal structure of the TSN domain of *Drosophila melanogaster* Tudor-SN. Using solution NMR, we show that the conformations in solution and in the crystal are very similar and characterize the backbone dynamics of the protein. Various putative ligands were tested in NMR titration experiments, and it was found that TSN binds specifically to sDMA or sDMA-containing ligands. The binding site maps to the aromatic cage of the Tudor domain, indicating that it is involved in

the specific recognition of sDMAs. These findings suggest that splicing regulation by Tudor-SN involves recognition of sDMA in the C-terminal tails of the spliceosomal Sm proteins and/or additional binding partners.

## Results

### Structure of the TSN domain from *D. melanogaster* Tudor-SN

Recombinant TSN protein was produced in *Escherichia coli*. An initial screen followed by condition optimization yielded crystals that diffracted to 2.1 Å (Table 1). The refined structure is composed of two chains, A and B (backbone coordinate RMSD, 1.09 Å), showing electron density for residues 699–915 and 699–913, respectively (Fig. 1b). The protein consists of an SN domain and a Tudor domain. Together, they form a compact double domain protein with an interface stabilized by a combination of electrostatic and hydrophobic interactions (Supplementary Fig. 1). The secondary structure comprises 12 β-strands and four α-helices. The Tudor domain is inserted

**Table 1**

<i>Data collection</i>	
Wavelength (Å)	1.54179
Space group	C121
<i>Cell dimensions</i>	
a (Å)	83.56
b (Å)	47.04
c (Å)	129.77
α (°)	90
β (°)	107.32
γ (°)	90
<i>Resolution</i>	
Total (Å)	19.64–2.10
Outer shell (Å)	2.22–2.10
R <sub>meas</sub> (%) <sup>a</sup>	4.4 (15.2)
R <sub>merged-F</sub> (%) <sup>a</sup>	4.4 (13.0)
I/σI <sup>a</sup>	24.4 (10.2)
Completeness (%) <sup>a</sup>	98.7 (97.8)
Redundancy <sup>a</sup>	3.63 (3.51)
<i>Refinement</i>	
Total no. of reflections	28,296
R <sub>work</sub> /R <sub>free</sub> <sup>b</sup>	0.227/0.269
<i>No. of atoms</i>	
Protein	3401
Water	303
<i>B-factors</i>	
Protein	24.8
Water	31.3
<i>RMSD</i>	
Bond lengths (Å)	0.007
Bond angles (°)	1.037
<i>Ramachandran values<sup>c</sup> (%)</i>	
Preferred regions	98.4
Allowed regions	1.4
Disallowed regions	0.2
PDB code	2WAC

Values in parentheses are for the highest-resolution shell.

<sup>a</sup> As defined in XDS.<sup>32</sup>

<sup>b</sup> As defined in REFMAC5.<sup>33</sup>

<sup>c</sup> Validated with MolProbity.<sup>34</sup>

between the second and the third strand ( $\beta 2$  and  $\beta 8$ ) of the SN  $\beta$ -barrel, connected by two relatively long linkers. The first linker, N-terminal of Tudor, comprises the first helix  $\alpha 1$ . Strands  $\beta 9$  and  $\beta 12$  form a short antiparallel  $\beta$ -sheet that docks the C-terminal helix  $\alpha 4$  onto the SN domain. The overall sequence identity (42%), between the TSN domain of *D. melanogaster* Tudor-SN and the human homologue [Protein Data Bank (PDB) code: 2HQE], is reflected in very similar three-dimensional structures, with a coordinate RMSD of 1.76 Å for the backbone atoms of 205 residues.

The SN domain (Fig. 1b) consists of the characteristic five-stranded  $\beta$ -barrel (OB-fold) flanked by three  $\alpha$ -helices. In human Tudor-SN, residues important for DNA binding are suggested to be present in SN1–4<sup>15</sup> but not in SN5.<sup>23</sup> This is also the case for the SN5 domain of *D. melanogaster* Tudor-SN where the loop between the third and the fourth  $\beta$ -sheet ( $\beta 8$ – $\beta 9$ ) is much shortened. Compared to wild-type SN (PDB code: 1EY0) residues important for calcium binding and catalysis,<sup>35</sup> D21, R35, D40, E43, and R87 are replaced in *Drosophila* Tudor-SN by L714, A815, A820, T823, and P856, respectively, thereby most likely rendering this domain catalytically inactive.

The Tudor domain (Fig. 1c) consists of five antiparallel  $\beta$ -strands and has an aromatic cage that strongly resembles human Tudor-SN (Fig. 1c). The aromatic cage residues (F760, Y767, Y783, Y786, and N788) are located in or between the first four  $\beta$ -strands ( $\beta 3$ – $\beta 6$ ; Figs. 1c and 2a). In other Tudor domains, the cage residues together form a cavity for recognition of methylated ligands.<sup>25,27,28</sup> The aromatic cages of *Drosophila* and human Tudor-SN are composed of identical residues (F740, Y746, Y763, Y766, and N768 in human Tudor-SN; UNIPROT accession code: Q7KZF4) and have a very similar three-dimensional arrangement (Fig. 1d). It is therefore very likely that the Tudor domain has similar binding partners in both species.

### Structure and dynamics of TSN in solution

We used NMR to characterize the structure and backbone dynamics of TSN in solution. The backbone amide resonances were assigned using standard triple-resonance techniques, on a <sup>15</sup>N,<sup>13</sup>C,<sup>2</sup>H-labeled sample. Ninety-five percent of backbone NMR signals could be assigned. Secondary chemical shift analysis<sup>37</sup> shows an excellent agreement with the secondary structure in the crystal structure (Fig. 2a). To characterize the three-dimensional fold in solution, we recorded <sup>1</sup>H<sup>N</sup>–<sup>15</sup>N residual dipolar couplings (RDCs) (Fig. 2b). The 96 experimental RDCs agree very well with the values back-calculated from the crystal coordinates, with an *R*-factor<sup>38</sup> of 0.19 (Fig. 2e). RDCs with larger deviations (>10 Hz) correspond to residues in loops or flanking secondary structures and might be affected by crystal packing.<sup>39</sup> The overall good agreement between the experimental and calculated RDC data indicates a highly similar structure of the TSN domain in solution. Alignment tensors fitted for the

Tudor and SN5 domain separately are identical within error. Although this does not exclude the presence of symmetric domain motions, the good agreement of the RDC data with the crystal structure indicates that such motions, if present at all, could be only of small amplitude. Together with the observed interdomain contacts in the crystal structure, this suggests that the TSN domain tumbles as a compact and rigid particle in solution.

We next recorded <sup>15</sup>N relaxation data [ $T_1$ ,  $T_2$ , and {<sup>1</sup>H}–<sup>15</sup>N heteronuclear Overhauser enhancement (NOE)] to characterize the backbone dynamics of the TSN domain (Fig. 2c and d). The average <sup>15</sup>N  $T_1$  and  $T_2$  relaxation times were 1130 ± 110 ms and 40.0 ± 4.0 ms, respectively.<sup>40</sup> The  $T_1/T_2$  ratio of 28.2 ± 6.2 corresponds to a correlation time of  $\tau_c \approx 17$  ns. The correlation time expected for the TSN domain obtained by HYDRONMR,<sup>41</sup>  $\tau_c \approx 19$  ns, is very similar, indicating that the protein tumbles as a monomer in solution. The heteronuclear NOE shows internal dynamics at subnanosecond time-scales for the termini of the protein and for the  $\alpha 1$ – $\beta 3$  loop preceding the Tudor domain (residues 744–749). The same stretch of residues also exhibits reduced  $T_1/T_2$  ratios (Fig. 2c). The variations in  $T_1/T_2$  ratios most likely reflect the anisotropy of the diffusion tensor. For example, the elevated ratio for amides in helix  $\alpha 1$  is consistent with its orientation along the main axis of the diffusion tensor.

Taken together, we find that the solution conformation of *Drosophila* TSN is very similar to that of the crystal structure. The <sup>15</sup>N relaxation data indicate that the TSN domain is monomeric and that its Tudor and SN domains form a compact fold and tumble together in solution. This finding is further supported by the presence of a network of electrostatic and hydrophobic interactions that stabilize the relative orientation of the two domains (Supplementary Fig. 1).

### Ligand binding properties of Tudor-SN

We performed NMR titrations to study the binding of TSN with putative ligands (Fig. 3). AR\*GR\*G (1) and AGRGRG (2) are derived from the C-terminal tails of Sm proteins, which have been shown to bind the Tudor domain of SMN.<sup>24,25</sup> These tails comprise RG repeats with arginines that can be symmetrically dimethylated *in vivo*. In addition, we tested binding to sDMA (3) and asymmetrically dimethylated arginines (aDMAs, 4) and to 7-methylguanosine (8) and *N*<sup>2</sup>,*N*<sup>2</sup>,7-trimethylguanosine (9). Finally, monomethyllysine (5), dimethyllysine (6), and trimethyllysine (7) were included because methylated lysines of histone tails have been found to interact with other Tudor domains.<sup>27,28</sup> Ligands were screened for binding using <sup>1</sup>H,<sup>15</sup>N-heteronuclear single quantum correlation (HSQC) spectra recorded on <sup>15</sup>N-labeled TSN. Molecules 5–9 did not induce any significant chemical shift perturbations (CSPs) even at high concentrations (Supplementary Figs. 2 and 3). For ligands 1–4, NMR titrations were analyzed

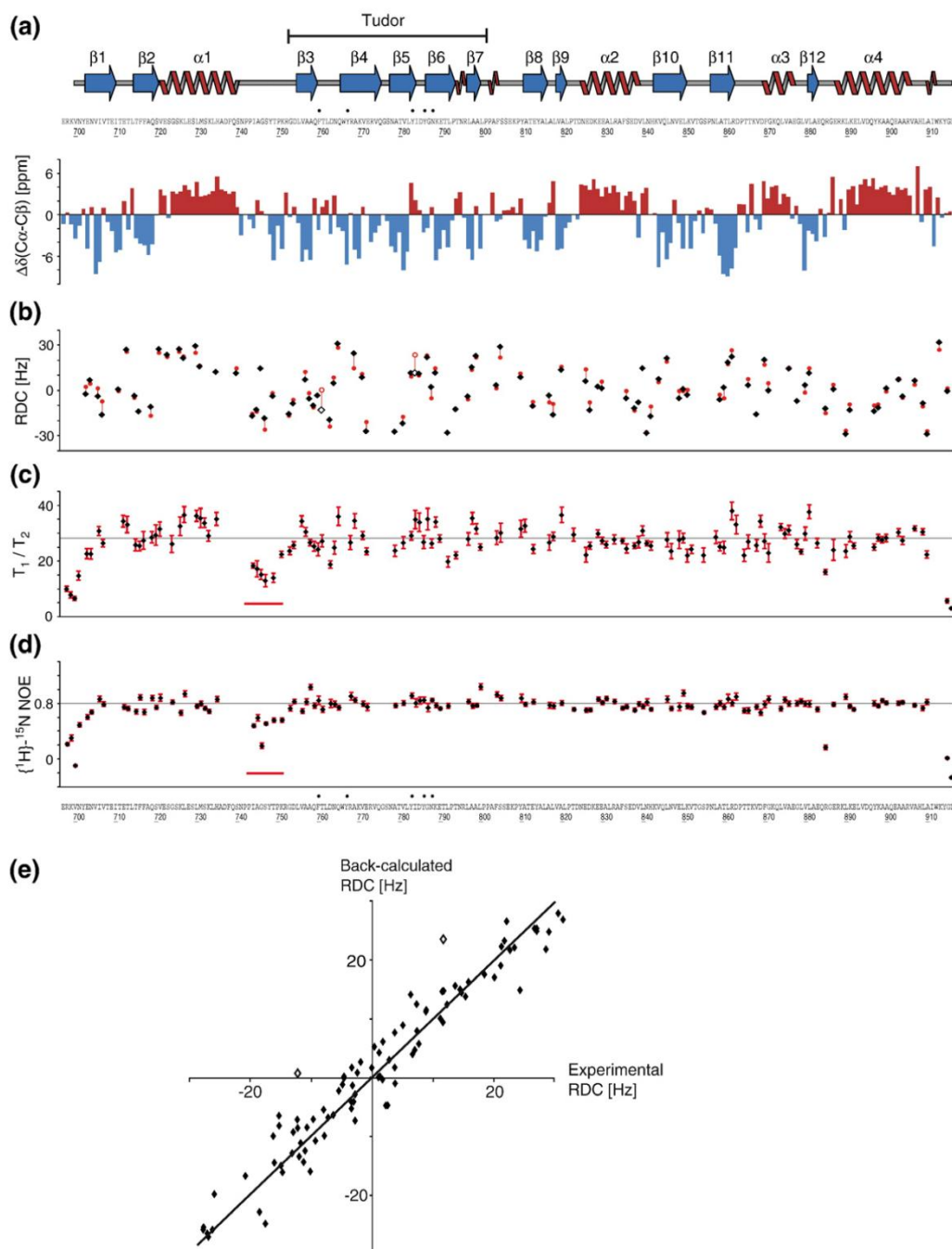


**Fig. 2.** Comparison of crystallography and NMR data. (a) The secondary structure as defined in the crystal structure by DSSP.<sup>36</sup> Filled circles indicate aromatic cage residues. Below, secondary chemical shifts,  $\Delta\delta(^{13}\text{C}^\alpha - ^{13}\text{C}^\beta)$ . Positive (red) and negative (blue) values indicate  $\alpha$ -helical and  $\beta$ -strand conformation, respectively. (b)  $^1\text{H}-^{15}\text{N}$  RDCs. Experimental (black boxes) values compared to back-calculated values from the crystal structure (red circles). Residues exhibiting a large discrepancy ( $>10$  Hz) are shown as open boxes and circles (see the text). (c)  $^{15}\text{N}$  NMR relaxation data. The average ratio of  $T_1/T_2$  relaxation times (28.2) is indicated with a gray line. A flexible loop with reduced  $T_1/T_2$  ratio is marked with a red line. The error was calculated by using  $T_1$  and  $T_2$  with an uncertainty of one standard deviation as estimated by Monte Carlo simulations. (d)  $^{15}\text{N}$  heteronuclear NOE. The average value (0.80) is indicated with a gray line. A flexible loop with reduced values is marked with a red line. The error was calculated as the standard deviation of the noise in the spectrum divided by the intensity of the reference peak. (e) Experimental RDCs *versus* back-calculated values from the crystal structure ( $R$ -factor=0.19). Residues exhibiting a large discrepancy ( $>10$  Hz) are shown as open boxes (see the text).



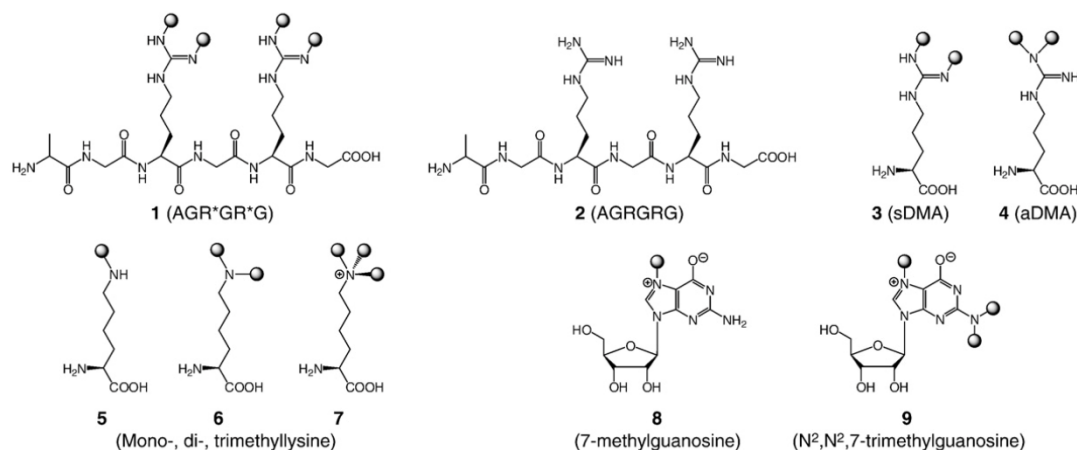


**Fig. 3.** Ligands used for NMR titrations. Spheres symbolize methylation modifications.

quantitatively to derive the binding affinities and map the binding sites of the ligands onto the TSN structure.

A striking difference was seen for the binding of methylated and nonmethylated ARGGRG peptides to the TSN domain (Fig. 4a). Upon addition of **1**, we observed many NMR signals shifting with increasing ligand concentration. These signals correspond to residues of the aromatic cage (F760, Y767, Y783, Y786, and N788; Fig. 4a, second column) or to residues in close spatial proximity. The binding affinity corresponds to a dissociation constant of  $K_d = 660 \pm 70 \mu\text{M}$  based on fitting titration curves for all peaks with  $\text{CSP} > 0.1 \text{ ppm}$  (Table 2). On the other hand, for the corresponding nonmethylated peptide (**2**), hardly any CSPs were observed, even at a ratio of 1:12 (protein:ligand), indicating a significantly weaker interaction (Fig. 4a, right column).

We then analyzed the titration experiments with single-arginine residues in two methylation states (**3** and **4**; Fig. 4b). The titration of sDMA gave rise to CSPs comparable to peptide **1** affecting the same aromatic cage residues (Fig. 4b, middle column). The binding affinity was determined to  $K_d = 720 \pm 100 \mu\text{M}$ , somewhat lower than that for the methylated peptide. The aDMA ligand exhibited a reduced

binding to the same region of the Tudor domain. The observed shifts at a ratio of 1:12 (protein:aDMA) are comparable to the ones seen for sDMA at a protein:ligand ratio of 1:2. This is reflected in an almost 10-fold reduced binding affinity,  $K_d \sim 5 \pm 2 \text{ mM}$  (Table 2).

All available CSPs were extracted for both **1** and **3**, at a protein:ligand ratio of 1:6 (Fig. 5a and b). Both ligand titrations give rise to a similar profile of CSPs, suggesting that only the sDMA residue is recognized by the Tudor domain. There are three major clusters exhibiting large CSPs, two are centered on the aromatic cage residues and a third one is found on the N-terminal helix  $\alpha 1$ . This helix is in the vicinity of the aromatic cage and is packed against the Tudor domain. Mapping of the CSPs onto the surface of the crystal structure shows that the affected residues are located within and around the aromatic cage (Fig. 5c and d).

The electrostatic surface potential of the TSN domain (Fig. 5e) shows a rather negatively charged area in the region of the aromatic cage. This is consistent with binding of ligands containing methylated arginines but makes an interaction with negatively charged molecules, such as RNA or DNA, improbable.

**Fig. 4.** NMR titration experiments with methylated ligands. (a) Titration of methylated and nonmethylated peptides, **1** and **2**, to the TSN domain. Left: overlay of  $^1\text{H}$ ,  $^{15}\text{N}$ -HSQC spectra of TSN, 0.2 mM, with different amounts of ligands. Residues in the aromatic cage are labeled. Reference spectrum is in black. Red, green, and blue spectra correspond to a protein:ligand ratio of 1:1, 1:3, and 1:12, respectively, of ligand **1**. The magenta spectrum corresponds to a protein:ligand ratio of 1:12 of ligand **2**. Middle column: Each of the resonances assigned to the aromatic cage residues are zoomed in. The perturbation at a protein:ligand ratio of 1:12 is indicated by arrows, black for **1** and magenta for **2**. If no shift is observed, this is marked by a cross. Right column: The CSP, calculated as  $\text{CSP} = \sqrt{\delta H(\text{ppm})^2 + 0.1 \times \delta N(\text{ppm})^2}$ , for each residue in the aromatic cage plotted against ligand concentration. Black and magenta curves are fitted to binding data of **1** and **2**, respectively. Both titrations were performed at 900 MHz. (b) Titration of methylated arginines, **3** and **4**, to the TSN domain. Left: overlay of  $^1\text{H}$ ,  $^{15}\text{N}$ -HSQC spectra of TSN, 0.1 mM, with different amounts of ligands. Residues in the aromatic cage are labeled. Reference spectrum is in black. Red, green, and blue spectra correspond to a protein:ligand ratio of 1:1, 1:3, and 1:12, respectively, of ligand **3**. The magenta spectrum corresponds to a protein:ligand ratio of 1:12 of ligand **4**. Middle column: Each of the resonances assigned to the aromatic cage residues are zoomed in. The perturbation at a protein:ligand ratio of 1:12, is indicated by arrows, black for **3** and magenta for **4**. Right column: The CSP for each residue in the aromatic cage plotted against ligand concentration. Black and magenta curves are fitted to binding data of **3** and **4**, respectively. Titrations of **3** and **4** were performed at 900 and 600 MHz, respectively.

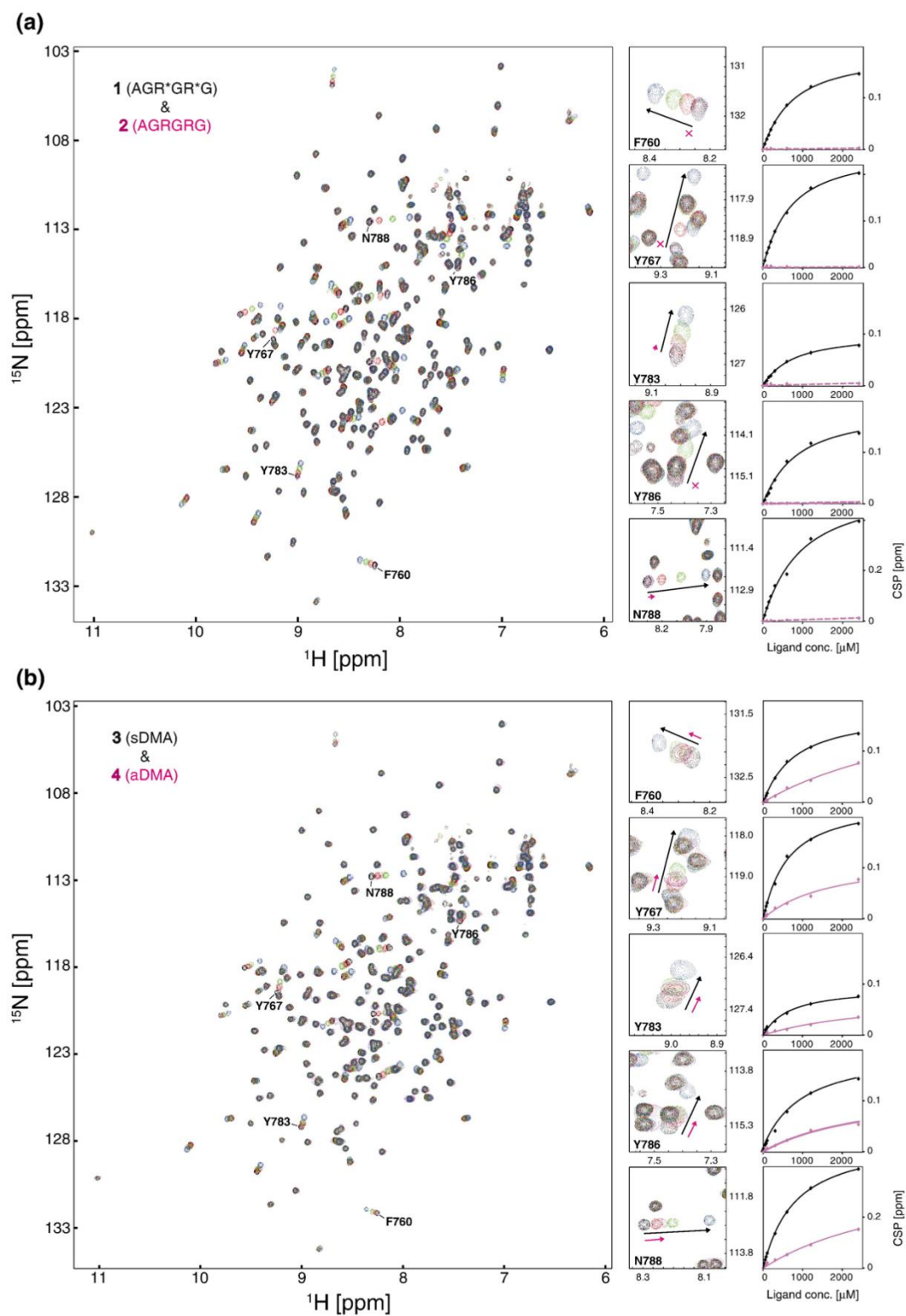


Fig. 4 (legend on previous page)

**Table 2**

Ligand	$K_d$
<b>1</b> (AGR*GR*G)	$660 \pm 70 \mu\text{M}$
<b>2</b> (AGRGRG)	ND
<b>3</b> (sDMA)	$720 \pm 100 \mu\text{M}$
<b>4</b> (aDMA)	$\sim 5 \pm 2 \text{ mM}$

ND, not detectable.

Altogether, these data indicate that the aromatic cage of the Tudor domain mediates specific recognition of a symmetrically methylated arginine side chain by Tudor-SN.

## Discussion

By combining crystallography and solution NMR, we show that the TSN domains of *D. melanogaster* and human Tudor-SN have very similar three-

dimensional structures and that the Tudor and SN domains interact and tumble together in solution. NMR titrations with putative ligands demonstrated that TSN preferentially binds sDMA, alone or in a peptide, via the aromatic cage of the Tudor domain. Furthermore, the binding motif discriminates binding of sDMA against aDMA. The aromatic cage of TSN consists of four aromatic residues and one asparagine, each residue making up one side of the binding cavity. The *Drosophila* and human TSN domain are structurally similar. Specifically, the corresponding aromatic cages are virtually identical, suggesting that both proteins have the same interaction partners *in vivo*. The specific recognition of sDMA suggests that this methylation mark is a prerequisite for the binding of TSN to its ligands.

The binding affinity of the TSN domain for the peptide comprising sDMAs (**1**) is slightly higher compared to sDMA alone (**3**) (Table 2). An increased apparent binding affinity would be consistent with the recognition of a single sDMA by the Tudor

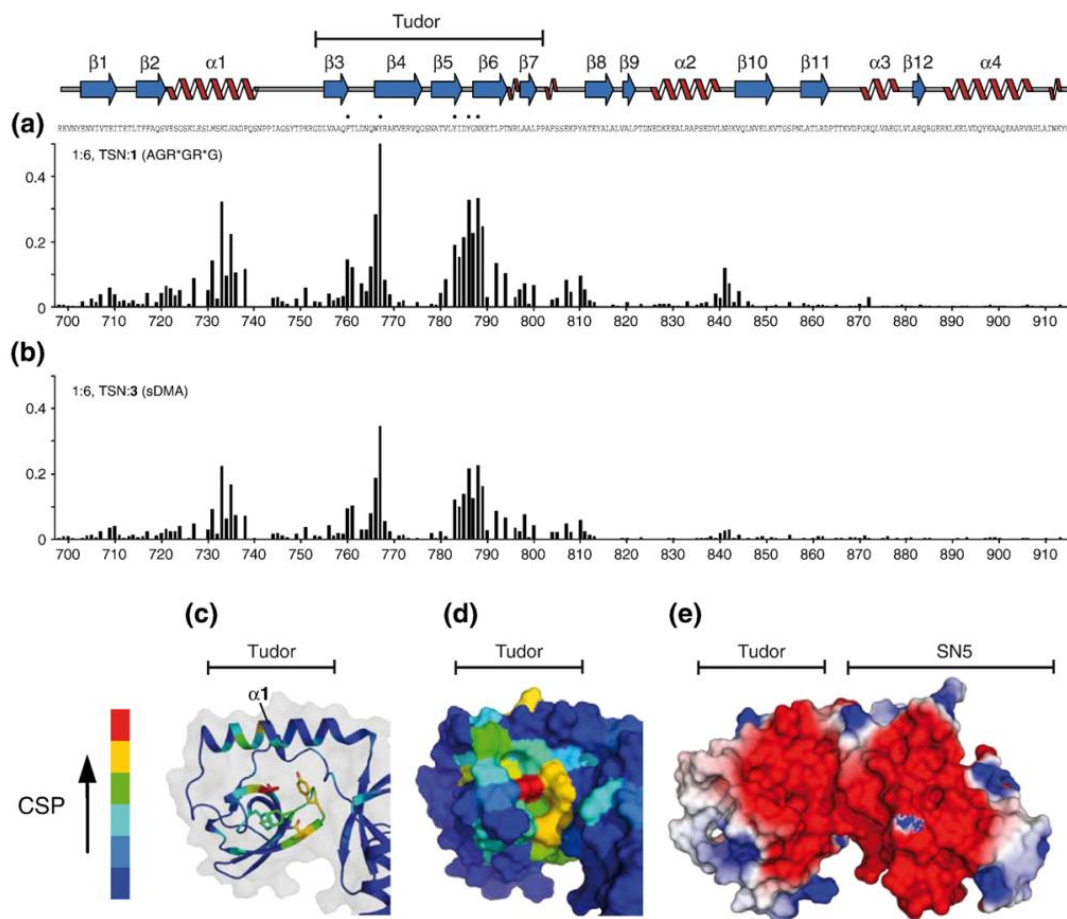


**Fig. 5.** Mapping of binding site onto the crystal structure of the TSN domain: CSP per residue for (a) **1** at a protein:ligand ratio of 1:6, (b) **3** at a protein:ligand ratio of 1:6, and (c) **1** at a protein:ligand ratio of 1:6 mapped onto the crystal structure of the TSN domain. Close-up of the Tudor domain with the aromatic cage residues highlighted as sticks. Coloring goes from blue (no or weak CSP) over light blue, cyan, green, and yellow to red (strong CSP). Same view as in Fig. 1b, right. (d) Surface representation of the mapped CSPs. Same data, view, and coloring as in (c). (e) Surface potential of the TSN domain. Contoured at  $-1.5 k_B \text{Te}^{-1}$  (red) and  $1.5 k_B \text{Te}^{-1}$  (blue). Same view as in (c).



domain, as two ligand motifs in the peptide (ligand 1) yield a statistical factor to the apparent  $K_d$ .<sup>42</sup> Similarly, Sprangers *et al.* observed a significantly enhanced affinity between the SMN Tudor domain and an RG peptide, compared to sDMA alone.<sup>25</sup> Given that in all Tudor domain/methyllysine ligand complexes reported so far, only a single methylated lysine residue is accommodated by the aromatic cage, it is likely that TSN and other sDMA binding Tudor domains also recognize just a single sDMA residue. Overall, the binding affinity of TSN to methylated ligands is weaker compared to that of SMN Tudor and other Tudor domains (Supplementary Table 1). Potentially, additional residues flanking the sDMA

residues in spliceosomal Sm and Lsm proteins<sup>43</sup> may contribute to the interaction. It is also possible that interactions involving other regions of the Tudor-SN protein may contribute to snRNP binding *in vivo*.

There is evidence that Tudor-SN is involved in various cellular processes such as transcription<sup>3,4</sup> and cleavage of edited dsRNAs.<sup>14</sup> However, recent data<sup>5</sup> and the fact that Tudor-SN has an aromatic cage very similar to that of the SMN Tudor domain<sup>24</sup> (Fig. 6a) strongly argue that the Tudor domain is important for a function of Tudor-SN in splicing regulation. The only difference between aromatic cages in the TSN and SMN Tudor domains is the

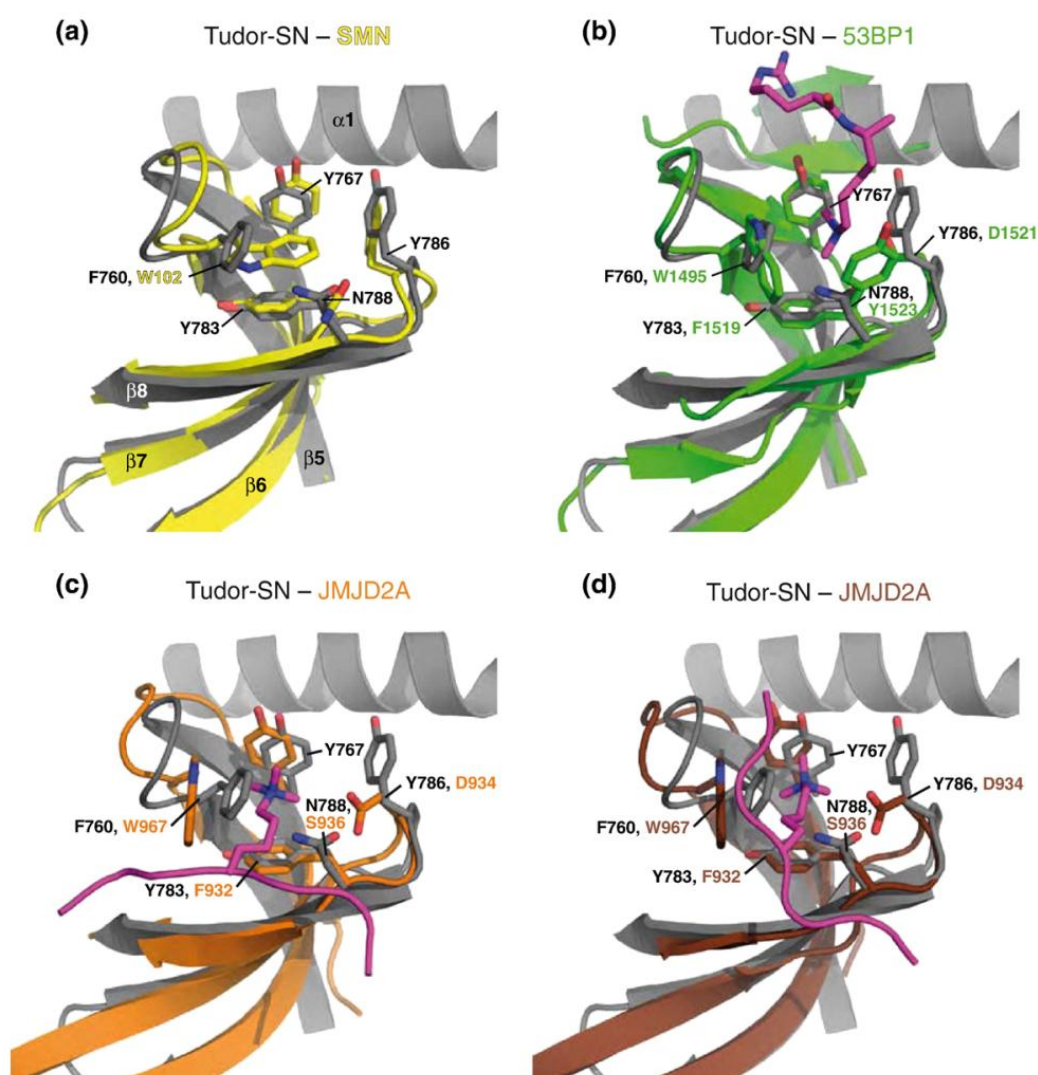


**Fig. 6.** Comparison of the aromatic cage in Tudor-SN with other proteins and analysis of ligand binding modes. Side chains of residues in the Tudor-SN aromatic cage are shown and labeled together with substitutions found in the other proteins. For clarity, only essential parts of the Tudor domains and surrounding structures are shown. Tudor-SN is shown in gray. Superposition of TSN (a) to SMN Tudor (yellow; PDB code: 1MHN), (b) to the 53BP1 tandem Tudor domain in complex with H4K20me2 (green; PDB code: 2IGO), (c) to the JMJD2A tandem hybrid Tudor domain in complex with H3K4me3 (orange; PDB code: 2GFA), and (d) to the JMJD2A tandem hybrid Tudor domain in complex with H4K20me3 (brown; PDB code: 2QQS). Peptide ligands are in magenta.

substitution of F760 by tryptophan in SMN (Fig. 6a). The link to a function in splicing regulation is further supported by our titration data, which shows that the TSN domain has a strong binding preference for sDMAs over other methylated ligands. In line with these data, it has been shown that mutations in the aromatic cage of the human TSN domain (F740, Y746, Y763, or Y766) diminish the interaction to several snRNPs.<sup>23</sup> Double mutants show no binding of snRNPs.

Tudor-SN was first described as a coactivator of transcription by forming a complex with the viral protein EBNA-2.<sup>1</sup> EBNA-2 has an RG-repeat region, which is methylated *in vivo*, and binds to the SMN protein by this motif.<sup>44</sup> Our binding studies suggest how Tudor-SN might interact with EBNA-2. The similarities of the aromatic cages (Fig. 6a) point towards an overlap in binding specificity of Tudor-SN and SMN for methylated binding partners. Interestingly, the Tudor domains of SPF30 and TDRD3 have also been shown to recognize sDMA-methylated Sm proteins, consistent with a conservation of their aromatic cages.<sup>26</sup>

To date, atomic resolution structures are only available for Tudor domains bound to methylated lysines.<sup>45</sup> Albeit the existence of an aromatic cage is common to Tudor domains, the residues involved in the recognition of methylated histone tails by 53BP1 and JMJD2A are distinct from the TSN and SMN Tudor domains. Residues F760, Y783, Y786, and N788, which define the aromatic cage in TSN, are replaced by W1495, F1519, D1521, and Y1523, respectively, in 53BP1 Tudor (Fig. 6b). The 53BP1 Tudor domain recognizes the dimethylated lysine in H4K20me2 mainly using these residues.<sup>27</sup> The aromatic cage of the JMJD2A hybrid tandem domain is similar to that of 53BP1 with a conserved aspartate that is involved in methyllysine binding<sup>28</sup> (Fig. 6c). However, again, the aromatic cage residues F760, Y783, and N788 in TSN are substituted by W967, F932, and S936, respectively, in JMJD2A as well. Compared to 53BP1, the orientation of the H3K4me3 peptide relative to the aromatic cages is different. With respect to the binding orientation of the ligand peptide relative to the aromatic cage of the TSN domain, our NMR titration data suggest that the sDMA peptide may bind in a similar orientation as seen in the 53BP1–H4K20me2 complex. Most of the CSPs are observed for residues in the aromatic cage and, additionally, helix  $\alpha 1$  in TSN. There are little chemical shift changes involving the  $\beta 6$ , as should be expected if the orientation of the ligand would resemble the JMJD2A–H3K4me3 binding mode (Fig. 6c). A further similarity with the 53BP1 binding topology is the presence of an additional interaction surface involving helix  $\alpha 1$  in Tudor-SN. Interestingly, the structure of JMJD2A bound to a different histone tail (H4K20me3)<sup>46</sup> exhibits yet another binding mode of the methylated ligand (Fig. 6d). This suggests that the binding orientation of the methylated ligand relative to the aromatic cage depends on both the ligand and the specific binding pocket presented.

The fact that none of the methylated lysines binds to the extended Tudor domain can, in part, be explained by the distinct composition of the aromatic cage (Fig. 6b–d). For example, the aspartate found in these Tudor domains, and not in Tudor-SN, has been linked to the selectivity for **6** over **7**<sup>27</sup> by forming a hydrogen bond to the ammonium hydrogen. On the other hand, **5** is probably too small to fill the binding cavity in Tudor-SN and to engage interactions required for strong binding.

Taken together, available structural and biochemical data indicate a conserved binding motif for sDMA recognition by a subset of Tudor domains that are distinct from Tudor domains that recognize methyl lysine residues. Structure determination of a Tudor domain–sDMA complex will be required to elucidate the atomic details of this interaction.

5' cap snRNA analogues, such as **8** and **9** (Fig. 3), have also been proposed as putative ligands of Tudor-SN. However, in our NMR titrations, both ligands produce very small chemical shift changes (Supplementary Fig. 3). This suggests that Tudor-SN does not bind to the 5' cap of snRNAs in the spliceosome. Consistent with the titration data, it has been demonstrated that antibodies specific against the trimethylated guanosine cap can efficiently co-immunoprecipitate human Tudor-SN in complex with snRNPs.<sup>5</sup> Thus, the methylated 5' cap of the snRNA is freely available for binding to the antibody and not involved in the interaction between Tudor-SN and snRNPs.

The negative potential surface at the sDMA binding site (Fig. 5e) and UV-crosslink data (A. D. J. Scadden, personal communication) indicate that there is, at best, an extremely weak interaction of the TSN domain with RNA or DNA. A similar negatively charged surface exists in human Tudor-SN,<sup>23</sup> and Li *et al.* found that the TSN domain does not contribute to dsRNA binding.<sup>15</sup> Therefore, it is probable that the implications of Tudor-SN in different biological processes, that is, splicing and RNA editing, might involve distinct regions of the protein. While recognition of dsRNA presumably involves the four N-terminal SN domains, the regulation of splicing is linked to sDMA recognition by the Tudor domain in the C-terminus of Tudor-SN. Further studies should elucidate the molecular details of these interactions and their role for the different biological functions of the Tudor-SN protein.

## Materials and Methods

### Cloning, protein expression, and purification

Several constructs with variations in the N-terminus of the TSN domain in Tudor-SN from *D. melanogaster* were created using standard cloning protocols. The constructs used for NMR and X-ray crystallography included residues 697–916 and 700–916, respectively. The gene and protein sequence of full-length Tudor-SN from *D. melanogaster* can be found at Ensembl (accession code: FBGN0035121). Both gene fragments were inserted in a modified pETM-11



vector [European Molecular Biology Laboratory (EMBL)] containing a His<sub>6</sub>-tag for purification, a Z-tag for increased protein solubility, both at the N-terminus, and a tobacco etch virus cleavage site for removal of the tags. Proteins were expressed with high yields (>50 mg/L) in *E. coli* BL21 (DE3) and LB medium at 20 °C overnight after induction at an optical density of 0.8 with 1 mM IPTG. After sonication and ultracentrifugation, the protein was bound to Ni<sup>2+</sup>-resin (Ni-NTA Agarose, Qiagen) and subsequently washed with low- and high-salt buffer, as well as with buffer containing 30 mM imidazole. The eluted protein was buffer exchanged before tobacco etch virus cleavage (room temperature, overnight), and the cleaved tags were removed by a second Ni<sup>2+</sup> column. The sample was then further purified by size-exclusion chromatography (HiLoad 16/60 Superdex 75, GE Healthcare Biosciences). Nonlabeled samples for crystallography were kept in a standard Tris buffer (20 mM Tris, pH 6.8, 300 mM NaCl, and 1 mM β-mercaptoethanol) at a concentration of 2 mM (50 mg/ml). Plasmids were sequenced and protein samples were checked by mass spectrometry.

Isotopically labeled protein samples for NMR studies were expressed in minimal medium (M9) enriched with the isotopes needed and purified in the same way as described above. For triple-resonance experiments, a triple-labeled sample was prepared using <sup>15</sup>NH<sub>4</sub>Cl and [U-<sup>13</sup>C]-D-glucose as sole nitrogen and carbon source, respectively, and expressed in 90% <sup>2</sup>H<sub>2</sub>O. For other NMR experiments, <sup>15</sup>N-labeled protein was used. NMR samples were kept in sodium phosphate buffer (50 mM NaPO<sub>4</sub>, pH 6.8, 300 mM NaCl, and 1 mM DTT) at concentrations ranging from 0.8 to 1.6 mM (20–40 mg/ml).

### Crystallization and structure determination

Screening for crystallization conditions and data collection was carried out at EMBL Heidelberg. Crystals were grown in hanging drops with 1 μl protein solution (40 mg/ml) and 1 μl precipitant (20% polyethylene glycol 3350, 100 mM Bis-Tris, pH 5.5, and 200 mM NaCl) at 20 °C. Crystals appeared during the first week and were flash-frozen in liquid nitrogen after cryoprotection using the same buffer as above but with 23% polyethylene glycol 3350 and 10% ethylene glycol. A 2.1-Å data set was collected using an in-house diffractor system equipped with a rotating anode X-ray source, osmic mirrors, a MAR345 plate detector, and cryocooling.

The diffraction data were processed with the XDS program package.<sup>32</sup> Phasing the data was done by molecular replacement (Phaser<sup>47</sup>) using human Tudor-SN (PDB code: 2HQE) as a search model (42% identity). The model had been prepared manually by deleting loops and mutating nonidentical residues to alanines. The SN and the Tudor domain were split up and searched for separately. Two molecules of the protein were found in the asymmetric unit, and the solution was refined in rounds with REFMAC5<sup>33</sup> and by manual model correction in Coot.<sup>48</sup> TLS refinement<sup>49</sup> was used as well as one round of simulated annealing refinement with PHENIX.<sup>50</sup> Water molecules were added with ARP/wARP<sup>51</sup> as implemented in REFMAC5. M699 in the refined structure is a cloning artifact. MolProbity<sup>34</sup> was used for structure validation. See Table 1 for structure statistics.

Secondary structure was assigned with a DSSP<sup>36</sup> algorithm. RMSD values were calculated in MOLMOL.<sup>52</sup> In the case of comparing chains A and B in the structure solution, RMSD was determined over the backbone atoms of 215 residues. The corresponding number for comparing

chain A with human Tudor-SN (PDB code: 2HQE) was 205. Based on a sequence alignment (Fig. 1a), the residues just before or after gaps were removed before the calculation.

PyMOL<sup>53</sup> was used for molecular graphics and DELPHI<sup>54</sup> was used for calculating surface potentials.

### NMR spectroscopy

NMR measurements were carried out at 305 K on Bruker 900-, 600-, and 500-MHz spectrometers equipped with cryoprobes and pulsed field gradients. Spectra were processed with NMRPipe<sup>55</sup> and analyzed in NMRView<sup>56</sup> (ver. 5.0.4). For assignment of protein backbone resonances, the following 3D heteronuclear experiments (<sup>2</sup>H decoupled TROSY: transverse relaxation optimized spectroscopy versions) were recorded on a 0.8-mM triple-labeled protein sample: HNCA, HNCACB, HN(CO)CA, and HN(CO)(CA)CB.<sup>57</sup> (H)CC(CO)NH-TOCSY (total correlation spectroscopy) and <sup>15</sup>N NOE spectroscopy-HSQC (120 ms mixing time) spectra were also recorded to facilitate assignment.<sup>57</sup> The secondary chemical shift analysis was done in NMRView.<sup>56</sup>

Relaxation measurements were performed at 600 MHz proton Larmor frequency with a 0.5-mM <sup>15</sup>N-labeled sample.<sup>58</sup> *T*<sub>1</sub> was measured in an interleaved fashion at 12 relaxation delays ranging from 21 to 2580 ms. Similarly, *T*<sub>2</sub> was measured at 10 time points in the range of 11–123 ms. These data and the {<sup>1</sup>H}-<sup>15</sup>N heteronuclear NOE were evaluated with the relaxation analysis packages of NMRView<sup>56</sup> (ver. 4.1.3). The average of these relaxation parameters were calculated for residues fulfilling certain criteria as described previously<sup>40</sup> with errors estimated as one standard deviation of included values. The correlation time (*τ*<sub>c</sub>) was estimated using the ratio of averaged *T*<sub>1</sub> and *T*<sub>2</sub> values and compared to a theoretical value obtained with HYDRONMR<sup>41</sup> using standard input parameters at 305 K.

<sup>1</sup>H<sup>N</sup>-<sup>15</sup>N RDCs were recorded in a two-dimensional, doublet-separated, sensitivity-enhanced HSQC experiment with (J+D) splitting in the nitrogen dimension.<sup>59</sup> The reference spectrum was recorded on a 0.6-mM <sup>15</sup>N, <sup>13</sup>C, <sup>2</sup>H-labeled sample, whereas the concentration of the oriented sample was 0.2 mM. The protein was aligned using a liquid crystalline phase media composed of 3.5 w/w% pentaethylene glycol (Sigma) and hexanol at a molar ratio of 1:0.84 (pentaethylene glycol:hexanol).<sup>60</sup> This gave rise to a 17-Hz splitting of the <sup>2</sup>H<sub>2</sub>O signal. The 96 RDCs that could be extracted were analyzed with DC.<sup>61</sup> The *R*-factor<sup>38</sup> was computed as

$$R = \sqrt{\frac{\sum_{i=0}^N (RDC_{Exp} - RDC_{Calc})^2}{2 \times N \times D_a^2 \times \frac{4 + 3R_h^2}{5}}}$$

where *RDC*<sub>Exp</sub> and *RDC*<sub>Calc</sub> are the experimental and the calculated value of the RDC, respectively, *D*<sub>a</sub> is the axial component of the alignment tensor, and *R*<sub>h</sub> is the rhombicity. The two latter values were determined to *D*<sub>a</sub> = 15.2 and *R*<sub>h</sub> = 0.556.

### Binding studies and determination of binding affinities

To investigate ligand binding, we recorded <sup>1</sup>H,<sup>15</sup>N-HSQC spectra at appropriate ranges of titration points at different field strengths (see figure legends). Titrations with peptides and methylated guanosines were performed at a protein concentration of 0.2 mM with sDMA and aDMA, and for methylated lysines, they were performed at 0.1 mM. The peptides (2) with and without

sDMA modification were purchased from Peptide Specialty Laboratories (Heidelberg, Germany). Compounds **8** and **9** were bought from MP Biomedicals and Biolog (Germany), respectively. Methylated amino acids such as sDMA, aDMA, and methylated lysines were purchased from Sigma, Calbiochem, and Bachem (USA), respectively. All ligands were used without further purification. The ligands were titrated into the protein samples in small volumes of highly concentrated solutions leading to negligible dilution. No pH effects were observed.

The ligand binding occurred in the fast-exchange regime, and peaks were manually traced in the NMR spectra. Binding affinities were determined with an NMRView plug-in from Kevin Gardner (University of Texas Southwestern Medical Center) together with scripts written by Bernd Simon (EMBL). CSPs were fitted to

$$\text{CSP} = \frac{\text{CSP}_{\max} \times \left( ([L] + [P_{\text{tot}}] + K_d) - \sqrt{([L] + [P_{\text{tot}}] + K_d)^2 - 4 \times [L] \times [P_{\text{tot}}]} \right)}{2 \times [P_{\text{tot}}]}$$

where  $\text{CSP}_{\max}$  is the CSP at ligand saturation,  $[L]$  is the ligand concentration,  $[P_{\text{tot}}]$  is the total protein concentration, and  $K_d$  is the equilibrium dissociation constant. Only peaks with  $\text{CSP}_{\max} > 0.1$  ppm were used for calculating the  $K_d$ , and signals exhibiting severe overlap were omitted. A total of 14, 12, and 7 peaks were included in the calculations for the methylated peptide, sDMA, and aDMA, respectively. The average  $K_d$  value is given together with an estimated error of one standard deviation for the fitted titration curves.

#### Accession codes

Protein structure coordinates and structure factors have been deposited at the PDB (accession code: 2WAC).

#### Acknowledgements

We thank Elena Conti and Jerome Basquin (MPI Martinsried) for access to their crystallization facilities, Atlanta Cook (MPI Martinsried) and Michael Groll (TU München) for help during structure determination, Andreas Lingel (Genentech, Inc.) for initial work, Bernd Simon (EMBL Heidelberg) for support with the NMR data, and Deirdre Scadden (University of Cambridge) for useful discussions.

A.F. acknowledges a PhD fellowship from Helmholtz Zentrum München. A.M. is supported by a PhD fellowship (SFRH/BD/22323/2005) from the Portuguese Foundation for Science and Technology. This work was supported by the Deutsche Forschungsgemeinschaft (Sa 823/5) and European Commission (3D Repertoire, LSHG-CT-2005-512028).

#### Supplementary Data

Supplementary data associated with this article can be found, in the online version, at [doi:10.1016/j.jmb.2009.02.018](https://doi.org/10.1016/j.jmb.2009.02.018)

#### References

- Tong, X., Drapkin, R., Yalamanchili, R., Mosialos, G. & Kieff, E. (1995). The Epstein-Barr virus nuclear protein 2 acidic domain forms a complex with a novel cellular coactivator that can interact with TFIIE. *Mol. Cell. Biol.* **15**, 4735–4744.
- Paukku, K., Yang, J. & Silvennoinen, O. (2003). Tudor and nuclease-like domains containing protein p100 function as coactivators for signal transducer and activator of transcription 5. *Mol. Endocrinol.* **17**, 1805–1814.
- Yang, J., Aittomaki, S., Pesu, M., Carter, K., Saarinen, J., Kalkkinen, N. *et al.* (2002). Identification of p100 as a coactivator for STAT6 that bridges STAT6 with RNA polymerase II. *EMBO J.* **21**, 4950–4958.
- Levenson, J. D., Koskinen, P. J., Orrico, F. C., Rainio, E. M., Jalkanen, K. J., Dash, A. B. *et al.* (1998). Pim-1 kinase and p100 cooperate to enhance c-Myb activity. *Mol. Cell.* **2**, 417–425.
- Yang, J., Valineva, T., Hong, J., Bu, T., Yao, Z., Jensen, O. N. *et al.* (2007). Transcriptional co-activator protein p100 interacts with snRNP proteins and facilitates the assembly of the spliceosome. *Nucleic Acids Res.* **35**, 4485–4494.
- Listerman, I., Sapra, A. K. & Neugebauer, K. M. (2006). Cotranscriptional coupling of splicing factor recruitment and precursor messenger RNA splicing in mammalian cells. *Nat. Struct. Mol. Biol.* **13**, 815–822.
- Lin, S., Coutinho-Mansfield, G., Wang, D., Pandit, S. & Fu, X. D. (2008). The splicing factor SC35 has an active role in transcriptional elongation. *Nat. Struct. Mol. Biol.* **15**, 819–826.
- Phatnani, H. P. & Greenleaf, A. L. (2006). Phosphorylation and functions of the RNA polymerase II CTD. *Genes Dev.* **20**, 2922–2936.
- Bass, B. L. (2002). RNA editing by adenosine deaminases that act on RNA. *Annu. Rev. Biochem.* **71**, 817–846.
- Scadden, A. D. & O'Connell, M. A. (2005). Cleavage of dsRNAs hyper-edited by ADARs occurs at preferred editing sites. *Nucleic Acids Res.* **33**, 5954–5964.
- Ohlson, J., Pedersen, J. S., Haussler, D. & Ohman, M. (2007). Editing modifies the GABA(A) receptor subunit alpha3. *RNA*, **13**, 698–703.
- Schoft, V. K., Schopoff, S. & Jantsch, M. F. (2007). Regulation of glutamate receptor B pre-mRNA splicing by RNA editing. *Nucleic Acids Res.* **35**, 3723–3732.
- Chen, L. L., DeCero, J. N. & Carmichael, G. G. (2008). Alu element-mediated gene silencing. *EMBO J.* **27**, 1694–1705.
- Scadden, A. D. (2005). The RISC subunit Tudor-SN binds to hyper-edited double-stranded RNA and promotes its cleavage. *Nat. Struct. Mol. Biol.* **12**, 489–496.
- Li, C. L., Yang, W. Z., Chen, Y. P. & Yuan, H. S. (2008). Structural and functional insights into human Tudor-SN, a key component linking RNA interference and editing. *Nucleic Acids Res.* **36**, 3579–3589.
- Yang, W., Chendrimada, T. P., Wang, Q., Higuchi, M., Seeburg, P. H., Shiekhattar, R. & Nishikura, K. (2006). Modulation of microRNA processing and expression through RNA editing by ADAR deaminases. *Nat. Struct. Mol. Biol.* **13**, 13–21.
- Kawahara, Y., Zinshteyn, B., Sethupathy, P., Iizasa, H., Hatzigeorgiou, A. G. & Nishikura, K. (2007). Redirection of silencing targets by adenosine-to-inosine editing of miRNAs. *Science*, **315**, 1137–1140.
- Caudy, A. A., Ketting, R. F., Hammond, S. M., Denli, A. M., Bathorn, A. M., Tops, B. B. *et al.* (2003). A



- micrococcal nuclease homologue in RNAi effector complexes. *Nature*, **425**, 411–414.
19. Paukku, K., Kalkkinen, N., Silvennoinen, O., Kontula, K. K. & Lehtonen, J. Y. (2008). p100 increases AT1R expression through interaction with AT1R 3'-UTR. *Nucleic Acids Res.* **36**, 4474–4487.
  20. Valineva, T., Yang, J., Palovuori, R. & Silvennoinen, O. (2005). The transcriptional co-activator protein p100 recruits histone acetyltransferase activity to STAT6 and mediates interaction between the CREB-binding protein and STAT6. *J. Biol. Chem.* **280**, 14989–14996.
  21. Callebaut, I. & Mornon, J. P. (1997). The human EBNA-2 coactivator p100: multidomain organization and relationship to the staphylococcal nuclease fold and to the tudor protein involved in *Drosophila melanogaster* development. *Biochem. J.* **321**, 125–132.
  22. Ponting, C. P. (1997). P100, a transcriptional coactivator, is a human homologue of staphylococcal nuclease. *Protein Sci.* **6**, 459–463.
  23. Shaw, N., Zhao, M., Cheng, C., Xu, H., Saarikettu, J., Li, Y. *et al.* (2007). The multifunctional human p100 protein 'hooks' methylated ligands. *Nat. Struct. Mol. Biol.* **14**, 779–784.
  24. Selenko, P., Sprangers, R., Stier, G., Buhler, D., Fischer, U. & Sattler, M. (2001). SMN tudor domain structure and its interaction with the Sm proteins. *Nat. Struct. Mol. Biol.* **8**, 27–31.
  25. Sprangers, R., Groves, M. R., Sinning, I. & Sattler, M. (2003). High-resolution X-ray and NMR structures of the SMN-Tudor domain: conformational variation in the binding site for symmetrically dimethylated arginine residues. *J. Mol. Biol.* **327**, 507–520.
  26. Cote, J. & Richard, S. (2005). Tudor domains bind symmetrical dimethylated arginines. *J. Biol. Chem.* **280**, 28476–28483.
  27. Botuyan, M. V., Lee, J., Ward, I. M., Kim, J. E., Thompson, J. R., Chen, J. & Mer, G. (2006). Structural basis for the methylation state-specific recognition of histone H4-K20 by 53BP1 and Crb2 in DNA repair. *Cell*, **127**, 1361–1373.
  28. Huang, Y., Fang, J., Bedford, M. T., Zhang, Y. & Xu, R. M. (2006). Recognition of histone H3 lysine-4 methylation by the double tudor domain of JMJD2A. *Science*, **312**, 748–751.
  29. Buhler, D., Raker, V., Luhrmann, R. & Fischer, U. (1999). Essential role for the tudor domain of SMN in spliceosomal U snRNP assembly: implications for spinal muscular atrophy. *Hum. Mol. Genet.* **8**, 2351–2357.
  30. Sanders, S. L., Portoso, M., Mata, J., Bahler, J., Allshire, R. C. & Kouzarides, T. (2004). Methylation of histone H4 lysine 20 controls recruitment of Crb2 to sites of DNA damage. *Cell*, **119**, 603–614.
  31. Mouaikel, J., Verheggen, C., Bertrand, E., Tazi, J. & Bordonne, R. (2002). Hypermethylation of the cap structure of both yeast snRNAs and snoRNAs requires a conserved methyltransferase that is localized to the nucleolus. *Mol. Cell*, **9**, 891–901.
  32. Kabsch, W. (1993). Automatic processing of rotation diffraction data from crystals of initially unknown symmetry and cell constants. *J. Appl. Crystallogr.* **26**, 795–800.
  33. Murshudov, G. N., Vagin, A. A. & Dodson, E. J. (1997). Refinement of macromolecular structures by the maximum-likelihood method. *Acta Crystallogr., Sect. D: Biol. Crystallogr.* **53**, 240–255.
  34. Davis, I. W., Leaver-Fay, A., Chen, V. B., Block, J. N., Kapral, G. J., Wang, X. *et al.* (2007). MolProbity: all-atom contacts and structure validation for proteins and nucleic acids. *Nucleic Acids Res.* **35**, W375–W383.
  35. Libson, A. M., Gittis, A. G. & Lattman, E. E. (1994). Crystal structures of the binary Ca<sup>2+</sup> and pdTp complexes and the ternary complex of the Asp21→Glu mutant of staphylococcal nuclease. Implications for catalysis and ligand binding. *Biochemistry*, **33**, 8007–8016.
  36. Kabsch, W. & Sander, C. (1983). Dictionary of protein secondary structure: pattern recognition of hydrogen-bonded and geometrical features. *Biopolymers*, **22**, 2577–2637.
  37. Wishart, D. S. & Sykes, B. D. (1994). The <sup>13</sup>C chemical-shift index: a simple method for the identification of protein secondary structure using <sup>13</sup>C chemical-shift data. *J. Biomol. NMR*, **4**, 171–180.
  38. Clore, G. M. & Garrett, D. S. (1999). R-factor, free R, and complete cross-validation for dipolar coupling refinement of NMR structures. *J. Am. Chem. Soc.* **121**, 9008–9012.
  39. Eyal, E., Gerzon, S., Potapov, V., Edelman, M. & Sobolev, V. (2005). The limit of accuracy of protein modeling: influence of crystal packing on protein structure. *J. Mol. Biol.* **351**, 431–442.
  40. Tjandra, N., Kuboniwa, H., Ren, H. & Bax, A. (1995). Rotational dynamics of calcium-free calmodulin studied by <sup>15</sup>N-NMR relaxation measurements. *Eur. J. Biochem.* **230**, 1014–1024.
  41. Garcia de la Torre, J., Huertas, M. L. & Carrasco, B. (2000). HYDRONMR: prediction of NMR relaxation of globular proteins from atomic-level structures and hydrodynamic calculations. *J. Magn. Reson.* **147**, 138–146.
  42. Kelly, R. C., Jensen, D. E. & von Hippel, P. H. (1976). DNA "melting" proteins. IV. Fluorescence measurements of binding parameters for bacteriophage T4 gene 32-protein to mono-, oligo-, and polynucleotides. *J. Biol. Chem.* **251**, 7240–7250.
  43. Brahms, H., Raymackers, J., Union, A., de Keyser, F., Meheus, L. & Luhrmann, R. (2000). The C-terminal RG dipeptide repeats of the spliceosomal Sm proteins D1 and D3 contain symmetrical dimethylarginines, which form a major B-cell epitope for anti-Sm autoantibodies. *J. Biol. Chem.* **275**, 17122–17129.
  44. Barth, S., Liss, M., Voss, M. D., Dobner, T., Fischer, U., Meister, G. & Grasser, F. A. (2003). Epstein-Barr virus nuclear antigen 2 binds via its methylated arginine-glycine repeat to the survival motor neuron protein. *J. Virol.* **77**, 5008–5013.
  45. Corsini, L. & Sattler, M. (2007). Tudor hooks up with DNA repair. *Nat. Struct. Mol. Biol.* **14**, 98–99.
  46. Lee, J., Thompson, J. R., Botuyan, M. V. & Mer, G. (2008). Distinct binding modes specify the recognition of methylated histones H3K4 and H4K20 by JMJD2A-tudor. *Nat. Struct. Mol. Biol.* **15**, 109–111.
  47. McCoy, A. J., Grosse-Kunstleve, R. W., Adams, P. D., Winn, M. D., Storoni, L. C. & Read, R. J. (2007). Phaser crystallographic software. *J. Appl. Crystallogr.* **40**, 658–674.
  48. Emsley, P. & Cowtan, K. (2004). Coot: model-building tools for molecular graphics. *Acta Crystallogr., Sect. D: Biol. Crystallogr.* **60**, 2126–2132.
  49. Winn, M. D., Isupov, M. N. & Murshudov, G. N. (2001). Use of TLS parameters to model anisotropic displacements in macromolecular refinement. *Acta Crystallogr., Sect. D: Biol. Crystallogr.* **57**, 122–133.
  50. Adams, P. D., Grosse-Kunstleve, R. W., Hung, L. W., Ioerger, T. R., McCoy, A. J., Moriarty, N. W. *et al.* (2002). PHENIX: building new software for automated crystallographic structure determination. *Acta Crystallogr., Sect. D: Biol. Crystallogr.* **58**, 1948–1954.
  51. Perrakis, A., Morris, R. & Lamzin, V. S. (1999).



- Automated protein model building combined with iterative structure refinement. *Nat. Struct. Biol.* **6**, 458–463.
52. Koradi, R., Billeter, M. & Wuthrich, K. (1996). MOLMOL: a program for display and analysis of macromolecular structures. *J. Mol. Graphics* **14**, 51–55, 29–32.
  53. DeLano, W. L. (2002). The PyMOL Molecular Graphics System DeLano Scientific, San Carlos, CA.
  54. Rocchia, W., Alexov, E. & Honig, B. (2001). Extending the applicability of the nonlinear Poisson–Boltzmann equation: multiple dielectric constants and multi-valent ions. *J. Phys. Chem. B*, **105**, 6507–6514.
  55. Delaglio, F., Grzesiek, S., Vuister, G. W., Zhu, G., Pfeifer, J. & Bax, A. (1995). NMRPipe: a multidimensional spectral processing system based on UNIX pipes. *J. Biomol. NMR*, **6**, 277–293.
  56. Johnson, B. A. & Blevins, R. A. (1994). NMRView: a computer program for the visualization and analysis of NMR data. *J. Biomol. NMR*, **4**, 603–614.
  57. Sattler, M., Schleucher, J. & Griesinger, C. (1999). Heteronuclear multidimensional NMR experiments for the structure determination of proteins in solution employing pulsed. *Prog. Nucl. Magn. Reson. Spectrosc.* **34**, 93–158.
  58. Farrow, N. A., Muhandiram, R., Singer, A. U., Pascal, S. M., Kay, C. M., Gish, G. *et al.* (1994). Backbone dynamics of a free and phosphopeptide-complexed Src homology 2 domain studied by <sup>15</sup>N NMR relaxation. *Biochemistry*, **33**, 5984–6003.
  59. Cordier, F., Dingley, A. J. & Grzesiek, S. (1999). A doublet-separated sensitivity-enhanced HSQC for the determination of scalar and dipolar one-bond J-couplings. *J. Biomol. NMR*, **13**, 175–180.
  60. Ruckert, M. & Otting, G. (2000). Alignment of biological macromolecules in novel nonionic liquid crystalline media for NMR experiments. *J. Am. Chem. Soc.* **122**, 7793–7797.
  61. Kontaxis, G., Delaglio, F. & Bax, A. (2005). Molecular fragment replacement approach to protein structure determination by chemical shift and dipolar homology database mining. *Methods Enzymol.* **394**, 42–78.

### 3.3. Supplementary material

#### Supplementary Table 1

Protein domains and their affinity to different methylated ligands.

Protein	Domain	Ligand	K <sub>D</sub>	Reference
SMN	Tudor	(R*G) <sub>4</sub>	low μM	1
SMN	Tudor	R*	high μM	1
JMJD2A	Tudor	H3K4me3	0.50 ± 0.03 μM, 10.4 μM	2, 3
JMJD2A	Tudor	H4K20me3	0.4 ± 0.03 μM	2
53BP1	Tudor	H4K20me1	52.9 ± 2.2 μM	4
53BP1	Tudor	H4K20me2	19.7 ± 0.7 μM	4
HP1	Chromodomain	H3K9me2	2.1 μM	5
HP1	Chromodomain	H3K9me3	1.9 μM	5
dSfmbt	MBT repeat	H3K9me1	7 ± 2 μM	6
dSfmbt	MBT repeat	H3K9me2	9 ± 2 μM	6
dSfmbt	MBT repeat	H3K9me3	110 ± 2 μM	6
dSfmbt	MBT repeat	H4K20me1	8 ± 1 μM	6
dSfmbt	MBT repeat	H4K20me2	12 ± 3 μM	6
dSfmbt	MBT repeat	H4K20me3	130 ± 15 μM	6
BPTF	PHD Finger	H3K4me1	ND	7
BPTF	PHD Finger	H3K4me2	5.0 μM	7
BPTF	PHD Finger	H3K4me3	2.7 μM	7
RAG2	PHD Finger	H3K4me0	499 ± 55 μM	8
RAG2	PHD Finger	H3K4me1	118 ± 36 μM	8
RAG2	PHD Finger	H3K4me2	60 ± 20 μM	8
RAG2	PHD Finger	H3K4me3	4.15 ± 0.21 μM	8

R\* - symmetrically dimethylated arginine (sDMA); ND - not detectable

<sup>1</sup> Sprangers et al. (2008). High-resolution X-ray and NMR structures of the SMN Tudor domain: conformational variation in the binding site for symmetrically dimethylated arginine residues. *J Mol Biol* 327, 507-20

<sup>2</sup> Lee et al. (2008). Distinct binding modes specify the recognition of methylated histones H3K4 and H4K20 by JMJD2A-tudor. *Nat Struct Mol Biol* 15, 109-11

<sup>3</sup> Huang, et al. (2006). Recognition of histone H3 lysine-4 methylation by the double tudor domain of JMJD2A. *Science* 312, 748-51

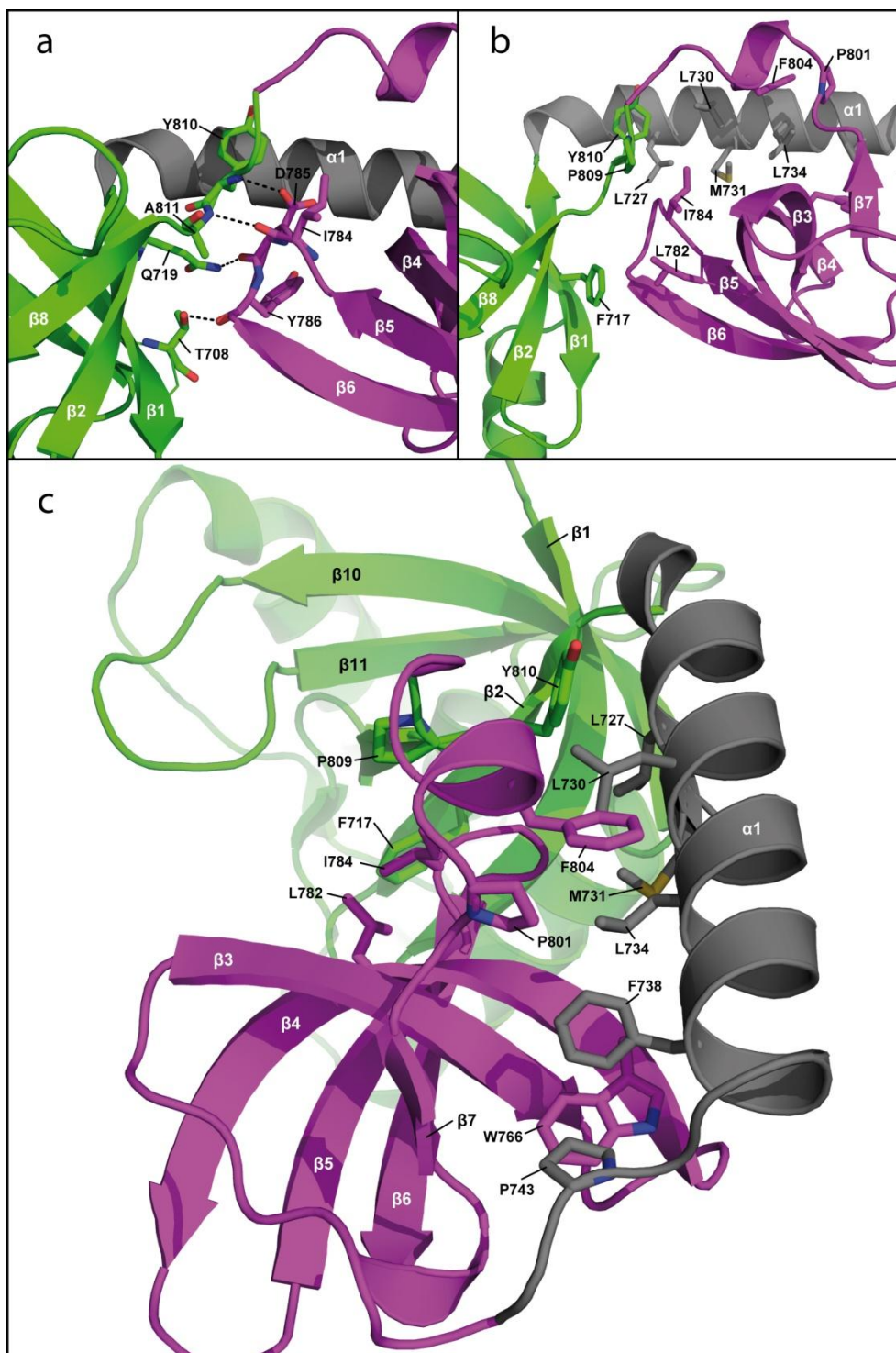
<sup>4</sup> Botuyan et al. (2006). Structural basis for the methylation state-specific recognition of histone H4-K20 by 53BP1 and Crb2 in DNA repair. *Cell* 127, 1361-73

<sup>5</sup> Nielsen et al. (2002) Structure of the HP1 chromodomain bound to histone H3 methylated at lysine 9. *Nature* 416, 103-107

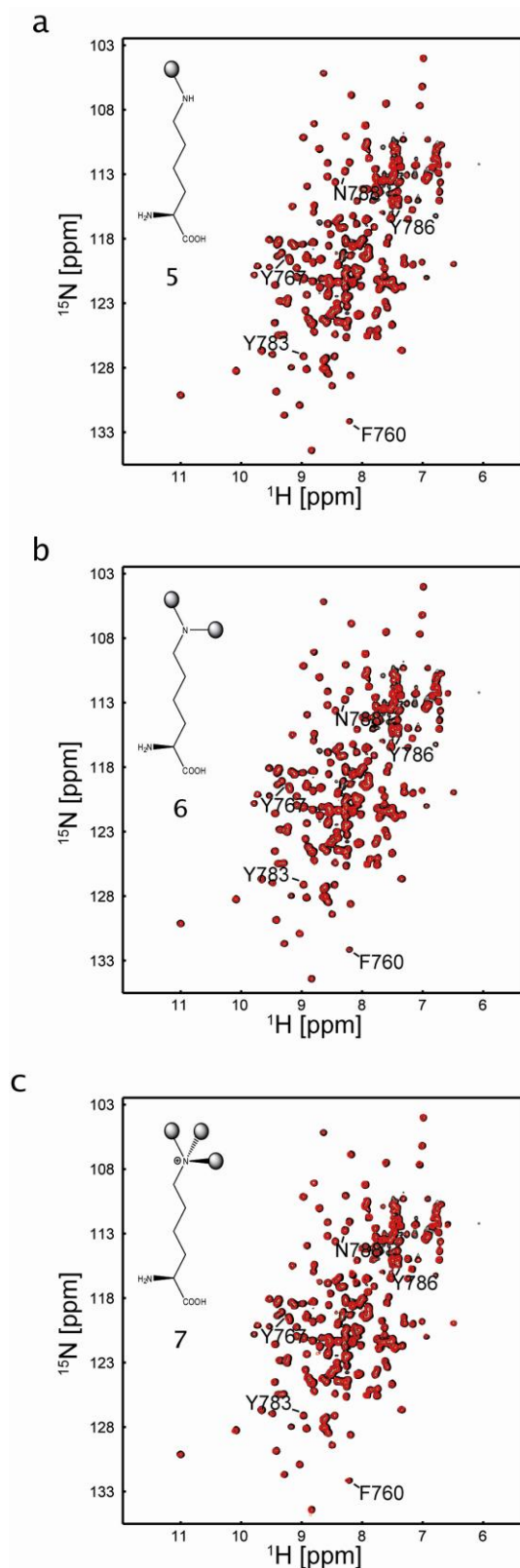
<sup>6</sup> Klymenko et al. (2006) A Polycomb group protein complex with sequence-specific DNA-binding and selective methyl-lysine-binding activities. *Genes Dev.* 20, 1110-22

<sup>7</sup> Li et al. (2006) Molecular basis for site-specific read-out of histone H3K4me3 by the BPTF PHD finger of NURF. *Nature* 442, 91-95

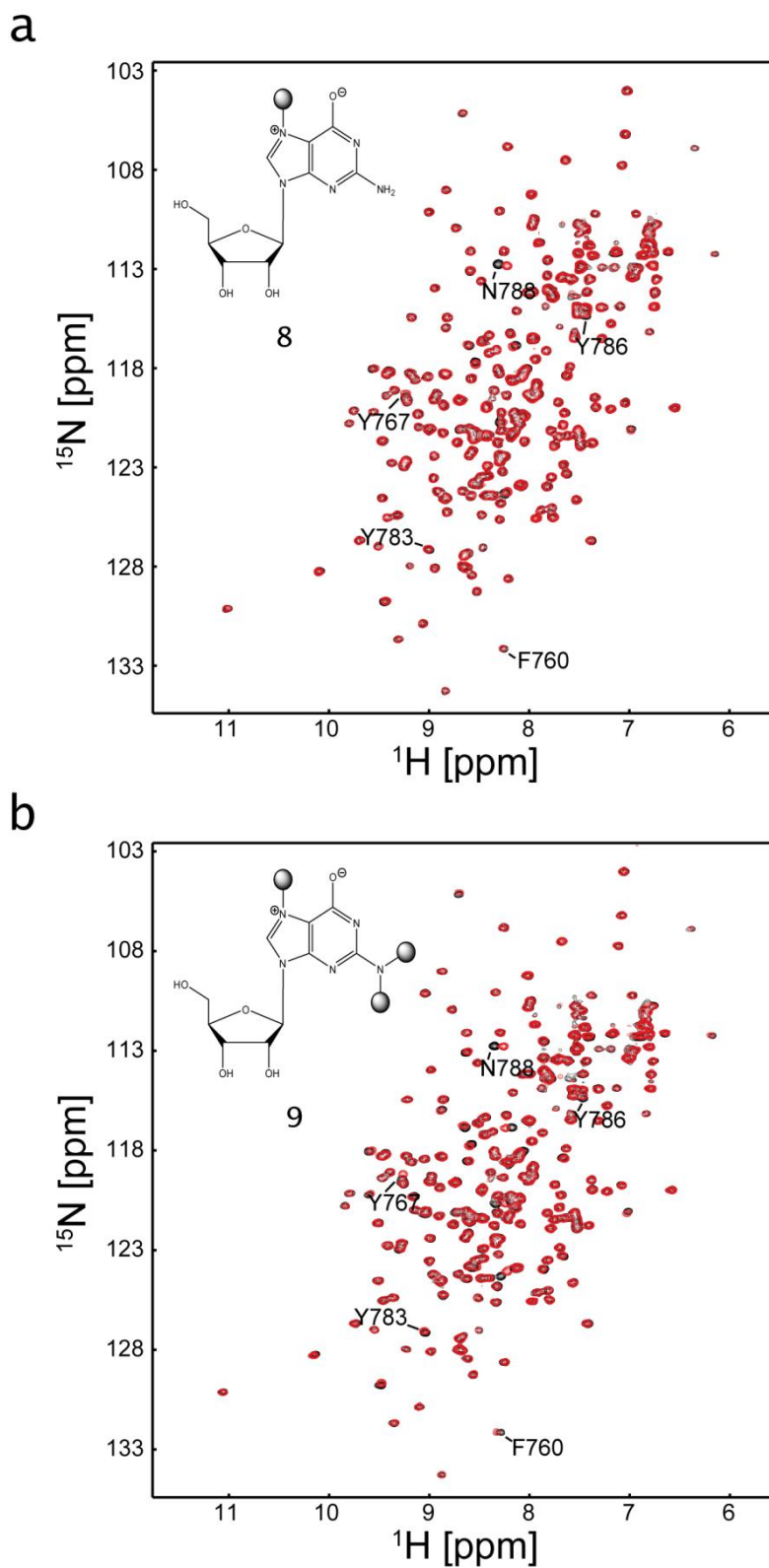
<sup>8</sup> Adam et al. (2007) RAG2 PHD finger couples histone H3 lysine 4 trimethylation with V(D)J recombination. *Nature* 450, 1106-10



**Supplementary Figure 1.** Hydrophobic and electrostatic interactions in the interface between SN5 (green),  $\alpha 1$  (grey) and the Tudor domain (magenta). (a) Residues with side-chains or backbone atoms taking part in electrostatic interactions (dotted lines). (b, c) Side-chains of residues making hydrophobic interactions.



**Supplementary Figure 2.** NMR titrations of methylated lysines. Residues in the aromatic cage of TSN are labeled (a) Titration of **5** (monomethyllysine) to TSN. Reference spectrum in black [0.1 mM], and in red at protein:ligand ratio of 1:12. (b) Titration of **6** (dimethyllysine) to TSN. Reference spectrum in black [0.1 mM], and in red at protein:ligand ratio of 1:12. (c) Titration of **7** (trimethyllysine) to TSN. Reference spectrum in black [0.1 mM], and in red at protein:ligand ratio of 1:12. All three titrations were performed at 500 MHz.



**Supplementary Figure 3.** NMR titrations of methylated guanosines, mimicking the 5' cap of snRNAs. Residues in the aromatic cage of TSN are labeled (a) Titration of **8** (7-methylguanosine) to TSN. Reference spectrum in black [0.2mM], and in red at protein:ligand ratio of 1:12. (b) Titration of **9** ( $N^2,N^2,7$ -trimethylguanosine) to TSN. Reference spectrum in black [0.2mM], and in red at protein:ligand ratio of 1:12. Both titrations were performed at 600 MHz.

## Chapter 4

---

### NMR structure of an atypical Tudor domain

#### 4.1. Summary

Epigenetic regulation of transcription is an increasingly appreciated area of research\*, which has deepened our understanding of gene expression greatly. We are now in a better position to understand, not only how cells "remember" which cell type they belong to, but also how regulatory information is passed along during cell divisions. This is not only important in developmental biology, but also in the fields of stem cell and tumor biology.

The Polycomblike (Pcl) protein is a subunit of a larger complex, involved in methylation of histone tails.<sup>17</sup> Through changes in chromatin structure, and not of the DNA itself, these complexes regulated the access of the transcriptional machinery to the genes.<sup>172</sup> Thus, Pcl is thought to be involved in epigenetic regulation of gene expression, at the level of chromatin remodeling. However, the molecular mechanism for its function is not understood, and we set out to characterize one particular structural domain of Pcl.

This paper presents the three-dimensional structure, as well as a ligand binding study, of the Tudor domain of *Drosophila* Polycomblike. The Tudor domain of Pcl (Pcl-Tudor) was of special interest, since members of this family of domains previously has been shown to bind methylated arginines and lysines (see Chapter 3). Such modified residues are present in the histone tails. Therefore Pcl-Tudor could be suggested, to target the chromatin remodeling complex to the histones.

In contrast to the hypothesis, our data show that Pcl-Tudor has no affinity for any known Tudor ligand. This observation can be explained by analyzing the NMR structure. Pcl-Tudor has a classical overall Tudor-fold, but exhibits an untypical composition of residues in its putative binding site. By structural comparisons to other Tudor domains, we suggest these differences make Pcl-Tudor incapable of binding our tested ligands. In the article, we further suggest divergent functions of *Drosophila* and human Pcl proteins, as well as an possible hydrophobic interaction site on Pcl-Tudor.

This work was a collaboration with the group of Dr. Jürg Müller at EMBL Heidelberg.

\* A search on ISI Web of Knowledge shows a steady increase of publications since the mid-nineties.



## 4.2 Published manuscript

# ***Structure of an atypical Tudor domain in the Drosophila Polycomblike protein***

Published in *Protein Science*

Received 19 May 2010; Revised 12 July 2010; Accepted 14 July 2010

DOI: 10.1002/pro.476

Anders Friberg<sup>1,2,†</sup>, Anna Oddone<sup>3,4,†</sup>, Tetyana Klymenko<sup>3</sup>, Jürg Müller<sup>3</sup>  
& Michael Sattler<sup>1,2\*</sup>

† These authors contributed equally to this work

<sup>1</sup> Institute of Structural Biology, Helmholtz Zentrum München, Ingolstädter Landstr. 1, 85764 Neuherberg, Germany

<sup>2</sup> Munich Center for Integrated Protein Science at Chair of Biomolecular NMR, Department Chemie, Technische Universität München, Lichtenbergstr. 4, 85747 Garching

<sup>3</sup> European Molecular Biology Laboratory (EMBL), Meyerhofstr. 1, 69117 Heidelberg, Germany

<sup>4</sup> Centre for Genomic Regulation (CRG), Doctor Aiguader 88, 08003 Barcelona, Spain

\* Correspondence: [sattler@helmholtz-muenchen.de](mailto:sattler@helmholtz-muenchen.de)

Tel: +49(0)89-28913418; Fax: +49(0)89-28913869

### Keywords

NMR, Polycomblike, Pcl, PRC2, Tudor, aromatic cage, methyllysine, sDMA, posttranslational modification, transcriptional regulation

### Abbreviations

Pcl, *Drosophila* Polycomblike; Pcl-Tudor, the Tudor domain of Pcl, PRC2, Polycomb repressive complex 2; PcG, Polycomb group; NMR, nuclear magnetic resonance; HSQC, heteronuclear single quantum correlation; NOE, nuclear Overhauser effect; sDMA, symmetrically dimethylated arginine; aDMA, asymmetrically dimethylated arginine.



## *Abstract*

Posttranslational modifications of histone tails are among the most prominent epigenetic marks and play a critical role in transcriptional control at the level of chromatin. The Polycomblike (Pcl) protein is part of a histone methyltransferase complex (Pcl-PRC2) responsible for high levels of histone H3 K27 trimethylation. Studies in *Drosophila* larvae suggest that Pcl is required for anchoring Pcl-PRC2 at target genes, but how this is achieved is unknown. Pcl comprises a Tudor domain and two PHD fingers. These domains are known to recognize methylated lysine or arginine residues and could contribute to targeting of Pcl-PRC2.

Here, we report an NMR structure of the Tudor domain from *Drosophila* Pcl (Pcl-Tudor) and binding studies with putative ligands. Pcl-Tudor contains an atypical, incomplete aromatic cage that does not interact with known Tudor domain ligands, such as methylated lysines or arginines. Interestingly, human Pcl orthologs exhibit a complete aromatic cage, suggesting that they may recognize methylated lysines. Structural comparison with other Tudor domains suggests that Pcl-Tudor may engage in intra- or intermolecular interactions through an exposed hydrophobic surface patch.

## *Introduction*

Epigenetic regulation of gene expression has emerged as one of the key determinants of cell fate and of maintenance of cell identity. Linked to this, many transcriptional regulators have been found to act at the level of chromatin. Among those chromatin modifiers, the Polycomb/Trithorax system is a highly conserved machinery that is essential for controlling expression of developmental regulator genes in both animals and plants. It is implicated in transcriptional control of genes during development,<sup>1</sup> in stem cells,<sup>2</sup> in X-inactivation<sup>3</sup> and tumor biology<sup>4</sup> of mammals, as well as in flowering time in plants<sup>5</sup>.

The Polycomb group (PcG) of proteins are known developmental regulators. PcG proteins are conserved from plants to humans and are considered as general factors engaged in transcriptional repression.<sup>6</sup> Polycomb proteins exist in four distinct multiprotein complexes: Pleiohomeotic repressive complex (PHO-RC), the Polycomb repressive complexes 1 and 2 (PRC1 and PRC2)<sup>7</sup> and the recently described Polycomb repressive deubiquitinase (PR-DUB)<sup>8</sup>. Among those, PRC2 is a histone methyltransferase for lysine 27 of histone 3 (H3K27). Studies in *Drosophila* suggest that mono- and dimethylation of H3K27 (H3K27me1/me2) is widespread,<sup>9</sup> whereas trimethylation (H3K27me3) is confined to genes regulated by the PcG machinery. Biochemical purifications isolated two different forms of the complex: PRC2 and Pcl-PRC2.<sup>10-12</sup> In *Drosophila*, genome-wide H3K27me1/me2 is generated by PRC2 whereas Pcl-PRC2 is responsible for the high levels of H3K27me3 at target genes to allow PcG repression.<sup>10</sup>

At present the specific role of Pcl in H3K27 trimethylation by PRC2-Pcl is not clear. *In vitro*, *Drosophila* PRC2 and Pcl-PRC2 have largely similar enzymatic activities for generating H3K27me1, me2 and me3.<sup>10</sup> However, *in vitro* histone methylation by reconstituted human PRC2 is enhanced when supplemented by Pcl1.<sup>12</sup> Studies in *Drosophila* larvae suggest that Pcl is required for anchoring PRC2 at PcG target genes.<sup>13</sup> The human homologs of Pcl are known as PHF1 (Pcl1), MTF2 (Pcl2) and PHF19 (Pcl3).

Full-length *Drosophila* Pcl comprises 1043 amino acids (115 kDa; Figure 1A) and is expressed in all cell nuclei during embryonic development, as well as in larval salivary glands where it co-localizes with other PcG proteins on polytene chromosomes.<sup>14</sup> Pcl contains two plant homeodomains (PHDs), which mediate binding to E(z),<sup>15</sup> and a Tudor domain (Pcl-Tudor; Figure 1A,B). PHD fingers and Tudor domains from several proteins are known to recognize methylated amino acids in histones or other proteins. Specifically, Tudor domains have previously been shown to bind methylated lysines in histone tails<sup>16,17</sup>, and methylated arginines in Sm proteins<sup>18-21</sup>. Recently, Tudor domains have been implicated in the selection of piRNAs by interacting with symmetrically dimethylated arginines (sDMAs) in Piwi proteins.<sup>22</sup> The binding of methylated ligands involves a so-called “aromatic cage”. The aromatic cage of Tudor domains comprises five residues, i.e. usually three to four aromatic side chains supplemented by small polar or charged residues.<sup>21</sup> Together these residues create a hydrophobic binding pocket with affinity for a methylated ligand.

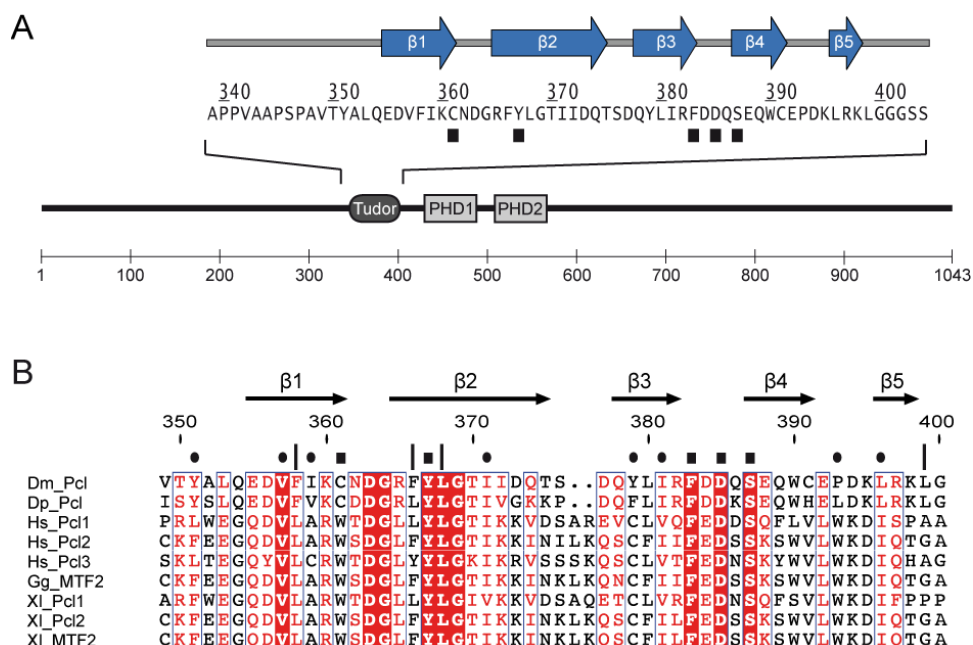


**Figure 1. Domain architecture of Polycomblike (Pcl) and sequence comparison of Pcl-Tudor homologs.** (A) Domain architecture of full-length Pcl from *D. melanogaster* and secondary structure topology of Pcl-Tudor: β-sheets are colored blue. Filled black boxes indicate aromatic cage residues that form the ligand binding site in canonical Tudor domains. (B) Multiple sequence alignment of Pcl Tudor domains from different organisms. Arrows indicate the β-strands in the Tudor domain. The numbering on top corresponds to *Drosophila* Pcl. Important residues in Pcl-Tudor are highlighted. Key: ■ Putative binding site residues; ● Hydrophobic core residues; | Residues in an additional hydrophobic surface patch.

A possible function of Pcl could be to target the Pcl-PRC2 complex via its Tudor or PHD domains by binding methylated residues in the histone tails. To address the role of the Tudor domain of *Drosophila* Pcl, we determined its three-dimensional structure by NMR spectroscopy and studied its ligand binding properties. Testing several typical Tudor domain ligands no high-affinity interaction was found. This result is rationalized based on the domain structure, which reveals that *Drosophila* Pcl-Tudor contains an atypical, incomplete aromatic cage. Differences in the aromatic cages of *Drosophila* and human Pcl Tudor domains suggest divergent molecular functions. A hydrophobic surface patch on Pcl-Tudor suggests that it may engage in additional intra- or intermolecular interactions.

## *Results and discussion*

### **Solution structure of Pcl-Tudor from *D. melanogaster***

Recombinant Pcl-Tudor (residues 339-404) was expressed in *Escherichia coli* at high yields. This construct resulted in a well dispersed 2D  $^1\text{H},^{15}\text{N}$  HSQC spectrum, indicating the protein was amenable for structural studies by NMR. A stable protein sample for further analysis required the use of a strong reducing agent to keep cysteine residues in a reduced state. The three-dimensional structure of Pcl-Tudor (Figure 2A-C) was determined by NMR, using standard experiments for assignments and derivation of distance restraints.<sup>23</sup> Out of the 69 residues in the expression construct, 52 residues (349 to 400) define the tertiary fold with high precision (RMSD < 1 Å; Figure 2C,3D) and good structural statistics (Table 1).

Pcl-Tudor comprises five anti-parallel  $\beta$ -sheets, which together form a characteristic  $\beta$ -barrel (Figure 2A). The  $\beta$ -barrel is closed by an interaction of  $\beta 5$  with  $\beta 1$ , and is stabilized by a hydrophobic core including Y351, V357, I359, I371, Y379, I381, P393 and L396 (Supp. Fig. 1A). Similar to other Tudor domains, the second  $\beta$ -strand is slightly bent around I372, thereby making a hydrogen bond possible between both of the backbone amides of I372 and D373 to the backbone oxygen of Y379. Secondary chemical shift values confirm the secondary structure seen in the structure (Figure 3A).

The side chains forming the putative binding pocket — the “aromatic cage” — are found in or close to the  $\beta 1$ - $\beta 2$  and  $\beta 3$ - $\beta 4$  loops (Figure 2B). The residues in Pcl-Tudor corresponding to the aromatic cage are: C361, Y367, F383, D385 and S387. Notably, the expected binding pocket of Pcl-Tudor is wider than other Tudor domains known to bind methylated ligands (Supp. Fig 2A). This might be a result of the absence of large aromatic residues in Pcl-Tudor, which are present in other Tudor domains. Particularly, the cysteine residue in position 361 is atypical for this type of domain. In addition, Pcl-Tudor exhibits a hydrophobic patch on the surface of the  $\beta$ -barrel, consisting of F358, F366, L368 and L399 (Figure 6B).

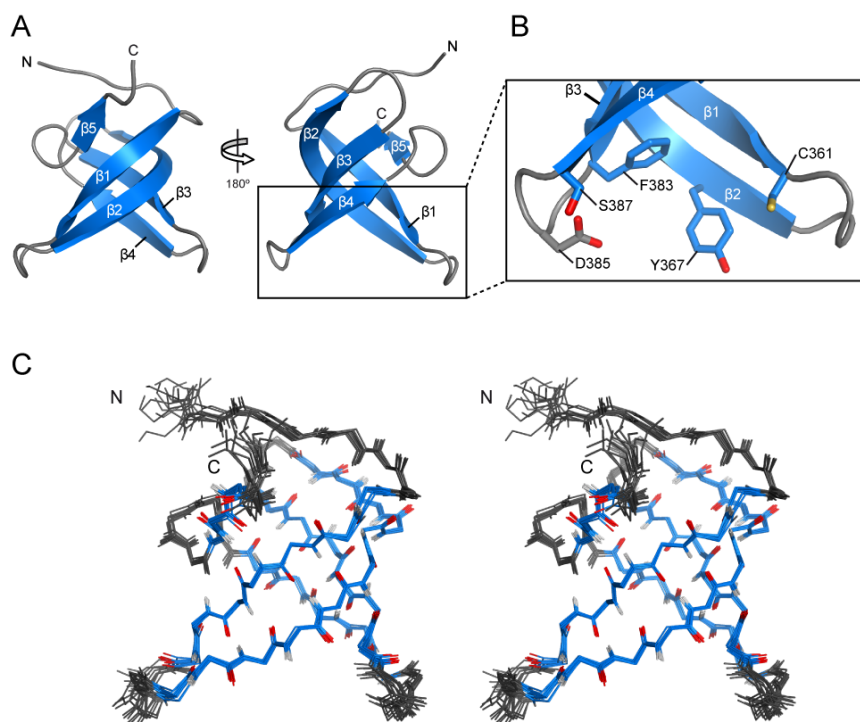


**Figure 2. Solution structure of Pcl-Tudor.** (A) NMR structure of Pcl-Tudor.  $\beta$ -sheets (blue) are numbered according to Figure 1A. (B) Detailed view of the putative binding site. Residues corresponding to the "aromatic cage" are shown in stick representation. (C) Stereo view of the ten lowest energy structures from the NMR calculation, displayed as a wire model of the protein backbone.

**Table 1**

<b>Structure calculation restraints</b>	
Distance restraints <sup>a</sup>	1579
Intra-residue	304
Inter-residue	
Short-range ( $ i-j  = 1$ )	333
Medium-range ( $1 <  i-j  < 5$ )	161
Long-range ( $ i-j  > 5$ )	781
Dihedral restraints (PHI + PSI)	88
<b>Quality analysis</b>	
Coordinate precision (Å) <sup>b,*</sup>	
N, C $\alpha$ , C'	0.29 $\pm$ 0.07
Heavy atoms	0.74 $\pm$ 0.04
Restraint RMSD <sup>c</sup>	
Distance restraints (Å)	0.011 $\pm$ 0.002
Dihedral restraints (°)	0.528 $\pm$ 0.043
Deviation from idealized geometry <sup>d</sup>	
Bond lengths (Å)	0.016
Bond angles (°)	1.3
Ramachandran values (%) <sup>e,*</sup>	
Preferred regions	91.9
Allowed regions	8.1
Generously allowed regions	0
Disallowed regions	0
WhatIf analysis <sup>f,*</sup>	
1 <sup>st</sup> generation packing	1.036 $\pm$ 0.145
2 <sup>nd</sup> generation packing	1.671 $\pm$ 0.367
Ramachandran plot appearance	0.485 $\pm$ 0.437
Chi-1/Chi-2 rotamer normality	-1.936 $\pm$ 0.442
Backbone conformation	0.051 $\pm$ 0.501

<sup>a</sup> 3243 resonances out of 3716 were assigned by CYANA

<sup>b</sup> Given as the cartesian RMSD of the ten lowest in energy models to their mean structure

<sup>c</sup> Analyzed by iCING. No restraints were violated by more than 0.2 Å or 3° in any of the models.

<sup>d</sup> PDB validation and deposition server (ADIT).

<sup>e</sup> With Procheck.

<sup>f</sup> Structure Z-scores, a positive number is better than average.

\* For residue 349-400.

## Protein backbone dynamics

NMR  $^{15}\text{N}$  relaxation data ( $T_1$ ,  $T_2$  and heteronuclear  $\{^1\text{H}\}$ - $^{15}\text{N}$  NOE) agree well with the calculated ensemble of structural models (Figure 3B,C). Our data show that the boundaries between less defined and well-defined protein backbone, at the N- and C-termini, correlate with the presence and absence, respectively, of fast motions (Figure 3B-D). No increased flexibility on fast (sub nanosecond) timescales is observed for the loops flanking the putative binding site. The reduced structural precision of these two loops probably results from paucity of distance restraints for these residues, but could also reflect slow motions in the millisecond timescale. The average  $^{15}\text{N}$   $T_1$  and  $T_2$  values were determined to be  $621 \pm 26$  ms and  $90 \pm 6.0$  ms, respectively. The ratio of  $T_1/T_2$  (6.9) corresponds to a correlation time of  $\tau_c^{\text{exp}} \approx 7.7$  ns. An estimation of the correlation time by HYDRONMR,<sup>24</sup> using our calculated structural model, gives approximately  $\tau_c^{\text{calc}} \approx 5.2$  ns. Taken together, this indicates that Pcl-Tudor is a monomer in solution, consistent with size exclusion chromatography data (Supp. Fig. 1B).

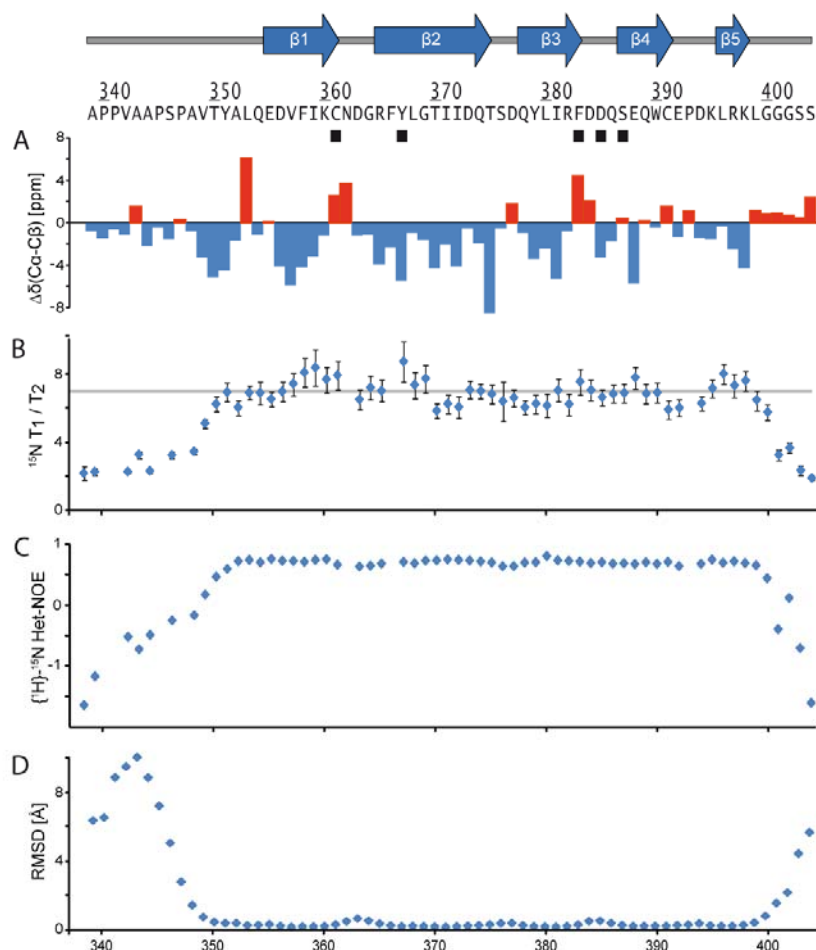


**Figure 3. Secondary chemical shifts and  $^{15}\text{N}$  relaxation data.** (A) Secondary chemical shifts,  $\Delta\delta(^{13}\text{C}\alpha\text{-}^{13}\text{C}\beta)$ . Positive (red) and negative (blue) values indicate  $\alpha$ -helical and  $\beta$ -strand conformation, respectively. (B)  $^{15}\text{N}$  NMR relaxation data. The average ratio of  $T_1/T_2$  (6.9) is indicated by a gray line. The error bars are derived by Monte Carlo simulations in NMRviewJ<sup>32</sup> (v8.0). (C)  $\{^1\text{H}\}$ - $^{15}\text{N}$  heteronuclear NOE indicates flexible N- and C-termini of Pcl-Tudor. (D) Backbone RMSD. The RMSD of the backbone atoms (N, C $\alpha$  and C') in the calculated ensemble of ten lowest energy structures.

## Ligand binding studies

The role of Pcl in trimethylation of H3K27 or in recruitment of PRC2 to target genes is still unknown. To obtain insight into the molecular interactions of Pcl, we performed binding studies using our Pcl-Tudor construct with putative ligands. In a series of NMR titrations and isothermal titration calorimetry (ITC) experiments, we primarily tested known Tudor ligands and their derivatives, i.e. molecules containing arginines and lysines in different methylation states. In addition, we included compounds that were suggested to bind to Tudor domains, e.g. acetyl-lysine (a different epigenetic modification), Xist RNA (a proposed targeting factor for PRC2<sup>3</sup>) and methylated guanosines (another molecule found in different methylation states). Table 2 lists all the ligands tested.

Despite our efforts, no ligand showing strong affinity for Pcl-Tudor could be identified. Figure 4 shows typical results of NMR titration experiments, here using a mixture of methylated lysines and methylated arginines (a), as well as unmodified histone tails (b). No chemical shift changes could be observed, hence indicating that Pcl-Tudor does not bind any of the Tudor ligands characterized to date, nor any of the additional ligands tested here. Similarly, ITC measurements failed to provide evidence that Pcl-Tudor interacts with various histone tail peptides containing methylated lysine residues (Maxim Nekrasov and J.M., unpublished data).

We found that the three-dimensional structure of the Tudor domain of *Drosophila* Pcl (Pcl-Tudor) comprises the typical  $\beta$ -barrel fold of Tudor domains, but lacks an intact aromatic cage. This particular structural feature of Pcl-Tudor provides an explanation for the lack of binding to known ligands of Tudor domains: without a complete aromatic cage, the methylated residue cannot be properly coordinated. Methylated amino acids can exist in different methylation states, which demands a specific and well-tuned recognition. Slight differences in the aromatic cage of Tudor domains provide selectivity for certain ligands.<sup>21</sup> To date, only structures of methylated lysines in complex with Tudor domains have been reported. A structural comparison of Pcl-Tudor with available structures of Tudor domain-ligand complexes as well as to its human homologs provides a rationale for the distinct binding properties and highlights the diversity of Tudor domains, as described in the following.

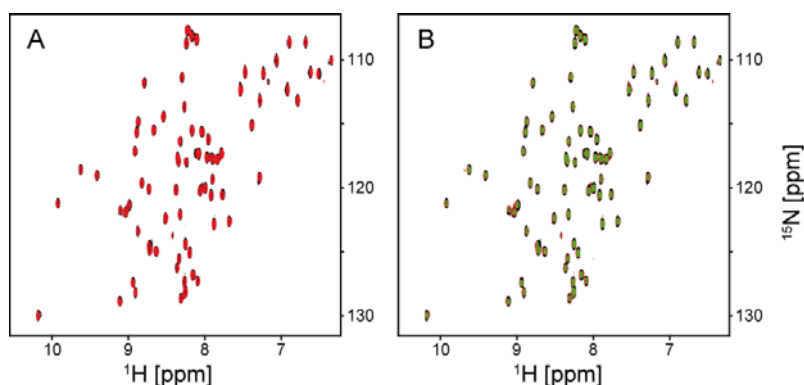


**Figure 4. Ligand titrations followed by NMR.** A reference  $^1\text{H}$ ,  $^{15}\text{N}$  HSQC spectrum (black) was measured on a  $^{15}\text{N}$ -labeled 100  $\mu\text{M}$  Pcl-Tudor sample. (A) Red spectrum, 1:5 protein:ligand ratio using a mixture of various modified amino acids (sDMA, aDMA, mono-, di- and trimethylated lysine). (B) Red spectrum, 1:5 protein:ligand ratio with unmodified H3 peptide. Green spectrum, 1:5 protein:ligand ratio of unmodified H4 peptide.

**Table 2**

Ligands tested by NMR	Final protein to ligand ratio
sDMA, aDMA, Kme1, Kme2, Kme3 (mixture)	1:5
R (unmodified)	1:20
AGRGRG	1:5
AGR*GR*G (R* = sDMA)	1:5
H3 (2-29)	1:5
H3K27me3	1:5
H3R2 sDMA	1:5
H3R17 sDMA	1:5
H3R26 sDMA	1:5
H4 (2-21)	1:5
H4R3 sDMA	1:5
Acetyllysine	1:5
Xist RNA 14mer	1:2
7-methylguanosine	1:5
N <sup>2</sup> ,N <sup>2</sup> ,7-trimethylguanosine	1:5

sDMA - symmetrically dimethylated arginine  
aDMA - asymmetrically dimethylated arginine  
Kme1 - monomethylated lysine  
Kme2 - dimethylated lysine  
Kme3 - trimethylated lysine

### Structural comparison with methyllysine recognition by 53BP1 Tudor

The first Tudor domain of 53BP1 has been proposed to be required for targeting the protein to DNA double-strand breaks by recognition of H3K20me2.<sup>16</sup> The interaction with dimethyllysine ( $K_D = 20 \mu\text{M}$ ) is mediated by an intact aromatic cage, comprising W1495, Y1502, F1519, D1521 and Y1523. The aspartate is thought to be critical for high affinity and selectivity, due to its capability of forming a hydrogen bond to the side-chain amino group of the ligand. Pcl-Tudor contains an aspartate in the equivalent position. However, Pcl-Tudor only has two aromatic side-chains in the binding pocket, Y367 and F383. W1495 of 53BP1, shown by mutational analysis to be essential for ligand binding, is replaced by a cysteine in Pcl-Tudor (Figure 5A). Also Y1523 of 53BP1 is substituted in Pcl-Tudor by a small non-aromatic residue, namely S387. The overall sequence identity between Pcl-Tudor and 53BP1 is 23% (Figure 5F).

### Structural comparison of *Drosophila* and human Pcl Tudor domains

Structures of the Tudor domains of Pcl1, Pcl2 and Pcl3, the human homologs of *Drosophila* Pcl, have been deposited in the PDB (Accession codes: 2E5P, 2EQJ and 2E5Q). The sequence identity between the *Drosophila* Pcl-Tudor and its human homologs is 28%, 32% and 24% for Pcl1, Pcl2 and Pcl3, respectively (Figure 1B). The structures of human and *Drosophila* Pcl Tudor domains are similar and all contain a rather wide putative binding pocket (Supp. Fig. 2D). However, an interesting difference is that the aromatic cage of all three human homologs comprises a conserved and characteristic tryptophan, which in *Drosophila* Pcl is replaced by a cysteine (C361) (Figure 5B,F and Supp. Fig. 2B,C). By structural



comparisons we find that the aromatic cage residues of the homologous Pcl1-3 proteins are identical to the tandem hybrid Tudor domain of JMJD2A (Figure 5C).<sup>17</sup> The JMJD2A Tudor domain binds trimethylated lysines in histone tails, both H3K4me3 and H4K20me3<sup>25</sup>, and it was shown that a mutation of the tryptophan to histidine abolishes binding of JMJD2A to H3K4me3.<sup>17</sup> These results are in line with our data since we do not observe any binding of H3K4me3 by ITC or of Kme3 by NMR to Pcl-Tudor, which lacks the conserved tryptophan. On the other hand, it is tempting to hypothesize that Pcl1-3 would interact with trimethylated lysines, considering the striking similarity of the putative binding sites in Pcl1-3 and JMJD2A (Figure 5C).

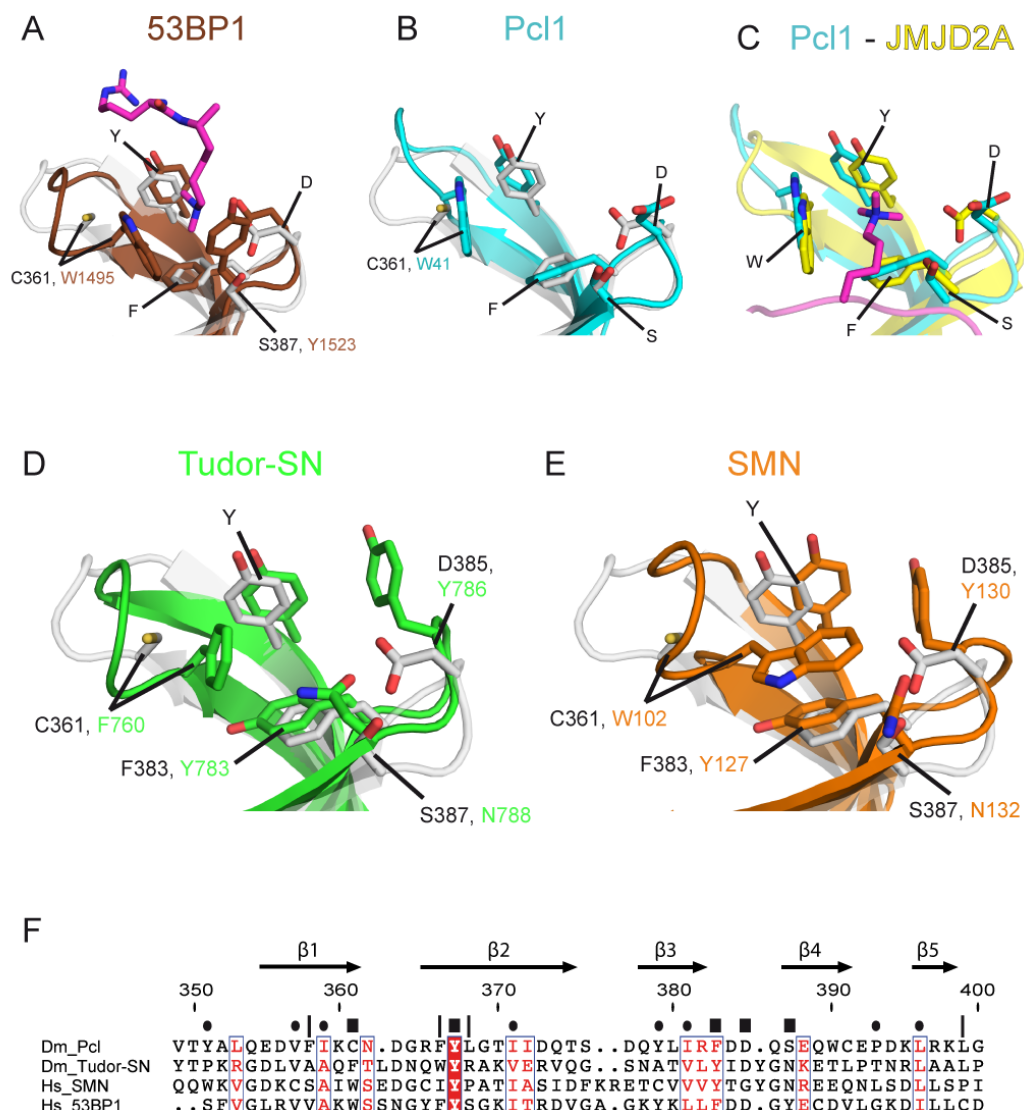


**Figure 5. Comparison of Pcl-Tudor with other Tudor domains.** (A, B) Side chains corresponding to the aromatic cage are highlighted as sticks in Pcl-Tudor and other Tudor domains, only substitutions are labeled with residue numbers. Superposition of Pcl-Tudor (lightgray) with (A) the first 53BP1 tandem Tudor domain in complex with H4K20me2 (brown; 2IGO.pdb; ligand in magenta) and (B) Pcl1 (cyan; 2E5P.pdb). (C) Superposition of the human homolog Pcl1 (cyan; 2E5P.pdb) and the hybrid Tudor domain of JMJD2A in complex with H3K4me3 (yellow; 2GFA.pdb). Note the identical composition of residues in the binding site. The peptide ligand is shown in magenta. (D, E) Similar to (A, B), superposition of Pcl-Tudor (gray) and, (D) Tudor-SN (green; 2WAC.pdb), (E) SMN (orange; 1MHN.pdb). (F) Multiple sequence alignment of *Drosophila* Pcl-Tudor and Tudor domains known to bind methylated lysines or methylated arginines. Symbols and numbering as in Figure 1B.



## Structural comparison to methylarginine-binding Tudor domains

The multifunctional Tudor-SN protein contains a methylarginine-binding Tudor domain also comprising an intact aromatic cage (Figure 5D). The binding site is composed of F760, Y767, Y783, Y786 and N788, providing the protein with selectivity for sDMA over aDMA ( $K_D = 720 \mu\text{M}$  and  $\sim 5 \text{ mM}$ , respectively).<sup>21</sup> The major difference compared to the methyllysine-binding 53BP1, is a spatial rearrangement of a small polar residue, D1521 and N788 in 53BP1 and Tudor-SN, respectively. Again, as in the case of 53BP1, compared to Tudor-SN Pcl-Tudor displays substitutions making an interaction with methylated arginines unlikely. F760, Y783, Y786 and N788 of Tudor-SN are replaced by C361, F383, D385 and S387 in Pcl-Tudor, respectively, and the overall sequence identity between Pcl-Tudor and the Tudor domain of Tudor-SN is only 13% (Figure 5F).

Similarly to Tudor-SN, also the Survival of Motor Neuron (SMN) protein interacts with methylated arginines.<sup>18,19,26,27</sup> Apart from one substitution their aromatic cages are identical in composition.<sup>21</sup> Compared to SMN, Pcl-Tudor exhibits major differences in the aromatic cage (Figure 5E). C361, F383, D385 and S387 in Pcl-Tudor are replaced by W102, Y127, Y130 and N132 in SMN, respectively, and the overall sequence identity between these two Tudor domains is 13% (Figure 5F).

## A putative interaction surface in Pcl-Tudor

Taken together, Pcl-Tudor adopts the characteristic overall fold of other Tudor domains, but exhibits major differences in the putative binding site that most likely renders it incapable of binding any of the established Tudor ligands. We cannot exclude the possibility that the atypical aromatic cage of Pcl-Tudor could recognize a ligand distinct from the ones included tested in this study. Also, additional domains in Pcl or in other binding partners might be needed for ligand recognition. These could, for example, associate with Pcl-Tudor to complete the aromatic cage, thus recreating the canonical binding pocket of Tudor domains, or they could recognize additional parts of the histone tails, leading to efficient substrate recognition. Methyllysine-binding modules such as PHD fingers are often found associated in proteins that play an important role in epigenetic regulation, and are likely to function cooperatively. Recently, PHF8, a human histone demethylase was reported to function in such modular fashion.<sup>28</sup> The demethylase activity of PHF8 resides in a Jumonji domain, with H3K9me2 and H3K27me2 as substrates. It was shown that the demethylase activity is enhanced and more specific if a H3K4me3 mark is present that interacts with a neighboring PHD domain.

We note that a distinct hydrophobic patch at the surface of Pcl-Tudor, remote from the aromatic cage, could be used as an interaction site for other domains or proteins (Figure 6; Supp. Fig. 3). Hydrophobic residues in this region are found in other Tudor domains, e.g. in SMN, 53BP1 and in the human homologs of Pcl (Figure 1B,5F). In some structures of Tudor-containing proteins, for example in Tudor-SN

(2WAC.pdb)<sup>21</sup> and TDRD2 (3FDR.pdb)<sup>29</sup>, the hydrophobic patch is covered by secondary structure elements extending from the Tudor domain, thereby forming an intramolecular hydrophobic interface (Figure 6). In the case of Tudor-SN, this arrangement stabilizes the inter-domain interaction to a neighboring nuclease domain, making the two domains tumble together as one unit in solution.<sup>21</sup> Moreover, in the structure of the human histone methyltransferase SETD1B (3DLM.pdb) such additional hydrophobic interaction surfaces are found between three consecutive Tudor domains (Supp. Fig. 3). Hence, it could be suggested that other domains or proteins interact with Pcl-Tudor using this structural feature. An additional factor interacting with Pcl-Tudor might increase ligand affinity and affect its binding specificity, possibly by complementing the incomplete aromatic cage of the Tudor domain.

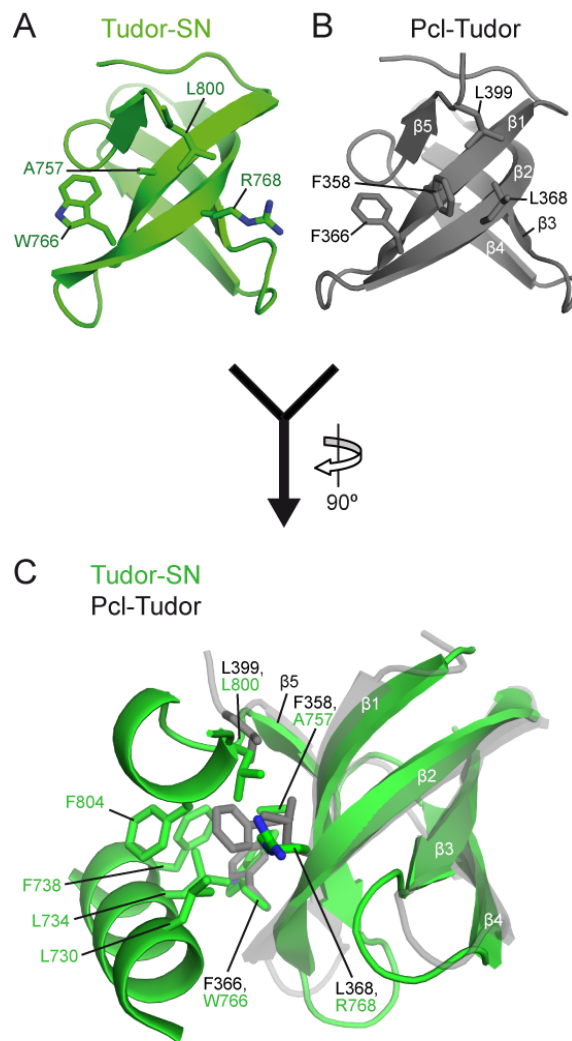


**Figure 6. Potential interaction site on *Drosophila* Pcl-Tudor.** (A) Hydrophobic patch residues in Tudor-SN (green). (B) A corresponding hydrophobic patch can be found in Pcl-Tudor (gray). (C) The Tudor domain of Tudor-SN forms a hydrophobic interaction with residues from neighboring secondary structures.

## Conclusion

In this study, we reported the structure of the Tudor-domain of Pcl from *Drosophila melanogaster* and, based on its structural features, rationalized our ligand binding results. While the overall structure represents a canonical Tudor fold it harbors an atypical incomplete aromatic cage. Pcl-Tudor shows no affinity for any of the typical known Tudor domain ligands, i.e. methylated lysines, methylated arginines, or other putative ligands tested. The Tudor domain of *Drosophila* Pcl may thus not directly participate in the recognition of post-translational modifications on histone proteins. However, it cannot be excluded that full-length Pcl contains such a function. Future studies, including the analysis of the Tudor domain in the context of larger portions of the Pcl protein should help to establish the role of Pcl in transcriptional repression and perhaps identify other, currently uncharacterized Tudor ligands.

## Materials and Methods

### Cloning, protein expression and purification

Residues 339-404 of Polycomblike (Pcl) from *Drosophila melanogaster* (Uniprot: Q24459) were cloned into a modified pET-24d vector using standard protocols. The fusion protein comprises a GFP (Green Fluorescence Protein) tag to facilitate purification. This protein construct was expressed in *Escherichia coli* BL21 (DE3) pLysS (Novagen) using kanamycin for selection. A 10mL lysogeny broth (LB) pre-culture was inoculated with a single colony from a transformation plate. The pre-culture was used to start larger 1L cultures, containing LB or M9 minimal medium for labeling with  $^{15}\text{N}$  or  $^{15}\text{N}/^{13}\text{C}$ . Upon reaching optical density (OD) of 0.6 cultures were put at 20°C and, after 30min of cooling, induced over night with 0.2 mM IPTG (Isopropyl  $\beta$ -D-1-thiogalactopyranoside).

Recombinant protein was purified by sonicating the harvested cell pellet in 25mL Lysis buffer (20 mM TRIS pH 7.5, 300 mM NaCl, 10 mM imidazole, 1 mM DTT and 0.02%  $\text{NaN}_3$ ), also including protease inhibitors, RNase, lysozyme and 0.2% IGEPAL. After high-speed centrifugation (20000rpm, 30min) and filtering, the supernatant was applied three times to Ni-NTA Agarose resin (Qiagen). Several rounds of washing were performed, with: Lysis buffer including 0.2% IGEPAL, Lysis buffer, Lysis buffer with high salt concentration (1M NaCl), Lysis buffer with high imidazole concentration (30 mM imidazole). Finally, the protein was eluted by applying 10mL of a buffer containing 20 mM TRIS pH 7.5, 300 mM NaCl, 330 mM imidazole, 1 mM DTT and 0.02%  $\text{NaN}_3$ . TEV (tobacco etch virus) protease was added to the sample and incubated overnight at 4°C. To remove the cleaved GFP tag the sample was passed three times over a second Ni-NTA column. A last purification step included size exclusion chromatography (HiLoad, Superdex 75 16/60, GE Healthcare). In this step, the protein was buffer-exchanged into the NMR buffer (20 mM sodium phosphate pH 6.3, 25 mM NaCl and 2 mM fresh DTT or TCEP, 0.02%  $\text{NaN}_3$ ).

### NMR spectroscopy and structure determination

Protein backbone and amino acid side chain assignments were done by using  $^{15}\text{N}/^{13}\text{C}$  labeled samples at a concentration of 0.25 mM. For this purpose, several multidimensional heteronuclear experiments were acquired:  $^1\text{H},^{15}\text{N}$  HSQC,  $^1\text{H},^{13}\text{C}$  HSQC, HNCA, HNCACB, CBCA(CO)NH, (H)CC(CO)NH-TOCSY, H(CC)(CO)NH-TOCSY, H(C)CH-TOCSY.<sup>23</sup> To obtain distance restraints for structure calculation a series of NOE-based experiments were recorded: 2D  $^1\text{H}$  homonuclear NOESY,  $^1\text{H},^{15}\text{N}$  HSQC-NOESY,  $^1\text{H},^{13}\text{C}$  HMQC-NOESY (aliphatic and aromatic versions). Assignment of the aromatic ring systems was enabled by another two experiments, (HB)CB(CG,CD)HD and (HB)CB(CG,CD,CE)HE.<sup>30</sup> All experiments were performed at 298.5 K on Bruker 900, 750, 600 and 500 MHz spectrometers equipped with pulsed field gradients. The data were processed with NMRPipe<sup>31</sup> for NMRView<sup>32</sup>.

Automatic assignment of the NOESY spectra and derivation of distance restraints were accomplished using CYANA v2.1.<sup>33</sup> TALOS+ was used to predict dihedral angle restraints.<sup>34</sup> Hundred structures were calculated and further water-refined<sup>35</sup> by use of RECOORD scripts<sup>36</sup> with CNS<sup>37</sup>. The ten lowest energy structures were selected as a representative ensemble. Structure validation was performed using Molprobity<sup>38</sup> and iCing<sup>39</sup> (including PROCHECK<sup>40</sup> and WHATCHECK<sup>41</sup>). Secondary structure definition were based on DSSP algorithms<sup>42</sup> as implemented in Procheck and Pymol, together with manual inspection.

To study the dynamical properties of the protein backbone  $^{15}\text{N}$   $T_1$ ,  $T_2$  and  $\{^1\text{H}\}$ - $^{15}\text{N}$  heteronuclear NOE were measured on a 1 mM  $^{15}\text{N}$ -labeled sample (600 MHz proton Larmor frequency) as described previously.<sup>43</sup>  $T_1$  was measured in an interleaved fashion with 14 different relaxation delays, varying from 21 ms to 2160 ms. Similarly,  $T_2$  was determined by using eight time points ranging from 11 ms to 190 ms. Duplicate time points were used for error estimation. The data was analyzed using the relaxation module integrated in NMRViewJ (v. 8.0). Average values were based on residues selected on specific criteria<sup>44</sup> and errors estimated as one standard deviation of included values. The correlation time ( $\tau_c$ ) of the protein molecule is estimated using the ratio of averaged  $T_1$  and  $T_2$  values.<sup>45</sup> HYDRONMR was used with standard parameter settings at 298.5 K.<sup>24</sup>

Images for structure comparisons were generated with Pymol.<sup>46</sup> The structure of Pcl2 (2EQJ.pdb), one of the human homologs, was deposited as originating from mouse. However, the amino acid sequence is identical to human and used accordingly. Sequence alignments were performed with ProbCons<sup>47</sup> (<http://probcons.stanford.edu>) and SSM<sup>48</sup> ([www.ebi.ac.uk/msd-srv/ssm](http://www.ebi.ac.uk/msd-srv/ssm)) using standard settings. Only the sequence of Pcl-Tudor that was well-defined in the NMR ensemble (residue 349 to 400) was included. The alignments were compared to structural data if available.

### **Binding studies**

Binding of putative ligands was investigated by NMR titrations. All NMR experiments were performed at 298.5 K with the protein in: 20 mM sodium phosphate pH 6.3, 25 mM NaCl and 2 mM fresh DTT or TCEP and 0.02%  $\text{NaN}_3$ . For NMR titrations samples of 100-200  $\mu\text{M}$  of  $^{15}\text{N}$  labeled protein were prepared. Ligands were then added in increasing amounts and binding followed by consecutive acquisition of 2D  $^1\text{H}$ ,  $^{15}\text{N}$  HSQC spectra. All ligands investigated are listed in Table 2. All compounds were purchased except the 14mer Xist RNA, which was produced by *in vitro* transcription.<sup>49</sup>

### *Accession codes*

Atom coordinates and restraint files have been deposited at the Protein Data Bank (accession code 2XK0). NMR chemical shifts have been deposited at Biological Magnetic Resonance Data Bank (accession code 17050).

### *Acknowledgements*

We thank Gunter Stier (EMBL Heidelberg) for help with designing and preparing the Tudor-Pcl expression plasmids; Maxim Nekrasov and Vladimir Rybin (EMBL Heidelberg) for ITC measurements. We thank Kostas Tripsianes, Alex Beribisky and Iren Wang for discussions and reading of the manuscript. A.F. is supported by a PhD fellowship from Helmholtz Zentrum München (HMGU), and by the International PhD program in Protein Dynamics from Elitenetzwerk Bayern. We acknowledge NMR measurement time at the Bavarian NMR Centre, Garching, Germany. This work was supported by the European Commission (3D Repertoire, LSHG-CT-2005-512028) and the Deutsche Forschungsgemeinschaft.

## References

1. Breiling A, Sessa L, Orlando V (2007) Biology of polycomb and trithorax group proteins. *Int Rev Cytol* 258:83-136.
2. Pietersen AM, van Lohuizen M (2008) Stem cell regulation by polycomb repressors: postponing commitment. *Curr Opin Cell Biol* 20:201-207.
3. Zhao J, Sun BK, Erwin JA, Song JJ, Lee JT (2008) Polycomb proteins targeted by a short repeat RNA to the mouse X chromosome. *Science* 322:750-756.
4. Bracken AP, Helin K (2009) Polycomb group proteins: navigators of lineage pathways led astray in cancer. *Nat Rev Cancer* 9:773-784.
5. Henderson IR, Dean C (2004) Control of Arabidopsis flowering: the chill before the bloom. *Development* 131:3829-3838.
6. Schwartz YB, Kahn TG, Nix DA, Li XY, Bourgon R, Biggin M, Pirrotta V (2006) Genome-wide analysis of Polycomb targets in *Drosophila melanogaster*. *Nat Genet* 38:700-705.
7. Simon JA, Kingston RE (2009) Mechanisms of polycomb gene silencing: knowns and unknowns. *Nat Rev Mol Cell Biol* 10:697-708.
8. Scheuermann JC, de Ayala Alonso AG, Oktaba K, Ly-Hartig N, McGinty RK, Fraterman S, Wilm M, Muir TW, Muller J (2010) Histone H2A deubiquitinase activity of the Polycomb repressive complex PR-DUB. *Nature advance online publication*.
9. Ebert A, Schotta G, Lein S, Kubicek S, Krauss V, Jenuwein T, Reuter G (2004) Su(var) genes regulate the balance between euchromatin and heterochromatin in *Drosophila*. *Genes Dev* 18:2973-2983.
10. Nekrasov M, Klymenko T, Fraterman S, Papp B, Oktaba K, Kocher T, Cohen A, Stunnenberg HG, Wilm M, Muller J (2007) Pcl-PRC2 is needed to generate high levels of H3-K27 trimethylation at Polycomb target genes. *EMBO J* 26:4078-4088.
11. Sarma K, Margueron R, Ivanov A, Pirrotta V, Reinberg D (2008) Ezh2 requires PHF1 to efficiently catalyze H3 lysine 27 trimethylation in vivo. *Mol Cell Biol* 28:2718-2731.
12. Cao R, Wang H, He J, Erdjument-Bromage H, Tempst P, Zhang Y (2008) Role of hPHF1 in H3K27 methylation and Hox gene silencing. *Mol Cell Biol* 28:1862-1872.
13. Savla U, Benes J, Zhang J, Jones RS (2008) Recruitment of *Drosophila* Polycomb-group proteins by Polycomblike, a component of a novel protein complex in larvae. *Development* 135:813-817.
14. Lonie A, D'Andrea R, Paro R, Saint R (1994) Molecular characterisation of the Polycomblike gene of *Drosophila melanogaster*, a trans-acting negative regulator of homeotic gene expression. *Development* 120:2629-2636.
15. O'Connell S, Wang L, Robert S, Jones CA, Saint R, Jones RS (2001) Polycomblike PHD fingers mediate conserved interaction with enhancer of zeste protein. *J Biol Chem* 276:43065-43073.
16. Botuyan MV, Lee J, Ward IM, Kim JE, Thompson JR, Chen J, Mer G (2006) Structural basis for the methylation state-specific recognition of histone H4-K20 by 53BP1 and Crb2 in DNA repair. *Cell* 127:1361-1373.
17. Huang Y, Fang J, Bedford MT, Zhang Y, Xu RM (2006) Recognition of histone H3 lysine-4 methylation by the double tudor domain of JMJD2A. *Science* 312:748-751.
18. Sprangers R, Groves MR, Sinning I, Sattler M (2003) High-resolution X-ray and NMR structures of the SMN Tudor domain: conformational variation in the binding site for symmetrically dimethylated arginine residues. *J Mol Biol* 327:507-520.

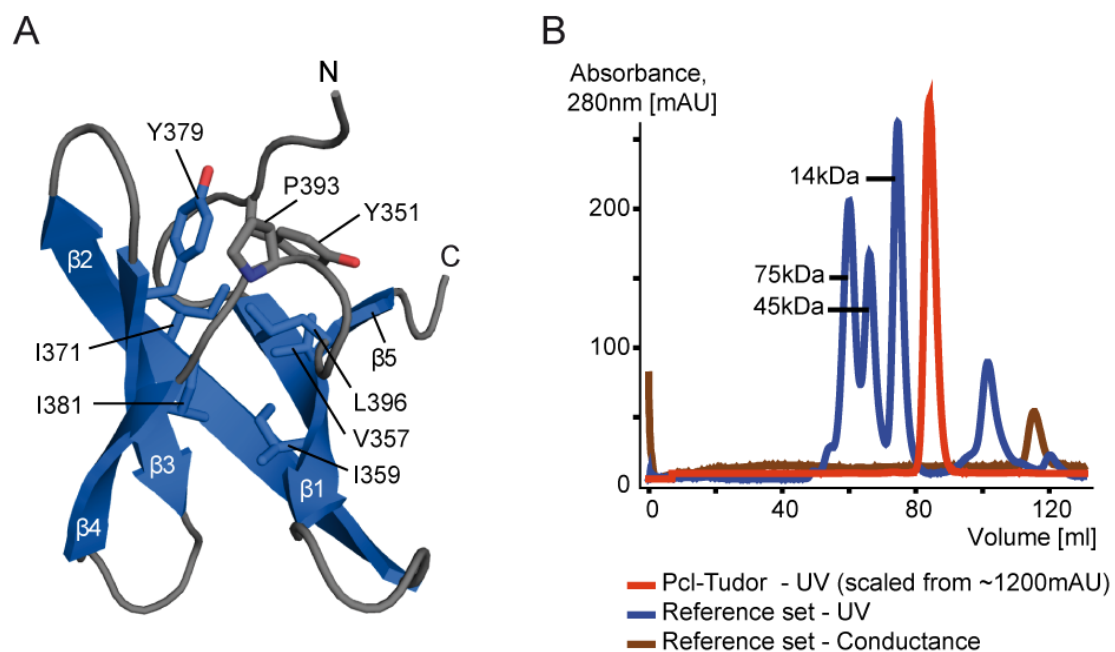
19. Selenko P, Sprangers R, Stier G, Buhler D, Fischer U, Sattler M (2001) SMN tudor domain structure and its interaction with the Sm proteins. *Nat Struct Biol* 8:27-31.
20. Shaw N, Zhao M, Cheng C, Xu H, Saarikettu J, Li Y, Da Y, Yao Z, Silvennoinen O, Yang J, Liu ZJ, Wang BC, Rao Z (2007) The multifunctional human p100 protein 'hooks' methylated ligands. *Nat Struct Mol Biol* 14:779-784.
21. Friberg A, Corsini L, Mourao A, Sattler M (2009) Structure and ligand binding of the extended Tudor domain of *D. melanogaster* Tudor-SN. *J Mol Biol* 387:921-934.
22. Reuter M, Chuma S, Tanaka T, Franz T, Stark A, Pillai RS (2009) Loss of the Mili-interacting Tudor domain-containing protein-1 activates transposons and alters the Mili-associated small RNA profile. *Nat Struct Mol Biol* 16:639-646.
23. Sattler M, Schleucher J, Griesinger C (1999) Heteronuclear multidimensional NMR experiments for the structure determination of proteins in solution employing pulsed. *Progress in Nuclear Magnetic Resonance Spectroscopy* 34:93-158.
24. Garcia de la Torre J, Huertas ML, Carrasco B (2000) HYDRONMR: prediction of NMR relaxation of globular proteins from atomic-level structures and hydrodynamic calculations. *J Magn Reson* 147:138-146.
25. Lee J, Thompson JR, Botuyan MV, Mer G (2008) Distinct binding modes specify the recognition of methylated histones H3K4 and H4K20 by JMJD2A-tudor. *Nat Struct Mol Biol* 15:109-111.
26. Brahms H, Raymackers J, Union A, de Keyser F, Meheus L, Luhrmann R (2000) The C-terminal RG dipeptide repeats of the spliceosomal Sm proteins D1 and D3 contain symmetrical dimethylarginines, which form a major B-cell epitope for anti-Sm autoantibodies. *J Biol Chem* 275:17122-17129.
27. Friesen WJ, Massenet S, Paushkin S, Wyce A, Dreyfuss G (2001) SMN, the product of the spinal muscular atrophy gene, binds preferentially to dimethylarginine-containing protein targets. *Mol Cell* 7:1111-1117.
28. Horton JR, Upadhyay AK, Qi HH, Zhang X, Shi Y, Cheng X (2010) Enzymatic and structural insights for substrate specificity of a family of jumonji histone lysine demethylases. *Nat Struct Mol Biol* 17:38-43.
29. Chen C, Jin J, James DA, Adams-Cioaba MA, Park JG, Guo Y, Tenaglia E, Xu C, Gish G, Min J, Pawson T (2009) Mouse Piwi interactome identifies binding mechanism of Tdrkh Tudor domain to arginine methylated Miwi. *Proc Natl Acad Sci U S A* 106:20336-20341.
30. Yamazaki T, Forman-Kay JD, Kay LE (1993) Two-dimensional NMR experiments for correlating carbon-13.beta. and proton.delta./epsilon. chemical shifts of aromatic residues in 13C-labeled proteins via scalar couplings. *Journal of the American Chemical Society* 115:11054-11055.
31. Delaglio F, Grzesiek S, Vuister GW, Zhu G, Pfeifer J, Bax A (1995) NMRPipe: a multidimensional spectral processing system based on UNIX pipes. *J Biomol NMR* 6:277-293.
32. Johnson BA, Blevins RA (1994) NMR View: A computer program for the visualization and analysis of NMR data. *Journal of Biomolecular NMR* 4:603-614.
33. Guntert P (2004) Automated NMR structure calculation with CYANA. *Methods Mol Biol* 278:353-378.
34. Shen Y, Delaglio F, Cornilescu G, Bax A (2009) TALOS+: a hybrid method for predicting protein backbone torsion angles from NMR chemical shifts. *J Biomol NMR* 44:213-223.
35. Linge JP, Williams MA, Spronk CA, Bonvin AM, Nilges M (2003) Refinement of protein structures in explicit solvent. *Proteins* 50:496-506.



36. Nederveen AJ, Doreleijers JF, Vranken W, Miller Z, Spronk CA, Nabuurs SB, Guntert P, Livny M, Markley JL, Nilges M, Ulrich EL, Kaptein R, Bonvin AM (2005) RECOORD: a recalculated coordinate database of 500+ proteins from the PDB using restraints from the BioMagResBank. *Proteins* 59:662-672.
37. Brunger AT, Adams PD, Clore GM, DeLano WL, Gros P, Grosse-Kunstleve RW, Jiang JS, Kuszewski J, Nilges M, Pannu NS, Read RJ, Rice LM, Simonson T, Warren GL (1998) Crystallography & NMR system: A new software suite for macromolecular structure determination. *Acta Crystallogr D Biol Crystallogr* 54:905-921.
38. Davis IW, Leaver-Fay A, Chen VB, Block JN, Kapral GJ, Wang X, Murray LW, Arendall WB, 3rd, Snoeyink J, Richardson JS, Richardson DC (2007) MolProbity: all-atom contacts and structure validation for proteins and nucleic acids. *Nucleic Acids Res* 35:W375-383.
39. Geerten W, Vuister JFD, Alan W.S. da Silva. iCing v2.0, <http://nmr.cmbi.ru.nl/icing/iCing.html>.
40. Laskowski RA, Rullmannn JA, MacArthur MW, Kaptein R, Thornton JM (1996) AQUA and PROCHECK-NMR: programs for checking the quality of protein structures solved by NMR. *J Biomol NMR* 8:477-486.
41. Vriend G, Sander C (1993) Quality control of protein models: directional atomic contact analysis. *Journal of Applied Crystallography* 26:47-60.
42. Kabsch W, Sander C (1983) Dictionary of protein secondary structure: pattern recognition of hydrogen-bonded and geometrical features. *Biopolymers* 22:2577-2637.
43. Farrow NA, Muhandiram R, Singer AU, Pascal SM, Kay CM, Gish G, Shoelson SE, Pawson T, Forman-Kay JD, Kay LE (1994) Backbone dynamics of a free and phosphopeptide-complexed Src homology 2 domain studied by <sup>15</sup>N NMR relaxation. *Biochemistry* 33:5984-6003.
44. Tjandra N, Kuboniwa H, Ren H, Bax A (1995) Rotational dynamics of calcium-free calmodulin studied by <sup>15</sup>N-NMR relaxation measurements. *Eur J Biochem* 230:1014-1024.
45. Daragan VA, Mayo KH (1997) Motional model analyses of protein and peptide dynamics using and NMR relaxation. *Progress in Nuclear Magnetic Resonance Spectroscopy* 31:63-105.
46. DeLano WL. (2002). The PyMOL Molecular Graphics System. DeLano Scientific, San Carlos, CA, USA.
47. Do CB, Mahabhashyam MS, Brudno M, Batzoglou S (2005) ProbCons: Probabilistic consistency-based multiple sequence alignment. *Genome Res* 15:330-340.
48. Krissinel E, Henrick K (2004) Secondary-structure matching (SSM), a new tool for fast protein structure alignment in three dimensions. *Acta Crystallogr D Biol Crystallogr* 60:2256-2268.
49. Duszczuk MM, Zanier K, Sattler M (2008) A NMR strategy to unambiguously distinguish nucleic acid hairpin and duplex conformations applied to a Xist RNA A-repeat. *Nucleic Acids Res* 36:7068-7077.

### 4.3. Supplementary material

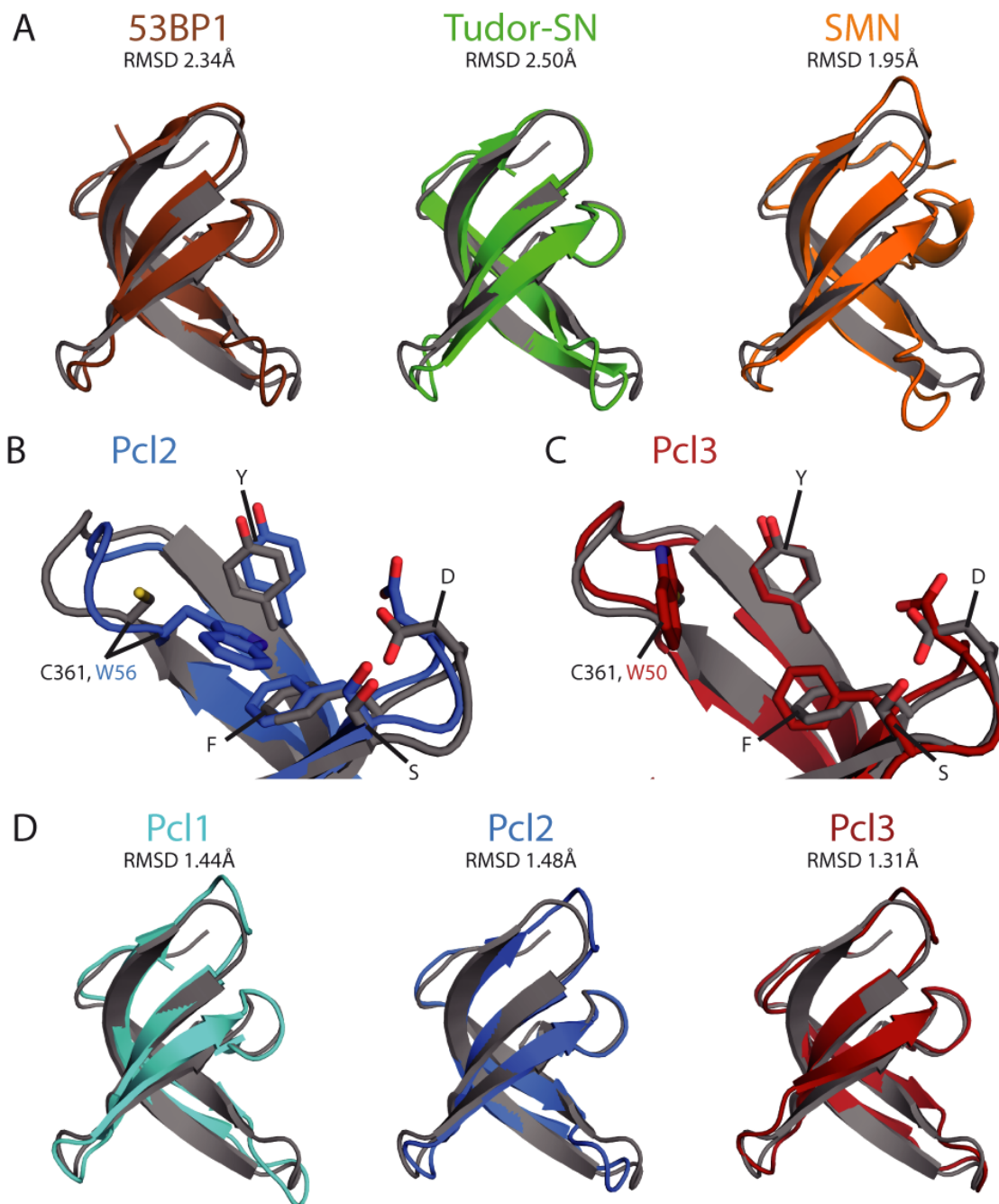
#### Supplementary Figure 1



Hydrophobic core of Pcl-Tudor and size exclusion chromatography data.

- (A) NMR structure of *Drosophila* Pcl-Tudor with residues in its stabilizing hydrophobic core highlighted as sticks.
- (B) Size exclusion chromatography suggests that Pcl-Tudor is a monomer in solution. The theoretical molecular weight of a monomer is 7.6kDa.

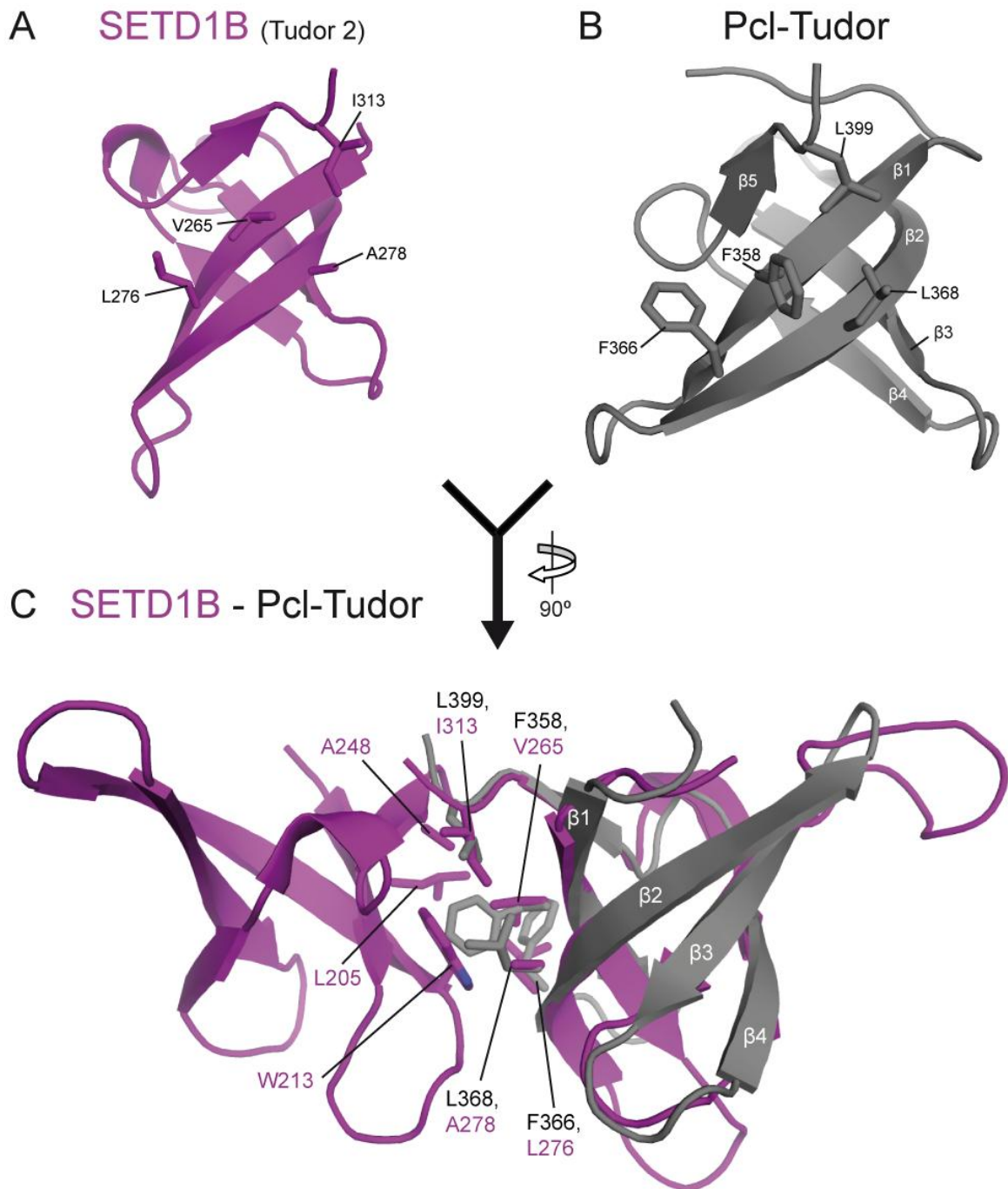
## Supplementary Figure 2



Structural comparison of Pcl-Tudor to other Tudor domains.

- (A) Comparison of the overall fold of Pcl-Tudor. RMSD was calculated by pair-wise fit of C $\alpha$  coordinates. Superposition of Pcl-Tudor (gray) and proteins known to bind methylated lysines or methylated arginines: the first Tudor domain of 53BP1 (brown; 2IGO.pdb), Tudor-SN (green; 2WAC.pdb) and SMN (orange; 1MHN.pdb).
- (B, C) Side chains corresponding to the aromatic cage are highlighted as sticks in Pcl-Tudor and two of its human homologs, only substitutions are labeled with residue numbers. Superposition of Pcl-Tudor (gray) and, (B) Pcl2 (blue; 2EQJ.pdb), (C) to Pcl3 (blue; 2E5Q.pdb).
- (D) Similar to (A), superposition of Pcl-Tudor (gray) and the human homologs: Pcl1 (cyan; 2E5P.pdb), Pcl2 (blue; 2EQJ.pdb) and Pcl3 (blue; 2E5Q.pdb).

## Supplementary Figure 3



Potential interaction site on *Drosophila* Pcl-Tudor. Comparison to SETD1B.

- (A) Hydrophobic patch residues in SETD1B (magenta).
- (B) A corresponding hydrophobic patch can be found in Pcl-Tudor (gray).
- (C) The Tudor domain of SETD1B forms a hydrophobic interaction with non-polar residues from another neighboring Tudor domain.



### Structural characterization of the RES complex

#### 5.1. Summary

The RES complex is required for efficient splicing, but is also involved in the retention of unspliced pre-mRNA in the nucleus. RES is composed of three proteins: Snu17, Bud13, and Pml1, and is found in yeast as well as humans. Snu17 acts as the central binding platform onto which the other two proteins bind. Pml1 contains a FHA domain for which the structure has been solved, however, the complex as such has resisted structural elucidation and has so far only been studied biochemically. Here, we address the assembly of the complex from a structural point of view. The efforts were mainly focused on the binary interaction of Snu17: Bud13, and to a minor extent on Snu17: Pml1.

Our data shows that Bud13 interacts with Snu17 via a linear peptide motif. In summary, the results suggest a strong and specific interaction between Snu17 and Bud13. The affinity was determined to be in the low nanomolar range by ITC ( $K_D \sim 6$  nM). The binding is suggested to be similar to protein-peptide complexes known as UHM-ULM complexes, although, including a few novel features. The peptide motif in Bud13 was analyzed using a combination of NMR and ITC measurements. Approximately 25 residues of a Bud13 peptide interact with Snu17 and include, in addition to the characteristic tryptophan, a C-terminal helix which forms upon binding. NMR data collection was made possible by construct optimization, as well as extensive screening of sample and experimental conditions.

The observations are in agreement with mutational analysis of Snu17, which suggest a rather large interaction surface, which is slightly different to that described previously for other UHM-ULM complexes. Future work includes full structural elucidation of a Snu17: Bud13 complex and additional mutational studies. These studies are anticipated to shed light on how the subunits of RES fulfill their functions. No structural details regarding the interaction of Snu17 and Pml1 could be established up to this point.

This work was done in close collaboration with the groups of Dr. Bertrand Séraphin, (CGM, Gif-Sur-Yvette, France) and Dr. Herman van Tilbeurgh (IBBMC, Orsay, France).



## 5.2. Introduction

Removal of non-coding introns from the pre-mRNA is a key step in the maturation of mRNA before it is exported into the cytoplasm for translation.<sup>48</sup> Regulation of splicing is closely connected to the assembly of the spliceosome, as this dynamic cellular machine of megadalton size is assembled in a stepwise manner at every new round of splicing.<sup>44</sup> The RES complex comprises three proteins, Snu17, Bud13 and Pml1, and is required for efficient splicing and nuclear retention of the unspliced pre-mRNA. The trimeric complex was discovered in 2004 during an effort to confirm the composition of Splicing Factor 3b (SF3b) in yeast.<sup>46</sup> The SF3b complex is associated with the U2 small nuclear ribonucleoprotein (snRNP) and had previously been described in humans. Snu17 was thought to be the yeast homolog of human p14, a protein responsible for branch point recognition during the spliceosome assembly. However, tandem-affinity purification (TAP) of Snu17 did not pull out partners of SF3b but the two other proteins of the RES complex as we now know it. The RES complex has also been shown to be conserved in humans and *Drosophila melanogaster*.<sup>45,173,174</sup>

The subunits of the RES complex are not essential for viability, but high-temperature growth of either Snu17 or Bud13 deletion strains is significantly reduced.<sup>46</sup> Snu17 was initially known as IST3 for 'increased sodium tolerance'<sup>175</sup>, while Bud13 had been correlated to 'bud selection site'.<sup>176</sup> Pml1 was discovered along with the characterization of the RES complex and named 'pre-mRNA leakage protein 1'.<sup>46</sup> RES is an acronym for retention and splicing.

The knowledge on how and when the RES complex interacts with the spliceosome is limited. Based on biochemical evidence it is known that the RES complex fulfills its function prior to the first splicing reaction. Deletion of either Snu17 or Bud13 in yeast limits the first splicing reaction, leading to the formation of the lariat, both *in vitro* and *in vivo*.<sup>46,177</sup> Although, this effect is the strongest for weak 5' splice sites at high-temperature growth.<sup>46</sup> Data from mass spectrometry indicates that components of the RES complex are present in affinity-purified B and C complexes of the spliceosome<sup>45</sup>, as well as in the yeast penta-snRNP<sup>178</sup>. This is in line with findings suggesting that the RES complex interacts with the U2 snRNP,<sup>177</sup> since the U2 snRNP only leaves the spliceosome after the second splicing reaction. Furthermore, a yeast-two-hybrid screen has suggested that Bud13 interacts with SF3b, a U2 snRNP-associated complex.<sup>179</sup> Bud13 has also been reported to co-purify with Cef1<sup>180</sup>, a protein related to splicing and which is part of the penta-snRNP of yeast<sup>178</sup> as well as in complex with Prp19<sup>45</sup>. However, being somewhat disputed it now seems to be evident that the RES complex is not stably associated with the U2 snRNA, or any other snRNA.<sup>46,177</sup> Together with the dispensable nature of RES complex for viability, this suggest a relatively dynamic and weak interaction with the spliceosome during splicing.

Nuclear retention of unspliced pre-mRNA can be attributed to the direct effect of preventing pre-mRNA from being exported, or the indirect effect of a factor targeting an

unspliced pre-mRNA to the spliceosome.<sup>181</sup> Hence, pre-mRNA leakage to the cytoplasm is often observed if the splicing function of the cell is diminished. One example, Mlp1 is localized to the nuclear pore and hinder export of pre-mRNA, which makes it an example of a protein with a direct effect on nuclear retention.<sup>80</sup> A similar function has been described for Pml39.<sup>182</sup> On the other hand, deletion of Mer1 in yeast leads to the leakage of specific pre-mRNAs, but its function is not uncoupled from splicing and Mer1 is therefore an example of indirect nuclear retention.<sup>183</sup> Interestingly, both Snu17 and Bud13 are suggested to be necessary to the function of Mer1.<sup>183,184</sup>

In the case of the RES complex, Pml1 is likely involved in direct nuclear retention of pre-mRNAs. In contrast, Snu17 and Bud13 deletions only exhibit indirect pre-mRNA leakage, since they are connected to a decrease of splicing efficiency.<sup>46</sup> Moreover, purine-rich exonic sequences have been suggested to play an important role for direct nuclear retention of pre-mRNA.<sup>185</sup> Modulation of nuclear retention and splicing by small molecules has been shown possible, and could be considered for future development of antitumor drugs.<sup>186</sup>

Extensive biochemical analysis of the RES complex provided evidence that Snu17 acts as a central binding platform for Bud13 and Pml1.<sup>187,188</sup> No direct binary interaction has been detected between Bud13 and Pml1. Snu17 was first described as containing a classical RNA recognition motif (RRM), since it contains the characteristic RNP1 and RNP2 sequences.<sup>177</sup> RRM s are among the most abundant protein domains and are common in splicing proteins and have been extensively characterized.<sup>189</sup> Nonetheless, new and compelling data show that the RRM of Snu17 is responsible for binding a peptide motif in the C-terminus of Bud13 ( $K_D \sim 2-7$  nM).<sup>187,188</sup> Thus, the RRM of Snu17 belongs to a small sub-family known as U2AF homology motifs (UHMs), which contain degenerated RRM s that evolved to interact with tryptophan-containing peptides instead (Figure 4.2.1 A,C).<sup>190</sup> The UHM of Snu17 is well conserved in higher eukaryotes (Figure 4.2.1 B). The peptidic interaction motifs are called UHM linear motifs (ULMs). W232 of Bud13 has been suggested to be essential for the interaction by both ITC (isothermal titration calorimetry) and SEC (size-exclusion chromatography) experiments<sup>187</sup>. Intriguingly, this is contradicted by *in vivo* co-expression and purification data of a W232A mutated His6:Snu17-Bud13 operon.<sup>188</sup> The molecular understanding of the interaction of Snu17 and Bud13 indicates that the Snu17-Bud13 interaction may differ from the canonical UHM-ULM type of interaction.

In addition, the C-terminal region of Snu17 is suggested to be necessary for binding of Pml1 ( $K_D \sim 1$   $\mu$ M).<sup>187,188</sup> However, biochemical or structural details regarding the nature of the interaction are missing. It is not clear whether the C-terminus of Snu17 functions as a linear motif interacting with a structural domain in Pml1<sup>188</sup>, or, if it together with the UHM domain forms an additional binding site for residues protruding from Pml1<sup>187</sup>. The full RES complex (71 kDa) has resisted structural characterization due to widespread structural flexibility within the individual proteins.<sup>187</sup> However, the structure of the forkhead-associated (FHA) domain in Pml1 was recently solved by two groups

independently.<sup>188,191</sup> It contains an 11-stranded  $\beta$ -sandwich and three short helical regions. Both reported structures start at around residue 50, indicating a flexible N-terminus. Additionally, it was shown that residues 52-61 are important for stability of the domain as they act as a clamp stabilizing  $\beta_3$  and  $\beta_6$ .<sup>191</sup> FHA domains are known to interact with peptides comprising phosphorylated threonines.<sup>192,193</sup> Such phosphopeptides bind to the loops at one edge of the  $\beta$ -sandwich of the FHA domain. Nevertheless, a link between phosphorylation and splicing regulation by the RES complex has yet to be established. Up to now, no phospholigand has been established (library screening; Mark Brooks, personal communication), and an *in vivo* reporter assay suggest that splicing is not affected by mutations in the putative binding cleft of Pml1.<sup>188</sup> A direct interaction between RNA and the RES complex has so far not been observed.

In summary, the functions of the RES complex are poorly understood and are so far not assigned to specific subunits or domains. Biochemically the organization of the RES complex has been laid out, but molecular details of the intramolecular interactions and the functions are yet to be ascertained. Here, we report an initial structural analysis of the assembly of the RES complex. The focus lies on the interaction between Bud13 and Snu17, which is believed to act as a central binding platform in the complex. These two proteins interact through a novel UHM/ULM-type of interaction, comprising an approximately 25 residue long peptide motif in Bud13. A full structural elucidation of this protein-peptide complex is ongoing.

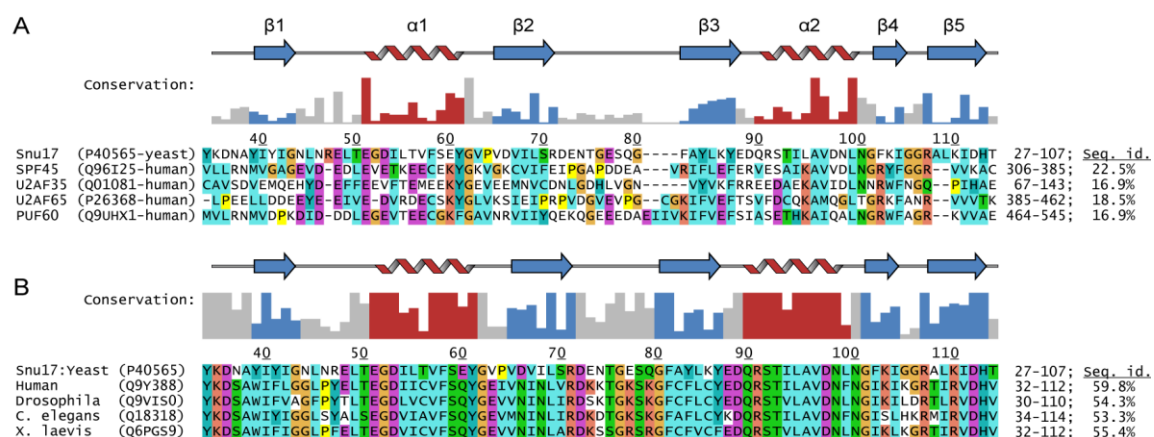


**Figure 5.2.1 Multiple sequence alignment of Snu17 UHM to other UHMs and to homologs in eukaryotic species.**

(A) Snu17 UHM aligned to known human UHMs. Red and blue columns in the conservation graph indicate  $\alpha$ -helices and  $\beta$ -strands, respectively. Uniprot accession codes in brackets. Numbering above the alignment is according to the expression construct of Snu17<sup>1-113</sup>, while the original residue numbering is indicated on the right side. The sequence identity to Snu17 is given at the far right. (B) Alignment of Snu17 UHM to the homolog of higher eukaryotic species. Similar features as in (A). (C) Homology model of Snu17 UHM based on free SPF45 (2PE8.pdb).  $\beta$ -strands (blue) and  $\alpha$ -helices (red) are numbered as in (A).

## 5.3. Results

### Initial analysis of full-length proteins

Characterization of full-length constructs of individual proteins indicated that all three contain flexible regions (Figure 5.3.1 A-C).  $^1\text{H}$ ,  $^{15}\text{N}$  HSQC spectra of  $\text{Snu17}^{\text{FL}}$ ,  $\text{Bud13}^{\text{FL}}$  and  $\text{Pml1}^{\text{FL}}$  show overlapping and intense signals around 8 ppm, indicative of unfolded or partially unfolded regions. Dispersed resonances, belonging to the folded FHA and UHM domain of  $\text{Pml1}^{\text{FL}}$  and  $\text{Snu17}^{\text{FL}}$ , respectively, were visible. In solution, unbound  $\text{Bud13}^{\text{FL}}$  can be suggested not to contain any elements of secondary structure.<sup>187</sup> A spectrum was also recorded of  $^{15}\text{N}$  labeled  $\text{Snu17}^{\text{FL}}$  in a reconstituted RES complex (Figure 5.3.1 D). This spectrum was of such poor quality that it suggested partial aggregation in the sample. No further NMR experiments were done on the full complex. These results confirmed what was known and expected from the proteins<sup>187</sup>, however, it was now clear why earlier crystal screens had failed; this was either due to flexibility in the complex, especially in Bud13, or due to aggregation of the protein samples. To extend our structural understanding of the complex, we decided to only study isolated domains and their binary interactions (Figure 5.3.1).

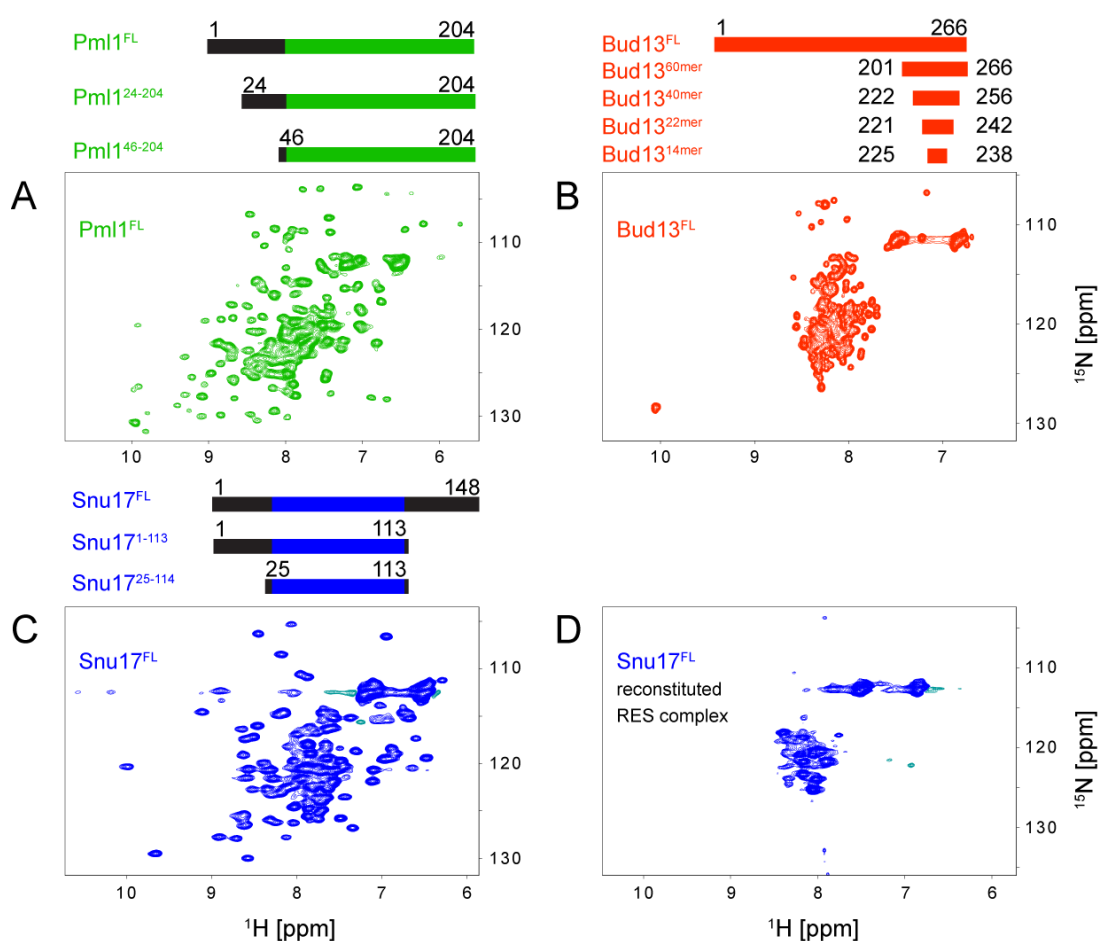


**Figure 5.3.1**  $^1\text{H}$ ,  $^{15}\text{N}$  HSQC spectra of individual proteins and of the full RES complex. (A)  $\text{Pml1}^{\text{FL}}$  (B)  $\text{Bud13}^{\text{FL}}$  (C)  $\text{Snu17}^{\text{FL}}$  (D) Reconstituted RES complex with  $^{15}\text{N}$  labeled  $\text{Snu17}^{\text{FL}}$ . All measurements were done at 300K. Additionally, common constructs referred to in the text, are illustrated. In the case of Pml1 and Snu17, the green and blue area indicates the folded FHA and UHM/RRM domains, respectively.

## The interaction between Snu17 and Bud13.

It was not obvious how to obtain sufficient amounts of stable Snu17 protein for structural studies. Many different problems were solved before the actual analysis of the complexes started. Firstly, it was decided upon to use a shorter construct, Snu17<sup>1-113</sup>, as the C-terminus was flexible. A <sup>1</sup>H, <sup>15</sup>N HSQC spectrum of Snu17<sup>1-113</sup> showed that the UHM domain was still intact in the shorter construct (Figure 5.3.2 A). Removing the N-terminus as well diminishes the purification yield in our hands. Secondly, Snu17<sup>1-113</sup> was very unstable as shown by H/D-exchange experiments (Figure 5.3.3 A-B) and it precipitated heavily over time. However, at low concentrations Snu17<sup>1-113</sup> could be used for ligand titrations. It was discovered that 10% DMSO stabilized the protein sufficiently that backbone experiments to be recorded and analyzed. The UHM structure was not heavily perturbed upon addition of DMSO as indicated by a <sup>1</sup>H, <sup>15</sup>N HSQC spectrum (Figure 5.3.7 A). General shifts, and not specific or isolated ones, are expected since the buffer has different properties. Third, to increase expression yields Snu17<sup>1-113</sup> was produced as inclusion bodies and refolded (see 5.6 *Materials and Methods*). Comparing spectra from either procedure shows that the UHM structure is identical (Figure 5.3.2 B). Finally, it was noticed that binding of Bud13 to Snu17<sup>1-113</sup> increased stability and improved behavior of the sample. The increased stability was for example shown by a thermofluor assay and hydrogen/deuterium-exchange (H/D-exchange; Figure 5.3.3 C-E). Binding of a Bud13 peptide increased the melting point of Snu17 by ~5°C. The hydrogen exchange experiment indicates the presence of stable elements of secondary structure that agree well with a homology model (Figure 5.3.3 F). Because of this, we ended our efforts to solve the structure of Snu17<sup>1-113</sup> alone, and focused on a structure of ligand-complex with a section of Bud13.

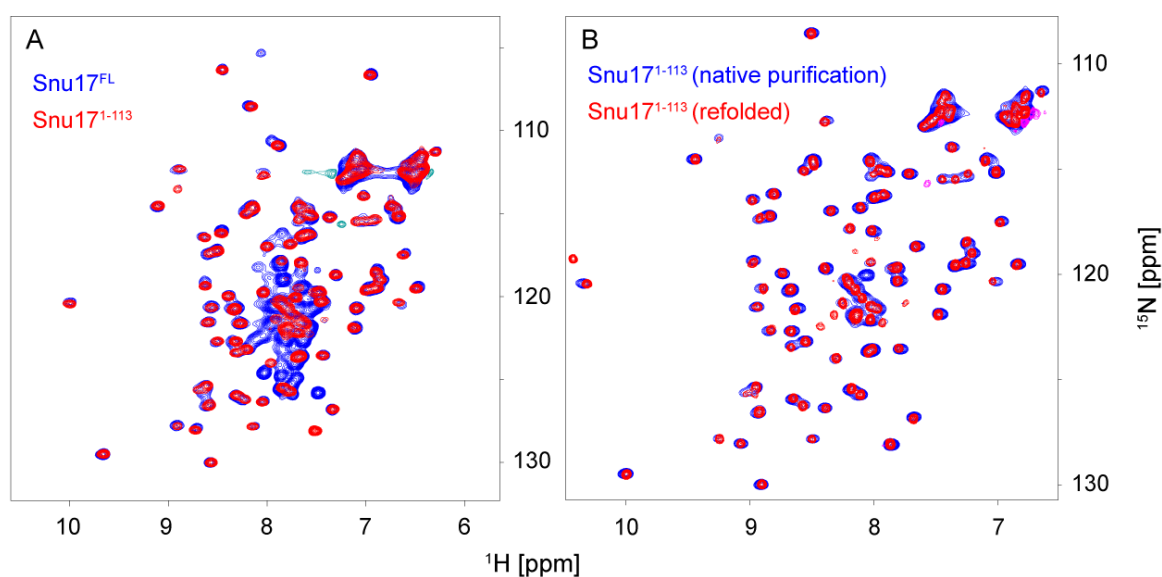


**Figure 5.3.2 Optimization of Snu17 construct and expression procedures.** (A) Comparison of Snu17<sup>FL</sup> and Snu17<sup>1-113</sup> by NMR. The UHM domain is still intact in the shorter construct. (B) Comparison of Snu17<sup>1-113</sup> purified under native and denaturing conditions. Identical spectra indicate that the refolding procedure worked. All <sup>1</sup>H, <sup>15</sup>N HSQC spectra recorded at 300K on 100  $\mu$ M samples.

An evident result of the stabilizing effect of DMSO was that the time to concentrate the protein sample was decreased dramatically. This suggests a more compact protein structure that does not get trapped in the filter pores of the concentration device. A standard set of backbone assignment experiments were recorded on a 250  $\mu\text{M}$   $^{15}\text{N}/^{13}\text{C}$  double-labeled Snu17<sup>1-113</sup> sample at 298K. Of the 120 residues in the expression construct, 87 (72%) could be assigned. Nevertheless, approximately 84% of the backbone amides of the UHM domain, which was of most interest to us, were assigned. Most of the non-assigned residues were in loops or at the domain termini. A chemical shift index (CSI) analysis points towards the existence of the expected secondary structure elements of an RRM/UHM domain (Figure 5.3.4 A). CSI analysis compares the chemical shift of C $\alpha$  and C $\beta$ , which depends on the secondary structure, to a database and gives an estimate of the propensity of  $\alpha$ -helices or  $\beta$ -strand.

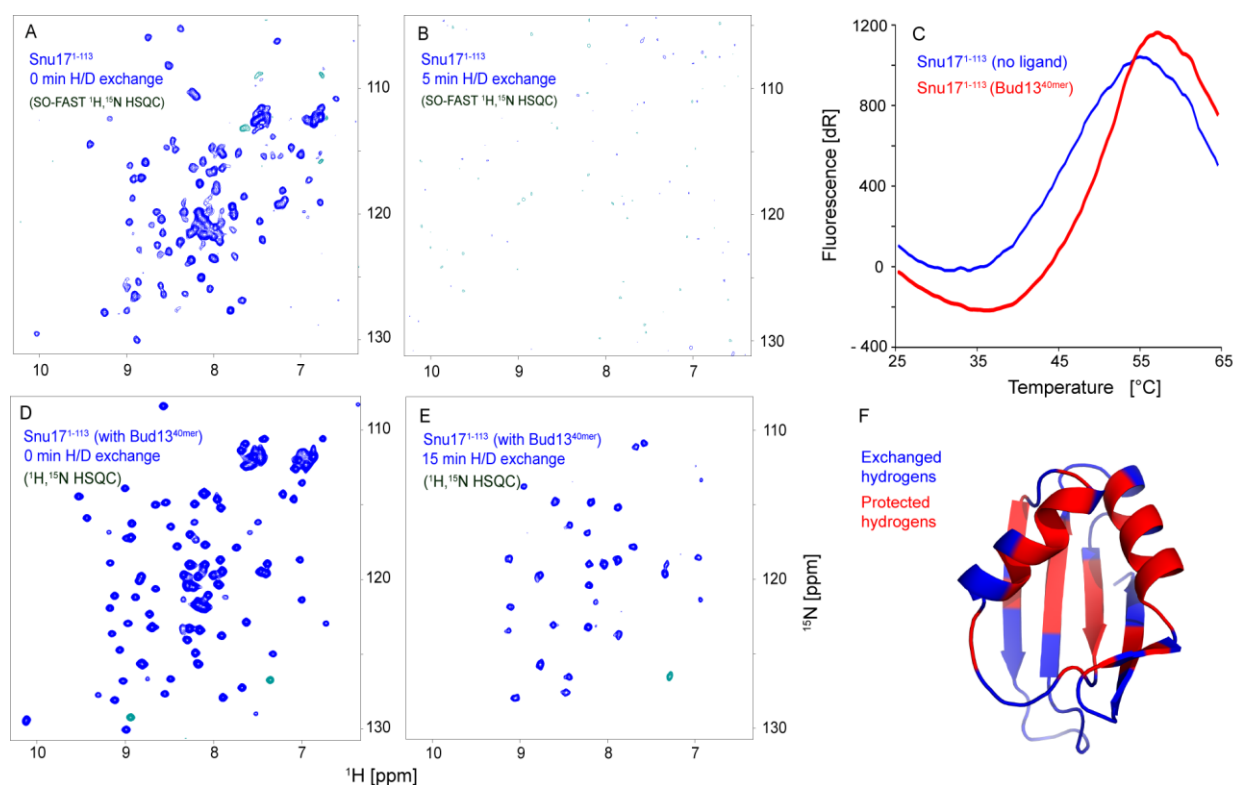


**Figure 5.3.3 Stability of Snu17<sup>1-113</sup> with and without a ligand.** (A-B) H/D exchange of Snu17<sup>1-113</sup> without any ligand. Within 5 min all amide protons have exchanged. (C) Thermal stability of Snu17<sup>1-113</sup> is increased by  $\sim 5^\circ\text{C}$  when bound to Bud13<sup>40mer</sup>. The difference to the initial fluorescence is plotted against the temperature, for Snu17<sup>1-113</sup> with ligand (red) and without (blue). (D-E) H/D exchange of Snu17<sup>1-113</sup> bound to Bud13<sup>40mer</sup>. After 15 min approximately 30 amide protons have not exchanged. This means they are involved in hydrogen bonds, and indicate that the UHM domain of the complex has a more stable fold. (F) H/D exchange data plotted onto a homology model of Snu17 UHM (2pe8.pdb). The result indicates which hydrogen atoms are exchanged (blue) and which are protected (red).



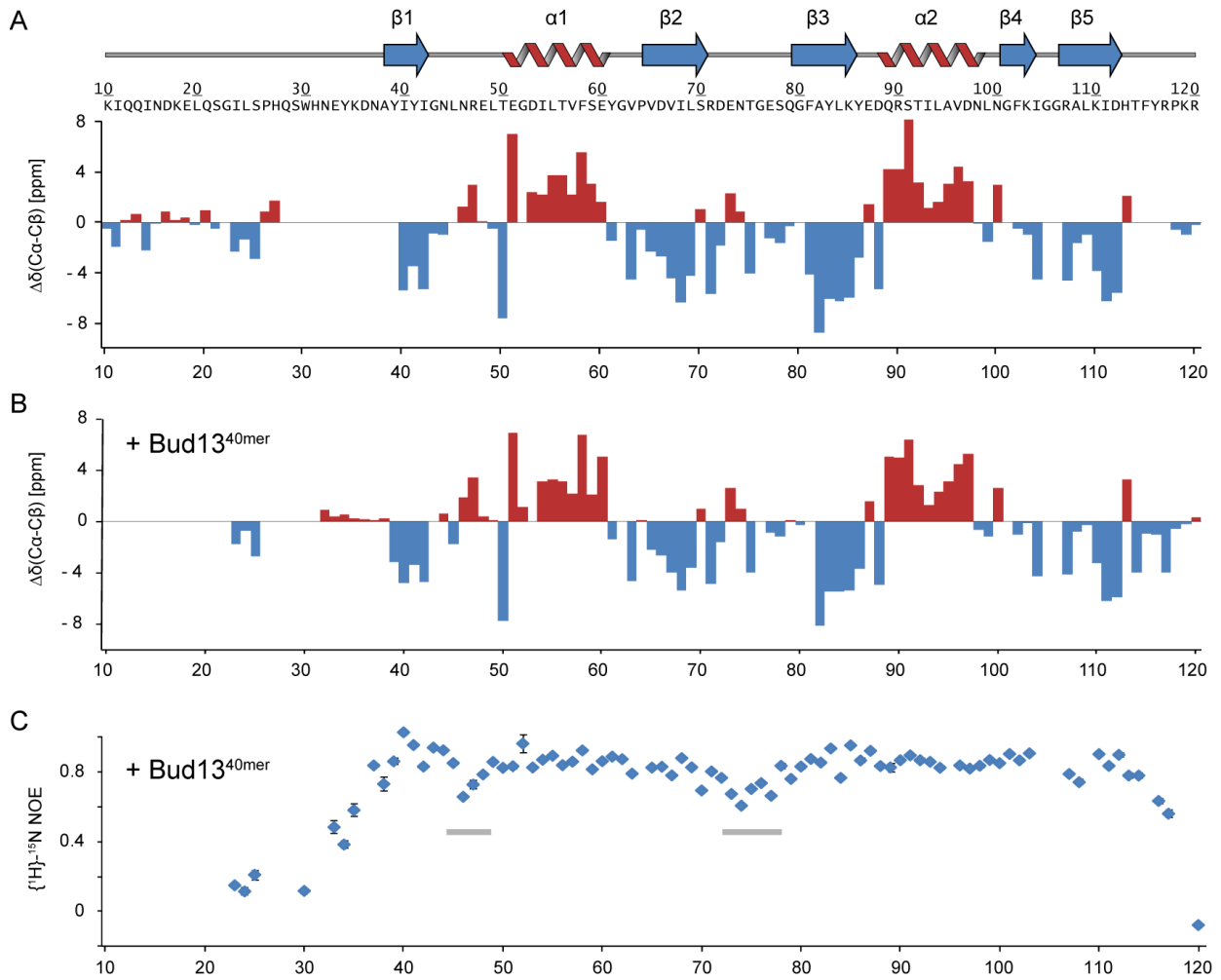


**Figure 5.3.4 Analysis of secondary structure and residue flexibility in Snu17<sup>1-113</sup> by NMR.** Residue numbering in the plot is from the expression construct.  $\beta$ -strands (blue arrows) and  $\alpha$ -helices (red) found in a homology model are indicated above the plots (Figure 4.2.1 C). (A) CSI analysis of free Snu17<sup>1-113</sup> (B) CSI analysis of Snu17<sup>1-113</sup> bound to Bud13<sup>40mer</sup>. Both plots show that the expected secondary structure elements are present in Snu17<sup>1-113</sup> in solution. (C) {<sup>1</sup>H}-<sup>15</sup>N heteronuclear NOE measurements confirm a folded UHM domain, with flexible termini and two slightly flexible loops (grey bars).

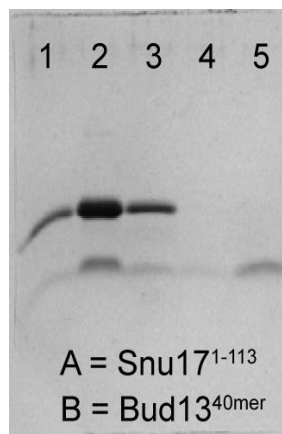
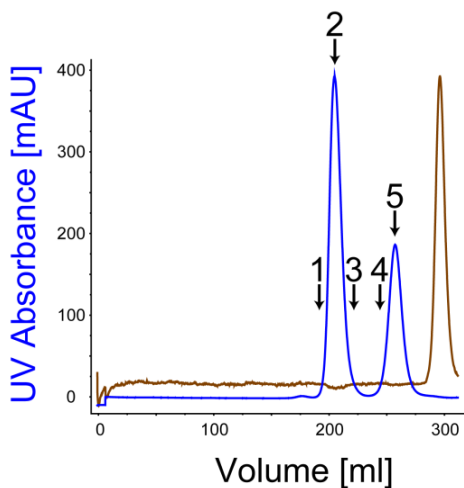


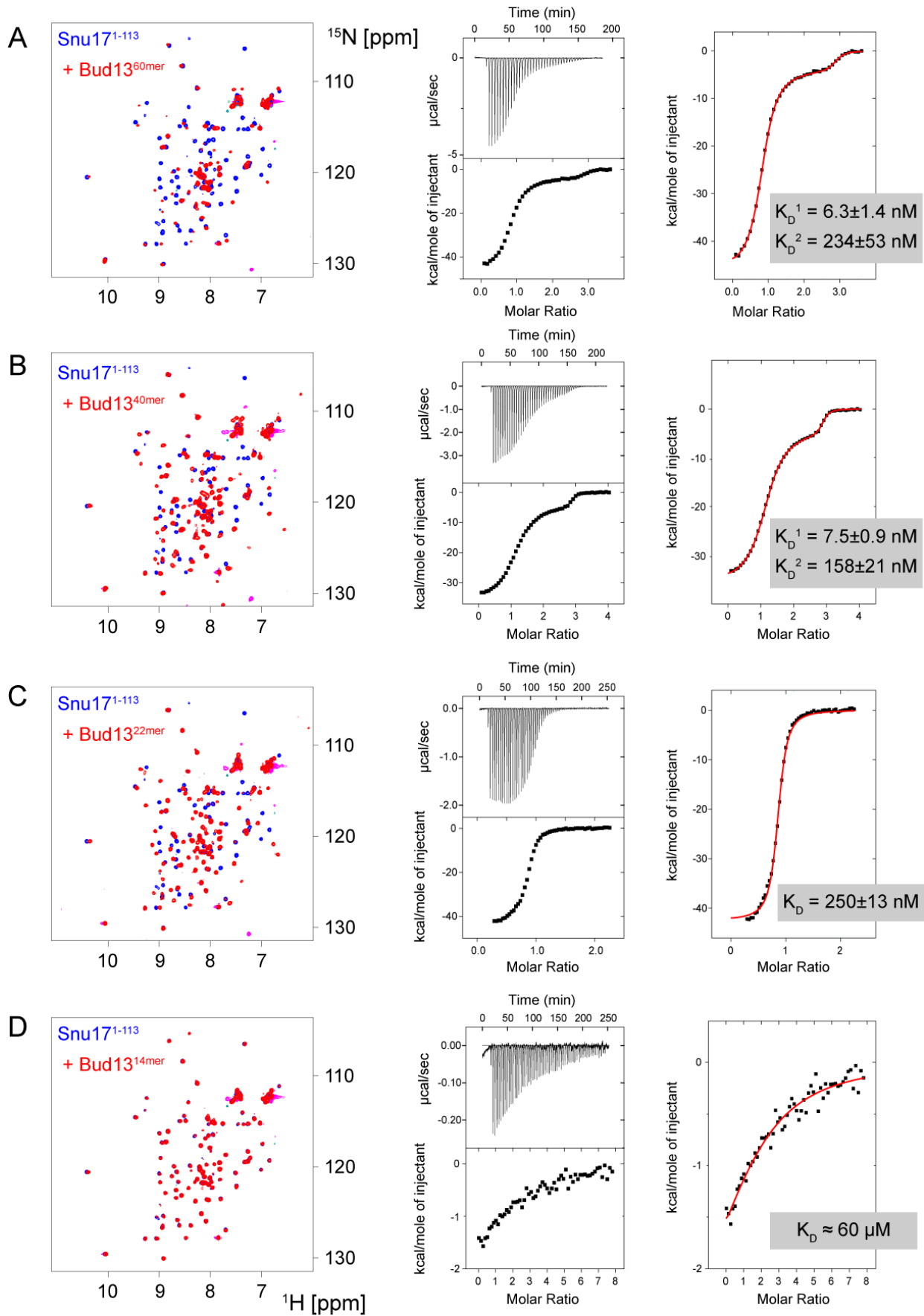
**Figure 5.3.5 Size exclusion chromatography of a complex containing Snu17<sup>1-113</sup> and Bud13<sup>40mer</sup>.**

The analysis of a sample containing an excess of Bud13 shows that fractions of the major peak contains the complex. The 10kDa difference between the fragments could be well resolved using Tricine-containing SDS-PAGE gels. Next to the UV curve (blue) is the conductance (brown), showing a separate buffer peak.

Next, we mapped the binding of Bud13 onto Snu17 and optimized the length of the interacting Bud13 peptide. This was done by a combination of NMR and ITC. First, we tested a 60mer recombinant peptide that already had been shown to interact with Snu17<sup>FL</sup>.<sup>188</sup> We could confirm binding of the Bud13<sup>60mer</sup> to Snu17<sup>1-113</sup> by NMR (Figure 5.3.6 A). This rather long peptide induced extensive chemical shift perturbations but also aggregation of the protein sample. Line broadening and low signal to noise could be observed. This excluded this peptide from any structural studies. Upon titration of a shorter recombinant peptide, Bud13<sup>40mer</sup>, similar shifts were induced but the quality of the spectrum remained high (Figure 5.3.6 B). Additionally, two purchased peptides were tested, a 22mer and a 14mer, Bud13<sup>22mer</sup> and Bud13<sup>14mer</sup>, respectively. Bud13<sup>22mer</sup> exhibited strong binding, but addition of Bud13<sup>14mer</sup> only resulted in weak chemical shift changes (Figure 5.3.6 C,D). This initially told us that the 22mer could be considered a minimal interaction motif. However, after additional studies this conclusion had to be revised.

The ligands were further characterized by ITC to understand the thermodynamics driving the interaction. All four ligands showed affinity for Snu17<sup>1-113</sup>, but in very different regimes (Figure 5.3.6 A-D; right columns). Both the isotherms of Bud13<sup>60mer</sup> and Bud13<sup>40mer</sup> could only be fitted to equations for a two-site binding model. They did so with similar affinities,  $K_{D1} = 6.3 \pm 1.4$  nM and  $K_{D2} = 234 \pm 53$  nM for Bud13<sup>60mer</sup> and,  $K_{D1} = 7.5 \pm 0.9$  nM and  $K_{D2} = 158 \pm 21$  nM for Bud13<sup>40mer</sup>. This together with the NMR data show that the extra residues of the 60mer do not add any increased affinity. In contrast to the longer recombinant peptides, Bud13<sup>22mer</sup> exhibits a one-site binding isotherm,  $K_D = 250 \pm 13$  nM. Bud13<sup>14mer</sup> interacts with Snu17<sup>1-113</sup> in similar fashion but only relatively weakly,  $K_D \approx 60$   $\mu$ M. Overall, this fits well with the NMR data. The 14mer is too short to interact strongly with Snu17. Generally all ligands displayed a large negative enthalpy contribution counteracted by a negative entropy.

It is important to note that the ligand titrations by NMR were performed with 10% DMSO in the buffer, to prevent unbound Snu17<sup>1-113</sup> from precipitating. This was not the case for the ITC, where no DMSO was used, due to lower protein concentrations. To understand the discrepancies, especially between the behavior and affinity of the 14mer, DMSO was used as an injectant in an ITC experiment (Figure 5.3.7 B). The result implies that DMSO might induce Snu17<sup>1-113</sup> to achieve a more stable conformation, and as a result heat is released. Note that the stoichiometry is not one-to-one for the fit, thus, we are not observing a real binding event. Furthermore, we performed additional ITC experiments with the Bud13<sup>40mer</sup> in the presence of 10% and 0.5% DMSO (Figure 5.3.7 C-D). Even at such low levels of DMSO, the affinity for the peptide dropped to 12  $\mu$ M, which is three orders of magnitude lower than without DMSO present. Additionally, the second binding event vanished and the isotherm could be fit to a one-site binding model. In summary, DMSO does not perturb the structure a lot (Figure 5.3.7 A) but competes with the binding of Bud13.



See next page for figure legend.

**Figure 5.3.6 Optimization of the Bud13 ULM peptide by NMR titrations and ITC.** A 100  $\mu\text{M}$   $^{15}\text{N}$  labeled sample of Snu17<sup>1-113</sup> was titrated with four different Bud13 peptides. Titrations were done at 298K and to a ratio of 1:2, protein to ligand concentration. The same peptides were analyzed in ITC experiments. Importantly, in the NMR titrations 10% DMSO is present in the buffer, see also Figure 5.3.7. (A) Addition of Bud13<sup>60mer</sup> result in aggregation as indicated by a low signal-to-noise spectrum. Binding isotherm can be fitted by a two-binding site equation. (B) Similar ITC results were observed with Bud13<sup>40mer</sup>, however, no aggregation was observed. (C) Bud13<sup>22mer</sup> has lower affinity and can be fitted to a one-binding site equation. (D) Bud13<sup>14mer</sup> has a very low affinity and no induced shifts is observed by NMR. Probably due to the DMSO which weakens the interaction.

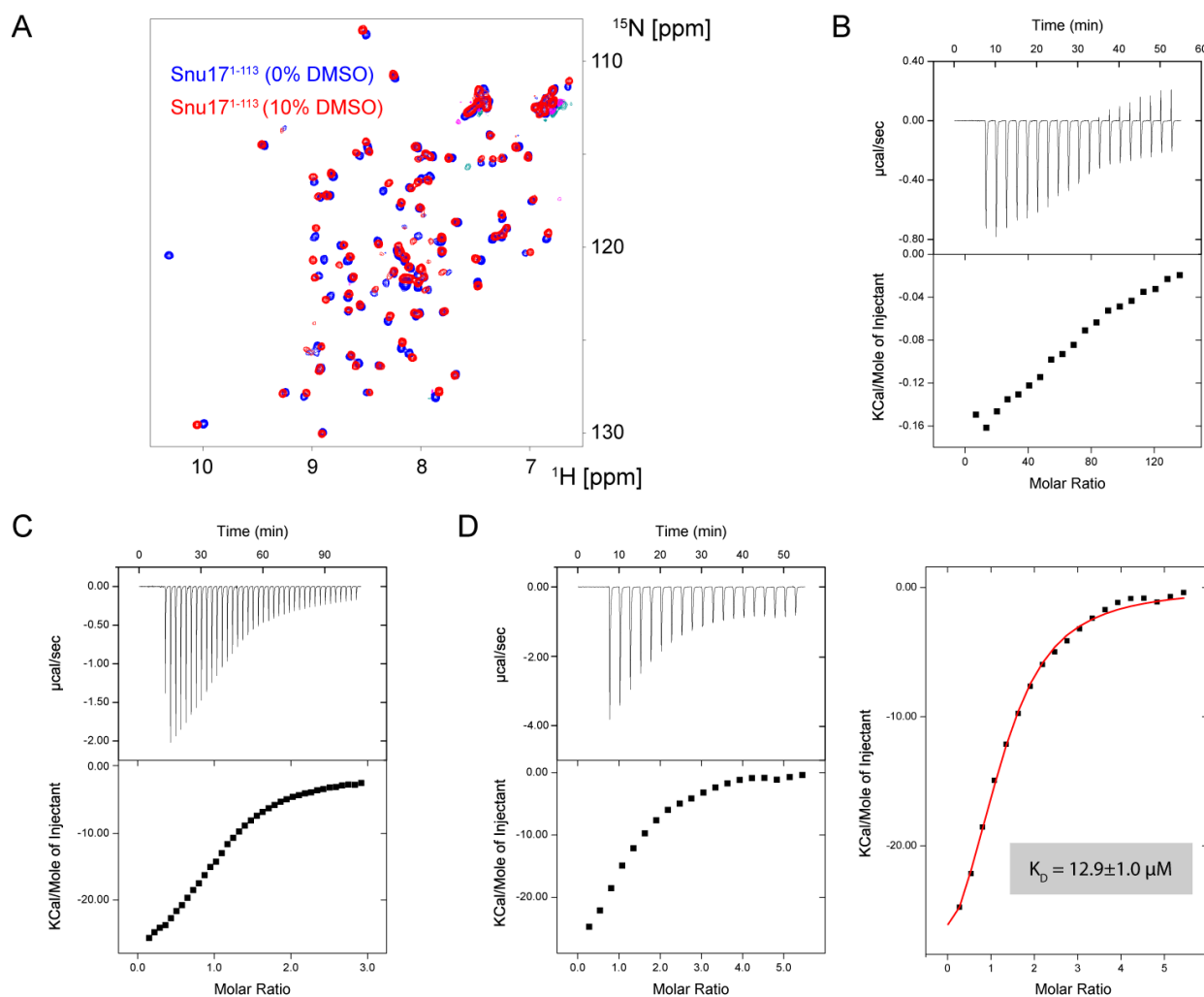


**Figure 5.3.7 DMSO was found to stabilize Snu17<sup>1-113</sup> and to weaken the interaction of Bud13<sup>40mer</sup>**

(A) DMSO increase the solubility of Snu17<sup>1-113</sup>, but has only slight effect on UHM domain fold. Comparison of Snu17<sup>1-113</sup> with (red) and without (blue) 10% DMSO. (B) The stabilizing effect might be observed as an exothermic process in a ITC measurement. Binding isotherm for injection of DMSO into a Snu17<sup>1-113</sup> sample. Note the high molar ratio of DMSO (C) The affinity between Snu17<sup>1-113</sup> and Bud13<sup>40mer</sup> is decreased with 10% DMSO present in the buffer. The data can be fitted to a one-binding site equation, which is not the case in the absence of DMSO (Figure 5.3.6 B). (D) Also 0.5% DMSO (70 mM) weakens the interaction.  $K_D = 12.9 \pm 1.0 \mu\text{M}$ .

Chemical shift perturbations (CSPs) induced by Bud13<sup>60mer</sup>, Bud13<sup>40mer</sup> and Bud13<sup>22mer</sup> were compared (Figure 5.3.8 A-B). Interestingly, there is hardly no difference between the recombinant 60mer and 40mer peptides. Bud13<sup>22mer</sup>, on the contrary, induce different CSPs than Bud13<sup>40mer</sup>. The CSPs of Bud13<sup>40mer</sup> and Bud13<sup>22mer</sup> on Snu17<sup>1-113</sup> were quantified and plotted for each residue. Despite the fact that the shifts are different, both peptides mostly affect the same residues (Figure 5.3.8 D-E). The highlighted region of perturbed backbone amide resonances coincide well with the expected binding site, as known from other UHM-ULM complexes (Figure 5.3.8 C; see 5.4 Discussion).

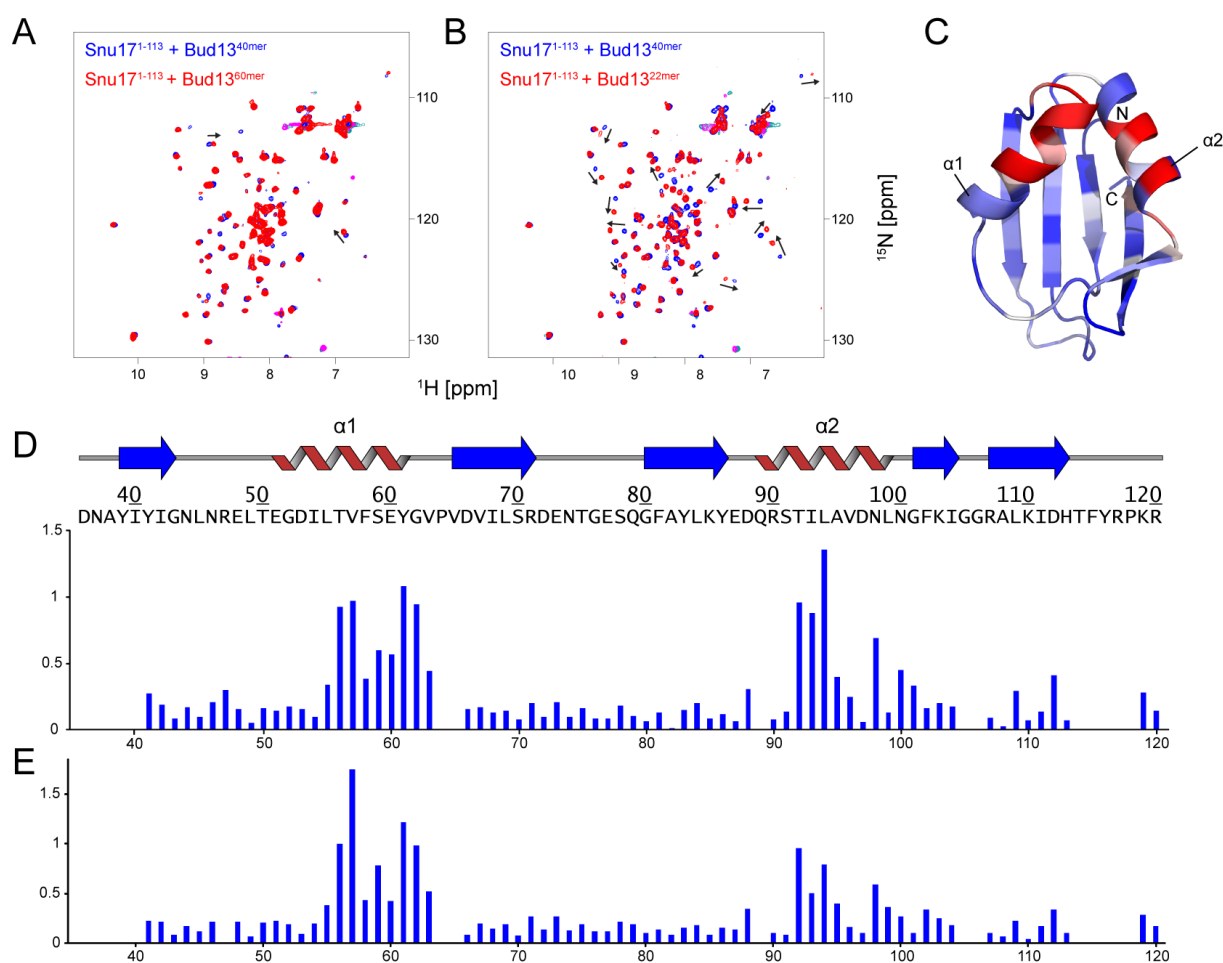


**Figure 5.3.8 Analysis of the Bud13 interaction site on Snu17, a comparison of peptides.** (A) Bud13<sup>40mer</sup> (blue) and Bud13<sup>60mer</sup> (red) induce similar chemical shift perturbations (CSPs) upon titration to Snu17<sup>1-113</sup>. Only slight differences can be observed (marked with black arrows). This indicates almost identical binding sites and binding modes, and is supported by the ITC data (see Figure 5.3.6 A-B). (B) In contrast, Bud13<sup>22mer</sup> (red) induce different shifts than Bud13<sup>40mer</sup> (blue). This suggests differences in the size of the interaction site, in binding mode, or in both. (C) The induced CSPs of Bud13<sup>40mer</sup> plotted onto a homology model of Snu17<sup>1-113</sup> (2pe8.pdb). The CSPs overlap well with the expected binding site of other known UHM-ULM complexes. Blue to red, through white, indicate increasing perturbations and are calculated as:  $CSP = \sqrt{\delta H [ppm]^2 + 0.1 \times \delta N [ppm]^2}$ . N- and C-terminus as well as  $\alpha$ -helix 1 and 2 are labeled. (D) As (C) but the CSPs plotted per residue in a column chart. Secondary structure definitions are taken from the homology model.  $\beta$ -strands are depicted as blue arrows and  $\alpha$ -helices in red. Numbering corresponds to our expression construct. (E) Same as (D) but with CSPs of Bud13<sup>22mer</sup>.

To gain knowledge about how many residues in Bud13 are involved in the interaction with Snu17, we next acquired several spectra of  $^{15}\text{N}$  labeled Bud13<sup>60mer</sup> and Bud13<sup>40mer</sup> in the presence of unlabeled Snu17<sup>1-113</sup> (Figure 5.3.9). In line with earlier findings, the 60mer peptide exhibited problems of aggregation. Both peptides show similar chemical shift changes upon binding to Snu17<sup>1-113</sup>. In total, approximately 25 shifting resonance were observed and expected to be involved in the interaction between Bud13<sup>40mer</sup> and Snu17<sup>1-113</sup>.

Evaluating all the available data, we decided to continue our work with the complex of Bud13<sup>40mer</sup> and Snu17<sup>1-113</sup>. Bud13<sup>60mer</sup> did not behave well, as also observed by SDS-PAGE where it gave fuzzy and jagged bands, indicating dimerization or oligomerization (data not shown). Bud13<sup>22mer</sup> behaved well and had strong affinity for Snu17, but was not available recombinantly. All efforts to express and purify shorter constructs of Bud13 (15-22 residues long) had failed. Furthermore, as clearly demonstrated Bud13<sup>14mer</sup> had only a very weak affinity for the UHM domain. On the other hand, Bud13<sup>40mer</sup> fulfilled the basic requirements by not inducing aggregation, having strong affinity and being obtainable in sufficient amount with  $^{15}\text{N}/^{13}\text{C}$  labeling. Additionally, the amount of chemical shift changes (Figure 5.3.8 B) and the rather different binding isotherm (Figure 5.3.6 B), convinced us this was the most interesting alternative.

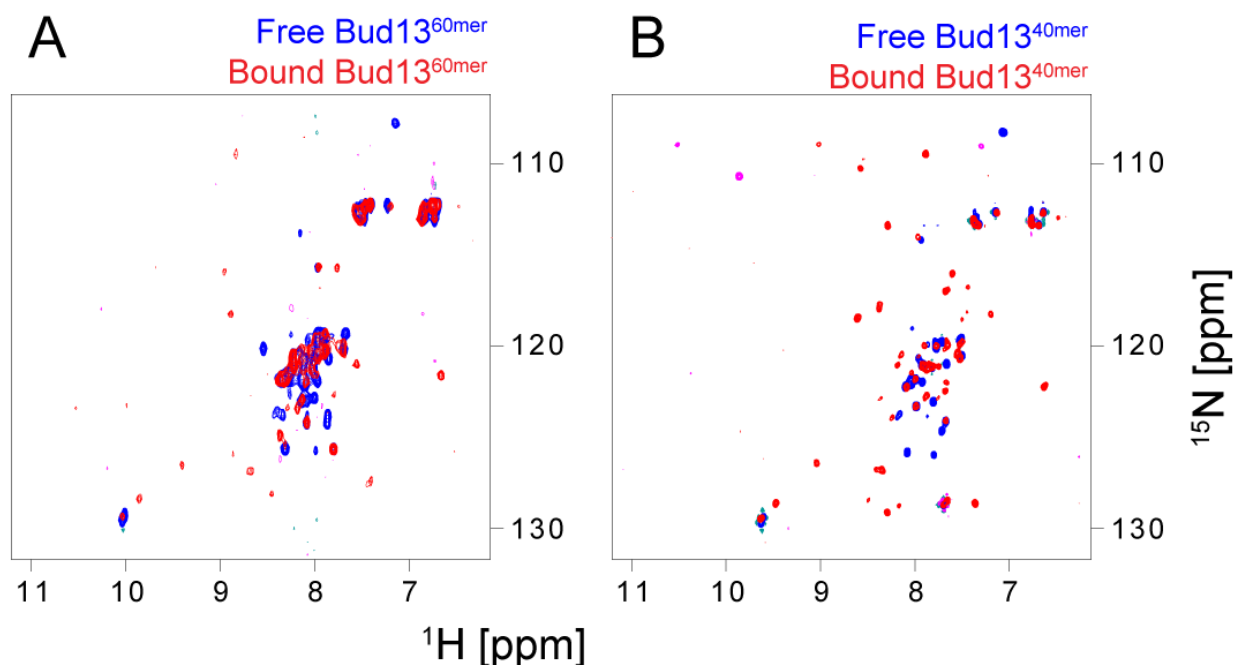


**Figure 5.3.9**  $^{15}\text{N}$  labeled recombinant Bud13 peptides titrated with unlabeled Snu17<sup>1-113</sup>. (A) Unbound Bud13<sup>60mer</sup> (blue) as well as in complex with Snu17<sup>1-113</sup> (Red). Decreased signal-to-noise suggest aggregation in the sample. (B) Same as (A) but with  $^{15}\text{N}$  labeled Bud13<sup>40mer</sup>. As relatively many resonances appear in new positions, a large interaction surface might be expected. Spectra were recorded at 298K with Snu17<sup>1-113</sup> in two times excess.



Both Bud13<sup>40mer</sup> and Snu17<sup>1-113</sup> were doubly-labeled and complexed to unlabeled counterparts. However, when prepared at high concentration, we realized that once more we had a problem of aggregation as indicated by a low quality HSQC spectrum. First, we tried to solve it by buffer optimization guided by a thermofluor assay (data not shown), as well as by re-constituting the complex using gelfiltration. The results were inconclusive and did not improve the quality of the sample. Even though counterintuitive, we also acquired NMR spectra at increased temperatures (Figure 5.3.10). This in fact solved our problems by increasing thermal energy and decreasing the correlation time of the complex. Faster tumbling of the protein complex leads to slower relaxation and sharper NMR signals. At high temperature the exchange of the peptide posed a problem to us. Due to the instability of free Snu17<sup>1-113</sup> an excess of Bud13<sup>40mer</sup> had to be used. A stable complex, yielding a high-quality NMR spectrum at 318K (45°C), required a 1:2.5 ratio of protein to peptide concentration.

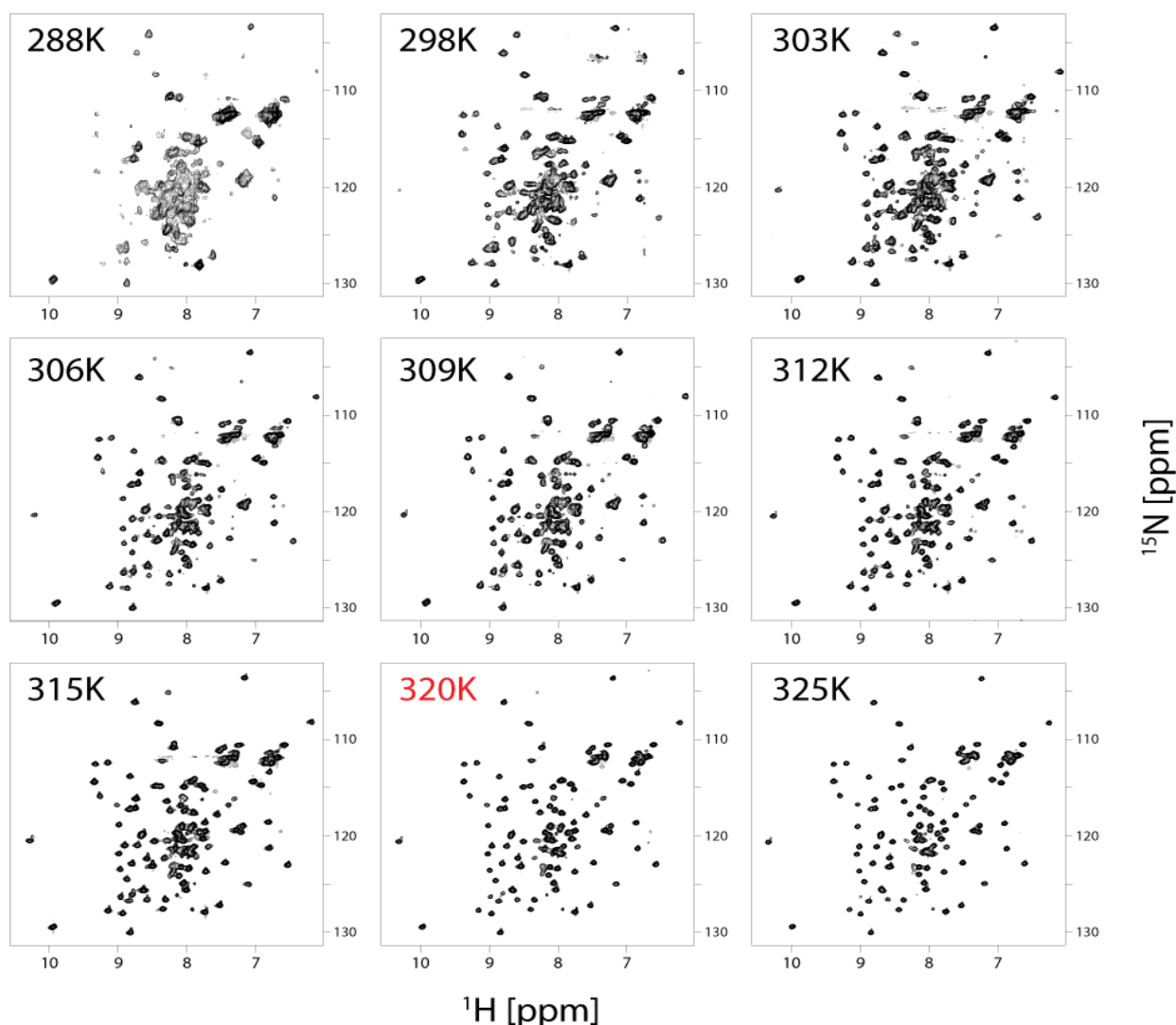


**Figure 5.3.10 High temperature is needed for recording high quality NMR data.** <sup>1</sup>H, <sup>15</sup>N HSQC spectra of a Snu17<sup>1-113</sup>: Bud13<sup>40mer</sup> complex at increasing temperatures. The quality of the spectra suggest aggregation at low temperature and monomeric behavior at high temperatures. At 320K the signals are sharp and the sample is stable. Increasing to 325K led to precipitation of protein.

The backbone amides of Bud13<sup>40mer</sup> could be assigned to an high extent (90%) and were analyzed by CSI (Figure 5.3.11 A-B). Intriguingly, the analysis suggests the formation of a helix in Bud13<sup>40mer</sup> upon binding to Snu17<sup>1-113</sup>. The helix is C-terminal to the tryptophan, which is characteristic and essential in all UHM-ULM interactions, and could be a reason to the differences observed in previous ITC measurements. Heteronuclear {<sup>1</sup>H}-<sup>15</sup>N NOE was recorded for Bud13<sup>40mer</sup> in complex and shows that almost all of the residues are rigid (Figure 5.3.11 C). Only a few residues at each terminus are designated flexible. The relaxation data is in agreement with the observation that numerous residues in the peptide are perturbed upon titration of Snu17<sup>1-113</sup> (Figure 5.3.9). Together with the CSI analysis, this data suggest that the interaction between Bud13 and Snu17 is not of the classical UHM-ULM type. A T<sub>2</sub> estimation by 1D jump-return spin-echo experiments with different relaxation delays, suggest that the complex tumbles as a monomer in solution (data not shown).<sup>194</sup>

The protein backbone amides of Snu17<sup>1-113</sup> in complex with Bud13<sup>40mer</sup> were assigned using a triple labeled sample (<sup>15</sup>N/<sup>13</sup>C/<sup>2</sup>H). As for Bud13<sup>40mer</sup> most flexible amides exchange to fast at high temperatures and are broadened out beyond detection. One positive thing about this is that the spectra get less crowded. 96% of the backbone amides of the UHM domain could be assigned. CSI analysis of the Snu17<sup>1-113</sup> complex suggests similar secondary structure elements as for the free protein (Figure 5.3.4 B). On the same sample also heteronuclear {<sup>1</sup>H}-<sup>15</sup>N NOE was recorded. This data show an almost rigid UHM domain flanked by flexible termini (Figure 5.3.4 C). Two slightly flexible regions might be expected around residue 46 and 74 in the Snu17<sup>1-113</sup> construct, which in a homology model of Snu17<sup>1-113</sup> correspond to two loops.

At the moment, we are at the stage of collecting and analyzing data for side-chain assignment and derivation of distance restraints. It appears promising, but difficulties may arise from the relatively intense CH signals coming from unfolded parts of Snu17<sup>1-113</sup>. These tend to disturb the baseline and to obscure less intense resonances. The protons and carbons of Bud13<sup>40mer</sup> are to be assigned using TOCSY-based experiments starting at the backbone amide. To be able to introduce correct distance restraints between Snu17<sup>1-113</sup> and Bud13<sup>40mer</sup>, <sup>13</sup>C-edited and <sup>13</sup>C,<sup>15</sup>N filtered experiments have been recorded. Initial analyses of such spectra have identified several intermolecular NOEs (Figure 5.3.12). These intermolecular restraints will be of crucial importance during the structure calculation of the protein peptide complex.

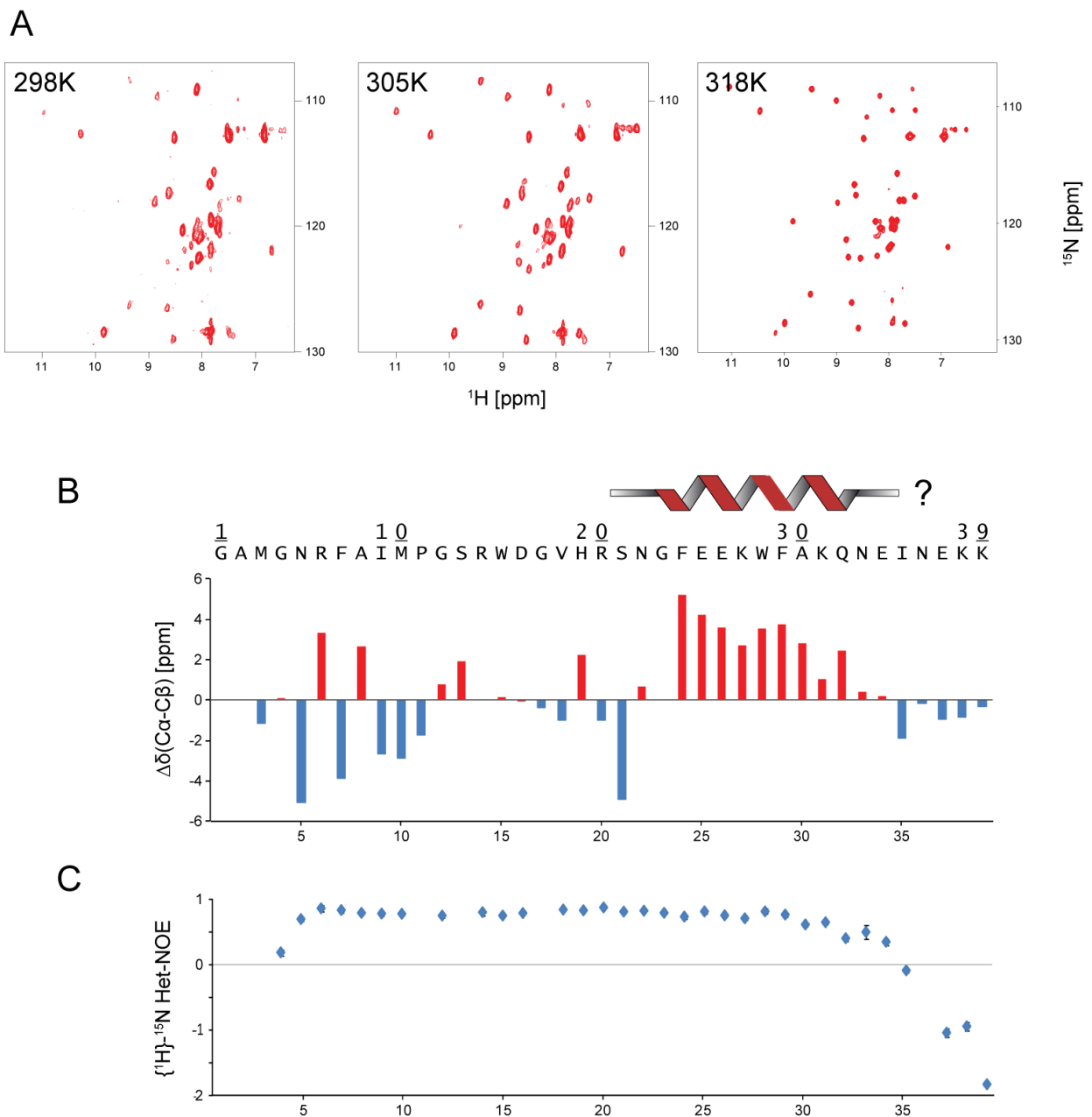


**Figure 5.3.11 NMR characterization of Bud13<sup>40mer</sup> in complex.** (A) <sup>1</sup>H, <sup>15</sup>N HSQC spectra of a 1:2.5 Snu17<sup>1-113</sup>, <sup>15</sup>N Bud13<sup>40mer</sup> sample at different temperatures. Backbone experiments recorded at 318K (45°C) were sharp and of more equal intensity. (B) Secondary chemical shift analysis suggests the presence of a helix in the bound Bud13 peptide. Numbering and sequence is from the expression construct. (C) <sup>1</sup>H-<sup>15</sup>N heteronuclear NOE analysis shows that ~25 residues are rigid and suggest that those amino acids interact more closely with the UHM domain of Snu17.

In collaboration, mutational data probing the *in vivo* interaction between Snu17 and Bud13 has been collected. In short, their studies show that a double mutant of Bud13<sup>FL</sup> (R231D, W232A) is not co-purified with Snu17<sup>FL</sup> when co-expressed in *E. coli*. Mutations in Snu17<sup>FL</sup> on the other hand are not as conclusive. A battery of single to quadruple mutations has been performed without abrogating the interaction completely. Although, one combination of mutations (F95A, K96D, I97A, V50W) exhibit a low-growth phenotype at high-temperature. This may be a sign of decreased affinity for Snu17 binding partners and/or indicate a non-intact structural domain. To clarify the results a combination of NMR and ITC experiments could be set up. Further mutations will have to be guided by structural data and therefore need to await our structure calculations.

To conclude, our findings so far provide us with a rich and interesting basis for further structural and biochemical work on the binary complex of Snu17<sup>1-113</sup> and Bud13<sup>40mer</sup>. The next stage is to make a thorough analysis of the NMR data and set up structural calculations. We then aim to extend our mutational analysis, to finally be able to fully characterize the molecular details of the Snu17: Bud13 interaction.

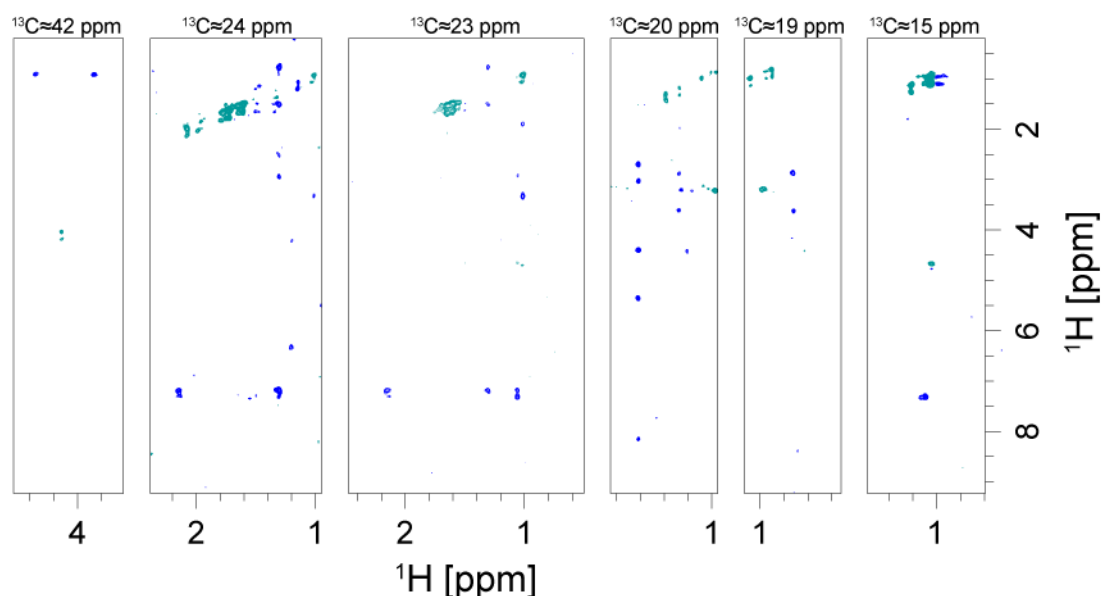


**Figure 5.3.12 Intermolecular NOEs for <sup>15</sup>N/<sup>13</sup>C labeled Snu17<sup>1-113</sup> in complex with Bud13<sup>40mer</sup>.** This <sup>13</sup>C-edited and double-filtered experiment shows that it is possible to record and define distance restraints between the UHM domain and the ULM peptide. The resonance frequency of the connected carbon atom was evolved, and the displayed carbon plane is indicated above each spectrum.

## Initial analysis of *Snu17: Pml1*

The interaction between *Snu17* and *Pml1* was to some extent studied by NMR. The initial work did not lead to any conclusive results, unfortunately, and is the reason why this part of the project was not pursued. Based on biochemical analysis and screening by NMR, a shorter construct of *Pml1* was selected for backbone assignment (Figure 5.3.13 C). 78% of *Pml1*<sup>46-204</sup> could be assigned using a triple-labeled sample and standard three-dimensional heteronuclear experiments. CSI analysis gives a comparable result to the secondary structures that are present in the crystal structure (Figure 5.3.13 A-B). Many of the assignments (64%) could be transferred to the full-length construct because of the intact FHA domain of *Pml1*<sup>46-204</sup>.

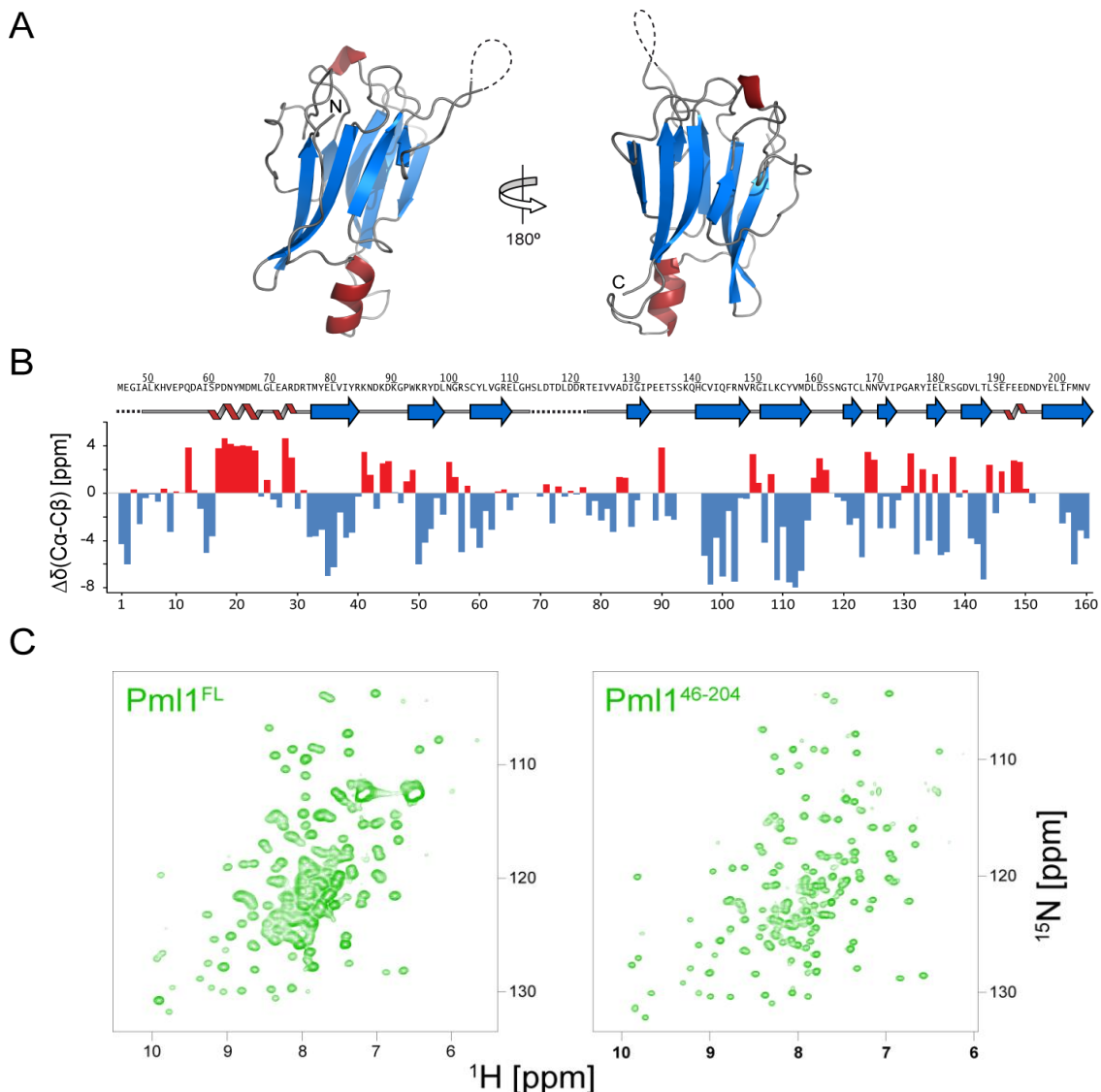
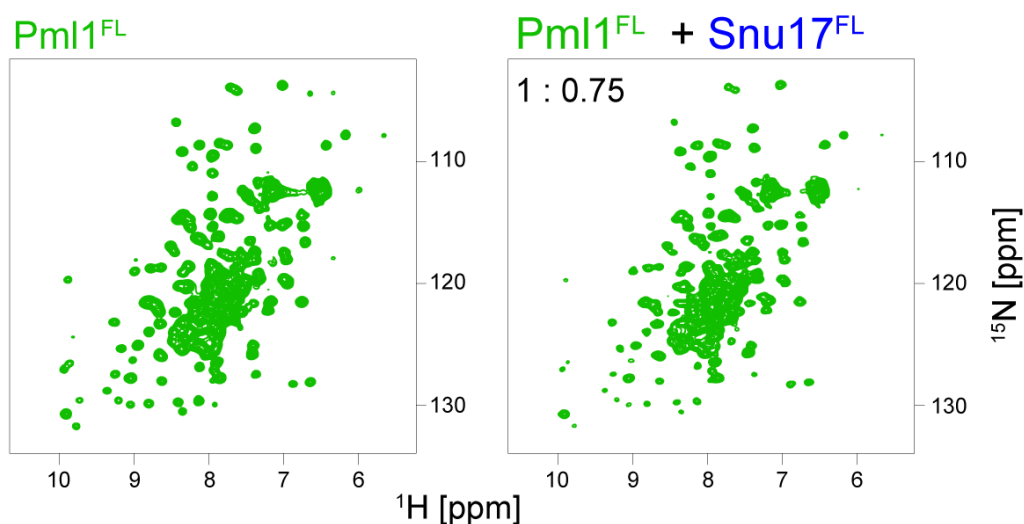


**Figure 5.3.13 Crystal structure of the FHA domain from *Pml1* and the NMR backbone assignment.** (A) The structure of the FHA domain from *Pml1* was solved by X-ray crystallography (2JKD.pdb).<sup>188</sup> A flexible loop is indicated with a dashed line.  $\beta$ -strands are depicted in blue and  $\alpha$ -helices in red. (B) CSI analysis of *Pml1*<sup>46-204</sup>. Above is the secondary structure topology, as in the crystal structure, and the sequence with numbering from the full-length protein. Below is the numbering as in the expression construct. (C) <sup>1</sup>H, <sup>15</sup>N HSQC spectra of *Pml1*<sup>FL</sup> (left) and *Pml1*<sup>46-204</sup> (right). *Pml1*<sup>46-204</sup> exhibits less overlap and an intact FHA domain. *Pml1*<sup>46-204</sup> was also the construct used for crystallization.

Upon titration of unlabeled Snu17<sup>FL</sup> to <sup>15</sup>N labeled Pml1<sup>FL</sup> no specific chemical shift perturbations could be observed (Figure 5.3.14 A). However, the signal intensities of resonances from residues in the folded FHA domain decreased in a general fashion. The reverse titration of unlabeled Pml1<sup>FL</sup> to <sup>15</sup>N labeled Snu17<sup>FL</sup> gave a similar but more unambiguous result (Figure 5.3.14 B). In both cases, our attempts to analyze the decrease in signal intensity quantitatively did not lead to any conclusions regarding the location of a binding site. Binding was evident but details were not.

A



B

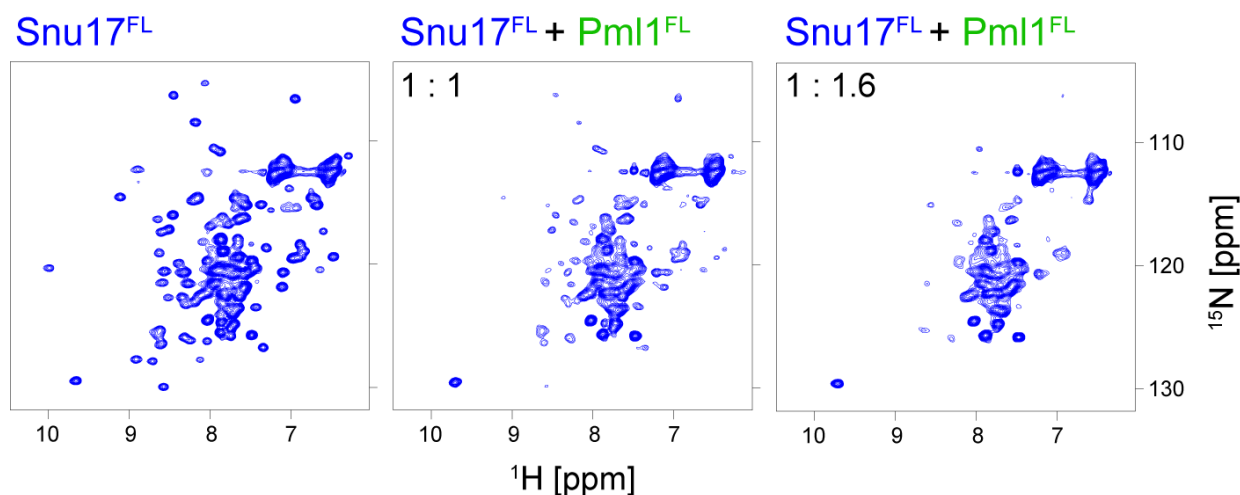


**Figure 5.3.14 Analysis of the Snu17<sup>FL</sup>:Pml1<sup>FL</sup> complex by NMR titrations.** (A) <sup>15</sup>N Pml1<sup>FL</sup> was titrated to a 1:0.75 ratio of Pml1<sup>FL</sup> to Snu17<sup>FL</sup>. Compared to free Pml1 (left), the intensity of signals from the FHA domain decrease in the presence of Snu17 (right). Further titration was not possible due to instability of Snu17<sup>FL</sup>. (B) The result was more evident when unlabeled Pml1<sup>FL</sup> was titrated against <sup>15</sup>N labeled Snu17<sup>FL</sup>. At 1:1 ratio of Snu17<sup>FL</sup> to Pml1<sup>FL</sup> (middle spectrum) most signals from the UHM domain are broadened out. The decrease in signal intensity of the sample continued when titrated to 1:1.6 (right spectrum). The titrations were followed by acquisition of <sup>1</sup>H,<sup>15</sup>N HSQC spectra with equal number of scans and at the same receiver gain. Experiments were recorded at 300K with samples ranging from 100-300  $\mu$ M in buffers in the absence of DMSO. Spectra are scaled using the strong intensity of the flexible side chain amides.

## 5.4. Discussion

The presented work describes how we used mainly biophysical techniques to analyze a stable sample of the UHM domain of Snu17 in complex with a peptide from Bud13; both NMR and ITC confirmed the interaction. We optimized the length of the Bud13 peptide and show that ~25 residues of Bud13<sup>40mer</sup> interact rigidly with Snu17. The interaction is expected to be of a similar type to those reported previously UHM-ULM complexes. The linear interaction motif in the peptide includes the characteristic tryptophan and, interestingly, a C-terminal helix, which is formed upon binding. ITC showed that inclusion of this helix increases affinity significantly. The predisposition for forming a helix at the C-terminus was appreciated early on in this work through bioinformatic analysis (JPRED<sup>195</sup>, PSIPRED<sup>196</sup>; data not shown). TALOS+, which compares Ca/Cβ chemical shifts to known structures, also predicts a helix at this position (data not shown).<sup>129</sup> The sequence of Bud13<sup>40mer</sup> is highly conserved in higher eukaryotes, although the sequence conservation is considerably lower at the C-terminus (Figure 5.4.1 A).

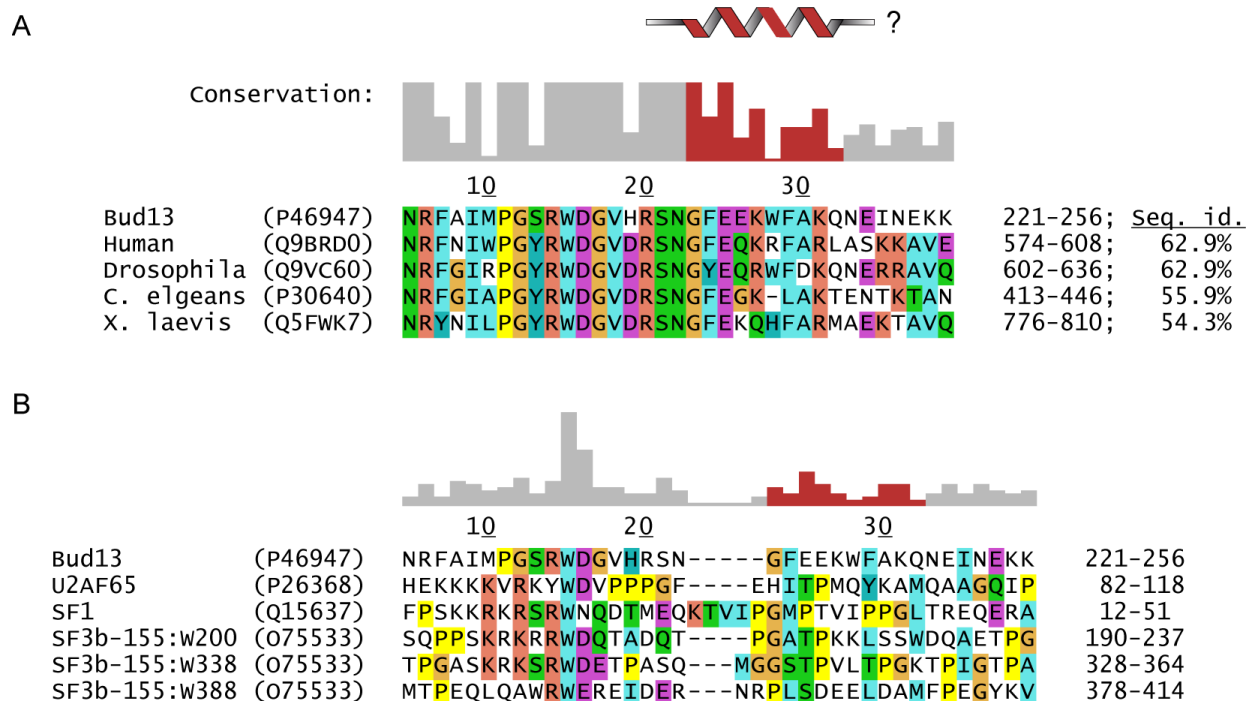


**Figure 5.4.1 Sequence alignment of Bud13<sup>40mer</sup> to eukaryotic homologs and to ULM sequences.**

Red columns in the conservation plot indicate residues suggested to form a helix upon binding to Snu17. Uniprot accession codes are given in brackets. Numbering above the alignment is according to the expression construct of Bud13<sup>40mer</sup>, while the original residue numbering is indicated on the right side. (A) Bud13<sup>40mer</sup> aligned to homologs from higher eukaryotic species. Sequence identity compared to Bud13 is shown on the far right of the alignment. (B) Bud13<sup>40mer</sup> aligned to characterized ULM sequences. Sequence identity to Bud13 is so low that no numbers were calculated.



In parallel to our structural biology effort by NMR, additional protein crystallization screens were performed, although, with a disappointing outcome. This can in part be explained by the aggregated appearance of the Bud13<sup>40mer</sup>:Snu17<sup>1-113</sup> complex at high concentrations and room temperature (Figure 5.3.10). High temperature NMR measurements make data acquisition possible and structure elucidation is now within reach.

Linear peptide motifs are being observed ever more increasingly in biology.<sup>197,198</sup> Such motifs act, for example, as interaction sites or modification sites and are important in cell compartment targeting and signaling cascades, as well as in other types of regulation. Several complexes of UHMs interacting with ULM peptides have been structurally characterized, both by NMR and X-ray crystallography. We performed a structural comparison to learn about similarities and differences of these structures to what is known about the Bud13<sup>40mer</sup>:Snu17<sup>1-113</sup> complex.

The first UHM-ULM interaction to be discovered was between U2AF35 and U2AF65, which also gave rise to the name: U2AF homology motif (UHM).<sup>190,199</sup> These two auxiliary factors are, together with the U2 snRNP, involved in the 3' splice site selection. The interaction between the two proteins of the heterodimer was shown to comprise the degenerated RRM domain of U2AF35 and a N-terminal peptide motif in U2AF65 (Figure 5.4.2 A).<sup>199</sup> At a first sight, this complex might be rather tempting to use as a template for Snu17 and Bud13. The ULM peptide modeled into the electron density is rather long (23 residues) and a C-terminal helix is also present. However, other important features include two tryptophan residues which dovetails the two subunits. One of the tryptophan residue originates from the UHM and the other from the peptide (Figure 5.4.2 A), as well as a polyproline stretch in the ULM, strongly kinking its backbone. This distinguishes the interactions since these attributes are not present in Snu17 or Bud13. A sequence alignment of the ULM peptide of U2AF65 and Bud13 clearly show the differences (Figure 5.4.1 B). The residues mentioned were all shown to be essential for low nanomolar affinity.<sup>199</sup> It could be argued that the C-terminal helix is induced by crystal contacts since it participates heavily in a helix bundle created by the arrangement of the asymmetric units into the crystallographic unit cell (data not shown). Additionally, the chemical shift perturbations induced by Bud13<sup>40mer</sup> do not overlap well with the position of the helix in the U2AF35 and U2AF65 complex (Figure 5.3.8 C).

U2AF65 not only contains a ULM, but also three RRM domains. One of these, the third RRM, turned out to be a UHM and bind a peptide from Splicing Factor 1 (SF1).<sup>200</sup> SF1 recognizes the branch point sequence of introns, and needs to be replaced by SF3b-155 during spliceosome assembly and the splicing reaction cycle.<sup>201</sup> A requirement for this is to break the interaction between the UHM of U2AF65 and the N-terminal ULM of SF1, which contribute a major part of SF1 affinity.<sup>202</sup> The molecular details of this interaction were previously demonstrated by structural studies using NMR in our laboratory (Figure 5.4.2 B).<sup>200</sup> The ULM of SF1 is shorter than that of

U2AF65, and has, in addition to the characteristic tryptophan, several positively-charged residues in the N-terminus (Figure 5.4.1 A). These residues contribute actively to binding due to corresponding negatively-charged residues on the  $\alpha 1$  helix of U2AF65.<sup>200</sup> Charge-reversing mutations abolishes the interaction, as does a tryptophan-to-alanine mutation. The ULM Bud13 contains no positively-charged residues at the N-terminus and, hence, not expected to be cross-reactive with U2AF65 (Figure 5.4.1 B).

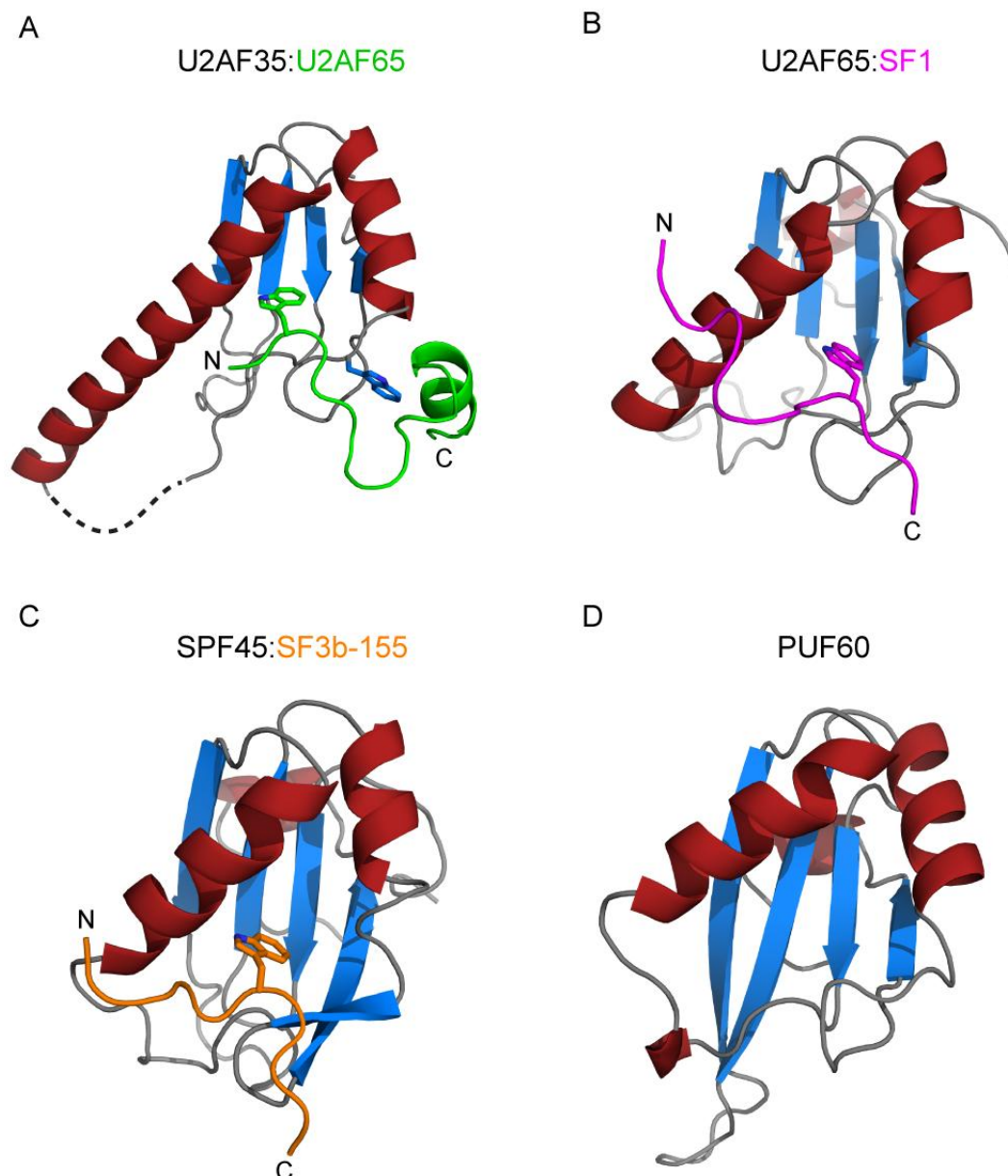


**Figure 5.4.2 Structures of UHM domains in complex with ULM peptides.**  $\beta$ -strands are depicted in blue and  $\alpha$ -helices in red. Termini of the ligand peptide are labeled. Note that the classical RNA binding site is on the back, across the  $\beta$ -sheet. (A) U2AF35 with the ULM peptide of U2AF65 (green; 1JMT.pdb). (B) U2AF65 with the ULM peptide of SF1 (magenta; 1OIP.pdb). (C) SPF45 with the ULM peptide of SF3b-155 (orange; 2PEH.pdb). (D) The UHM domain of PUF60 (3DXB.pdb). Characterized by ITC and NMR to bind several different ULMs, from SF3b-155, SF1 and U2AF65.

The proteins described thus far are involved in constitutive splicing, but unsurprisingly proteins in alternative splicing also utilize the UHM-ULM architecture. One possibility is that such proteins could compete with the constitutive splicing factors for exclusion or inclusion of certain exons.<sup>51</sup> Splicing factor SPF45 is a positive regulator for the exclusion of exon 6 in the FAS (CD95) gene, a splicing event known to regulate apoptosis.<sup>54</sup> SPF45 was shown to bind several ULMs, up to now those present in SF3b-155, U2AF65 and SF1. All three proteins are involved in 3' splice site definition together with the U2 snRNP. A crystal structure of SPF45 UHM bound to the fifth ULM of SF3b-155 has been solved (Figure 5.4.2 C).<sup>54</sup> The details of the interaction is relatively similar to the U2AF65:SF1 complex (Figure 5.3.1). Binding of a central tryptophan is enhanced by neighboring positively-charged residues. Furthermore, based on the structural data the authors designed numerous mutations to deconvolute the function of SPF45. The results suggest an interesting model for how networks of UHM-ULM interactions are required for alternative splicing.<sup>54</sup> Generally, there seem to be cross-reactivity between sets of UHMs and ULMs.

Also the UHM of PUF60 has been structurally and biochemically characterized (Figure 5.4.2 D).<sup>203</sup> PUF60 is a splicing factor closely related to U2AF65, but interacts, in contrast to U2AF65, specifically with the N-terminal ULMs of SF3b-155. Various interactions of PUF60 have been studied by both ITC and NMR, but up to now, only the free form of the protein has been crystallized. However, these interactions most likely have similar features as the U2AF65:SF1 and SPF45:SF3b-155 complexes (Figure 5.4.1 B-C). Surprisingly, a distinctive and flexible loop of the PUF60 UHM mediates homo-dimerization upon addition of SDS.<sup>203</sup>

In conclusion, we expect structural differences in the Snu17: Bud13 complex compared to the UHM-ULM structures presented above. The ULM of Bud13 is relatively long, as indicated by NMR relaxation data, and comprises no positively-charged residues. A ULM helix, evidently formed in Bud13<sup>40mer</sup>, has only been observed in the U2AF35:U2AF65 complex before, but is there preceded by a poly-proline stretch. Also, that type of helix-UHM interaction does not fit with our titration data. However, one explanation for this could be that the helix is not making any close contacts to the folded domain of Snu17, but is instead sticking out into the solution. Concerning the ITC data, the formation of a helix in Bud13<sup>40/60mer</sup> might be correlated to the two binding-event isotherm observed, since the helix residues are not present in the shorter Bud13<sup>22mer</sup>. Mutational data on Snu17 also suggest a relatively large interaction surface, since no combination of mutations so far abolished the interaction in the co-expression analysis of full-length construct. The mutations done were based on structural knowledge from the previously described UHM-ULM complexes (Figure 5.4.2).

To date, all UHMs characterized originate from proteins related to splice site recognition. It would be interesting to test the ULM-specificity of Snu17, since cross-reactivity has been shown between the other UHMs and their ULMs.<sup>54</sup> One question to be answered is if RES function might arise from and/or affect these functions by competition in a similar way alternative splicing proteins do. Data challenging such a hypothesis is the exceptionally strong affinity between Bud13 and Snu17 ( $K_D \approx 5$  nM). Purifications also propose that the RES complex is a stable heterotrimer.

There is one more related protein-peptide complex of interest to us, even though the binding mode of the peptide is completely different to previously described UHM-ULM structures. The complex of p14:SF3b155 exhibits what could be called a pseudo-RRM peptide complex (Figure 5.4.3 A).<sup>204</sup> It has been suggested that the binding mode of p14:SF3b-155 is similar to the Snu17:Pml1 interaction.<sup>191</sup> The hypothesis is that the C-terminal extension of Snu17 creates a binding pocket for the flexible N-terminal of Pml1. The RRM domain of p14 interacts with the branch point adenosine of intronic mRNA, but can simultaneously bind a SF3b-155 peptide. Interestingly, this is not occurring at the ULM site but at the classical RNA site. The SF3b-155 peptide occludes most of the classical RNA interaction site but does not abrogate RNA binding.<sup>204</sup> The three-dimensional structure of p14 with RNA has not been solved, but RNA binding by the classical RRM domain of U1A can be used as a model and for comparison (Figure 5.4.3 B-C).<sup>205,206</sup> We have only briefly addressed direct RNA binding by the RES complex, in particular by free Snu17. However, band shift analysis did not reveal any interaction with an oligonucleotide (5'-AAUUUGUGG-3') (data not shown).

In this respect, it would be of great interest to characterize how Snu17 binds Pml1 further. Our studies of the Snu17:Pml1 interaction are not conclusive, and are not fully in agreement with biochemical data<sup>187</sup> but suggest that the two proteins rather tumble together in solution. This would require a large interaction surface between the UHM of Snu17 and the FHA domain in Pml1. If only shorter peptide motifs from either protein make up the interaction, creating a so-called pearls-on-a-string arrangement, the HSQC spectra of the complex should be of better quality than they were (Figure 5.3.14). We observe a drastic decrease of most signals from residues in folded domains. Still, somehow Snu17 is able to bind two proteins at the same time, and it will most likely be yet another example of a degenerated RRM, which acquired new structural and functional features.

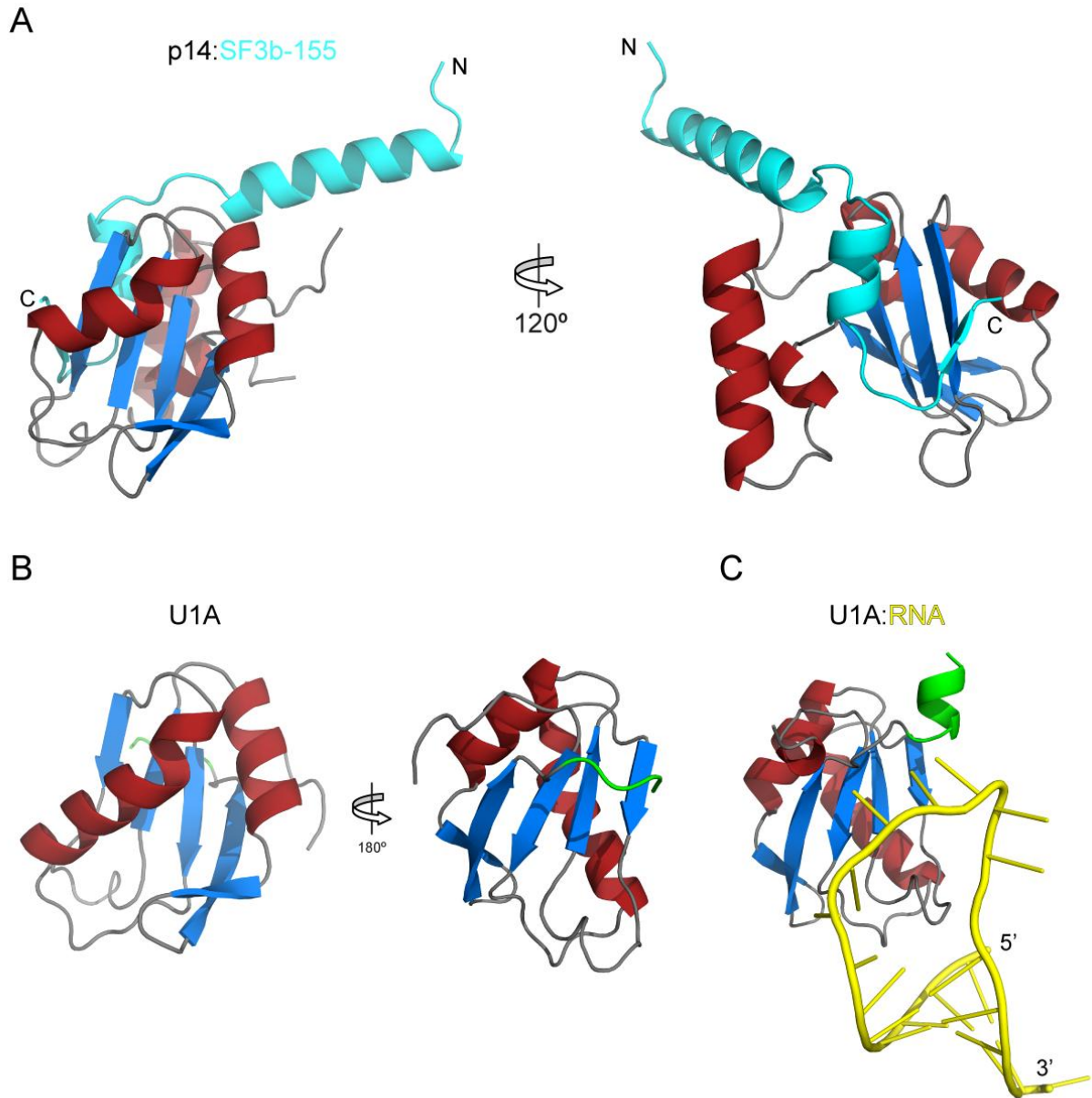


**Figure 5.4.3 A peptide motif of SF3b-155 interacts with p14 at the site where RNA binding occurs.**  $\beta$ -strands are depicted in blue and  $\alpha$ -helices in red. Termini of ligands are labeled. (A) SF3b-155 does not interact with p14 at the ULM binding site (left; 2F9D.pdb), but rather at the RNA binding site which lies across the  $\beta$ -sheet (right). Peptide ligand in cyan. (B) The U1A RRM without any ligand (1OIA.pdb). A C-terminal extension (green) occludes the RNA binding site. (C) Complex structure of U1A RRM with RNA (yellow; 1URN.pdb). The C-terminal extension (green) is flipped out and forms a helix.

## 5.5. Conclusions

RES function is required for splicing of a subfamily of introns, namely those with weak 5' splice sites, as well as for the retention of unspliced pre-mRNA.<sup>46</sup> We have reported ITC and NMR data that confirm binding of Snu17 to Bud13, which are two out of the three RES subunits. Closer analysis of the binary complex was made possible through optimization of constructs, buffers and measurements conditions. We suggest that the interaction is similar but different to known UHM-ULM interactions. In addition to the central and characteristic tryptophan of the ULM, Bud13 also includes an N-terminal helix, which increases the affinity. Moreover, sequence analysis and structural comparison of known complexes highlight features which are particular to the Snu17 UHM and Bud13 ULM. Such differences include electrostatic interactions not expected in the Snu17: Bud13 complex.

Future work includes spectral analysis and structure calculations of a complex containing Snu17<sup>1-113</sup> and Bud13<sup>40mer</sup>. Based on the three-dimensional structure we hope to suggest specific mutations confirming the structural model, and which finally abrogate the interaction *in vivo*. Hopefully such experiments can support the ongoing efforts to elucidate the function of the RES complex further, and resolve interaction details at the molecular level. One important task will be to understand how RES actually interacts with the pre-mRNA and affects splicing. Biochemical characterization of the proposed flexible C-terminal of Bud13 may answer these questions.

## 5.6. Materials and Methods

### Sample preparation

Several constructs of each protein in the RES complex from *Saccharomyces cerevisiae* were expressed, purified and analyzed in this study (Table 5.6.1). Cloning of all constructs into T7 based expression vectors was done in the laboratory of Herman van Tilbeurgh. They performed extensive crystallographic trials using these constructs. For the most important constructs, namely those two used for structural studies, the sample preparations procedures will be described in detail. Generally, standard techniques similar to the ones below were used to obtain pure protein samples of all other constructs. Rich lysogeny broth (LB) medium was used to prepare unlabeled samples. For NMR samples,  $^{15}\text{N}$  or  $^{15}\text{N}/^{13}\text{C}$  labeled, minimal M9 medium with  $^{15}\text{NH}_4\text{Cl}$  and  $^{13}\text{C}$ -glucose, as its sole nitrogen and carbon source, was utilized. Cultures were grown in  $^2\text{H}_2\text{O}$  in case  $^2\text{H}$ -labeling was needed.

For protocols see [www.helmholtz-muenchen.de/pepf](http://www.helmholtz-muenchen.de/pepf).

Plasmids were sequenced and purified proteins were checked by mass spectrometry (see Appendix A.2).

Table 5.6.1

Name of Construct	Gene	Residues <sup>a</sup>	Vector <sup>b</sup>	Tag <sup>c</sup>	Cleavable?	Comment
Snu17 <sup>FL</sup> (full-length)	Snu17	1-148	pET9	C-His	no	
Snu17 <sup>1-113</sup>	Snu17	1-113	pBS-3256	N-His	no	Used for structural studies
Snu17 <sup>25-113</sup>	Snu17	25-113	pET28	N-His	no	Low yield
Snu17 <sup>25-138</sup>	Snu17	25-138	pET28	N-His	no	Low yield
Bud13 <sup>FL</sup> (full-length)	Bud13	1-266	pET9	C-His	no	
Bud13 <sup>60mer</sup>	Bud13	201-266	pET9	C-His	no	
Bud13 <sup>40mer</sup>	Bud13	222-256	pETM30	N-GST	yes	Used for structural studies
Bud13 <sup>40mer-His</sup>	Bud13	222-256	pETM30	C-His	no	
Bud13 <sup>221-242</sup>	Bud13	221-242	pETM30	N-GST	yes	Low yield
Bud13 <sup>221-239</sup>	Bud13	221-239	pETM30	N-GST	yes	Low yield
Bud13 <sup>225-242</sup>	Bud13	225-242	pETM30	N-GST	yes	Low yield
Bud13 <sup>225-239</sup>	Bud13	225-239	pETM30	N-GST	yes	Low yield
Pml1 <sup>FL</sup> (full-length)	Pml1	1-204	pET9	C-His	no	
Pml1 <sup>24-204</sup>	Pml1	24-204	pET9	C-His	no	
Pml1 <sup>46-204</sup>	Pml1	46-204	pET21	C-His	no	Backbone assigned

<sup>a</sup> For certain important plasmids the protein sequence and mass spectrometry data are reported in Appendix A.2

<sup>b</sup> All vectors used kanamycin as their selection marker, except for pET21 which give ampicillin resistance.

<sup>c</sup> N/C designates a N-terminal or C-terminal tag. The GST tag also include a 6×Histidine-tag for purification.



Snu17<sup>1-113</sup> is poorly expressed at 20°C, but the soluble fraction of the protein could be used for initial experiments. However, it was recognized that at 37°C a large amount of protein was available as inclusion bodies. After transformation of the expression plasmid into *E. coli* Rosetta (DE3) (Novagen), a single colony was picked from the kanamycin selection plate for inoculation of a 10 mL overnight pre-culture. 2 mL of the pre-culture was added to 1 L of pre-heated medium and grown at 37°C (170 rpm) until OD 0.7 was reached. The culture was induced with 0.5mM IPTG for 4h at constant temperature. The culture was cooled down and harvested by centrifugation. The pellet was dissolved in 20 mL of buffer (20 mM TRIS pH 7.5, 300 mM NaCl, 10 mM imidazole, 1 mM DTT 0.02% NaN<sub>3</sub>, protease inhibitors, RNase, lysozyme and 0.2% IGEPAL) and sonicated for 5 min while cooling with ice-water (80% power, 50% cycle; UP200s, Dr Hielscher GmbH). Next, the sample was centrifuged using a two step procedure, 5 min at 5000 rpm and then 30 min at 20000 rpm. This allow efficient sedimentation of the high-density inclusion bodies and should give a sample of higher purity. The supernatant was discarded together with the viscous cell debris, and the whitish pellet was dissolved in 25 mL 8M urea (pH 7.5). The solution of dissolved inclusion bodies was applied three times to a gravity column filled with 4 mL of Ni<sup>2+</sup>-NTA resin (Qiagen) pre-equilibrated in 8M urea. The protein was then washed using 20 mL 8M urea, 20 mL 4M urea, 20 mL 4M urea + 1M NaCl and, finally, 20 mL 2M urea. The protein was then eluted using 10 mL Elution buffer (20 mM TRIS pH 7.5, 300 mM NaCl, 300 mM imidazole, 1 mM DTT and 0.02% NaN<sub>3</sub>) including 2M urea. To remove the remaining urea and to refold Snu17<sup>1-113</sup> the sample was diluted to approximately 150 μM and dialyzed against the NMR buffer (20 mM sodium phosphate pH 6.9, 150 mM NaCl and 1 mM DTT, 0.02% NaN<sub>3</sub>). The final sample was exceptionally clean and could be used without any further purification steps. The yield was usually around 50 mg/L medium. Due to its instability at high concentrations Snu17<sup>1-113</sup>, the protein could not be kept at higher concentration than 100μM. If a highly concentrated sample was needed Snu17<sup>1-113</sup> had to be complexed to Bud13 before a final concentration step. 10% DMSO also increased the stability of Snu17<sup>1-113</sup>, up to ~ 250 μM.

In comparison, Bud13<sup>40mer</sup> was expressed and purified using standard procedures. A 1 L culture was cooled for 20 min before induction with 0.5 mM IPTG over night at 20°C. This limits the stress on the cells and should increase the amount of soluble protein. The soluble fraction of Bud13<sup>40mer</sup> was purified by sonicating the harvested cell pellet in 25mL Lysis buffer (20 mM TRIS pH 7.5, 300 mM NaCl, 10 mM imidazole, 1 mM DTT and 0.02% NaN<sub>3</sub>), also including protease inhibitors, RNase, lysozyme and 0.2% IGEPAL. After high-speed centrifugation and filtering, the supernatant was applied three times to 3 mL Ni<sup>2+</sup>-NTA resin. Several rounds of washing (20 mL) were performed, with: Lysis buffer including 0.2% IGEPAL, Lysis buffer, Lysis buffer with high salt concentration (1M NaCl), Lysis buffer with high imidazole concentration (30 mM imidazole). Finally, the protein was eluted by applying 10mL of Elution Buffer. TEV (tobacco etch virus) protease was added to the sample and incubated overnight at

room temperature. A second nickel-column was not used, because most of the cleaved GST precipitated. The peptide sample was concentrated and further purified by size exclusion chromatography (HiLoad, Superdex 75 16/60 or 26/60, GE Healthcare). In this step, the protein was buffer-exchanged into NMR buffer. The final Snu17<sup>1-113</sup>:Bud13<sup>40mer</sup> sample was made as follows. Using the theoretical extinction coefficients the concentrations of the individual proteins were calculated (EXPASY: Protparam<sup>207</sup>). To avoid precipitation during high-temperature measurements, the amounts corresponding to a 1:2.5 ratio of Snu17<sup>1-113</sup> to Bud13<sup>40mer</sup> molarity was pooled, and subsequently concentrated in a 3 kDa MWCO concentrator.

Two shorter peptides of Bud13, Bud13<sup>22mer</sup> (221-242; ENRFAIMPGSRWDGVHRSNGFE) and Bud13<sup>14mer</sup> (225-238; AIMPGSRWDGVHRS), were purchased from Peptide Specialty Laboratories (Heidelberg, Germany), and extensively dialyzed before usage.

## *NMR*

Many different experiments were recorded to characterize our protein samples, constructs boundaries, buffer conditions, interaction sites, protein dynamics as well as the behavior of complexes. All NMR spectra were recorded on Bruker instruments (900, 750, 600 and 500 MHz) equipped with pulse field gradients, most of them also had cryo-cooled probe heads. For backbone assignments generally the following experiments were recorded: <sup>1</sup>H,<sup>15</sup>N HSQC, <sup>1</sup>H,<sup>13</sup>C HSQC, HNCA, HNCACB, CBCA(CO)NH, (H)CC(CO)NH-TOCSY and <sup>1</sup>H,<sup>15</sup>N HSQC-NOESY.<sup>125</sup> Regarding temperature settings and sample concentrations see each individual spectra. The recorded data was processed with NMRPipe/ NMRDraw<sup>123</sup> and visualized as well as analyzed in NMRView<sup>126</sup> (v5.0.4) and NMRViewJ (v8.0). Most spectra for figures were exported directly from Topspin v2.1 (Bruker). Secondary chemical shifts were used to validate assignments.<sup>128</sup> Protein backbone dynamics were studied by {<sup>1</sup>H}-<sup>15</sup>N heteronuclear NOE experiments, as described previously.<sup>137</sup> Errors were estimated as the standard deviation of the noise and propagated accordingly for each resonance. Hydrogen/Deuterium-exchange were recorded after lyophilization of the protein sample and the subsequent addition of <sup>2</sup>H<sub>2</sub>O. The measurements were carried out at 293K and 308K for ligand-free Snu17<sup>1-113</sup> and the complex, respectively.

## *ITC*

Isothermal titration calorimetry (ITC) was used to measure the affinity between Snu17<sup>1-113</sup> and different Bud13 constructs. Most of the measurements were performed with a VP-ITC (MicroCal Inc.) at 25°C using proteins samples in NMR buffer (see the purification protocols). The concentration of Snu17<sup>1-113</sup> in the cell (1440 µL) varied between 30-70 µM, while the syringe (300 µL) contained the ligands at concentrations ranging from 0.6 to 1.1 mM. Normally 40-80 injections were done over a period of 3-4 hours. To estimate the heat of dilution, the ligands were also injected into buffer. The result was then subtracted from the original measurement. The analysis of the ITC

data was done in Origin v7, according to the recommendations of the manufacturer. The experimental values are given  $\pm$  fitting error.

### *Thermoflour assay*

A thermoflour assay was used to characterize the stability of Snu17<sup>1-113</sup> with and without a ligand, as well as in different buffer conditions.<sup>208</sup> In brief, a fluorophore that change emission spectra upon interaction with hydrophobic residues is added to the sample. Upon thermal unfolding the hydrophobic core of the protein will be exposed and this process can be follow with a real-time PCR machine (Stratagene Mx3005P, Agilent Technologies Inc.). 50  $\mu$ L reactions of a wide range of buffers (varying salt and pH) were setup, including: 10 or 20  $\mu$ M protein, 5x of SYPRO-orange (5000x stock; Sigma-Aldrich). The assays were started at 25°C and heated with 3°C/min. Ligand induced stability were tested by adding a four-fold amount of peptide.

### *Homology modeling and sequence alignments*

A homology model of the UHM domain of Snu17 was built for mapping of chemical shift perturbations induced by titrations of ligands. The model was created using the free form of SPF45 (2pe8.pdb; 22.5% sequence identity) as a template and the web-based server of HHpred.<sup>209</sup> The backbone of the homology model was colored, for example to display chemical shift changes, by modifying the B-factor column of the pdb-file. The color bins were modified manually to give a reasonable appearance, meaning that very strong perturbations often were scaled down. Superposition of proteins structures were done in Pymol<sup>210</sup>, which also was used for rendering pictures. Secondary structure definitions were taken from the pdb-files or calculated by the DSSP-based<sup>211</sup> algorithm implemented in Pymol.

Multiple sequence alignments were done in ClustalX v2.0.<sup>212</sup> Sequences used were downloaded from Uniprot. Accession codes are given in the alignments. Homologs for Snu17 and Bud13 in higher eukaryotes were found in the literature and using PSI-BLAST at EMBL-EBI ([www.ebi.ac.uk](http://www.ebi.ac.uk)).<sup>45,174</sup>

### *Mutational studies*

Mutational studies of Snu17 and Bud13 were performed in the laboratory of Bertrand Séraphin (IGBMC, Paris). Mutants were suggested together with Mark Brooks, and were analyzed regarding their ability to form the complex when proteins were co-expressed, as well as in a growth phenotype assays. A number of single to quadruple mutants were designed to abrogate the interaction between Snu17 and Bud13. In short, for the co-expression assay site directed mutagenesis was directly performed on a available His-Snu17-Bud13-Pml1 operon. After expression in *E. coli* purification of the complex was done using the His-tag. A complementation assay of certain TAP-tagged mutants was performed in  $\Delta$ Snu17 and  $\Delta$ Bud13 yeast deletion strains to study growth at various temperatures (25, 30 and 37°C). The TAP-tag was used to control expression levels of mutant protein.

## Chapter 6

---

### Additional collaborations

During my thesis I had the opportunity to join and develop many collaborations. These projects, ranging from drug development to basic biochemical research, are briefly presented and discussed. The projects have been completed if not stated otherwise.

#### 6.1. Induction of apoptosis: Evaluation of a potential inhibitor

A collaboration with: Prof. Dr. Angelika Vollmar, Pharmaceutical Biology, LMU, Munich.

X-linked inhibitor of apoptosis protein (XIAP) is an important regulator of controlled cell death, and includes amongst others three Baculovirus IAP Repeat (BIR) domains.<sup>213</sup> XIAP inhibits apoptosis by binding caspases via its BIR domains. In particular, caspase-9 has been shown to interact with, and to be regulated by, BIR-3.<sup>214</sup> The rationale to develop molecules that bind BIR-3 is, that an induced release and activation of caspase 9 could result in apoptosis. Such compounds could therefore be used as an antitumor treatment. A drug candidate (T8) to modify the BIR-3/caspase-9 interaction had been developed using *in silico* methods, and provided the anticipated effect in *in vivo* experiments. In such experiments cultured cells were sensitized to etoposide, a known chemotherapeutic.

However, evidence on the molecular mechanism, whether the molecules actually interacted with BIR-3 or not, was missing. To resolve this question, we expressed and purified <sup>15</sup>N labeled samples of the BIR-2 and BIR-3 domains of human XIAP. Ligand binding was then analyzed by ligand titrations followed by consecutive acquisition of 2D <sup>1</sup>H, <sup>15</sup>N HSQC spectra. Based on the results, it was clear that T8 did not specifically interact with either BIR domain (Figure 6.1.1). A known ligand of BIR3 was used as a positive control, and induced the expected chemical shift perturbations, indicating binding. Thus, the sensitizing effect observed in the *in vivo* experiments, must have been caused by another process in the cells, modulated by the compound.

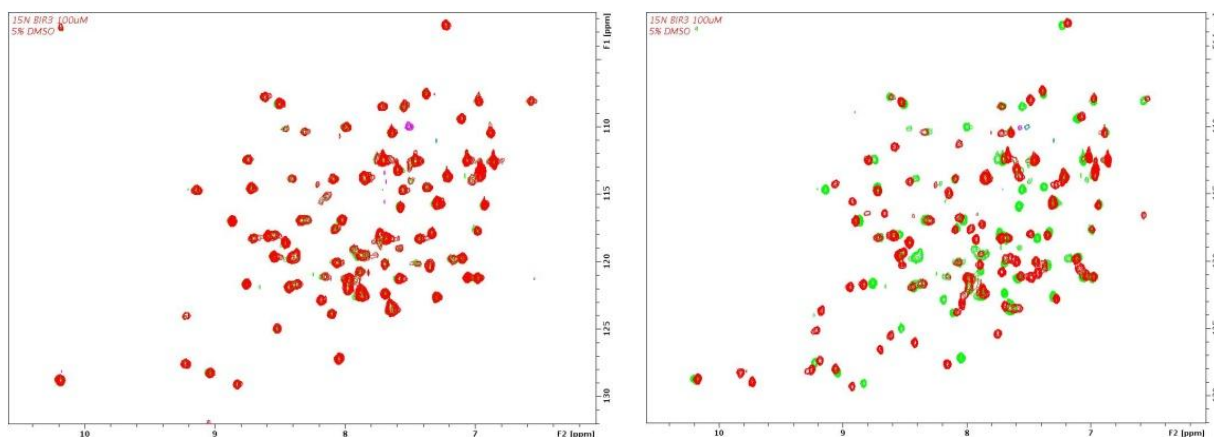


**Figure 6.1.1 Ligand titrations of a putative binder to XIAP (BIR-3 domain).** The reference spectrum (green) was recorded on a  $100\mu\text{M}$   $^{15}\text{N}$  labeled sample. At a ratio of 1:3 protein to ligand concentration with T8 (left, red spectrum), no chemical shift perturbations could be observed. In contrast, this was the case for a positive control at 1:1 (right, red spectrum ; ABT-11<sup>215</sup> from Abbott Laboratories). 5% DMSO was used in both experiments to increase ligand solubility.

## 6.2. Proposed interaction between viral LMP1 and human TRADD

A collaboration with: PD Dr. Arnd Kieser, Department of Gene Vectors, HMGU, Munich.

To hide from the human immune system, the Epstein-Barr virus (EBV) infects and transforms B-cells. This process makes the B-cells immortal, which in some patients can lead to development of certain types of tumors. The viral Latent Membrane Protein 1 (LMP1) is one of the key players orchestrating the manipulation of gene expression in the host cell, and is therefore interesting from a therapeutic point of view.<sup>216</sup> In particular, LMP1 had been proposed to interact with the human Tumor Necrosis Factor  $\alpha$  Receptor Associated Death Domain (TRADD) protein. In uninfected cells, TRADD is important for signaling during proliferation, as well as in progression of cell death. The interaction had been suggested to take place between the flexible and intracellular C-terminal domain of LMP1, and the N-terminal domain of TRADD.<sup>217</sup>

We expressed and purified several different constructs of LMP1 and TRADD, and studied the suggested interaction by NMR, ITC and analytical size exclusion chromatography (SEC) (Figure 6.2.1). In summary, our *in vitro* data show that, at best there is a very weak and unspecific interaction between those proteins. One possibility is that the interaction might be mediated by additional factors *in vivo*.

This project was the Bachelor's thesis of Christoph Hartmüller (TUM Biochemistry, 2009).

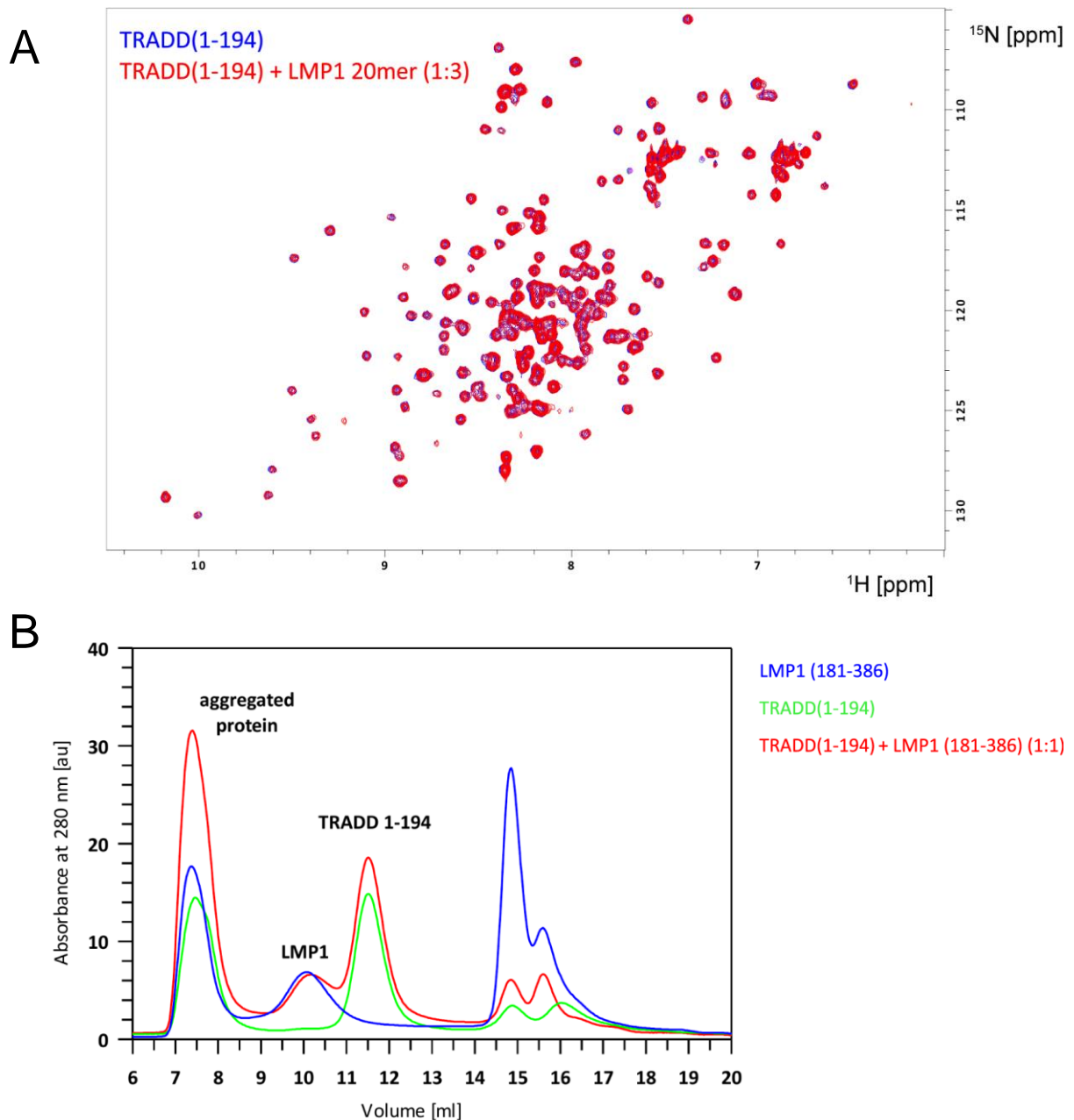


**Figure 6.2.1 Interaction studies of viral LMP1 and human TRADD.** (A) Ligand titration of a C-terminal LMP1 peptide (20mer) to  $^{15}\text{N}$  labeled TRADD $^{1-194}$ . Blue spectrum is a  $^1\text{H}$ ,  $^{15}\text{N}$  HSQC reference spectrum of 100  $\mu\text{M}$  TRADD $^{1-194}$ . Red spectrum is recorded at a ratio of 1:3, protein to ligand concentration. There are no chemical shift changes observed, indicating that there is no interaction between the LMP1 peptide and TRADD (B) Analytical size exclusion chromatography of individual proteins and of the putative complex. The red chromatogram shows that if mixed, the proteins still elute at volumes expected for them individually, again, indicating at best a very weak interaction.

### 6.3. Elucidation of a novel structural domain in EBNA-2

A collaboration with: Dr. Bettina Kempkes, Institute of Clinical and Molecular Biology, HMGU, Munich.

Epstein-Barr virus nuclear antigen 2 (EBNA-2) is a transcriptional co-activator essential for induction and maintenance of an EBV infection.<sup>218</sup> We have cloned, expressed and purified a domain from EBNA-2 which shows no sequence homology to any known protein. Previously, this part of the EBNA-2 protein has been described to be involved in the initial transformation of B-cells, as shown by functional assays.

Preliminary characterization indicates a folded domain with short flexible termini. The  $^1\text{H},^{15}\text{N}$  HSQC spectrum is well dispersed, and a complete set of triple resonance spectra for backbone/sidechain assignment have been recorded, as well as several NOESY spectra (Figure 6.3.1). The data is to be analyzed in the near future and used for structure determination. The structure will then be validated by mutational analysis. Furthermore, to extend the knowledge on the function of this domain, we will use the obtained information in *in vivo* assays.

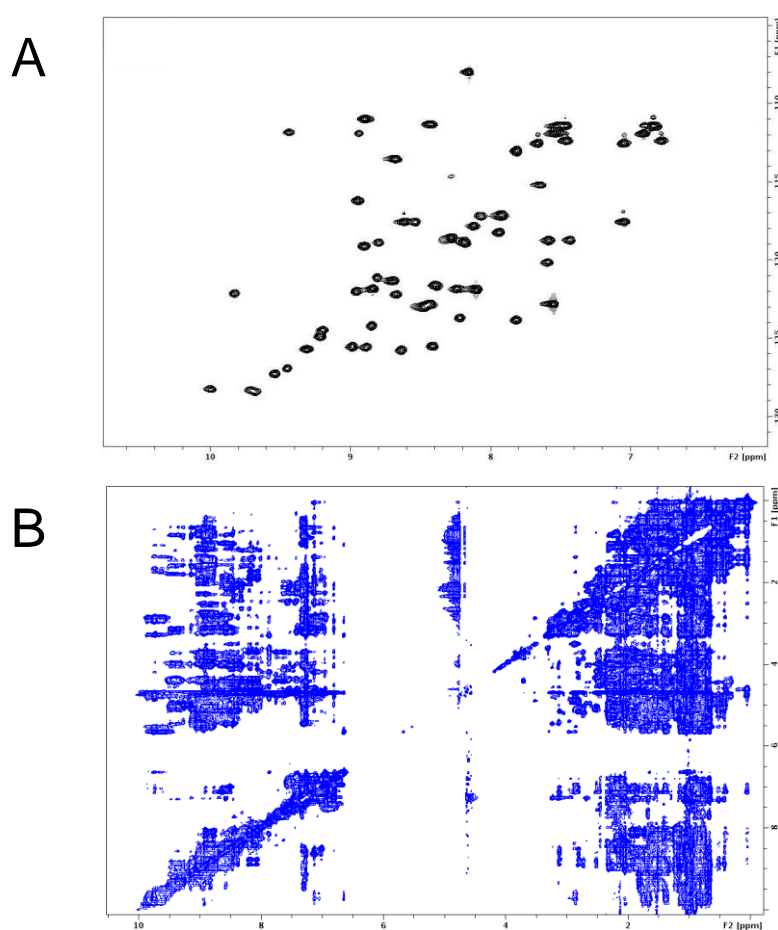


**Figure 6.3.1 Initial NMR analysis of an EBNA-2 fragment.** (A)  $^1\text{H},^{15}\text{N}$  HSQC and (B)  $^1\text{H}$  homonuclear 2D NOESY of a novel structural domain in EBNA-2. Both spectra indicate a folded domain and were recorded on a 300  $\mu\text{M}$   $^{15}\text{N}$  labeled sample.



## 6.4. Confirming inhibitors of Bcl-xl

A collaboration with: Dr. Thorsten Berg, Chemical Biology, MPI Biochemistry, Munich.

The aim of the project was to investigate the binding of small-molecule inhibitors to Bcl-xl. Bcl-xl is involved in regulation of apoptosis, programmed cell-death.<sup>108</sup> Apoptosis-related pathways, and modulation thereof, are highly attractive targets in oncology research. Several compounds had previously been identified in a peptide displacement assay using fluorescence polarization.

The binding of three compounds to Bcl-xl was confirmed by NMR, and their interaction sites were mapped onto the known structure of Bcl-xl (Figure 6.4.1). The molecules are expected to bind in the same site as known endogenous binders, i.e. peptides.<sup>219</sup> Furthermore, the strength of the interactions were estimated by ligand titrations. See Chapter 3 for details on such an analysis.

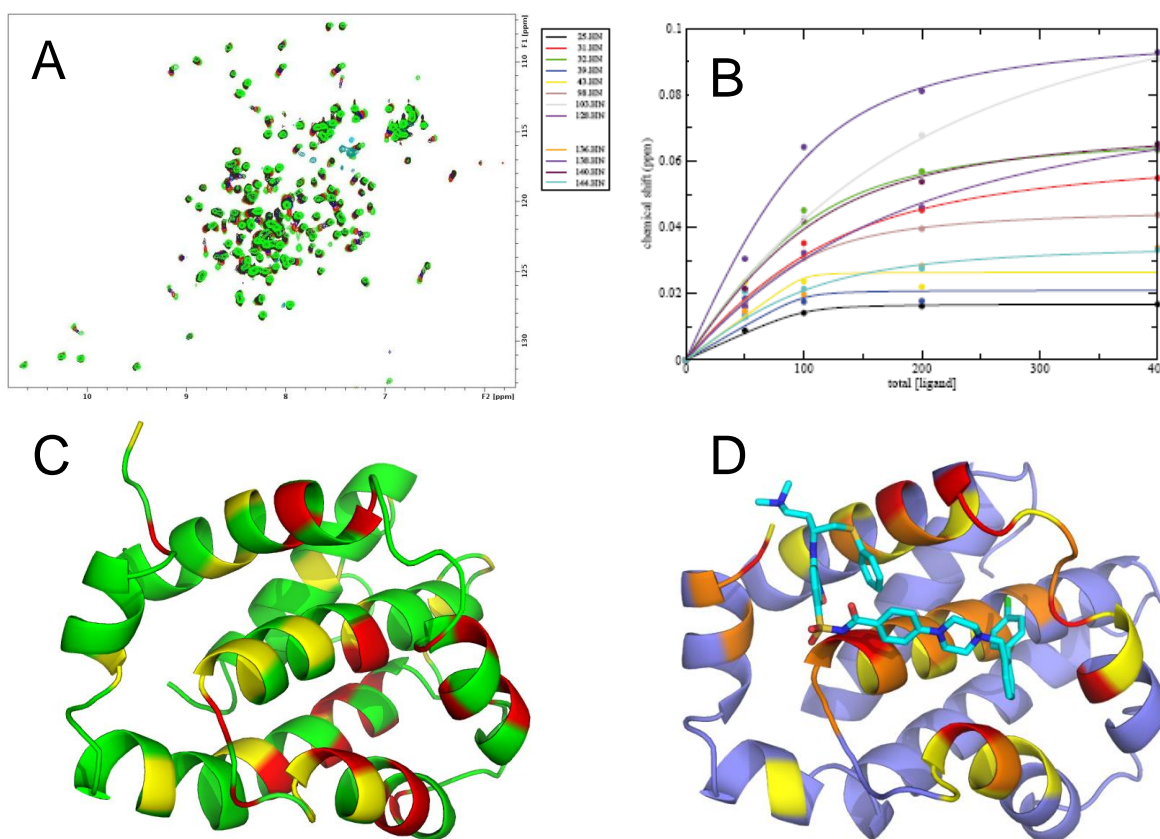


**Figure 6.4.1 Example of an inhibitor interacting with Bcl-xl.** (A) Overlay of  $^1\text{H}$ ,  $^{15}\text{N}$  HSQC spectra recorded at increasing amounts of the ligand. The endpoint was at a 1:4 ratio of protein to ligand concentration. (B) The observed chemical shift changes of several residues were fitted to a one-binding site equation, giving an approximation of the  $K_D$  to 50  $\mu\text{M}$ . (C) Chemical shift changes at a fourfold excess of the ligand mapped onto the structure of Bcl-xl (1LXL.pdb) using available backbone assignments. Red - major perturbations ( $> 0.1$  ppm); Orange - minor perturbations (0.02-0.1 ppm); Green - no ( $< 0.02$  ppm), or inconclusive perturbations. (D) The closest distance between a ligand (ABT-737<sup>219</sup>; 2YXJ.pdb) and the backbone amides of the apoprotein (1MAZ.pdb) is plotted onto the structure of the latter. Red  $< 3$  Å; Orange 3-5 Å; Yellow 5-7 Å; Light purple  $> 7$  Å. Peptide is shown in cyan. Please note, how our inhibitor induces chemical shift changes in equivalent areas, as where ABT-737 would be expected to. This analysis suggest that the ligand binds in the same site as ABT-737<sup>219</sup>.

## 6.5. STD NMR: Interaction of STAT5b with a putative ligand

A collaboration with: Dr. Thorsten Berg, Chemical Biology, MPI Biochemistry, Munich.

NMR analysis of high molecular weight targets is challenging, since the slow tumbling of a large molecule leads to fast relaxation of the NMR signal. This makes characterization of large complexes difficult. However, for a small exchanging ligand, it is possible to observe the slow decaying NMR signal of its unbound form. This is one of the ideas behind saturation transfer difference NMR (STD NMR).<sup>135</sup> STD NMR is a fast and reliable technique that only needs small amounts of non-labeled material.

In STD NMR, the protein, for example a receptor, is saturated using a series of pulses directed at a region of the chemical shift range, where the ligand has no resonances. This saturation spreads through the protein by spin diffusion and also to any ligand that might interact with the protein. The technique basically measures the difference between two consecutive measurements, with and without saturation. Importantly, this results in a spectrum similar to a normal 1D, only if there was an interaction taking place between the protein and the ligand.

STAT5b is a 90 kDa transcription factor that can be phosphorylated by receptor tyrosine kinases, and therefore important in transforming molecular signals into changes in gene expression.<sup>220</sup> A ligand to STAT5b had been identified in the laboratory of our collaborator, using a peptide displacement screen and fluorescence polarization. To confirm binding we performed STD NMR, in a D<sub>2</sub>O-based buffer to enhance signal to noise. The sample contained 20 μM STAT5b and 1 mM ligand (1:50).

Our NMR data confirms binding, and suggest that the ligand is interacting with STAT5b in a hydrophobic manner via its aromatic system (Figure 6.5.1).

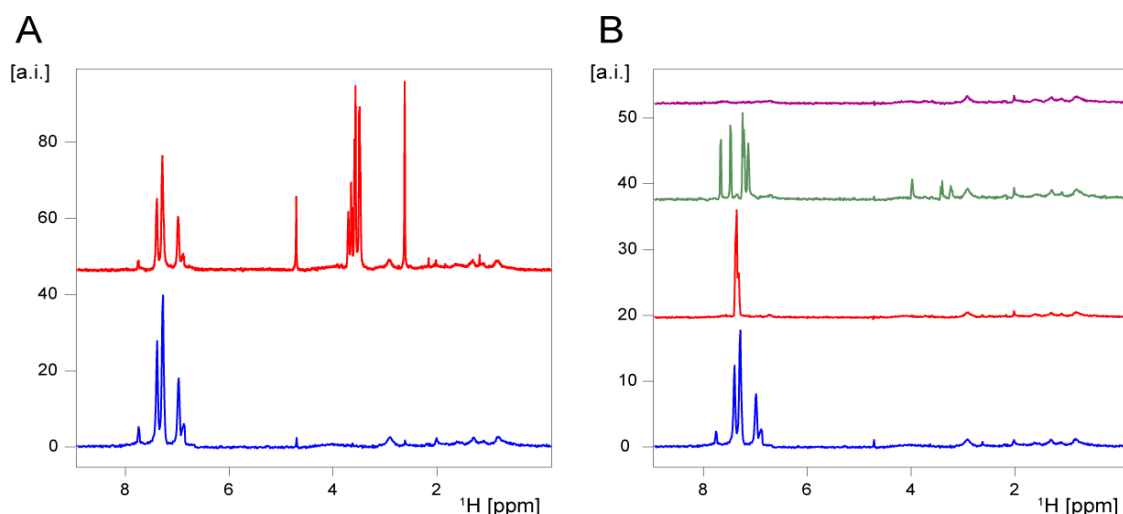


**Figure 6.5.1 STD NMR of STAT5b with different compounds.** (A) Red - Standard 1D of STAT5b and the of ligand of interest. Blue - STD spectrum of the same sample, showing STD signals for the compound (~8 ppm), but not for the buffer molecule (TRIS; ~4 ppm). The tested ligand binds. (B) STD spectra of STAT5b with other compounds. Magenta - Glucose (no interaction); Green - Tryptophan (interacts mostly with its aromatic protons, and less with H $\alpha$ /H $\beta$ ; by comparison of the intensities); Red - Molecule with a similar structure as the tested ligand (binding observed); Blue - Same as (A). Protein signals are observable in the background, since the protein always is saturated. (a.i. - arbitrary intensity)

## 6.6. Protein chemistry: Ligation of a modified peptide to SMN

A collaboration with: Prof. Dr. Christian Becker, Protein Chemistry, TUM, Munich.

The Tudor domain of human Survival of motor neuron (SMN) was one of the first domains of its kind to be characterized to bind methylated arginines (see Chapter 3).<sup>221,222</sup> However, the interaction of SMN to a single sDMA is relatively weak, with a  $K_D$  in the high micromolar range. This has hampered the structural determination of such a complex. To overcome this, we teamed up with Prof. Becker to ligate a short peptide comprising one sDMA to the C-terminus of SMN. The idea was to improve the apparent affinity of sDMA and, thereby facilitating structural characterization of the complex. The peptide was synthesized in-house and ligated to SMN prepared from a special intein-containing vector.<sup>223</sup>

Initial analysis of the ligated product by NMR has shown that the expected amide resonances of the SMN Tudor domain are perturbed (Figure 6.6.1). When plotted onto the structure of SMN Tudor, it is clear that the chemical shift changes localize to the described binding site, known as the aromatic cage. Furthermore, we have shown that the perturbations are highly similar to those observed when SMN is titrated with free sDMA.<sup>222</sup> This project is still ongoing, however, before continuing structural characterization of the ligated SMN Tudor, we need to improve the yield of the ligation reaction, as well as sample purity.

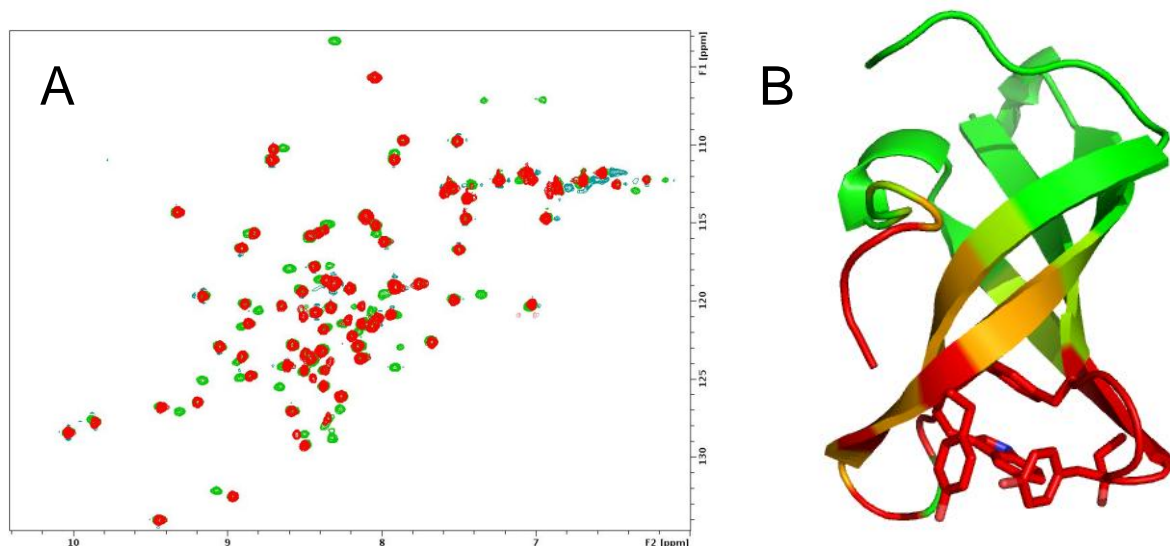


**Figure 6.6.1 Mapping of induced chemical shifts changes upon ligation of a sDMA-containing peptide to SMN.** (A)  $^1\text{H}$ ,  $^{15}\text{N}$ -HSQC spectra of non-ligated (red) and ligated SMN Tudor (green). (B) The chemical shift changes mapped onto the structure of SMN Tudor (1MHN.pdb). The characterized binding site, the so-called "aromatic cage" is highlighted as sticks. Red - major perturbations ( $> 0.1$  ppm); Orange - minor perturbations (0.02-0.1 ppm); Green - no ( $< 0.02$  ppm), or inconclusive perturbations.



# Acknowledgements

---

Where to start?! The last four years has truly been an exciting period of my life, of course with a lot of ups and downs, but in the end very, very rewarding. I've have learnt and experienced things I wouldn't have dreamt about during my studies, and you might know that I never planned to do a PhD, or to move abroad. My PhD studies has definitely been a lucky draw for me.

First and foremost my thanks and gratefulness goes to Michael Sattler. Thanks for the opportunity you gave me, and the for interesting projects to take part of. As usual in science (I know by now), many things that we tried and put our hopes to didn't succeed, but all in all I'm really satisfied with what we accomplished. And the struggle is part of the learning process, I hope...

Additionally, I want to mention all the collaborators who have contributed with their knowledge and data to our joint projects. I'm very grateful to the following people and their dedicated co-workers: Deirdre Scadden (University of Cambridge, Great Britain), Bertrand Séraphin (CGM, Gif-Sur-Yvette, France), Herman van Tilbeurgh (IBBMC, Orsay, France), Jürg Müller (EMBL, Heidelberg), Bettina Kempkes (HMGU, Munich), Arnd Kieser (HMGU, Munich), Angelika Vollmar (LMU Munich), Thorsten Berg (MPI Munich), Michael Groll (TUM, Munich) and Christian Becker (TUM, Munich).

What would the days in the lab have been without my dear colleagues? Just darn boring! Often feels like you by now belong to my extended family. I guess it comes from sharing so many tough days, and then having the contrast in the moments when things actually work out. Still, it might also be due to all nice (late) parties, dinners, trips and all the fun stuff going outside of the institute... Isn't it so, that the best thing sometimes, is to close the door to the lab, go for a beer, and then come back and try again? Well, ok maybe not the same day...

Thanks to all the guys at EMBL Heidelberg, where it all started in 2006. Gunther and Alex for giving me a kick-start in protein expression and purification. Fabi, Cameron, Lorenzo, Malgosia, Fred, Johanna for introducing me to the nightlife of HD! Bernd being there when the NMR instruments didn't understand me... or was it vice versa? Anna, thanks for sharing your Tudor project with me and, let's see when they find the real ligand? What haven't we tried, methylated DNA? Or, why not a combination of acetylated, phosphorylated and ubiquitinated H2A tails? Too expensive?!

Additionally, the rest of the HD people; Predocs of 2006 (and any other year!), Ivonne, Aga/Sebastian, WG-people – thanks to you all for making it such a great year!

Once in Munich it took some time to get settled, but luckily I, through fantastic coincidences came across my superb flat – Herzlichen Dank an Tanja, und die Familie Werner! I'm not sure if I'll ever live in a flat with a pool on the roof ever again...

Also, I want to express my gratitude to the people that made me feel so at home in this great city: Tamara and Miriam, for teaching me some Bavarian expressions. The Church crew (Alex, Feli, Nena, Sebastian, Florian, Til and the rest in Christkönig) for enjoying good food in Ristorante Italy. The Taizè people (Barbara, Berna, Rita, Anke – just so great that we by chance (?) ended up in that same cinema, my very first evening in Munich). Choir members of The Changing Voices, in particular Iris, Anke, Vanessa and Maren, one more concert to go! Lars-Anders – how big is the chance to meet an old classmate under such circumstances? Vera, for enjoying intense, and late, clubbing events, as much as me.

The graduate programs of ENB and HMGU have been very valuable to me. All people of ENB, thanks for arranging interesting workshops and retreats, but particularly for the great interest in the combination of science and friendship.

I'm very much in debt to the people of the Sattler lab, thanks for always helping out, and all the social behavior ;) Would probably be a dream (?) come true of any sociologist, to study this (international) group and its dynamics. My deepest gratefulness to all of you, hope to invite you soon to Sweden, or whatever country I may end up in. Just send me an e-mail a couple of days beforehand.

Postdocs: Fatiha, Kostas, Thomas, Toby, Iren (and Andre!) thanks for helping out when things got more tricky than expected. Toby, especially, for keeping track of the pulse programs. Kostas, for sharing the interest in Tudors. Fatiha - I'll call from anywhere if I have questions on relaxation, or for a good cake recipe! Thomas, for bringing a great party mood and fast-pulsing :) Iren, is there more Asian cakes and snacks to try, or have we had them all?

Gerd and Rainer, for hardware/software - it wouldn't work without you! (and for every now and then bringing stories about strange far-away countries into our coffee room) Waltraud, when is my contract finishing again!? :) Sorry for knocking your door so often, asking all those small annoying questions.

Predocs (I like that word) of the Sattler lab: It was always fun sharing the agony of protein purifications, and the setting-up of probably-not-successful NMR-experiments with you. Irina and Alex, my Russian is still not that good, but maybe some day I'll understand what Alex is talking about on the phone. Divita, how many times didn't that smile help me out. Don't stop - bring it on! Uli - thanks for enjoying electronica clubs and bringing me along, and that you choose to join the ENB as well... Sports was sort of missing in our (work) schedule, Hamed, thanks for never turning down the football/volleyball/ping pong opportunities. Elke, thanks for the exchange of ideas on job and outside-of-lab issues. Yun - I will never forget the day you first joined the lab, and just after a couple of hours, sat with a Maß on Oktoberfest. A great start in Germany!? Helge - this bittersweet wit you possess, fantastic! Will we see you in Lederhosen this year? Or, maybe it is rather for the Karneval? ;) The dames of the Dames' lab: Diana and Lisa, thanks for all the fun of internationality. Giambattista - associated Predoc? - an Italian wanting to leave Italy, it's not every day you meet one... Thanks for your never-ending interest in history (and Vikings!!), and the personal delivery of Mozzarella di Bufala. Johannes (and Miriam), I really liked our relaxed Sundays, with walks in the Englischer Garten and extended café sessions.

My appreciation also goes to the gate-keepers of the Garching lab, Gülden, Peijian and Steffi, as well as to our alumnus Serge. For your efforts to run the lab smoothly despite, our (not mine!!) forgotten flasks and falcons. Similarly, Arie, Ana and Heike, in the HMGU site, however, will you manage to steam that cappuccino milk without me...

A special thanks goes to André, for sharing many great moments in pubs, streets, labs and so on. Dr Wittek- Mourão, all the best with family life - and I hope to meet up with you, Mariola and David in Portugal in the near future!

To all of my friends in Sweden, I remember all your visits with warmth, as well as the intense weeks of holiday spent with you back home. My brothers in arms, David and Erik, when was the last time we spent a boring weekend somewhere? Kram på er!

And finally, above all, my deepest gratitude to mamma och pappa and Staffan, back in Stockholm. No words are enough. Thanks for love, your support and all encouragements.



## References

---

1. Crick F (1970) Central dogma of molecular biology. *Nature* 227:561-563.
2. Sourjik V, Armitage JP (2010) Spatial organization in bacterial chemotaxis. *EMBO J* 29:2724-2733.
3. Pera MF, Tam PP (2010) Extrinsic regulation of pluripotent stem cells. *Nature* 465:713-720.
4. Clapier CR, Cairns BR (2009) The biology of chromatin remodeling complexes. *Annu Rev Biochem* 78:273-304.
5. Fullwood MJ, Liu MH, Pan YF, Liu J, Xu H, Mohamed YB, Orlov YL, Velkov S, Ho A, Mei PH, Chew EG, Huang PY, Welboren WJ, Han Y, Ooi HS, Ariyaratne PN, Vega VB, Luo Y, Tan PY, Choy PY, Wansa KD, Zhao B, Lim KS, Leow SC, Yow JS, Joseph R, Li H, Desai KV, Thomsen JS, Lee YK, Karuturi RK, Herve T, Bourque G, Stunnenberg HG, Ruan X, Cacheux-Rataboul V, Sung WK, Liu ET, Wei CL, Cheung E, Ruan Y (2009) An oestrogen-receptor-alpha-bound human chromatin interactome. *Nature* 462:58-64.
6. Probst AV, Dunleavy E, Almouzni G (2009) Epigenetic inheritance during the cell cycle. *Nat Rev Mol Cell Biol* 10:192-206.
7. Breiling A, Sessa L, Orlando V (2007) Biology of polycomb and trithorax group proteins. *Int Rev Cytol* 258:83-136.
8. Bracken AP, Helin K (2009) Polycomb group proteins: navigators of lineage pathways led astray in cancer. *Nat Rev Cancer* 9:773-784.
9. Pietersen AM, van Lohuizen M (2008) Stem cell regulation by polycomb repressors: postponing commitment. *Curr Opin Cell Biol* 20:201-207.
10. Cheng X, Blumenthal RM (2008) Mammalian DNA methyltransferases: a structural perspective. *Structure* 16:341-350.
11. Klose RJ, Bird AP (2006) Genomic DNA methylation: the mark and its mediators. *Trends Biochem Sci* 31:89-97.
12. Amir RE, Van den Veyver IB, Wan M, Tran CQ, Francke U, Zoghbi HY (1999) Rett syndrome is caused by mutations in X-linked MECP2, encoding methyl-CpG-binding protein 2. *Nat Genet* 23:185-188.
13. Duszczak MM, Zanier K, Sattler M (2008) A NMR strategy to unambiguously distinguish nucleic acid hairpin and duplex conformations applied to a Xist RNA A-repeat. *Nucleic Acids Res* 36:7068-7077.
14. Zhao J, Sun BK, Erwin JA, Song JJ, Lee JT (2008) Polycomb proteins targeted by a short repeat RNA to the mouse X chromosome. *Science* 322:750-756.
15. Campos EI, Reinberg D (2009) Histones: annotating chromatin. *Annu Rev Genet* 43:559-599.
16. Clayton AL, Hazzalin CA, Mahadevan LC (2006) Enhanced histone acetylation and transcription: a dynamic perspective. *Mol Cell* 23:289-296.
17. Nekrasov M, Klymenko T, Fraterman S, Papp B, Oktaba K, Kocher T, Cohen A, Stunnenberg HG, Wilm M, Muller J (2007) Pcl-PRC2 is needed to generate high levels of H3-K27 trimethylation at Polycomb target genes. *EMBO J* 26:4078-4088.
18. Sanders SL, Portoso M, Mata J, Bahler J, Allshire RC, Kouzarides T (2004) Methylation of histone H4 lysine 20 controls recruitment of Crb2 to sites of DNA damage. *Cell* 119:603-614.
19. Choi JK, Kim YJ (2009) Implications of the nucleosome code in regulatory variation, adaptation and evolution. *Epigenetics* 4:291-295.
20. Cairns BR, Lorch Y, Li Y, Zhang M, Lacomis L, Erdjument-Bromage H, Tempst P, Du J, Laurent B, Kornberg RD (1996) RSC, an essential, abundant chromatin-remodeling complex. *Cell* 87:1249-1260.
21. Whitehouse I, Flaus A, Cairns BR, White MF, Workman JL, Owen-Hughes T (1999) Nucleosome mobilization catalysed by the yeast SWI/SNF complex. *Nature* 400:784-787.
22. Durand-Dubief M, Persson J, Norman U, Hartsuiker E, Ekwall K (2010) Topoisomerase I regulates open chromatin and controls gene expression in vivo. *EMBO J*.
23. Lodish H, Berk A, Kaiser C, Krieger M, Scott M, Bretscher A, Ploegh H, Matsudaira P. (2007). *Molecular Cell Biology*. Chp. 11, 447-454. 5th edit, W. H. Freeman.
24. Cramer P (2010) Towards molecular systems biology of gene transcription and regulation. *Biol Chem*.



25. Cramer P, Bushnell DA, Fu J, Gnatt AL, Maier-Davis B, Thompson NE, Burgess RR, Edwards AM, David PR, Kornberg RD (2000) Architecture of RNA polymerase II and implications for the transcription mechanism. *Science* 288:640-649.
26. Roeder RG (1996) The role of general initiation factors in transcription by RNA polymerase II. *Trends Biochem Sci* 21:327-335.
27. Phatnani HP, Greenleaf AL (2006) Phosphorylation and functions of the RNA polymerase II CTD. *Genes Dev* 20:2922-2936.
28. Cramer P, Armache KJ, Baumli S, Benkert S, Brueckner F, Buchen C, Damsma GE, Dengl S, Geiger SR, Jasiak AJ, Jawhari A, Jennebach S, Kamenski T, Kettenberger H, Kuhn CD, Lehmann E, Leike K, Sydow JF, Vannini A (2008) Structure of eukaryotic RNA polymerases. *Annu Rev Biophys* 37:337-352.
29. Dengl S, Cramer P (2009) Torpedo nuclease Rat1 is insufficient to terminate RNA polymerase II in vitro. *J Biol Chem* 284:21270-21279.
30. Rondon AG, Mischo HE, Kawauchi J, Proudfoot NJ (2009) Fail-safe transcriptional termination for protein-coding genes in *S. cerevisiae*. *Mol Cell* 36:88-98.
31. West S, Proudfoot NJ (2009) Transcriptional termination enhances protein expression in human cells. *Mol Cell* 33:354-364.
32. Laurencikiene J, Kallman AM, Fong N, Bentley DL, Ohman M (2006) RNA editing and alternative splicing: the importance of co-transcriptional coordination. *EMBO Rep* 7:303-307.
33. Moore MJ, Proudfoot NJ (2009) Pre-mRNA processing reaches back to transcription and ahead to translation. *Cell* 136:688-700.
34. Mayr B, Montminy M (2001) Transcriptional regulation by the phosphorylation-dependent factor CREB. *Nat Rev Mol Cell Biol* 2:599-609.
35. Ramji DP, Foka P (2002) CCAAT/enhancer-binding proteins: structure, function and regulation. *Biochem J* 365:561-575.
36. Bjorklund S, Gustafsson CM (2005) The yeast Mediator complex and its regulation. *Trends Biochem Sci* 30:240-244.
37. Koschubs T, Lorenzen K, Baumli S, Sandstrom S, Heck AJ, Cramer P (2010) Preparation and topology of the Mediator middle module. *Nucleic Acids Res* 38:3186-3195.
38. Garneau NL, Wilusz J, Wilusz CJ (2007) The highways and byways of mRNA decay. *Nat Rev Mol Cell Biol* 8:113-126.
39. Collier J, Parker R (2004) Eukaryotic mRNA decapping. *Annu Rev Biochem* 73:861-890.
40. Goldstrohm AC, Wickens M (2008) Multifunctional deadenylase complexes diversify mRNA control. *Nat Rev Mol Cell Biol* 9:337-344.
41. Houseley J, LaCava J, Tollervey D (2006) RNA-quality control by the exosome. *Nat Rev Mol Cell Biol* 7:529-539.
42. Lorentzen E, Conti E (2005) Structural basis of 3' end RNA recognition and exoribonucleolytic cleavage by an exosome RNase PH core. *Mol Cell* 20:473-481.
43. Conti E, Izaurralde E (2005) Nonsense-mediated mRNA decay: molecular insights and mechanistic variations across species. *Curr Opin Cell Biol* 17:316-325.
44. Wahl MC, Will CL, Luhrmann R (2009) The spliceosome: design principles of a dynamic RNP machine. *Cell* 136:701-718.
45. Bessonov S, Anokhina M, Will CL, Urlaub H, Luhrmann R (2008) Isolation of an active step I spliceosome and composition of its RNP core. *Nature* 452:846-850.
46. Dziembowski A, Ventura AP, Rutz B, Caspary F, Faux C, Halgand F, Laprevote O, Seraphin B (2004) Proteomic analysis identifies a new complex required for nuclear pre-mRNA retention and splicing. *EMBO J* 23:4847-4856.
47. Yang J, Valineva T, Hong J, Bu T, Yao Z, Jensen ON, Frilander MJ, Silvennoinen O (2007) Transcriptional co-activator protein p100 interacts with snRNP proteins and facilitates the assembly of the spliceosome. *Nucleic Acids Res* 35:4485-4494.
48. Kramer A (1996) The structure and function of proteins involved in mammalian pre-mRNA splicing. *Annu Rev Biochem* 65:367-409.
49. Smith DJ, Query CC, Konarska MM (2008) "Nought may endure but mutability": spliceosome dynamics and the regulation of splicing. *Mol Cell* 30:657-666.
50. Lin S, Coutinho-Mansfield G, Wang D, Pandit S, Fu XD (2008) The splicing factor SC35 has an active role in transcriptional elongation. *Nat Struct Mol Biol* 15:819-826.
51. Chen M, Manley JL (2009) Mechanisms of alternative splicing regulation: insights from molecular and genomics approaches. *Nat Rev Mol Cell Biol* 10:741-754.
52. Guo W, Bharmal SJ, Esbona K, Greaser ML (2010) Titin diversity--alternative splicing gone wild. *J Biomed Biotechnol* 2010:753675.

53. Kishore S, Stamm S (2006) The snoRNA HBII-52 regulates alternative splicing of the serotonin receptor 2C. *Science* 311:230-232.
54. Corsini L, Bonnal S, Basquin J, Hothorn M, Scheffzek K, Valcarcel J, Sattler M (2007) U2AF-homology motif interactions are required for alternative splicing regulation by SPF45. *Nat Struct Mol Biol* 14:620-629.
55. Wang ET, Sandberg R, Luo S, Khrebtkova I, Zhang L, Mayr C, Kingsmore SF, Schroth GP, Burge CB (2008) Alternative isoform regulation in human tissue transcriptomes. *Nature* 456:470-476.
56. Zhang Z, Lotti F, Dittmar K, Younis I, Wan L, Kasim M, Dreyfuss G (2008) SMN deficiency causes tissue-specific perturbations in the repertoire of snRNAs and widespread defects in splicing. *Cell* 133:585-600.
57. Mauger DM, Lin C, Garcia-Blanco MA (2008) hnRNP H and hnRNP F complex with Fox2 to silence fibroblast growth factor receptor 2 exon IIIc. *Mol Cell Biol* 28:5403-5419.
58. Feng Y, Chen M, Manley JL (2008) Phosphorylation switches the general splicing repressor SRp38 to a sequence-specific activator. *Nat Struct Mol Biol* 15:1040-1048.
59. Le Hir H, Seraphin B (2008) EJC's at the heart of translational control. *Cell* 133:213-216.
60. Proudfoot N (2000) Connecting transcription to messenger RNA processing. *Trends Biochem Sci* 25:290-293.
61. Jepson JE, Reenan RA (2008) RNA editing in regulating gene expression in the brain. *Biochim Biophys Acta* 1779:459-470.
62. Ohman M (2007) A-to-I editing challenger or ally to the microRNA process. *Biochimie* 89:1171-1176.
63. Iizasa H, Wulff B-E, Alla NR, Maragkakis M, Megraw M, Hatzigeorgiou A, Iwakiri D, Takada K, Wiedmer A, Showe L, Lieberman P, Nishikura K Editing of EBV-encoded BART6 microRNAs controls their dicer targeting and consequently affects viral latency. *Journal of Biological Chemistry*.
64. Li CL, Yang WZ, Chen YP, Yuan HS (2008) Structural and functional insights into human Tudor-SN, a key component linking RNA interference and editing. *Nucleic Acids Res* 36:3579-3589.
65. Scadden AD (2005) The RISC subunit Tudor-SN binds to hyper-edited double-stranded RNA and promotes its cleavage. *Nat Struct Mol Biol* 12:489-496.
66. Decher N, Streit AK, Rapedius M, Netter MF, Marzian S, Ehling P, Schlichthorl G, Craan T, Renigunta V, Kohler A, Dodel RC, Navarro-Polanco RA, Preisig-Muller R, Klebe G, Budde T, Baukowitz T, Daut J (2010) RNA editing modulates the binding of drugs and highly unsaturated fatty acids to the open pore of Kv potassium channels. *EMBO J* 29:2101-2113.
67. Ohlson J, Pedersen JS, Haussler D, Ohman M (2007) Editing modifies the GABA(A) receptor subunit alpha3. *RNA* 13:698-703.
68. Schoft VK, Schopoff S, Jantsch MF (2007) Regulation of glutamate receptor B pre-mRNA splicing by RNA editing. *Nucleic Acids Res* 35:3723-3732.
69. Scadden AD, Smith CW (2001) RNAi is antagonized by A-->I hyper-editing. *EMBO Rep* 2:1107-1111.
70. Nishikura K (2006) Editor meets silencer: crosstalk between RNA editing and RNA interference. *Nat Rev Mol Cell Biol* 7:919-931.
71. Yang W, Chendrimada TP, Wang Q, Higuchi M, Seeburg PH, Shiekhattar R, Nishikura K (2006) Modulation of microRNA processing and expression through RNA editing by ADAR deaminases. *Nat Struct Mol Biol* 13:13-21.
72. Kawahara Y, Zinshteyn B, Sethupathy P, Iizasa H, Hatzigeorgiou AG, Nishikura K (2007) Redirection of silencing targets by adenosine-to-inosine editing of miRNAs. *Science* 315:1137-1140.
73. Athanasiadis A, Rich A, Maas S (2004) Widespread A-to-I RNA editing of Alu-containing mRNAs in the human transcriptome. *PLoS Biol* 2:e391.
74. Chen LL, DeCervo JN, Carmichael GG (2008) Alu element-mediated gene silencing. *EMBO J* 27:1694-1705.
75. Batzer MA, Deininger PL (2002) Alu repeats and human genomic diversity. *Nat Rev Genet* 3:370-379.
76. Martinez HD, Jasavala RJ, Hinkson I, Fitzgerald LD, Trimmer JS, Kung HJ, Wright ME (2008) RNA editing of androgen receptor gene transcripts in prostate cancer cells. *J Biol Chem* 283:29938-29949.
77. Strambio-De-Castillia C, Niepel M, Rout MP (2010) The nuclear pore complex: bridging nuclear transport and gene regulation. *Nat Rev Mol Cell Biol* 11:490-501.
78. Kohler A, Hurt E (2007) Exporting RNA from the nucleus to the cytoplasm. *Nat Rev Mol Cell Biol* 8:761-773.

79. Huang Y, Steitz JA (2005) SRprises along a messenger's journey. *Mol Cell* 17:613-615.
80. Galy V, Gadal O, Fromont-Racine M, Romano A, Jacquier A, Nehrbass U (2004) Nuclear retention of unspliced mRNAs in yeast is mediated by perinuclear Mlp1. *Cell* 116:63-73.
81. Bolinger C, Boris-Lawrie K (2009) Mechanisms employed by retroviruses to exploit host factors for translational control of a complicated proteome. *Retrovirology* 6:8.
82. Akhtar A, Gasser SM (2007) The nuclear envelope and transcriptional control. *Nat Rev Genet* 8:507-517.
83. Ahmed S, Brickner JH (2007) Regulation and epigenetic control of transcription at the nuclear periphery. *Trends Genet* 23:396-402.
84. Besse F, Ephrussi A (2008) Translational control of localized mRNAs: restricting protein synthesis in space and time. *Nat Rev Mol Cell Biol* 9:971-980.
85. Martin KC, Ephrussi A (2009) mRNA localization: gene expression in the spatial dimension. *Cell* 136:719-730.
86. Lecuyer E, Yoshida H, Parthasarathy N, Alm C, Babak T, Cerovina T, Hughes TR, Tomancak P, Krause HM (2007) Global analysis of mRNA localization reveals a prominent role in organizing cellular architecture and function. *Cell* 131:174-187.
87. Anderson P, Kedersha N (2009) RNA granules: post-transcriptional and epigenetic modulators of gene expression. *Nat Rev Mol Cell Biol* 10:430-436.
88. Fire A, Xu S, Montgomery MK, Kostas SA, Driver SE, Mello CC (1998) Potent and specific genetic interference by double-stranded RNA in *Caenorhabditis elegans*. *Nature* 391:806-811.
89. Carthew RW, Sontheimer EJ (2009) Origins and Mechanisms of miRNAs and siRNAs. *Cell* 136:642-655.
90. Khvorova A, Reynolds A, Jayasena SD (2003) Functional siRNAs and miRNAs exhibit strand bias. *Cell* 115:209-216.
91. Liu Q, Paroo Z (2010) Biochemical principles of small RNA pathways. *Annu Rev Biochem* 79:295-319.
92. Liu J, Valencia-Sanchez MA, Hannon GJ, Parker R (2005) MicroRNA-dependent localization of targeted mRNAs to mammalian P-bodies. *Nat Cell Biol* 7:719-723.
93. Lu J, Getz G, Miska EA, Alvarez-Saavedra E, Lamb J, Peck D, Sweet-Cordero A, Ebert BL, Mak RH, Ferrando AA, Downing JR, Jacks T, Horvitz HR, Golub TR (2005) MicroRNA expression profiles classify human cancers. *Nature* 435:834-838.
94. Svoboda P, Flemr M (2010) The role of miRNAs and endogenous siRNAs in maternal-to-zygotic reprogramming and the establishment of pluripotency. *EMBO Rep* 11:590-597.
95. Tsai MC, Manor O, Wan Y, Mosammamaparast N, Wang JK, Lan F, Shi Y, Segal E, Chang HY (2010) Long noncoding RNA as modular scaffold of histone modification complexes. *Science* 329:689-693.
96. Yap KL, Li S, Munoz-Cabello AM, Raguz S, Zeng L, Mujtaba S, Gil J, Walsh MJ, Zhou MM (2010) Molecular interplay of the noncoding RNA ANRIL and methylated histone H3 lysine 27 by polycomb CBX7 in transcriptional silencing of INK4a. *Mol Cell* 38:662-674.
97. Kanhere A, Viiri K, Araujo CC, Rasaiyaah J, Bouwman RD, Whyte WA, Pereira CF, Brookes E, Walker K, Bell GW, Pombo A, Fisher AG, Young RA, Jenner RG (2010) Short RNAs are transcribed from repressed polycomb target genes and interact with polycomb repressive complex-2. *Mol Cell* 38:675-688.
98. Guang S, Bochner AF, Burkhart KB, Burton N, Pavelec DM, Kennedy S (2010) Small regulatory RNAs inhibit RNA polymerase II during the elongation phase of transcription. *Nature* 465:1097-1101.
99. Malone CD, Hannon GJ (2009) Small RNAs as guardians of the genome. *Cell* 136:656-668.
100. Xu Z, Wei W, Gagneur J, Perocchi F, Clauder-Munster S, Camblong J, Guffanti E, Stutz F, Huber W, Steinmetz LM (2009) Bidirectional promoters generate pervasive transcription in yeast. *Nature* 457:1033-1037.
101. Astbury WT (1961) Molecular biology or ultrastructural biology? *Nature* 190:1124.
102. Watson JD, Crick FH (1953) Molecular structure of nucleic acids; a structure for deoxyribose nucleic acid. *Nature* 171:737-738.
103. Studier FW, Rosenberg AH, Dunn JJ, Dubendorff JW (1990) Use of T7 RNA polymerase to direct expression of cloned genes. *Methods Enzymol* 185:60-89.
104. Peti W, Page R (2007) Strategies to maximize heterologous protein expression in *Escherichia coli* with minimal cost. *Protein Expr Purif* 51:1-10.
105. Edwards AM, Arrowsmith CH, Christendat D, Dharamsi A, Friesen JD, Greenblatt JF, Vedadi M (2000) Protein production: feeding the crystallographers and NMR spectroscopists. *Nat Struct Biol* 7 Suppl:970-972.

106. Biegert A, Mayer C, Remmert M, Soding J, Lupas AN (2006) The MPI Bioinformatics Toolkit for protein sequence analysis. *Nucleic Acids Res* 34:W335-339.
107. Fuhrmann M, Hausherr A, Ferbitz L, Schodl T, Heitzer M, Hegemann P (2004) Monitoring dynamic expression of nuclear genes in *Chlamydomonas reinhardtii* by using a synthetic luciferase reporter gene. *Plant Mol Biol* 55:869-881.
108. Sattler M, Liang H, Nettlesheim D, Meadows RP, Harlan JE, Eberstadt M, Yoon HS, Shuker SB, Chang BS, Minn AJ, Thompson CB, Fesik SW (1997) Structure of Bcl-xL-Bak peptide complex: recognition between regulators of apoptosis. *Science* 275:983-986.
109. Bonneau F, Lenherr ED, Pena V, Hart DJ, Scheffzek K (2009) Solubility survey of fragments of the neurofibromatosis type 1 protein neurofibromin. *Protein Expr Purif* 65:30-37.
110. Hart DJ, Tarendeau F (2006) Combinatorial library approaches for improving soluble protein expression in *Escherichia coli*. *Acta Crystallogr D Biol Crystallogr* 62:19-26.
111. Aslanidis C, de Jong PJ (1990) Ligation-independent cloning of PCR products (LIC-PCR). *Nucleic Acids Res* 18:6069-6074.
112. Li MZ, Elledge SJ (2007) Harnessing homologous recombination in vitro to generate recombinant DNA via SLIC. *Nat Methods* 4:251-256.
113. Lesage A (2009) Recent advances in solid-state NMR spectroscopy of spin  $I=1/2$  nuclei. *Phys Chem Chem Phys* 11:6876-6891.
114. Freeman R (1995) A short history of NMR. *Chemistry of Heterocyclic Compounds* 31:1004-1005.
115. Overhauser AW (1953) Polarization of Nuclei in Metals. *Physical Review* 92:411.
116. Ernst RR, Anderson WA (1966) Application of Fourier Transform Spectroscopy to Magnetic Resonance. *Review of Scientific Instruments* 37:93-102.
117. Aue WP, Bartholdi E, Ernst RR (1976) Two-dimensional spectroscopy. Application to nuclear magnetic resonance. *The Journal of Chemical Physics* 64:2229-2246.
118. Foster MP, McElroy CA, Amero CD (2007) Solution NMR of large molecules and assemblies. *Biochemistry* 46:331-340.
119. Sprangers R, Velyvis A, Kay LE (2007) Solution NMR of supramolecular complexes: providing new insights into function. *Nat Methods* 4:697-703.
120. Kovacs H, Moskau D, Spraul M (2005) Cryogenically cooled probes--a leap in NMR technology. *Progress in Nuclear Magnetic Resonance Spectroscopy* 46:131-155.
121. Rossi P, Swapna GV, Huang YJ, Aramini JM, Anklin C, Conover K, Hamilton K, Xiao R, Acton TB, Ertekin A, Everett JK, Montelione GT (2010) A microscale protein NMR sample screening pipeline. *J Biomol NMR* 46:11-22.
122. Piotto M, Saudek V, Sklenar V (1992) Gradient-tailored excitation for single-quantum NMR spectroscopy of aqueous solutions. *J Biomol NMR* 2:661-665.
123. Delaglio F, Grzesiek S, Vuister GW, Zhu G, Pfeifer J, Bax A (1995) NMRPipe: a multidimensional spectral processing system based on UNIX pipes. *J Biomol NMR* 6:277-293.
124. Sørensen OW, Eich GW, Levitt MH, Bodenhausen G, Ernst RR (1984) Product operator formalism for the description of NMR pulse experiments. *Progress in Nuclear Magnetic Resonance Spectroscopy* 16:163-192.
125. Sattler M, Schleucher J, Griesinger C (1999) Heteronuclear multidimensional NMR experiments for the structure determination of proteins in solution employing pulsed. *Progress in Nuclear Magnetic Resonance Spectroscopy* 34:93-158.
126. Johnson BA, Blevins RA (1994) NMR View: A computer program for the visualization and analysis of NMR data. *Journal of Biomolecular NMR* 4:603-614.
127. Volk J, Herrmann T, Wuthrich K (2008) Automated sequence-specific protein NMR assignment using the memetic algorithm MATCH. *J Biomol NMR* 41:127-138.
128. Wishart DS, Sykes BD (1994) The  $^{13}\text{C}$  chemical-shift index: a simple method for the identification of protein secondary structure using  $^{13}\text{C}$  chemical-shift data. *J Biomol NMR* 4:171-180.
129. Shen Y, Delaglio F, Cornilescu G, Bax A (2009) TALOS+: a hybrid method for predicting protein backbone torsion angles from NMR chemical shifts. *J Biomol NMR* 44:213-223.
130. Cavalli A, Salvatella X, Dobson CM, Vendruscolo M (2007) Protein structure determination from NMR chemical shifts. *Proc Natl Acad Sci U S A* 104:9615-9620.
131. Shen Y, Vernon R, Baker D, Bax A (2009) De novo protein structure generation from incomplete chemical shift assignments. *J Biomol NMR* 43:63-78.
132. Robustelli P, Kohlhoff K, Cavalli A, Vendruscolo M (2010) Using NMR Chemical Shifts as Structural Restraints in Molecular Dynamics Simulations of Proteins. *18:923-933*.
133. Stockman BJ, Dalvit C (2002) NMR screening techniques in drug discovery and drug design. *Progress in Nuclear Magnetic Resonance Spectroscopy* 41:187-231.

134. Shuker SB, Hajduk PJ, Meadows RP, Fesik SW (1996) Discovering high-affinity ligands for proteins: SAR by NMR. *Science* 274:1531-1534.
135. Mayer M, Meyer B (2001) Group Epitope Mapping by Saturation Transfer Difference NMR To Identify Segments of a Ligand in Direct Contact with a Protein Receptor. *Journal of the American Chemical Society* 123:6108-6117.
136. Sanchez-Pedregal VM, Reese M, Meiler J, Blommers MJ, Griesinger C, Carlomagno T (2005) The INPHARMA method: protein-mediated interligand NOEs for pharmacophore mapping. *Angew Chem Int Ed Engl* 44:4172-4175.
137. Farrow NA, Muhandiram R, Singer AU, Pascal SM, Kay CM, Gish G, Shoelson SE, Pawson T, Forman-Kay JD, Kay LE (1994) Backbone dynamics of a free and phosphopeptide-complexed Src homology 2 domain studied by <sup>15</sup>N NMR relaxation. *Biochemistry* 33:5984-6003.
138. Sprangers R, Selenko P, Sattler M, Sinning I, Groves MR (2003) Definition of domain boundaries and crystallization of the SMN Tudor domain. *Acta Crystallogr D Biol Crystallogr* 59:366-368.
139. Sprangers R, Kay LE (2007) Quantitative dynamics and binding studies of the 20S proteasome by NMR. *Nature* 445:618-622.
140. Jaravine VA, Zhuravleva AV, Permi P, Ibraghimov I, Orekhov VY (2008) Hyperdimensional NMR Spectroscopy with Nonlinear Sampling. *Journal of the American Chemical Society* 130:13182-13182.
141. Guntert P (2004) Automated NMR structure calculation with CYANA. *Methods Mol Biol* 278:353-378.
142. Linge JP, O'Donoghue SI, Nilges M (2001) Automated assignment of ambiguous nuclear overhauser effects with ARIA. *Methods Enzymol* 339:71-90.
143. Tjandra N, Bax A (1997) Direct measurement of distances and angles in biomolecules by NMR in a dilute liquid crystalline medium. *Science* 278:1111-1114.
144. Zweckstetter M, Bax A (2001) Characterization of molecular alignment in aqueous suspensions of Pf1 bacteriophage. *J Biomol NMR* 20:365-377.
145. Ruckert M, Otting G (2000) Alignment of Biological Macromolecules in Novel Nonionic Liquid Crystalline Media for NMR Experiments. *Journal of the American Chemical Society* 122:7793-7797.
146. Lorieau J, Yao L, Bax A (2008) Liquid Crystalline Phase of G-Tetrad DNA for NMR Study of Detergent-Solubilized Proteins. *Journal of the American Chemical Society* 130:7536-7537.
147. Kummerlöwe G, Auernheimer J, Lendlein A, Luy B (2007) Stretched Poly(acrylonitrile) as a Scalable Alignment Medium for DMSO. *Journal of the American Chemical Society* 129:6080-6081.
148. Zweckstetter M (2008) NMR: prediction of molecular alignment from structure using the PALES software. *Nat Protoc* 3:679-690.
149. Kontaxis G, Delaglio F, Bax A (2005) Molecular fragment replacement approach to protein structure determination by chemical shift and dipolar homology database mining. *Methods Enzymol* 394:42-78.
150. Dosset P, Hus JC, Marion D, Blackledge M (2001) A novel interactive tool for rigid-body modeling of multi-domain macromolecules using residual dipolar couplings. *J Biomol NMR* 20:223-231.
151. Simon B, Madl T, Mackereth CD, Nilges M, Sattler M (2010) An efficient protocol for NMR-spectroscopy-based structure determination of protein complexes in solution. *Angew Chem Int Ed Engl* 49:1967-1970.
152. Bax A, Kontaxis G, Tjandra N (2001) Dipolar couplings in macromolecular structure determination. *Methods Enzymol* 339:127-174.
153. Zhang Q, Stelzer AC, Fisher CK, Al-Hashimi HM (2007) Visualizing spatially correlated dynamics that directs RNA conformational transitions. *Nature* 450:1263-1267.
154. Tolman JR, Flanagan JM, Kennedy MA, Prestegard JH (1997) NMR evidence for slow collective motions in cyanometmyoglobin. *Nat Struct Biol* 4:292-297.
155. Lange OF, Lakomek NA, Fares C, Schroder GF, Walter KF, Becker S, Meiler J, Grubmüller H, Griesinger C, de Groot BL (2008) Recognition dynamics up to microseconds revealed from an RDC-derived ubiquitin ensemble in solution. *Science* 320:1471-1475.
156. Brunger AT, Adams PD, Clore GM, DeLano WL, Gros P, Grosse-Kunstleve RW, Jiang JS, Kuszewski J, Nilges M, Pannu NS, Read RJ, Rice LM, Simonson T, Warren GL (1998) Crystallography & NMR system: A new software suite for macromolecular structure determination. *Acta Crystallogr D Biol Crystallogr* 54:905-921.
157. Schwieters CD, Kuszewski JJ, Tjandra N, Clore GM (2003) The Xplor-NIH NMR molecular structure determination package. *J Magn Reson* 160:65-73.

158. Madl T, Bermel W, Zangger K (2009) Use of relaxation enhancements in a paramagnetic environment for the structure determination of proteins using NMR spectroscopy. *Angew Chem Int Ed Engl* 48:8259-8262.
159. Spronk CAEM, Nabuurs SB, Krieger E, Vriend G, Vuister GW (2004) Validation of protein structures derived by NMR spectroscopy. *Progress in Nuclear Magnetic Resonance Spectroscopy* 45:315-337.
160. Geerten W, Vuister JFD, Alan W.S. da Silva. iCing v2.0, <http://nmr.cmbi.ru.nl/icing/iCing.html>.
161. Laskowski RA, Rullmann JA, MacArthur MW, Kaptein R, Thornton JM (1996) AQUA and PROCHECK-NMR: programs for checking the quality of protein structures solved by NMR. *J Biomol NMR* 8:477-486.
162. Vriend G, Sander C (1993) Quality control of protein models: directional atomic contact analysis. *Journal of Applied Crystallography* 26:47-60.
163. Clore GM, Garrett DS (1999) R-factor, Free R, and Complete Cross-Validation for Dipolar Coupling Refinement of NMR Structures. *Journal of the American Chemical Society* 121:9008-9012.
164. Deisenhofer J, Epp O, Miki K, Huber R, Michel H (1985) Structure of the protein subunits in the photosynthetic reaction centre of *Rhodospseudomonas viridis* at 3[angst] resolution. *Nature* 318:618-624.
165. Cramer P, Bushnell DA, Kornberg RD (2001) Structural basis of transcription: RNA polymerase II at 2.8 angstrom resolution. *Science* 292:1863-1876.
166. Ban N, Nissen P, Hansen J, Moore PB, Steitz TA (2000) The complete atomic structure of the large ribosomal subunit at 2.4 A resolution. *Science* 289:905-920.
167. Sayre D (2002) X-Ray Crystallography: The Past and Present of the Phase Problem. *Structural Chemistry* 13:81-96.
168. Price WN, 2nd, Chen Y, Handelmann SK, Neely H, Manor P, Karlin R, Nair R, Liu J, Baran M, Everett J, Tong SN, Forouhar F, Swaminathan SS, Acton T, Xiao R, Luft JR, Lauricella A, DeTitta GT, Rost B, Montelione GT, Hunt JF (2009) Understanding the physical properties that control protein crystallization by analysis of large-scale experimental data. *Nat Biotechnol* 27:51-57.
169. Dong A, Xu X, Edwards AM, Chang C, Chruszcz M, Cuff M, Cymborowski M, Di Leo R, Egorova O, Evdokimova E, Filippova E, Gu J, Guthrie J, Ignatchenko A, Joachimiak A, Klostermann N, Kim Y, Korniyenko Y, Minor W, Que Q, Savchenko A, Skarina T, Tan K, Yakunin A, Yee A, Yim V, Zhang R, Zheng H, Akutsu M, Arrowsmith C, Avvakumov GV, Bochkarev A, Dahlgren LG, Dhe-Paganon S, Dimov S, Dombrovski L, Finerty P, Jr., Flodin S, Flores A, Graslund S, Hammerstrom M, Herman MD, Hong BS, Hui R, Johansson I, Liu Y, Nilsson M, Nedyalkova L, Nordlund P, Nyman T, Min J, Ouyang H, Park HW, Qi C, Rabeh W, Shen L, Shen Y, Sukumard D, Tempel W, Tong Y, Tresagues L, Vedadi M, Walker JR, Weigelt J, Welin M, Wu H, Xiao T, Zeng H, Zhu H (2007) In situ proteolysis for protein crystallization and structure determination. *Nat Methods* 4:1019-1021.
170. Brunger AT (1992) Free R value: a novel statistical quantity for assessing the accuracy of crystal structures. *Nature* 355:472-475.
171. Christodoulou J, Larsson G, Fucini P, Connell SR, Pertinhez TA, Hanson CL, Redfield C, Nierhaus KH, Robinson CV, Schleucher J, Dobson CM (2004) Heteronuclear NMR investigations of dynamic regions of intact *Escherichia coli* ribosomes. *Proceedings of the National Academy of Sciences of the United States of America* 101:10949-10954.
172. Simon JA, Kingston RE (2009) Mechanisms of polycomb gene silencing: knowns and unknowns. *Nat Rev Mol Cell Biol* 10:697-708.
173. Deckert J, Hartmuth K, Boehringer D, Behzadnia N, Will CL, Kastner B, Stark H, Urlaub H, Luhrmann R (2006) Protein composition and electron microscopy structure of affinity-purified human spliceosomal B complexes isolated under physiological conditions. *Mol Cell Biol* 26:5528-5543.
174. Herold N, Will CL, Wolf E, Kastner B, Urlaub H, Luhrmann R (2009) Conservation of the protein composition and electron microscopy structure of *Drosophila melanogaster* and human spliceosomal complexes. *Mol Cell Biol* 29:281-301.
175. Entian KD, Schuster T, Hegemann JH, Becher D, Feldmann H, Guldener U, Gotz R, Hansen M, Hollenberg CP, Jansen G, Kramer W, Klein S, Kotter P, Kricke J, Launhardt H, Mannhaupt G, Maierl A, Meyer P, Mewes W, Munder T, Niedenthal RK, Ramezani Rad M, Rohmer A, Romer A, Hinnen A, et al. (1999) Functional analysis of 150 deletion mutants in *Saccharomyces cerevisiae* by a systematic approach. *Mol Gen Genet* 262:683-702.
176. Ni L, Snyder M (2001) A genomic study of the bipolar bud site selection pattern in *Saccharomyces cerevisiae*. *Mol Biol Cell* 12:2147-2170.

177. Gottschalk A, Bartels C, Neubauer G, Luhrmann R, Fabrizio P (2001) A novel yeast U2 snRNP protein, Snu17p, is required for the first catalytic step of splicing and for progression of spliceosome assembly. *Mol Cell Biol* 21:3037-3046.
178. Stevens SW, Ryan DE, Ge HY, Moore RE, Young MK, Lee TD, Abelson J (2002) Composition and functional characterization of the yeast spliceosomal penta-snRNP. *Mol Cell* 9:31-44.
179. Wang Q, He J, Lynn B, Rymond BC (2005) Interactions of the yeast SF3b splicing factor. *Mol Cell Biol* 25:10745-10754.
180. Ohi MD, Link AJ, Ren L, Jennings JL, McDonald WH, Gould KL (2002) Proteomics analysis reveals stable multiprotein complexes in both fission and budding yeasts containing Myb-related Cdc5p/Cef1p, novel pre-mRNA splicing factors, and snRNAs. *Mol Cell Biol* 22:2011-2024.
181. Fasken MB, Corbett AH (2009) Mechanisms of nuclear mRNA quality control. *RNA Biol* 6:237-241.
182. Palancade B, Zuccolo M, Loeillet S, Nicolas A, Doye V (2005) Pml39, a novel protein of the nuclear periphery required for nuclear retention of improper messenger ribonucleoproteins. *Mol Biol Cell* 16:5258-5268.
183. Spingola M, Armisen J, Ares M, Jr. (2004) Mer1p is a modular splicing factor whose function depends on the conserved U2 snRNP protein Snu17p. *Nucleic Acids Res* 32:1242-1250.
184. Scherrer FW, Jr., Spingola M (2006) A subset of Mer1p-dependent introns requires Bud13p for splicing activation and nuclear retention. *RNA* 12:1361-1372.
185. Taniguchi I, Masuyama K, Ohno M (2007) Role of purine-rich exonic splicing enhancers in nuclear retention of pre-mRNAs. *Proc Natl Acad Sci U S A* 104:13684-13689.
186. Kaida D, Motoyoshi H, Tashiro E, Nojima T, Hagiwara M, Ishigami K, Watanabe H, Kitahara T, Yoshida T, Nakajima H, Tani T, Horinouchi S, Yoshida M (2007) Spliceostatin A targets SF3b and inhibits both splicing and nuclear retention of pre-mRNA. *Nat Chem Biol* 3:576-583.
187. Trowitzsch S, Weber G, Luhrmann R, Wahl MC (2008) An unusual RNA recognition motif acts as a scaffold for multiple proteins in the pre-mRNA retention and splicing complex. *J Biol Chem* 283:32317-32327.
188. Brooks MA, Dziembowski A, Quevillon-Cheruel S, Henriot V, Faux C, van Tilbeurgh H, Seraphin B (2009) Structure of the yeast Pml1 splicing factor and its integration into the RES complex. *Nucleic Acids Res* 37:129-143.
189. Clery A, Blatter M, Allain FH (2008) RNA recognition motifs: boring? Not quite. *Curr Opin Struct Biol* 18:290-298.
190. Kielkopf CL, Lucke S, Green MR (2004) U2AF homology motifs: protein recognition in the RRM world. *Genes Dev* 18:1513-1526.
191. Trowitzsch S, Weber G, Luhrmann R, Wahl MC (2009) Crystal structure of the Pml1p subunit of the yeast precursor mRNA retention and splicing complex. *J Mol Biol* 385:531-541.
192. Durocher D, Henckel J, Fersht AR, Jackson SP (1999) The FHA domain is a modular phosphopeptide recognition motif. *Mol Cell* 4:387-394.
193. Byeon IJ, Li H, Song H, Gronenborn AM, Tsai MD (2005) Sequential phosphorylation and multisite interactions characterize specific target recognition by the FHA domain of Kif67. *Nat Struct Mol Biol* 12:987-993.
194. Plateau P, Gueron M (1982) Exchangeable proton NMR without base-line distortion, using new strong-pulse sequences. *Journal of the American Chemical Society* 104:7310-7311.
195. Cole C, Barber JD, Barton GJ (2008) The Jpred 3 secondary structure prediction server. *Nucleic Acids Res* 36:W197-201.
196. McGuffin LJ, Bryson K, Jones DT (2000) The PSIPRED protein structure prediction server. *Bioinformatics* 16:404-405.
197. Puntervoll P, Linding R, Gemund C, Chabanis-Davidson S, Mattingsdal M, Cameron S, Martin DM, Ausiello G, Brannetti B, Costantini A, Ferre F, Maselli V, Via A, Cesareni G, Diella F, Superti-Furga G, Wyrwicz L, Ramu C, McGuigan C, Gudavalli R, Letunic I, Bork P, Rychlewski L, Kuster B, Helmer-Citterich M, Hunter WN, Aasland R, Gibson TJ (2003) ELM server: A new resource for investigating short functional sites in modular eukaryotic proteins. *Nucleic Acids Res* 31:3625-3630.
198. Gould CM, Diella F, Via A, Puntervoll P, Gemund C, Chabanis-Davidson S, Michael S, Sayadi A, Bryne JC, Chica C, Seiler M, Davey NE, Haslam N, Weatheritt RJ, Budd A, Hughes T, Pas J, Rychlewski L, Trave G, Aasland R, Helmer-Citterich M, Linding R, Gibson TJ (2010) ELM: the status of the 2010 eukaryotic linear motif resource. *Nucleic Acids Res* 38:D167-180.
199. Kielkopf CL, Rodionova NA, Green MR, Burley SK (2001) A novel peptide recognition mode revealed by the X-ray structure of a core U2AF35/U2AF65 heterodimer. *Cell* 106:595-605.

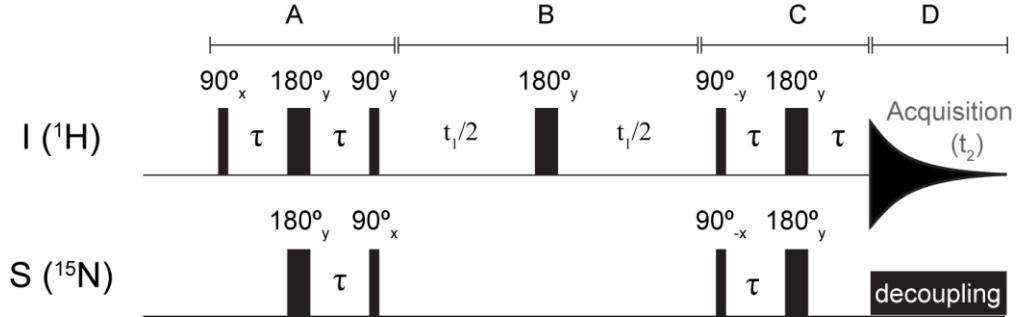


200. Selenko P, Gregorovic G, Sprangers R, Stier G, Rhani Z, Kramer A, Sattler M (2003) Structural basis for the molecular recognition between human splicing factors U2AF65 and SF1/mBBP. *Mol Cell* 11:965-976.
201. Das R, Zhou Z, Reed R (2000) Functional association of U2 snRNP with the ATP-independent spliceosomal complex E. *Mol Cell* 5:779-787.
202. Berglund JA, Abovich N, Rosbash M (1998) A cooperative interaction between U2AF65 and mBBP/SF1 facilitates branchpoint region recognition. *Genes Dev* 12:858-867.
203. Corsini L, Hothorn M, Stier G, Rybin V, Scheffzek K, Gibson TJ, Sattler M (2009) Dimerization and protein binding specificity of the U2AF homology motif of the splicing factor Puf60. *J Biol Chem* 284:630-639.
204. Schellenberg MJ, Edwards RA, Ritchie DB, Kent OA, Golas MM, Stark H, Luhrmann R, Glover JN, MacMillan AM (2006) Crystal structure of a core spliceosomal protein interface. *Proc Natl Acad Sci U S A* 103:1266-1271.
205. Nagai K, Oubridge C, Jessen TH, Li J, Evans PR (1990) Crystal structure of the RNA-binding domain of the U1 small nuclear ribonucleoprotein A. *Nature* 348:515-520.
206. Oubridge C, Ito N, Evans PR, Teo CH, Nagai K (1994) Crystal structure at 1.92 Å resolution of the RNA-binding domain of the U1A spliceosomal protein complexed with an RNA hairpin. *Nature* 372:432-438.
207. Wilkins MR, Gasteiger E, Bairoch A, Sanchez JC, Williams KL, Appel RD, Hochstrasser DF (1999) Protein identification and analysis tools in the Expasy server. *Methods Mol Biol* 112:531-552.
208. Ericsson UB, Hallberg BM, Detitta GT, Dekker N, Nordlund P (2006) Thermofluor-based high-throughput stability optimization of proteins for structural studies. *Anal Biochem* 357:289-298.
209. Soding J, Biegert A, Lupas AN (2005) The HHpred interactive server for protein homology detection and structure prediction. *Nucleic Acids Res* 33:W244-248.
210. DeLano WL. (2002). The PyMOL Molecular Graphics System. DeLano Scientific, San Carlos, CA, USA.
211. Kabsch W, Sander C (1983) Dictionary of protein secondary structure: pattern recognition of hydrogen-bonded and geometrical features. *Biopolymers* 22:2577-2637.
212. Larkin MA, Blackshields G, Brown NP, Chenna R, McGettigan PA, McWilliam H, Valentin F, Wallace IM, Wilm A, Lopez R, Thompson JD, Gibson TJ, Higgins DG (2007) Clustal W and Clustal X version 2.0. *Bioinformatics* 23:2947-2948.
213. Liu Z, Sun C, Olejniczak ET, Meadows RP, Betz SF, Oost T, Herrmann J, Wu JC, Fesik SW (2000) Structural basis for binding of Smac/DIABLO to the XIAP BIR3 domain. *Nature* 408:1004-1008.
214. Holcik M, Korneluk RG (2001) XIAP, the guardian angel. *Nat Rev Mol Cell Biol* 2:550-556.
215. Oost TK, Sun C, Armstrong RC, Al-Assaad AS, Betz SF, Deckwerth TL, Ding H, Elmore SW, Meadows RP, Olejniczak ET, Oleksijew A, Oltersdorf T, Rosenberg SH, Shoemaker AR, Tomaselli KJ, Zou H, Fesik SW (2004) Discovery of potent antagonists of the antiapoptotic protein XIAP for the treatment of cancer. *J Med Chem* 47:4417-4426.
216. Kieser A (2008) Pursuing different 'TRADDs': TRADD signaling induced by TNF-receptor 1 and the Epstein-Barr virus oncoprotein LMP1. *Biol Chem* 389:1261-1271.
217. Kieser A, Kaiser C, Hammerschmidt W (1999) LMP1 signal transduction differs substantially from TNF receptor 1 signaling in the molecular functions of TRADD and TRAF2. *EMBO J* 18:2511-2521.
218. Maier S, Staffler G, Hartmann A, Hock J, Henning K, Grabusic K, Mailhammer R, Hoffmann R, Wilmanns M, Lang R, Mages J, Kempkes B (2006) Cellular target genes of Epstein-Barr virus nuclear antigen 2. *J Virol* 80:9761-9771.
219. Lee EF, Czabotar PE, Smith BJ, Deshayes K, Zobel K, Colman PM, Fairlie WD (2007) Crystal structure of ABT-737 complexed with Bcl-xL: implications for selectivity of antagonists of the Bcl-2 family. *Cell Death Differ* 14:1711-1713.
220. Muller J, Sperl B, Reindl W, Kiessling A, Berg T (2008) Discovery of chromone-based inhibitors of the transcription factor STAT5. *Chembiochem* 9:723-727.
221. Buhler D, Raker V, Luhrmann R, Fischer U (1999) Essential role for the tudor domain of SMN in spliceosomal U snRNP assembly: implications for spinal muscular atrophy. *Hum Mol Genet* 8:2351-2357.
222. Sprangers R, Groves MR, Sinning I, Sattler M (2003) High-resolution X-ray and NMR structures of the SMN Tudor domain: conformational variation in the binding site for symmetrically dimethylated arginine residues. *J Mol Biol* 327:507-520.
223. Durek T, Becker CF (2005) Protein semi-synthesis: new proteins for functional and structural studies. *Biomol Eng* 22:153-172.



# Appendices

## A.1 Product operator analysis of the HSQC pulse sequence



The initial magnetization is depending on the population of the energy states according to the Boltzmann distribution,

$$aI_z + bS_z$$

, where a and b are coefficients describing the individual amounts of polarization. These numbers will be omitted in the analysis. For a proton and nitrogen pair,  $a \approx 10b$ .

In the analysis the following rules have been applied to simplify calculations:

- 1) During spin-echoes there is no chemical evolution
- 2)  $\tau$  is set to  $1/4J$ , to accomplish complete coherence transfer. In the  $^1\text{H}-^{15}\text{N}$  amide pair, the J-coupling is  $\sim 90\text{Hz}$ .
- 3) During decoupling there is no coupling active between the I and S spin

**Part A:** (No chemical shift evolution; a spin-echo for spin I and spin S is always along the z-axis)

$$I_z + S_z \xrightarrow{(90^\circ_x)_I} -I_y + S_z \xrightarrow{\pi_{IS}} -I_y \cos \pi J_{IS} \tau + 2I_x S_z \sin \pi J_{IS} \tau + S_z$$

$$\xrightarrow{(180^\circ_y)_I} -I_y \cos \pi J_{IS} \tau - 2I_x S_z \sin \pi J_{IS} \tau + S_z$$

$$\xrightarrow{(180^\circ_y)_S} -I_y \cos \pi J_{IS} \tau + 2I_x S_z \sin \pi J_{IS} \tau - S_z$$

$$\xrightarrow{\pi_{IS}} -I_y \cos \pi J_{IS} \tau \cos \pi J_{IS} \tau + 2I_x S_z \cos \pi J_{IS} \tau \sin \pi J_{IS} \tau$$

$$\cos^2 A - \sin^2 A = \cos 2A$$

$$+ 2I_x S_z \sin \pi J_{IS} \tau \cos \pi J_{IS} \tau + I_y \sin \pi J_{IS} \tau \sin \pi J_{IS} \tau - S_z$$

$$2 \times \sin A \times \cos A = \sin 2A$$

$$= -I_y \cos 2\pi J_{IS} \tau + 2I_x S_z \sin 2\pi J_{IS} \tau - S_z$$

$$\xrightarrow{\tau = 1/4J} 2I_x S_z - S_z$$

$$\xrightarrow{(90^\circ_y)_I} -2I_z S_z - S_z \xrightarrow{(90^\circ_x)_S} 2I_z S_y + S_y$$

**Part B:** (No chemical shift evolution for the I spin, because of the  $180^\circ$  degree pulse. However, also the J-coupling is refocused due to this arrangement,)

$$2I_z S_y + S_y \xrightarrow{\Omega_S t_1} 2I_z S_y \cos \Omega_S t_1/2 - 2I_z S_x \sin \Omega_S t_1/2 + S_y \cos \Omega_S t_1/2 - S_x \sin \Omega_S t_1/2$$

$$\xrightarrow{(180^\circ_y)_I} -2I_z S_y \cos \Omega_S t_1/2 + 2I_z S_x \sin \Omega_S t_1/2 + S_y \cos \Omega_S t_1/2 - S_x \sin \Omega_S t_1/2$$

$$\xrightarrow{\Omega_S t_1} -2I_z S_y \cos \Omega_S t_1 + 2I_z S_x \sin \Omega_S t_1 + S_y \cos \Omega_S t_1 - S_x \sin \Omega_S t_1$$

**Part C:** Similar to A, but reversed and lacks the last 90° pulse, since we want to leave the magnetization precessing in the plane, where it can induce a signal in the probe coils.

$$\begin{aligned}
& -2I_z S_y \cos \Omega_S t_1 + 2I_z S_x \sin \Omega_S t_1 + S_y \cos \Omega_S t_1 - S_x \sin \Omega_S t_1 \\
& \xrightarrow{(90^\circ - y)_I} 2I_x S_y \cos \Omega_S t_1 - 2I_x S_x \sin \Omega_S t_1 + S_y \cos \Omega_S t_1 - S_x \sin \Omega_S t_1 \\
& \xrightarrow{(90^\circ - x)_S} -2I_x S_z \cos \Omega_S t_1 - 2I_x S_x \sin \Omega_S t_1 - S_z \cos \Omega_S t_1 - S_x \sin \Omega_S t_1 \\
& \xrightarrow{\pi J_{IS}} -2I_x S_z \cos \Omega_S t_1 \cos \pi J_{IS} \tau - I_y \cos \Omega_S t_1 \sin \pi J_{IS} \tau \\
& \quad -2I_x S_x \sin \Omega_S t_1 \quad * \quad * \text{ Double quantum operators do not evolve under J-coupling.} \\
& \quad -S_z \cos \Omega_S t_1 \\
& \quad -S_x \sin \Omega_S t_1 \cos \pi J_{IS} \tau - 2I_z S_y \sin \Omega_S t_1 \sin \pi J_{IS} \tau \\
& \xrightarrow{(180^\circ)_I (180^\circ)_S} -2I_x S_z \cos \Omega_S t_1 \cos \pi J_{IS} \tau - I_y \cos \Omega_S t_1 \sin \pi J_{IS} \tau \\
& \quad -2I_x S_x \sin \Omega_S t_1 + S_z \cos \Omega_S t_1 \\
& \quad + S_x \sin \Omega_S t_1 \cos \pi J_{IS} \tau + 2I_z S_y \cos \Omega_S t_1 \sin \pi J_{IS} \tau \\
& \xrightarrow{\pi J_{IS}} -2I_x S_z \cos \Omega_S t_1 \cos \pi J_{IS} \tau \cos \pi J_{IS} \tau - I_y \cos \Omega_S t_1 \cos \pi J_{IS} \tau \sin \pi J_{IS} \tau \\
& \quad - I_y \cos \Omega_S t_1 \sin \pi J_{IS} \tau \cos \pi J_{IS} \tau + 2I_x S_z \cos \Omega_S t_1 \sin \pi J_{IS} \tau \sin \pi J_{IS} \tau \\
& \quad -2I_x S_x \sin \Omega_S t_1 + S_z \cos \Omega_S t_1 \\
& \quad + S_x \sin \Omega_S t_1 \cos \pi J_{IS} \tau \cos \pi J_{IS} \tau + 2I_z S_y \sin \Omega_S t_1 \cos \pi J_{IS} \tau \sin \pi J_{IS} \tau \\
& = -2I_x S_z \cos \Omega_S t_1 \cos 2\pi J_{IS} \tau - I_y \cos \Omega_S t_1 \sin 2\pi J_{IS} \tau \\
& \quad -2I_x S_x \sin \Omega_S t_1 + S_z \cos \Omega_S t_1 + S_x \sin \Omega_S t_1 \cos \pi J_{IS} \tau \cos \pi J_{IS} \tau \\
& \quad + 2I_z S_y \sin \Omega_S t_1 \cos \pi J_{IS} \tau \sin \pi J_{IS} \tau \\
& \xrightarrow{\tau = 1/4J} -I_y \cos \Omega_S t_1 - 2I_x S_x \sin \Omega_S t_1 + S_z \cos \Omega_S t_1 + S_x \sin \Omega_S t_1 \cos \pi J_{IS} \tau \cos \pi J_{IS} \tau + 2I_z S_y \sin \Omega_S t_1 \cos \pi J_{IS} \tau \sin \pi J_{IS} \tau
\end{aligned}$$

Only the blue ( $I_y$ ) operator is observable, the other operators are not:  $2I_x S_x$  - multiple quantum operator;  $S_z$  - along z-axis, not detectable;  $S_x$  arises from initial S excitation which is, in the case of  $^{15}\text{N}$  nucleus, ten times less intense than the one arising from excitation of proton spin (can also be removed by phase cycling of the initial 90° pulse.);  $2I_z S_y$  - antiphase magnetization on spin S, and do not evolve to magnetization on I due to the decoupling during acquisition.

**Part D:** During acquisition, no J-coupling is active because of the decoupling pulse on spin S. Chemical shift of spin I is evolved, and relaxation will also clearly affect the FID.

$$-I_y \cos \Omega_S t_1 \xrightarrow{\Omega_S t_2} -I_y \cos \Omega_S t_1 \cos \Omega_I t_2 + I_x \cos \Omega_S t_1 \sin \Omega_I t_2$$

Comments: To "save" both anti-phase magnetization terms on spin S at the end of B part, a so-called *sensitivity enhanced HSQC (SE-HSQC)* sequence have been developed.<sup>125</sup> In order to achieve quadrature detection, the direction of the initial 90° pulse is changed sequentially. In addition, pulsed-field gradients can be incorporated to remove artifacts, and accomplish water-suppression as well as coherence selection.

## A.2 Sequence and mass spectra of selected RES expression constructs

### Snu17<sup>1-113</sup>

Uniprot: P40565

Residues: 1-113

Number of amino acids: 120

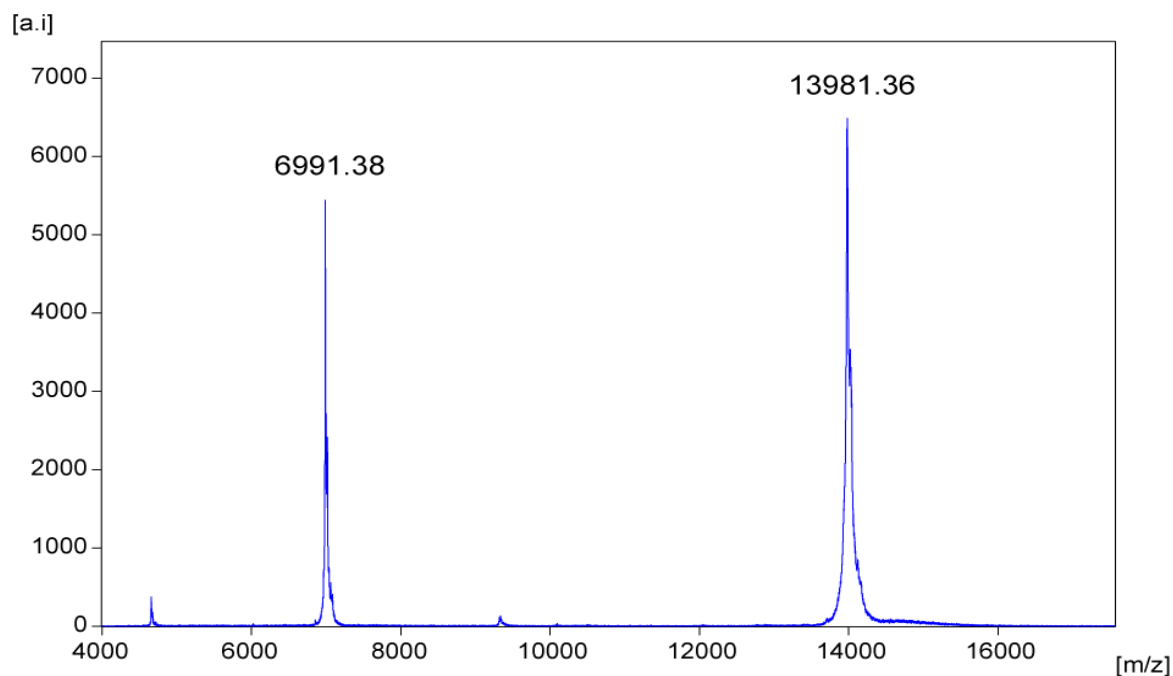
Molecular weight: 13979 Da

Extinction coefficient: 15930 M<sup>-1</sup> cm<sup>-1</sup> at 280 nm

Theoretical pI: 6.3

10            20            30            40            50            60  
MHHHHHMNK IQQINDKELQ SGILSPHQSW HNEYKDNAYI YIGNLNRELT EGDILTVFSE  
70            80            90            100           110           120  
YGV PVDVILS RDENTGESQG FAYLK YEDQR STILAVDNLN GFKIGGRALK IDHTFYRPKR

(Cloning artifacts in red)



# Bud13<sup>40mer</sup>

Uniprot: P46947

Residues: 221-256

Number of amino acids: 39

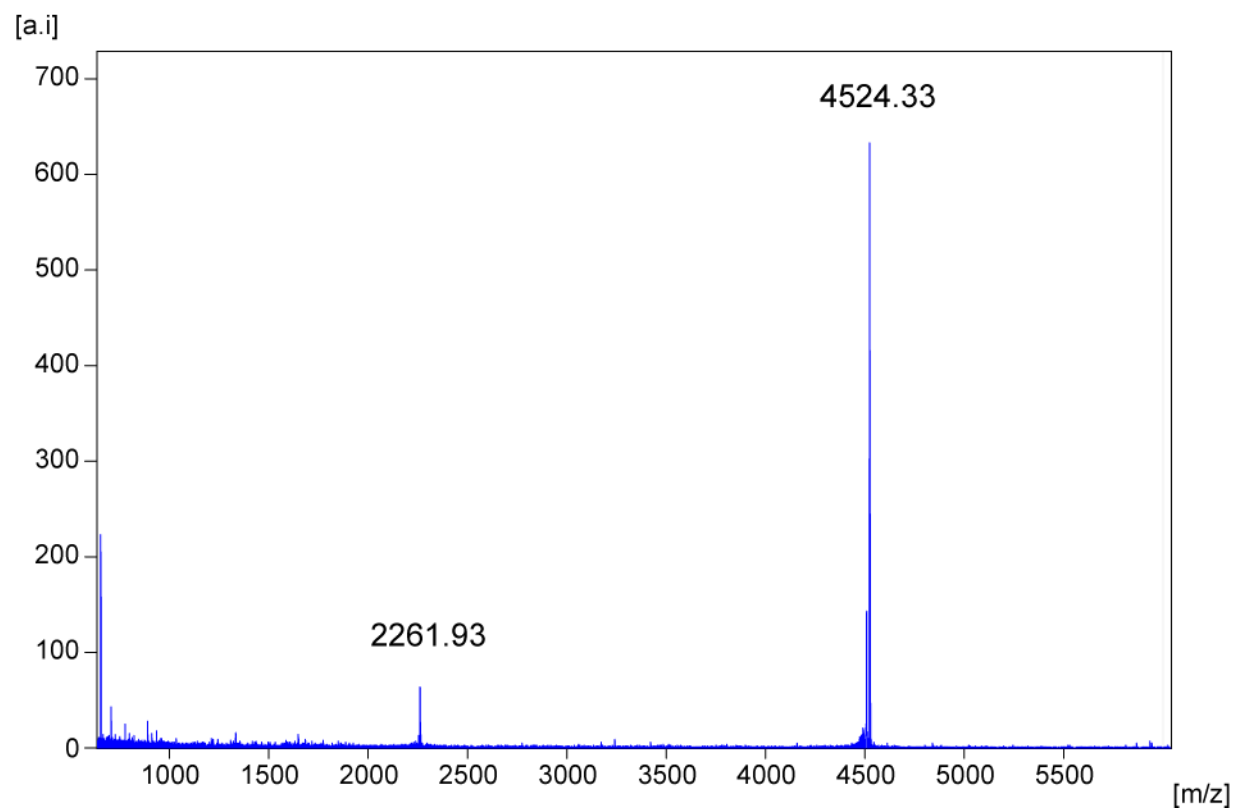
Molecular weight: 4524.0 Da

Extinction coefficient: 11000 M<sup>-1</sup> cm<sup>-1</sup> at 280 nm

Theoretical pI: 9.5

10                      20                      30                      39  
GAMGNRFAIM PGRWDGVHR SNGFEEKWFA KQNEINEKK

(Cloning artifacts in red)



## Pml1<sup>46-204</sup>

Uniprot: Q07930

Residues: 46-204

Number of amino acids: 166

Molecular weight: 19150 Da

Extinction coefficient: 17420 M<sup>-1</sup> cm<sup>-1</sup> at 280 nm

Theoretical pI: 5.1

10            20            30            40            50            60  
MEGIALKHVE PQDAISPDNY MDMLGLEARD RTMYELVIYR KNDKDKGPWK RYDLNGRSCY

70            80            90            100            110            120  
LVGRELGHSL DTDLDDRTEI VVADIGIPEE TSSKQHCVIQ FRNVRGILKC YVMDLDSSNG

130            140            150            160  
TCLNNVIPG ARYIELRSGD VLTLSEFEED NDYELIFMNV HHHHHH

(Cloning artifacts in red)

*no mass spectrometry data available for Pml1<sup>46-204</sup>*





# Abbreviations

1D, 2D, 3D	one-, two-, three-dimensional	NPC	nuclear pore complex
ADAR	adenosine deaminases that act on RNAs	P-bodies	processing bodies
aDMA	asymmetric dimethylated arginine	RISC	RNA-induced silencing complex
A-to-I	adenosine to inosine (RNA editing)	Pcl	Polycomblike protein
ATP	adenosine triphosphate	Pcl-Tudor	Tudor domain of Pcl
Bcl-xl	B-cell lymphoma-extra large	PCR	polymerase chain reaction
BIR	baculovirus IAP repeat	Pml1	pre-mRNA leakage protein 1
BIR-3	Baculoviral inhibition of apoptosis protein repeat (#3)	Pol II	RNA polymerase II
BMRB	Biological Magnetic Resonance Bank	poly(A)	polyadenosine
Bud13	bud site selection protein 13	ppm	parts per million
C/EBP	ccaat-enhancer-binding protein	PRE	paramagnetic relaxation enhancement
CREB	cAMP response element-binding	pre-mRNA	precursor messenger RNA
CSI	chemical shift index	RCS	remodel the structure of chromatin
CSP	chemical shift perturbation	RDC	residual dipolar coupling
CTD	C-terminal domain (usually of Pol II)	RES	retention and splicing
DMSO	dimethyl sulfoxide	RF	radio frequency
DNA	deoxyribonucleic acid	RNA	ribonucleic acid
DNMT	DNA methyltransferase	RNAi	RNA interference
dsRNA	double stranded RNA	RNase	ribonuclease
<i>E. coli</i>	<i>Escherichia coli</i>	RRM	RNA recognition motif
EBNA-2	Epstein-Barr virus nuclear antigen 2	rRNA	ribosomal RNA
EBV	Epstein-Barr virus	SAR-by-NMR	structure-activity relationships by NMR
eIF4E	eukaryotic translation initiation factor 4E	sDMA	symmetric dimethylated arginine
EJC	exon-junction complex	SDS-PAGE	sodium dodecyl sulfate polyacrylamide gel electrophoresis
FHA	forkhead-associated	SEC	size-exclusion chromatography
FID	free induction decay	siRNA	small interfering RNA
FM	frequency modulated	SMN	survival of motor neuron
FT	Fourier transform	snRNAs	small nuclear RNA
GABA	$\gamma$ -Aminobutyric acid	snRNP	small nuclear ribonucleoproteins
H/D-exchange	Hydrogen/Deuterium exchange	Snu17	small nuclear ribonucleoprotein associated protein 17
H3K27me3	tri-methylated lysine 27 of histone H3	STAT5b	signal transducer and activator of transcription 5B
HIV	human immunodeficiency virus	STD-NMR	saturation transfer difference NMR
HMQC	heteronuclear multiple quantum coherence	SWI/SNF	SWItch/Sucrose NonFermentable
HSQC	heteronuclear single quantum coherence	TEV	tobacco etch virus
$K_D$	dissociation constant	TF	transcription factor
kDa	kilo Dalton	TOCSY	total correlation spectroscopy
LMP1	latent membrane protein 1	TRADD	TNF receptor-associated death domain
MeCP2	methyl CpG binding protein 2	TREX	transcription/export (complex)
miRNA	microRNA	tRNA	transfer RNA
MRI	magnetic resonance imaging	TROSY	transverse relaxation optimized spectroscopy
mRNA	messenger RNA	TSN	the extended Tudor domain of Tudor-SN
mRNP	ribonucleoprotein particle	Tudor-SN	Tudor staphylococcal nuclease
MWCO	molecular weight cut-off	UHM	U2AF homology motif
NMD	nonsense mediated decay	ULM	UHM ligand motif
NMR	nuclear magnetic resonance	UV	ultraviolet
NOE	nuclear Overhauser effect	XIAP	x-linked inhibitor of apoptosis protein
NOESY	nuclear Overhauser effect spectroscopy		



# List of Figures

<b>Figure 1.1.1</b> Central dogma of molecular biology.....	6
<b>Figure 1.2.1</b> Overview of regulation in gene expression: From transcription to translation.....	7
<b>Figure 1.2.2</b> Chromatin is a dynamic structure.....	9
<b>Figure 1.2.3</b> Transcription initiation.....	10
<b>Figure 1.2.4</b> mRNA stability depends on the 5' cap and on a intact Poly(A)-tail.....	12
<b>Figure 1.2.5</b> Basics of pre-mRNA splicing.....	13
<b>Figure 1.2.6</b> RNA editing by ADARs.....	14
<b>Figure 1.2.7</b> The nuclear pore complex (NPC) controls mRNA export from the nucleus.....	16
<b>Figure 1.2.8</b> RNA interference (RNAi) in eukaryotic cells.....	19
<b>Figure 2.1.1</b> Basic workflow of molecular cloning for protein expression.....	22
<b>Figure 2.2.1</b> The Larmor frequency depends on the external magnetic field.....	25
<b>Figure 2.2.2</b> Basic explanation of the NMR phenomenon using the vector model.....	26
<b>Figure 2.2.3</b> Outline of NMR hardware setup and acquisition.....	27
<b>Figure 2.2.4</b> Evolution under J-coupling.....	30
<b>Figure 2.2.5</b> The basic version of the HSQC pulse sequence.....	31
<b>Figure 2.2.6</b> Multidimensional NMR.....	32
<b>Figure 2.2.7</b> J-couplings utilized in backbone assignment experiments.....	33
<b>Figure 2.2.8</b> Cartoon illustrating the backbone assignment strategy.....	33
<b>Figure 2.2.9</b> Ligand binding monitored by consecutive acquisition of $^1\text{H}$ , $^{15}\text{N}$ HSQC spectra.....	34
<b>Figure 2.2.10</b> The exchange rate of the ligand influence the appearance of a signal during titration.....	35
<b>Figure 2.2.11</b> $T_2$ measurements using the rate analysis module of NMRViewJ v8.....	36
<b>Figure 2.3.1</b> Basic workflow of X-ray crystallography.....	40
<b>Figure 5.2.1</b> Multiple sequence alignment of Snu17 UHM to other UHMs.....	88
<b>Figure 5.3.1</b> $^1\text{H}$ , $^{15}\text{N}$ HSQC spectra of individual proteins and of the full RES complex.....	89
<b>Figure 5.3.2</b> Optimization of Snu17 constructs, and expression procedures.....	90
<b>Figure 5.3.3</b> Stability of Snu17 $^{1-113}$ with and without a ligand.....	91
<b>Figure 5.3.4</b> Analysis of secondary structure and residue flexibility in Snu17 $^{1-113}$ by NMR.....	92
<b>Figure 5.3.5</b> Size exclusion chromatography of a complex containing Snu17 $^{1-113}$ and Bud13 $^{40mer}$ .....	92
<b>Figure 5.3.6</b> Optimization of the Bud13 ULM peptide by NMR titrations and ITC.....	95
<b>Figure 5.3.7</b> DMSO stabilizes Snu17 $^{1-113}$ and to weakens the interaction of Bud13 $^{40mer}$ .....	95
<b>Figure 5.3.8</b> Analysis of the Bud13 interaction site on Snu17, a comparison of peptides.....	96
<b>Figure 5.3.9</b> $^{15}\text{N}$ labeled recombinant Bud13 peptides titrated with unlabeled Snu17 $^{1-113}$ .....	97
<b>Figure 5.3.10</b> High temperature is needed for recording high quality NMR data.....	98
<b>Figure 5.3.11</b> NMR characterization of Bud13 $^{40mer}$ in complex.....	100
<b>Figure 5.3.12</b> Intermolecular NOEs for $^{15}\text{N}/^{13}\text{C}$ labeled Snu17 $^{1-113}$ in complex with Bud13 $^{40mer}$ .....	101
<b>Figure 5.3.13</b> Crystal structure of the FHA domain from Pml1 and the NMR backbone assignment.....	102
<b>Figure 5.3.14</b> Analysis of the Snu17 $^{FL}$ :Pml1 $^{FL}$ complex by NMR titrations.....	103
<b>Figure 5.4.1</b> Sequence alignment of Bud13 $^{40mer}$ to eukaryotic homologs and to ULM sequences.....	104
<b>Figure 5.4.2</b> Structures of UHM domains in complex with ULM peptides.....	106
<b>Figure 5.4.3</b> A peptide motif of SF3b-155 interacts with p14 at the site where RNA binding occurs.....	109
<b>Figure 6.1.1</b> Ligand titrations of a putative binder to XIAP (BIR-3 domain).....	116
<b>Figure 6.2.1</b> Interaction studies of viral LMP1 and human TRADD.....	117
<b>Figure 6.3.1</b> Initial NMR analysis of an EBNA-2 fragment.....	118
<b>Figure 6.4.1</b> Example of an inhibitor interacting with Bcl-xl.....	119
<b>Figure 6.5.1</b> STD NMR of STAT5b with different compounds.....	120
<b>Figure 6.6.1</b> Induced chemical shifts changes upon ligation of a sDMA-containing peptide to SMN.....	121



# Curriculum Vitae

---

München, October 2010

Anders Friberg  
Born 15th of June 1980  
Swedish citizen

E-mail: anders.friberg@kth.se  
Languages: Swedish, English and German

---

## Education

### 2006-2010

PhD thesis with Prof. Dr. Michael Sattler at EMBL (European Molecular Biology Laboratory, Heidelberg) and at Helmholtz Zentrum München / Technische Universität München. The title of my thesis was:

*Structure and molecular recognition of proteins linked to pre-mRNA splicing and transcriptional regulation.*

I was enrolled in the International PhD program 'Protein Dynamics in Health and Disease' of Elitenetzwerk Bayern.

### 2000 - 2005

M.Sc. in Biotechnology at the Royal Institute of Technology (KTH) in Stockholm. My studies were focused at biomolecular and organic chemistry. Study break during 2003. The Final Degree Project was carried out at Medivir AB in the autumn of 2005, and entitled: *Computational Mapping of Active Sites*

### Spring 2000

Attended a bible study program of Johannelunds Theological University College in Uppsala.

### 1996 - 1999

Attended the natural sciences program at Rudbeckskolan, Sollentuna (Upper secondary school).

My studies were focused on organic chemistry.

---

## Prior employments

### Winter 2006

Full-time position at Medivir AB. Applying the methods developed during my M.Sc. Final Degree project on a drug development project.

### Spring 2003

Full-time work at Apoteket AB, a pharmacy. Cashier and management of goods.

### 2002, 2003 & 2005

Manager at summer camps for ~40 teenagers, I was responsible for planning and implementation. This also included heading a team of 8-12 youth leaders.

### Autumn 1999

Research internship with Prof. Dr. Magnus Ingelman-Sundberg at the Unit of Molecular Toxicology of Karolinska Institutet. The work included molecular biology techniques for cloning, expression and purification of membrane proteins in yeast.

---

## Other merits

### *Elected for a local council in Sollentuna Församling*

During 2005-2006 I was elected board chairman for a district of Sollentuna Församling, a parish within Church of Sweden. The work included setting and controlling the budget, as well as developing the direction of activities in the congregation.

### *Scholarship holder of Church of Sweden*

Thanks to a scholarship from Church of Sweden I spent the autumn of 2003 in Malaysia. During this exchange program I visited projects connected to a partner church and worked at schools for handicapped, homes for neglected children etc.

### *Youth Leader*

Worked as a youth leader at summer confirmation camps in 1997-2001 and 2004.

Responsible for activities and discussion groups.

---

References and certificates will be provided at your request.

"Quality... you know what it is, yet you don't know what it is. But that's self-contradictory. But some things *are* better than others, that is, they have more quality. But when you try to say what the quality is, apart from the things that have it, it all goes *poof!* There's nothing to talk about. But if you can't say what Quality is, how do you know what it is, or how do you know that it even exists? If no one knows what it is, then for all practical purposes it doesn't exist at all. But for all practical purposes it really *does* exist. What else are the grades based on?

Why else would people pay fortunes some things and throw others in the trash pile? Obviously some things are better than others.. but what's the "betterness"?... So round and round you go, spinning mental wheels and nowhere finding anyplace to get traction. What the hell is Quality? What is it?"

*Zen and the Art of Motorcycle Maintenance,*

by Robert M. Pirsig

"Du bist frei. Nun lebe aus der Weisheit, die auch Gott dir geschenkt hat."

*Das Buch der Lebenskunst,*

by Benedictine Brother Anselm Grün, Münsterschwarzach